Characterisation of a novel interaction of dystrophin with caveolae in the heart.

Elena Marrosu

UCL Great Ormond Street Institute of Child Health

University College London

Thesis submitted to University College London in fulfilment

of the requirements for the title of Doctor of Philosophy

November 2021

Abstract

Patients living with Duchenne and Becker muscular dystrophy are characterised respectively by the loss of a functional dystrophin protein and the expression of a mutant dystrophin protein. Dilated cardiomyopathy (DCM) is the major cause of death in these patients and the molecular mechanisms causing DCM in these patients are still not completely established. In fact, the cardiac disease is treated with cardioprotective drugs that delay but do not prevent DCM as a targeted treatment for the heart is still not available due to this lack of knowledge.

 Previous findings showed that exclusively in the heart, the dystrophin glycoprotein complex includes cavin-1, an essential protein for the biogenesis of caveolae. Caveolae in the heart are involved in mechanisms of cardio protection, cardiac contraction, and cardiac conduction. Key caveolae accessory proteins include cavin-2, -3 and -4. More importantly, caveolar protein mutations have been linked to cardiomyopathy. My PhD thesis investigates the molecular interactions between cardiac dystrophin and cavins that are important for cardiac function and are affected by dystrophin gene mutations. I have characterised the distribution of cavin proteins in mouse, rat and dog models of Duchenne muscular dystrophy (DMD) comparing this distribution in explanted human heart and discovered that cavin-1 and -4 cardiac localisation is conserved across these different species. I have investigated the effect of the loss of full-length dystrophin in DMD mouse, rat and dog models finding different levels of disruption of cavin-1 and -4 that could be attributed by the expression of shorter dystrophin isoforms in these animal models. I have also tested the ability of five different

micro and mini-dystrophin (one of them is currently used in a clinical trial) constructs in restoring the physiological cardiac localisation of cavin-1 and -4 finding that none of them is able to do this.

Overall, my findings suggest that the cardiac localisation of cavins is dependent on the expression of dystrophin at the cardiomyocyte membrane and that the cavin binding domain could reside in the distal part of the dystrophin protein. This knowledge suggests new roles of dystrophin in the heart and could be useful for the design of the next gene therapy constructs and for the development of targeted cardiac therapies.

.

Impact statement

Duchenne and Becker muscular dystrophies are two neuromuscular conditions caused by mutations of the dystrophin gene. Duchenne patients are characterized by a severe skeletal muscle disease and dilated cardiomyopathy (DCM) whereas Becker patients show a more variable phenotype of skeletal muscle disease, but they also develop DCM. The major cause of death in Duchenne and Becker muscular dystrophies is cardiac failure. The molecular principles behind DCM in these diseases are poorly understood and current cardiac management in these patients involves cardio-protective drugs that delay the onset of DCM, but do not prevent it due to their lack of specificity. A promising therapeutic approach is adeno-associated virus (AAV) gene therapy that aim to systemically delivers a functional dystrophin cDNA. Because of the limited capacity of the AAV vector, dystrophin needs to be miniaturized (micro- and mini-dystrophin). Therefore, the dystrophin domains included in these mini and micro-dystrophin construct need to be carefully chosen to ensure the rescue of both the cardiac and skeletal muscle pathology. Dystrophin associates with different proteins in both skeletal and cardiac muscle but previous studies showed that cardiac dystrophin associates with a set of proteins that are not present in the dystrophin glycoprotein complex of skeletal muscle suggesting a cardiac specific role of dystrophin. Among these new proteins is cavin-1, that is essential for the formation of caveolae. Caveolae are membrane invaginations that in the heart play important roles for cardiac physiology and disease. Cavin-1 is part of a protein family that includes key caveolae accessory proteins such as cavin-2, -3 and -4. Because of the known involvement of caveolae in cardiac disease and function, a

disruption of cavins in DMD could be a hitherto unrecognised contributor to cardiac disease in DMD. Therefore, the aim of my PhD project was to characterise the association of cardiac dystrophin with the cavin proteins. The characterisation of these new molecular interactions adds new knowledge about the role of dystrophin in the heart and could be beneficial for the design of future gene therapy constructs and targeted cardiac therapies. The research I conducted for my PhD thesis led me to find that, when dystrophin is lost at the membrane of the mouse cardiomyocytes, the membrane localisation of cavin-1, -2 and -4 is also disrupted, supporting a prior study that showed an association of dystrophin with cavin-1. I have found that the distribution of cavin-1, -2 and -4 is conserved across different species such as rats, dogs, and humans and is affected in DMD rats and dogs by the loss of dystrophin as observed in mice. This knowledge could be useful when choosing an appropriate animal model for the study of caveolar proteins.

Using transgenic mice expressing five different micro and mini-dystrophin constructs, I found that none of them is able to recruit cavin-1 and -4 at the cardiomyocyte membrane they helped me narrowing down the dystrophin domains potentially involved in the cavin-1 and -4 binding. The results collected from my research demonstrated a new role of dystrophin in the membrane localisation of cavin proteins that is not only limited to the murine heart but also occurs in other species. Since mutations on cavin-1 and cavin-4 are associated with cardiac disease, the cardiac interaction between dystrophin and cavins should be considered for the design of the next gene therapy constructs.

Presentations and Publications

Presentations

1. 14th UK Neuromuscular Translational Research Conference (25th -26th March 2021), virtual conference. Poster presentation

2. 12th UK Neuromuscular Translational Research Conference (4th-5th April 2019), Newcastle. Oral presentation

3. 6th International Congress of Myology (25-28 March 2019). Bordeaux (FR). Poster presentation

4. ICH poster competition. Poster winner, 1st prize. UCL Great Ormond Street Institute of Child   Health, London (Nov 2018).

5. ICH Developmental Neuroscience 3 Minutes Thesis competition. Best oral presentation. UCL Great Ormond Street Institute of Child Health, London (Feb 2018).

Publications

1. Wang H and **Marrosu E**, Brayson D, Wasala NB, Johnson EK, Scott CS, Yue Y, Hau KL, Trask AJ, Froehner SC, Adams ME, Zhang L, Duan D, Montanaro F. "Proteomic analysis identifies key differences in the cardiac interactomes of dystrophin and micro-dystrophin". Hum Mol Genet. Jun 2021; 26;30(14):1321-1336.

Acknowledgements

I wish to express my sincere gratitude to my supervisors Doctor Federica Montanaro and Professor Jennifer Morgan for their constant support and guidance during these long four years of my PhD, in which we also experienced working during a pandemic.

I also want to thank Muscular Dystrophy UK for the trust they have had in our project and the fundings they provided to achieve it. Thank you to Doctor Dongheng Duan and his collaborators for providing me with precious samples and insightful opinions on my research. Thank you to Doctor Caroline Le Guiner who also kindly gave me important samples for my PhD project and to Professor Richard Piercy and his group for allowing me to work on their samples and for the helpful scientific discussions we had during my PhD journey.

I want to thank Professor Muntoni and all the past and present members of the Dubowitz Neuromuscular Centre that in these almost 8 years have become more like a second family to me than just a group of colleagues. A special thanks goes to Silvia Torelli, she has made everything easier for me, she was always present, always helpful, and supportive.

Thank you to the beautiful people and amazing scientists I met at the Institute of Child Health that became my friends. Pierpaolo, Sara, Francesco, Serena, and Veronica, I am honored to be their friend and colleague.

I have waited for this PhD for such a long time, I left my amazing parents to pursue my dream to be a scientist, a doctor. But they never left me, not for one second. Despite the physical distance they filled my life with

love, laughs, and support. They always taught me that I could do whatever I wanted to do and be whomever I wanted to be. They are my two pillars and without them I could not stand.

Endless gratitude goes to Valeria, my sister, my best friend, the better version of myself. She has believed in me since day one and I am blessed to share my life with her.

Lastly, but not least, my deepest gratitude goes to the best person I have ever met who I am lucky enough to also call my husband. The unconditional love, the patience, and the support he has given me in these years are priceless and I will be always grateful to him.

To my friend, Giulio

Table of contents

List of figures

List of tables

List of abbreviations

ABD	actin binding domain
BDM	Becker muscular dystrophy
C-terminus	Carboxy-terminus
Dag1	β-dystroglycan
DAPC	Dystrophin associated protein complex
DAPI	4′, 6-diamidino-2-phenylindole
DCM	dilated cardiomyopathy
DGC	dystrophin glycoprotein complex
DMD	Duchenne muscular dystrophy
DNC	Dubowitz Neuromuscular Centre
DP	dystrophin protein
Dtna	α-dystrobrevin
EDTA	ethylenediaminetetraacetic acid
FAM	6-Carboxyfluorescein
GOS Institute of child health	Great Ormond Street Institute of Child Health
H	Hinge region (followed by a number)
HPRT	hypoxanthine phosphoribosyltransferase1
IF	immunofluorescence
nNOS	Neuronal nitric oxide synthases

NPG	n-propyl-gallate
N-terminus	Amino-terminus
PBS	phosphate buffer saline
PCR	polymerase chain reaction
PDZ	PSD95=post synaptic density protein, Dlg1=Drosophila disc large tumor suppressor and zo-1=zonula occludens-1 protein
qRT-PCR	quantitative real time PCR
R	spectrin-like repeat (followed by a number)
RSB	Reducing sample buffer
Sgcb	β-sarcoglycan
SSPN	Sarcospan
Stna1	α1-syntrophin
Tris	tris(hydroxymethyl)aminomethane
VIC	2′-chloro-7′phenyl-1,4-dichloro-6 carboxyfluorescein
WB	western blot

Chapter 1. Introduction

1.1 The Duchenne Muscular Dystrophy gene and the dystrophin protein

The Duchenne Muscular Dystrophy (*DMD*) gene spanning over 2.2Mb (Tennyson, Klamut et al. 1995) is one of the largest human genes and is located in the short arm of the X chromosome (Kunkel, Monaco et al. 1985, Monaco, Neve et al. 1986, van Ommen, Verkerk et al. 1986). It contains eight promoters that drive the transcription of different dystrophin isoforms (**Figure 1 A**). The dystrophin protein isoforms are identified by the acronym Dp, that stands for dystrophin protein followed by a number that corresponds to the molecular weight and are expressed in different tissues (**Table 1**) at different times during development (Torelli, Ferlini et al. 1999). Three upstream promoters (**Figure 1 A**) initiate the transcription of three different full length dystrophin forms that have the same molecular weight but are differentially expressed in muscle, brain, and cerebellar Purkinje cells respectively, called Dp427m, Dp427c and Dp427p (**Figure 1 B**). The *DMD* gene also encodes for five shorter dystrophin isoforms initiated by five different promoters (**Figure 1 A**). The Dp260 isoform is expressed in the retina (D.M Pillers 1993), brain and cardiac muscle (V N D'Souza 1995). Dp140 has been reported in the Purkinje cells of the cerebellar cortex (Lidov 1995) and in kidney (Lidov 1997). Dp116 is expressed in the peripheral nervous system in the Schwann cells (Byers 1993), while Dp71 is mainly expressed in brain and liver (Austin 1995) but its mRNA is also found in muscle (Rapaport, Lederfein et al. 1992). The last isoform is Dp40 (Tozawa, Itoh et al.

2012), that lacks the C-terminus of Dp427, found in brain (Tozawa, Itoh et al. 2012, Doorenweerd, Mahfouz et al. 2018) (**Figure 1 B and table 1**).
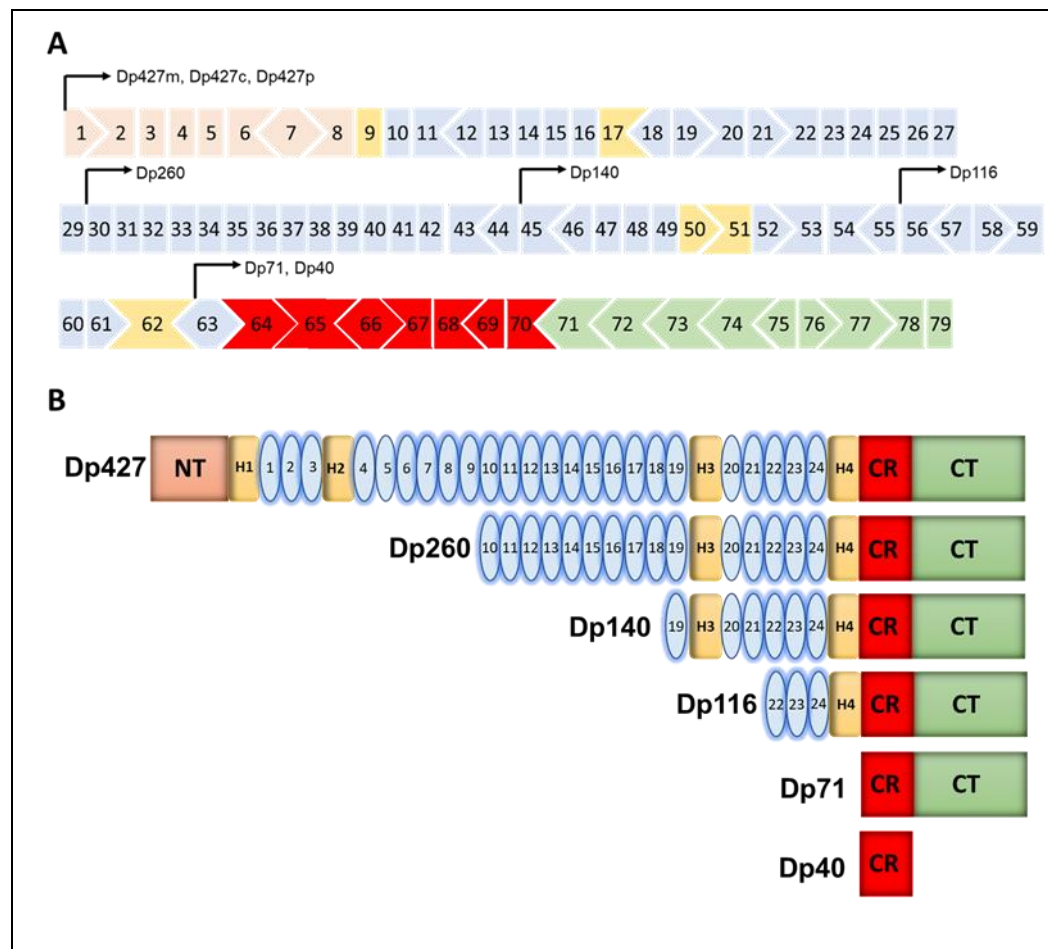
Figure 1. DMD exons, promoters, and tissue distribution of dystrophin isoforms.

*Schematic representation of DMD gene exons and the eight promoters. The chosen colours for the exons match the colours of the encoded dystrophin protein domains (**B**) that will be examined in detail in 1.1.1. **B.** Diagram of the different dystrophin protein isoforms. **NT**= N-terminus, **H1**, **H2**, **H3**, **H4**= Hinge 1, 2, 3 and 4. Numbered light blue oval-shapes= spectrin-like repeats of the rod domain. **CR**= Cysteine-rich domain. **CT**= C-terminus.*

Table 1. Tissue distribution of dystrophin isoforms.

Dystrophin isoforms	Tissue expression
Dp427	Cardiac and skeletal muscle Brain Cerebellar Purkinje cells
Dp260	Cardiac muscle Brain Retina
Dp140	Purkinje Kidney
Dp116	Schwann cells
Dp71	Brain Liver
Dp40	Brain

In skeletal and cardiac muscle, dystrophin has a structural role connecting the intracellular cytoskeleton to the extracellular matrix via several protein interactions (**Figure 2 and 3**), ensuring the membrane stabilisation during muscle contraction in order to avoid contraction-induced damage (Danialou 2001) (Petrof 1993). Furthermore, dystrophin functions as a scaffold, anchoring signalling proteins to the sarcolemma (Rando 2001) (Judge, Haraguchiln et al. 2006). To my knowledge there are not studies that elucidate the role of each specific isoform in different tissue. However, a study performed in brain found that the Dp427 isoform is expressed in neurons while Dp140 and Dp71 are expressed in glial cells. The three different isoforms present in different brain cells play different roles creating a link with specific proteins (Verghese 2021) .

1.1.1 Dystrophin protein domains and dystrophin interactions with the dystrophin glycoprotein complex

The fulfilment of the structural and signalling roles of dystrophin would not be possible without the interactions that dystrophin establishes with a set of proteins that come together to form the Dystrophin Glycoprotein Complex (DGC; **Figure 2 and 3**) (Ibraghimov-Beskrovnaya, Ervasti et al. 1992, Duggan, Gorospe et al. 1997). Dystrophin associates with members of the DGC because of its tertiary structure, made of 4 functional domains.

1) Actin-binding domain (ABD1)

The amino-terminal portion of dystrophin is responsible for anchoring the dystrophin protein to the cytoskeleton. It is called the actin-binding domain (ABD1) because of the presence of two calponin homology domains (CH1 and CH2) that bind with monomers of the cytoskeletal F-actin (Way M. 1992, Rybakova and Ervasti 1997). The ABD1 domain is very important for muscle membrane stability as it connects dystrophin to the contractile apparatus in skeletal muscle via the link with γ-actin (Rybakova, Patel et al. 2000). The ABD1 also associates with the contractile apparatus via the cytokeratin 19 intermediate filament protein (Stone, O'Neill et al. 2005).

2) Rod domain

The central portion of the dystrophin protein is called the rod domain and is composed of 24 spectrin-like repeats (R1 to R24) placed in tandem, plus four proline-rich regions called "hinges". Two hinges (H1 and H4) are located at its extremities and the other two hinges (H2 and H3) are within the rod domain allowing flexibility to the dystrophin protein (Koenig

and Kunkel 1990) (**Figure 2**). One of the roles carried out by the rod domain is to reinforce the structural role of dystrophin, in fact the region of the rod domain spanning from spectrin-like repeat R11 to R17 forms a second actin binding domain (ABD2) (Amann, Renley et al. 1998). Though lower affinity than ABD1 it likely serves to support the association of dystrophin with the cytoskeleton by ABD1 at the N-terminus of dystrophin. In skeletal muscle, dystrophin plays also a role in the organisation of the microtubule lattice via R20 to R23 of the rod damain (Belanto, Mader et al. 2014). *In vivo* studies on mdx[23] mice (a DMD mouse model that will be described in **1.3.2**) treated with adeno associated virus (AAV) vectors to deliver specific dystrophin spectrin-like repeats, revealed an interaction between membrane phospholipids and the R1-R3 / R10-R12 regions of dystrophin (Zhao, Kodippili et al. 2016) facilitating the interaction of dystrophin with the plasma membrane.

Another important molecular interaction happens between H4 and a transmembrane protein of the DGC: β-dystroglycan. Specifically, the C-terminus of β-dystroglycan binds with the WW motif present in H4 of the dystrophin rod domain (Ilsley, Sudol et al. 2002).

The rod domain has not only a structural role but also a signalling role. It is involved in binding members of the DGC involved in signaling, such as α-syntrophin that binds to R17 and β-syntrophin that binds to R22 (Adams, Odom et al. 2018). Alpha1-syntrophin is an important signalling protein that mediates the interaction of neuronal nitric oxide synthase (nNOS) with the DGC in skeletal muscle (Lai, Thomas et al. 2009, Lai, Zhao et al. 2013). In particular, nNOS binds the PDZ domain (PDZ stands for PSD95=post synaptic density protein , Dlg1=Drosophila disc

large tumor suppressor and zo-1=zonula occludens-1 protein that are the three proteins that first showed to share this domain) of α-syntrophin (Hillier B. J. 1999). nNOS is localised at the cytosolic surface of the sarcolemma and during muscle contraction nNOS produces nitric oxide (NO). When NO reaches the muscle vasculature it causes their dilation allowing sufficient blood flow to provide the correct amount of oxygen and nutrients that a contracting muscle requires (Suhr, Gehlert et al. 2013). In cardiac muscle, nNOS is not part of the DGC, as it is found in the sarcoplasmic reticulum and in the mitochondria (K. Y. Xu 1999, A. J. Kanai 2001, Johnson, Zhang et al. 2012).

3) Cysteine-rich domain

The third dystrophin domain is the cysteine-rich domain that can be subdivided into two functional sub-domains, the EF hand-like and the ZZ domain. The EF hand-like domain reinforces the binding of H4 with β-dystroglycan (Chung W. 1999, Rentschler S. 1999). The ZZ domain binds to calmodulin, a calcium-binding protein involved in muscle contraction, in a calcium-dependent manner (Anderson, Rogers et al. 1996). This ZZ domain is also involved in the binding with ankyrin-B, that is crucial to increase the closeness of dystrophin to the sarcolemma (Ayalon, Davis et al. 2008).

4) C-terminus

The last domain is the C-terminus that contains binding sites for α and β-syntrophins other than the ones present in the rod domain, but the major difference between the two binding types is that only the α-syntrophin that binds to the R17 is able to recruit nNOS (Adams, Odom et al. 2018).

The dystrophin C-terminus also interacts with the C-terminus of another member of the DCG called α-dystrobrevin via their respective coiled-coil regions (Blake D. J. 1995, Sadoulet-Puccio, Rajala et al. 1997) anchoring it to the sarcolemma (Sadoulet-Puccio, Rajala et al. 1997). Alpha-dystrobrevin has been shown to also interact with syntrophins (Peters M. F. 1997). On one hand the C-terminus of dystrophin is involved with binding to multiple proteins involved in signalling, on the other hand, studies performed in mice expressing a dystrophin lacking the C-terminus showed normal localisation of dystrobrevin and syntrophin. These observations suggest that both proteins do not require the C-terminus for their membrane localisation (Crawford G. E. 2000). Moreover, Rafael and colleagues showed that mice expressing a dystrophin protein lacking the C-terminus domain have normal muscle function (Rafael J. A. 1996).
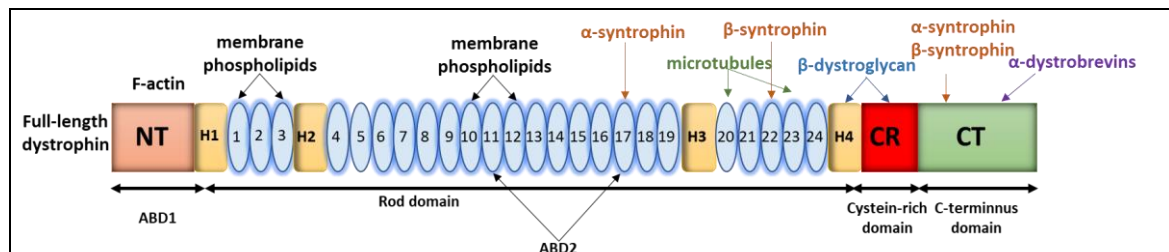
Figure 2. Schematic representation of the dystrophin domains and the interactions they are involved in.

NT= N-terminus, H1, H2, H3, H4= Hinge 1, 2, 3 and 4. Numbered light blue oval-shapes= spectrin-like repeats of the rod domain. CR= Cysteine-rich domain. CT= C-terminus. ABD = Actin binding domain.

1.1.2 Other members of the DGC

In **1.1.1** the members of the DGC that interact directly with dystrophin have been described. However, the DGC also includes other members (**Figure 3**) that do not associate directly with dystrophin but interact with the DGC proteins described in the previous section. For example, β-dystroglycan binds dystrophin but is also tightly associated with another member of the DGC, the extracellular protein α-dystroglycan (Ervasti and Campbell 1991). Alpha-dystroglycan acts as a receptor for extracellular ligands such as laminin, agrin and perlecan linking dystrophin to the extracellular matrix (Henry and Campbell 1996). Another protein family part of the DGC consists of six transmembrane proteins, α, β, γ, δ, ε and ζ sarcoglycan. Striated muscle is mainly composed of α, β, γ, δ sarcoglycans. Delta-sarcoglycan has been shown to interact with β-dystroglycan (Chan Y. M. 1998). Moreover, the sarcoglycans bind with the N-terminal region of α-dystrobrevin (Yoshida M. 2000). The binding between sarcoglycans and α-dystroglycan is important to stabilize the DGC (Yoshida, Hama et al. 2000). The last member of dystrophin glycoprotein complex is sarcospan (SSPN) that required the association with sarcoglycans for its stability (Crawford, Faulkner et al. 2000). Studies in sarcospan knock-out mice showed no disruption in the dystrophin glycoprotein complex (Lebakken C. S. 2000).
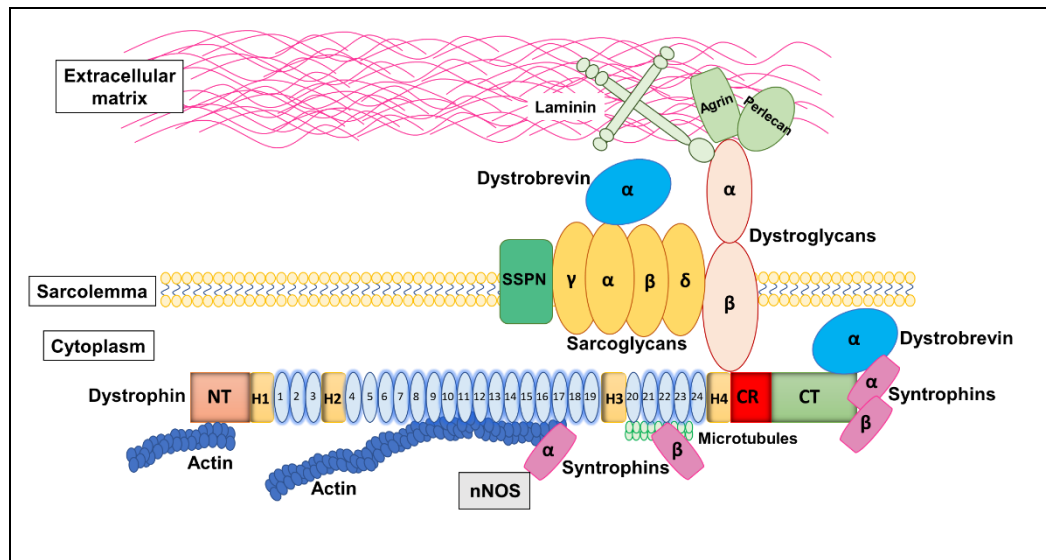
Figure 3. Diagram of the interaction of dystrophin with the dystrophin glycoprotein complex (DGC) and actin in skeletal muscle.

Schematic representation of how dystrophin links the actin cytoskeleton with the extracellular matrix via molecular interactions with actin, microtubules, and the dystrophin glycoprotein complex in skeletal muscle cells.

There is not only a difference in the tissue distribution of the dystrophin isoforms (**Table 1**) but there is also a difference in the proteins that dystrophin can assemble in these different tissues. In cardiac muscle the DCG includes proteins that are not found to be associated with dystrophin in skeletal muscle. The proteins that specifically associate with dystrophin in the heart are cavin-1, ahnak1, cypher, and CRYAB. Moreover, β2-syntrophin and α3-dystrobrevin have been found more abundant in cardiac muscle than in skeletal muscle (Johnson, Zhang et al. 2012). Several studies also focused on the specific distribution of the dystrophin isoforms in brain and the difference in the dystrophin associated proteins. As mentioned in 1.1.1, Dp427 isoform is expressed in neurons while Dp140 and Dp71 are expressed in glial cells. The brain DGC contains β-dystrobrevin but not the sarcoglycan complex.

Moreover, γ-1-syntrophin shown to be associated with the Dp427 isoform in neurons while γ2-syntrophin has been found associated with Dp71 in glial cells (Verghese 2021).

1.1.3 Utrophin, *in vivo* and *in vitro* differences with dystrophin

Utrophin is an autosomal paralogue of dystrophin. The utrophin gene is located on the human chromosome 6q24 and the mouse chromosome 10 (Buckle, Guenet et al. 1990) and its transcription is controlled by two differentially regulated promoters, A and B. These two promoters drive the transcription of two different mRNA isoforms that are translated in two full-length utrophin proteins, A-utrophin and B-utrophin (**Figure 4**). A and B-utrophin proteins have a 395kDa molecular weight and they share 80% amino acid identity with dystrophin (Tinsley, Blake et al. 1992). Utrophin A and B have a different N-terminus actin binding domain and a different expression pattern. A-utrophin has been found in muscle at the myotendinous and neuromuscular junctions and at the sarcolemma of regenerating myofibers (Helliwell, Man et al. 1992). B-utrophin is expressed in endothelial cells and blood vessels (Weir, Burton et al. 2002). Another three shorter utrophin isoforms have been reported: Up140, Up71 (Wilson, Putt et al. 1999), G-utrophin (Blake, Schofield et al. 1995) and their function is not yet fully understood. Like the dystrophin protein, utrophin consists of an actin binding N-terminus domain, a central rod domain, a cysteine-rich domain and C-terminus domain. One of the differences between dystrophin and utrophin is their spatiotemporal distribution. In fact, utrophin is present at the sarcolemma of human foetal skeletal muscle fibres while dystrophin is absent. At about 20 weeks of gestation, utrophin is gradually substituted by dystrophin at the sarcolemma and thereafter, utrophin is confined to

myotendinous and neuromuscular junctions, in the nerves and vasculature (Clerk, Sewry et al. 1992, Clerk, Strong et al. 1992, Clerk, Morris et al. 1993). Despite having a very similar amino acid identity with dystrophin (Tinsley, Blake et al. 1992), utrophin is not capable of localising nNOS to the sarcolemma (Li, Bareja et al. 2010) and binds to β-dystroglycan more weakly than does dystrophin (about 2-fold) (Ishikawa-Sakurai, Yoshida et al. 2004). Moreover, utrophin binds the actin filaments with only one continuous domain that spans from the N-terminus to spectrin-like repeat 10. Despite the different mode of association with actin, the binding affinity of dystrophin and utrophin for actin is very similar (Rybakova and Ervasti 2005). The presence of a single continuous high affinity actin binding domain in the utrophin protein versus the two low affinity actin binding sites of dystrophin remains unclear. Rybakova and Ervasti speculated that the role of the two low affinity dystrophin actin binding sites is to bind and unbind with actin more rapidly allowing dystrophin to function as a "shock absorber" during muscle stretch. Instead, the high affinity single actin binding domain of utrophin acts as a "molecular ruler" to define the length of costameric actin during muscle development. Another difference between dystrophin and utrophin is their binding with the microtubules. Studies performed on skeletal muscle of dystrophin deficient mice (mdx[23], **1.3.2**) and mdx[23] mice over expressing utrophin showed the disorganization of the microtubule lattice when compared to wild-type mice normally expressing dystrophin showing that utrophin does not binds with microtubules (Belanto, Mader et al. 2014).
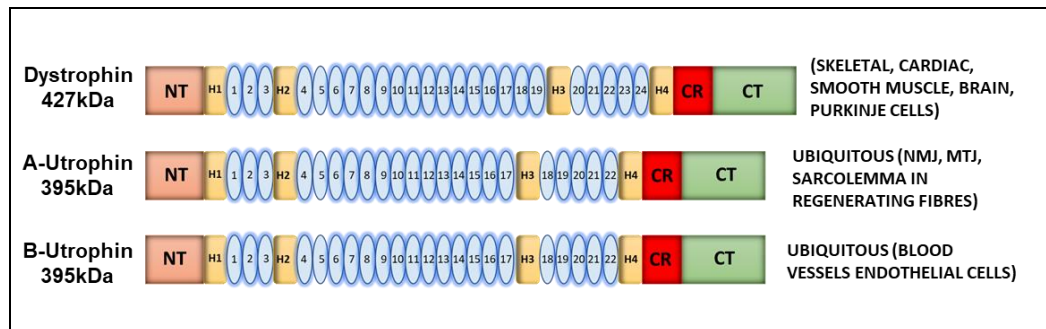
Figure 4. Comparison of the full-length dystrophin domains with the domains of A and B-utrophin.

Schematic representation of the domains of dystrophin and A and B utrophin. NT=N-terminus, H= hinge. Numbered light blue oval-shapes= spectrin-like repeats of the rod domain. CR= Cysteine-rich domain. CT= C-terminus.

1.2 Dystrophinopathies

Several mutations can occur in the *DMD* gene, the majority of which involve more than one exon and are classified as large mutations accounting for 80% of total mutations, of which 86% are deletions and 14% are duplications. The remaining 20% includes small mutations (smaller than one exon) of which the majority are point mutations (52%) that are nonsense in 50% of the cases and missense in 2% of the cases. Small mutations also include deletions (25%), splice site (14%) and insertions (9%). Mid-intronic mutations occur in only 0.3% of the cases (Bladen, Salgado et al. 2015). Mutations in the *DMD* gene cause dystrophinopathies that span from mild to severe diseases including Duchenne muscular dystrophy (DMD), Becker muscular dystrophy (BMD) and X-linked dilated cardiomyopathy (XLDCM). Although, dystrophinopathies show a X-linked inherited pattern, de novo mutations are also described by several independent studies being reported in 16%–35% of cases (Garcia, de Haro et al. 2014, Lee, Takeshima et al. 2014).

1.2.1 Duchenne muscular dystrophy

Duchenne muscular dystrophy has an incidence of about 1 in 5000 male live births (Mendell, Shilling et al. 2012, Moat, Bradley et al. 2013). Most of the mutations found in the dystrophin gene of DMD patients are deletions (60-70%), that can happen anywhere in the *DMD* gene but have been mostly observed in the region including exons 2-19 (Nakamura, Fueki et al. 2016) and the central region which includes exon 45-55 (Oudet, Hanauer et al. 1992, Nobile, Galvagni et al. 1995, Nakamura, Shiba et al. 2017). The region included between exon 2-20

and between exon 45-55 of the dystrophin gene are the two main mutational "hotspots" (Bladen, Salgado et al. 2015) (**Figure 5 A**). 5-15% of the patients present with duplications and the remaining 20% have small deletions or insertions or point mutations (Aartsma-Rus, Van Deutekom et al. 2006, Magri, Govoni et al. 2011). 90% of DMD cases are caused by mutations that disrupt the reading frame (out-of-frame mutations) leading to the production of a non-functional dystrophin according to the Monaco rule (Monaco, Bertelson et al. 1988, Aartsma-Rus, Van Deutekom et al. 2006). This rule was postulated in 1988, categorising out-of-frame mutations with the severe DMD phenotype and mutations that do not disrupt the reading frame (in-frame mutations) with the milder BMD phenotype. However, exceptions have been observed in DMD patients presenting with mutations that do not disrupt the reading frame but still develop a severe phenotype. In these cases, mutations affect too large portions of the *DMD* gene to result in a functional protein, or are located in crucial domains for dystrophin function stabilisation such as the cysteine-rich domain (Aartsma-Rus, Van Deutekom et al. 2006). Moreover, several patients with in-frame deletion or duplication of exon 5 resulted in out-of-frame transcripts due to alternative splicing events (Gualandi, Trabanelli et al. 2003).

DMD patients start to show muscle weakness and motor function deterioration at the age of 5-7 years becoming wheelchair dependent by 12 years of age (Yiu and Kornberg 2015). They show respiratory muscle decline from 12 years of age with a decrease of 4-8% per year in their vital capacity (Khirani, Ramirez et al. 2014) needing assisted ventilation by the age of 20 years (Mercuri, Bönnemann et al. 2019). About 30% of patients also show intellectual disability, attention deficit disorder and

autistic spectrum disorder (Ricotti, Mandy et al. 2016). DMD patients start to show cardiomyopathy by 9-10 years of age that progresses into dilated cardiomyopathy (DCM) eventually leading to cardiac failure (Eagle M 2002). Currently, there is no cure for Duchenne muscular dystrophy. Before the advent of nocturnal ventilation, respiratory failure was the major cause of death in DMD patients (Passamano, Taglia et al. 2012). Assisted ventilation increased their life expectancy to their late twenties to early thirties (Eagle M. 2002). Currently, the major cause of mortality in these patients is cardiac failure (Eagle M 2002, McNally, Kaltman et al. 2015, Birnkrant, Bushby et al. 2018).

DMD is extremely rare in females and has been described in one case of bi-allelic *DMD* mutation (Takeshita, Minami et al. 2017), and in some case reports associated with Turner disease (Ferrier, Bamatter et al. 1965, Chelly, Marlhens et al. 1986, Satre, Monnier et al. 2004) a genetic disorder in which part or the whole X chromosome is missing. DMD female carriers carrying a *DMD* mutation on one of the X chromosomes, are mostly asymptomatic when the normal allele compensates the mutated one. In rare cases the skewed inactivation of the normal allele causes the development of a DMD-like phenotype with skeletal muscle weakness occurring in approximately 2.5-19% of the cases and dilated cardiomyopathy occurring in the 7.3-16.7% of the cases (Ishizaki, Kobayashi et al. 2018).

1.2.2 Becker muscular dystrophy

Becker muscular dystrophy (BMD) is less common than DMD, it affects 1 in 11,000 to 19,000 live male births (Mah, Korngut et al. 2014). 60-70% of the mutations found in BMD patients are deletions. Duplications account for 20% of cases, while 5-10% are point mutations, small

deletions, or insertions (Aartsma-Rus, Van Deutekom et al. 2006). BMD patients have low levels of full-length dystrophin or express a partially functional dystrophin mostly (90%) due to in-frame mutations of the *DMD* gene (Hoffman, Fischbeck et al. 1988, Blake, Weir et al. 2002) **(Figure 5 B**). However, in 2% of BMD patients out-of-frame deletions and duplications have been found (Aartsma-Rus, Van Deutekom et al. 2006).

The disease course is quite variable: typically these patients start to manifest symptoms by the age of 15 or greater but most patients remain ambulant until the third decade of life (Yazaki, Yoshida et al. 1999). They rarely show cognitive impairments, that are reported only in isolated cases (North, Miller et al. 1996, Young, Barton et al. 2008). 70% of BMD patients develop cardiomyopathy with a variable age of onset and in some cases, this is not accompanied by skeletal muscle disease (Angelini, Fanin et al. 1996). Cardiac failure is the major cause of death in patients with BMD (Bushby, Muntoni et al. 2003) and will be discussed in **1.3**. 13.3% of BMD female carriers show skeletal muscle symptoms and dilated cardiomyopathy (Ishizaki, Kobayashi et al. 2018).

1.2.3 X-linked dilated cardiomyopathy

In 1987, Berko and Swift described a large family with 11 males showing dilated cardiomyopathy between 10 and 20 years old without skeletal muscle involvement, and 5 females showing progressive dilated cardiac involvement by the age of 40 and no skeletal muscle involvement (Berko and Swift 1987). In 1993 Tobin and colleagues linked this family's disorder to the *DMD* gene (Towbin, Hejtmancik et al. 1993). Simultaneously, Muntoni identified mutations in the dystrophin gene in a

separate family with dilated cardiomyopathy and no skeletal muscle involvement (Muntoni, Cau et al. 1993).

Patients with X-linked dilated cardiomyopathy (XLDCM) show absent or mild myopathy symptoms (Berko and Swift 1987, Lester, Femia et al. 2019). Immunohistochemical analyses of biopsies from XLDCM patients show a moderate reduction of dystrophin in skeletal muscles but a complete loss of dystrophin in cardiac muscle (Muntoni, Cau et al. 1993, Muntoni, Wilson et al. 1995, Bies, Maeda et al. 1997). They show variable age of onset of cardiac impairment, between 10 and 20 year of age (Yoshida, Ikeda et al. 1993) and variable severity of cardiac disease. In the most severe form, patients develop congestive heart failure before their 20s (Muntoni, Cau et al. 1993, Towbin, Hejtmancik et al. 1993). Female patients are characterized by a later age of onset of cardiomyopathy (between 40 and 50 year of age) with slower progression compared to male patients, but which is also fatal (Towbin, Hejtmancik et al. 1993, Cox and Kunkel 1997, Nakamura 2015). Since 1993, several dystrophin mutations have been discovered in patients with XLDCM, but the pathogenesis of this peculiar phenotype is still poorly understood. Tasaki's group proposed to classify XLDCM patients based on their dystrophin mutation. They identified a first group of patients with mutations in the region from the muscle promoter to exon 1, the second group comprised patients with a mutation in the central hot spot region centred around exons 48–49 and patients with mutations in other regions not included in the first and the second group were in the third group. The latter included patients with mutations in exon 9, the region between exons 2-7 and mutations in exon 11 (Tasaki, Yoshida et al. 2001). In 2004, Cohen and Muntoni (Cohen and Muntoni 2004)

divided the *DMD* mutations associated with XLDCM in two groups called A and B. Group A included mutations of the 5' end of the *DMD* gene, and also included mutations of the third group proposed by Tasaki. Thus, group A included mutations in the region from the muscle protomer to part of intron 1, exons 2-7, exon 9 and intron 11. According to their classification, mutations of group A differentially affect the splicing or the promoter usage of dystrophin in skeletal and cardiac muscle. Patients of this group had different levels of dystrophin in skeletal and cardiac muscle, with some patients having no detectable dystrophin in the heart and reduced dystrophin in skeletal muscle. Group B included patients with mutations in exon 29, exon 35 and exons 45-55. Patients with *DMD* mutations in these regions had no major differences in the amounts of dystrophin in their skeletal and cardiac muscles. A patient of group B, with a nonsense mutation in exons 29, showed a severe dystrophin reduction in both skeletal and cardiac muscle. Patients with deletions in the region between exons 45 and 55 showed almost normal levels of truncated dystrophin in the heart and very mild skeletal muscle involvement (**Figure 5 C**). The reason why mutations of group A involve only cardiac muscle is still not clear but in the past years several hypotheses have been formulated. The first hypothesis is that the regulation of the dystrophin gene transcription is different in skeletal and cardiac muscle. In this regard, Muntoni found that deletions involving the region from the muscle promoter and part of intron 1 result in the loss of the muscle dystrophin isoform (Dp427m) accompanied by the overexpression of the Purkinje-cell (Dp427p) and brain isoform (Dp427c) in skeletal but not in cardiac muscle resulting in XLDCM (Muntoni, Melis et al. 1995, Muntoni, Wilson et al. 1995). Moreover, an insertion mutation

of Alu-like sequences in intron 11 in a family with XLDCM results in the expression of both mutant and normal mRNA in skeletal muscle and in the expression of the mutant mRNA only in cardiac muscle (Ferlini, Galié et al. 1998). Another hypothesis is that, in cardiac muscle, the stability and the mechanism of protein binding of dystrophin is different from skeletal muscle. In this regard, Bies reported a 5' mutation associated with the loss of dystrophin and α-dystroglycan in cardiac muscle but not in skeletal muscle in a family affected by XLDCM speculating that this mutation may have caused a cardiac-specific change in dystrophin function (Bies, Maeda et al. 1997). Singh conducted a study on a missense mutation (Lys18Asn) located in the N-terminus of dystrophin found in a patient with XLDCM and no skeletal muscle myopathy (Feng, Yan et al. 2002), reporting that this mutation increases an anomalous folding of dystrophin protein causing protein instability (Singh, Bandi et al. 2014). The third hypothesis relates to the fact that XLDCM patients as well as BMD patients, if unaware of their cardiac condition, perform sport activities inducing mechanical stress on the dystrophin deficient heart (Melacini, Fanin et al. 1996). Myocardial damage caused by physical exercise has also been observed in dystrophin deficient mice (Nakamura, Yoshida et al. 2002). The last hypothesis is that some dystrophin mutations can disrupt dystrophin molecular interaction that occurs only in the heart and not in skeletal muscle. In fact, in the heart, dystrophin associates with proteins that not only are not present in the skeletal muscle DGC but that are also involved in cardiac muscle function and disease (Johnson, Zhang et al. 2012). The exact binding site of dystrophin for these new cardiac-specific proteins is currently unknown but is certainly a hypothesis that must be investigated.
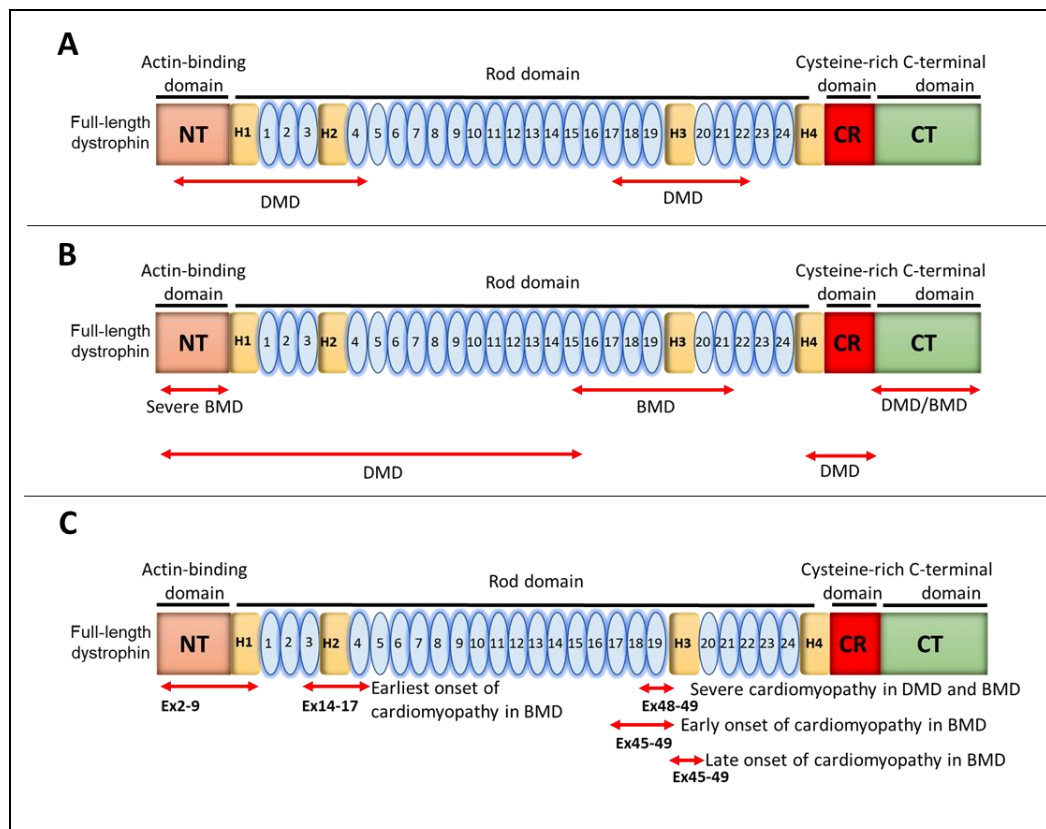
Figure 5. Dystrophin domains affected by out-of-frame and in-frame mutations.

(A and B). Schematic representation of the dystrophin domains mostly affected by out-of-frame mutations (A) and in-frame mutations (B) and the resulting dystrophic phenotypes. C. Mutations affecting different part of the dystrophin gene lead to a various onset of cardiomyopathy in DMD and BMD patients. NT=N-terminus, H= hinge. Numbered light blue oval-shapes= spectrin-like repeats of the rod domain. CR= Cysteine-rich domain. CT= C-terminus

1.3 Cardiac disease in Duchenne and Becker muscular dystrophy patients compared to cardiac impairments in DMD animal models

My PhD thesis aims to characterise a subset of cardiac-specific molecular interactions of dystrophin that, if impaired, could have an effect on cardiac physiology. My research also focuses on micro and mini-dystrophin constructs including one that is currently on a gene therapy clinical trial, that I used as a tool to identify the dystrophin binding domain for the new cardiac-specific molecular partners. Therefore, in the

following sections I will define the aspects of the cardiac disease in DMD and BMD patients and compare them with the cardiac impairments found in DMD mouse models (**1.3.2**) used for the study of the micro and mini-dystrophin constructs. I will also describe the cardiac impairments found in two other DMD animal models (rats **1.3.3** and dogs **1.3.4**) that I used in my research to study dystrophin cardiac molecular interactions.

1.3.1 Clinical manifestation of cardiac disease in Duchenne and Becker muscular dystrophy patients

As mentioned in **1.2.1** and **1.2.2**, both DMD and BMD patients develop cardiac impairment but at different stages of their life. More than 90% of 18-year-old DMD patients show cardiac dysfunction (Kamdar and Garry 2016). Current guidelines recommend the first cardiac evaluation at the time of the diagnosis of DMD, with biannual cardiac screening until 10 years of age, and annual screening after 10 years of age (Bushby, Finkel et al. 2010). This is because the recognition of cardiac disease symptoms can be challenging due to respiratory issues and the physical inactivity of these patients. Moreover, many DMD patients do not show the classic symptoms of heart failure, and this leads to a delay in the correct cardiac evaluation and a delayed pharmacological treatment (McNally, Kaltman et al. 2015). Sixty to 75% of patients with BMD present with cardiac disease and the age of onset varies from 7 years of age to their late twenties (Rajdev and Groh 2015). Most of them have asymptomatic cardiac involvement and show a wide range of cardiac manifestation, from imperceptible signs to severe cardiomyopathy (Srinivasan, Hornyak et al. 2005).

The first signs of cardiac disease that DMD patients show are usually detected by electrocardiographic examinations and are (Thrush, Allen et al. 2009, Santos, Costa Fde et al. 2010, Rajdev and Groh 2015)

•Sinus tachycardia: abnormally elevated heart rhythm (greater than 100 beats/min)

•Short PR interval: the period that elapses between the onsets of atrial depolarization (P wave) and the beginning of ventricular depolarization (QRS complex).

•Decreased S:R wave ratio in the precordial leads with tall R waves, inferolateral Q waves: The R wave refers to the early ventricular depolarisation, the S wave refers to the final depolarisation of the ventricles. An R wave amplitude that is greater than that of the S wave indicates cardiomyopathy.

 •Long QT interval: the QT interval is the time between the ventricular depolarisation and the ventricular repolarisation. An interval longer than 480 milliseconds is considered pathologic.

These electrocardiographic findings are associated with fibrosis of the inferior and inferolateral walls of the left ventricle. From about 14 years old patients often develop supraventricular and ventricular arrhythmias increasing the risk of sudden death (Rajdev and Groh 2015) and left ventricle ejection fraction declines. By 18 years of age, dilated cardiomyopathy with extensive cardiac fibrosis become overt in DMD patients (van Bockel, Lind et al. 2009).

Becker patients present similar electrocardiographic and echocardiographic impairments but with an average age of onset of 27 years.

1.3.2 Cardiac impairments in mdx[23] and mdx[5cv] mouse models

Since 1984 several mouse models for DMD have been characterised, each of them carries different point mutations and similar clinical presentation. For this project, mdx[23] (Bulfield, Siller et al. 1984) and mdx[5cv] mice have been used. The mdx[23] mouse model is the most widely used, it carries a spontaneous nonsense point mutation in exon 23 of the *Dmd* gene (**Figure 6**) that abolishes the expression of full-length dystrophin in skeletal and cardiac muscle (Sicinski, Geng et al. 1989). However, mdx[23] mice show presence of rare revertant myofibres (dystrophin-positive) and revertant cardiomyocytes in skeletal and cardiac muscle respectively, accounting for less than 1% (Hoffman, Morgan et al. 1990, Danko, Chapman et al. 1992, Nicholson 1993). Revertant myofibres or cardiomyocytes contain dystrophin due to the skipping of the mutated dystrophin exon during the transcriptional process restoring the open-reading frame (Lu, Morris et al. 2000). The percentage of revertant fibres in muscle biopsies from Duchenne patients spans from 0.1% to 7% (Fanin, Danieli et al. 1992, Angelini, Fanin et al. 1996). Mdx[23] mice show a peak of skeletal muscle damage such as necrosis and regeneration at about 4 weeks of age that plateaus thereafter (Dangain and Vrbova 1984). Significant severe symptoms of skeletal muscle disease are only visible by 2 years of age with the accumulation of fat and fibrosis and muscle weakness (Pastoret and Sebille 1995). Initially, mdx[23] mouse have normal cardiac function that

later evolves in a dilated cardiomyopathy, and they share many features with DMD patients, although the pathology is less severe. At 8 weeks of age, they have normal echocardiograms and normal ventricular cytosolic function (Quinlan, Hahn et al. 2004). However, when put under cardiac mechanical stress by the administration of the β adrenoceptor agonist isoproterenol, 8 week old mice show sarcolemmal injury and contractile dysfunction (Danialou, Comtois et al. 2001). Between 12 and 17 months of age they develop cardiac fibrosis and moderate changes of echocardiographic and electrocardiographic (ECG) parameters (Quinlan, Hahn et al. 2004). At 21 months of age, the equivalent of 62 year old human (Chamberlain, Metzger et al. 2007, Bostick, Yue et al. 2008) mdx[23] mice have myocardial fibrosis and calcification, abnormal enlargement of the left ventricle and the ECG shows the changes observed in DMD patients such as the reduction of the PR interval, a prolonged QT interval, and deep Q waves. They also show hemodynamic changes such as increases in both end-systolic and end-diastolic volume as a result of reduced contractility and chamber dilation leading to reduced ejection fraction, stroke volume and cardiac output (Bostick, Yue et al. 2008). Lifespan is reduced by 17% in female mice and 19% in male mice (approximately 22.5 months) compared to wild-type and they die of natural causes and not as a direct effect of the loss of dystrophin (Chamberlain, Metzger et al. 2007).

The other dystrophin deficient mice used for my PhD project are the mdx[5cv] mice (Im, Phelps et al. 1996). They carry a mutation in exon 10 of the dystrophin gene (**Figure 6**) that disrupts the expression of full-length dystrophin in both skeletal and cardiac muscle (Im, Phelps et al. 1996, Filareto, Maguire-Nguyen et al. 2018, Wang, Marrosu et al. 2021).

Compared to mdx[23] , mdx[5cv] mice have a 10-fold lower frequency of revertant fibres and cardiomyocytes (Danko, Chapman et al. 1992) making them a more suitable model for studies involving sensitive biochemical techniques such as co-immunoprecipitation using antibodies against the dystrophin protein. They also show a more severe skeletal muscle dysfunction than mdx[23] mice, such as a more severe exercise-induced fatigue (Beastrom, Lu et al. 2011). Mdx[5cv] mice show some of the conduction abnormalities that have been seen in DMD patients such as tall R waves. Shortened PR intervals mean they are also likely to experience accelerated atrioventricular conduction, and they show a mild increased vulnerability to ventricular arrhythmia. In terms of echocardiographic features, by 6 months of age mdx[5cv] mice exhibit cardiac fibrosis and cardiomyocyte hypertrophy (Wang, Marrosu et al. 2021). Mdx[23] and mdx[5cv] mice have a less severe cardiac phenotype and a slower progression of the cardiac disease. than DMD patients. Despite these differences, they represent a good model to study DMD cardiomyopathy as they recapitulate the majority of the cardiac impairment observed in DMD patients, they share the same genetic defect as DMD patients, and in addition they are easy to handle and readily available.

1.3.3 Rat model of DMD

The DMD rat model (DMD[mdx] rat) was generated in 2014 by Larcher and colleagues using transcription activator-like effector nucleases (TALEN) targeting exon 23 of the dystrophin gene (Larcher, Lafoux et al. 2014) (**Figure 6**). These rats do not express full-length dystrophin in either skeletal or cardiac muscle. They exhibit muscle fibre necrosis and interstitial fibrosis in skeletal muscle that results in decreased muscle

force and reduced locomotor activity (Larcher, Lafoux et al. 2014). Very recently, Szabo and colleagues (Szabo, Ebner et al. 2021) characterized the cardiovascular phenotype of the DMD[mdx] rat finding several similarities between their cardiac dysfunction and those observed in DMD patients. DMD[mdx] rats show a reduction in the ejection fraction by 3 months of age, and lower left ventricular pressure, dP/dtmax and dP/dtmin (that are the maximum and minimum rates of ventricular pressure development; they also develop contractile dysfunction (reduced ejection fraction) and progressive dilatation. Moreover, between 7 and 9 months of age they show left ventricular dilatation, cardiac inflammation, and fibrosis (Szabo, Ebner et al. 2021). The cardiovascular phenotype of DMD[mdx] rats is more severe and develops quickly (by 3 month of age) compared to the mouse models that develop dilated cardiomyopathy at 21 months of age, making the DMD[mdx] rats a suitable animal model for the study of cardiomyopathy in DMD.

1.3.4 Dog models of DMD

The golden retriever muscular dystrophy dog (GRMD) is the most studied DMD canine model for cardiomyopathy; it carries a naturally occurring splice site mutation in intron 6 of the dystrophin gene causing the loss of full-length dystrophin in both skeletal and cardiac muscle (Sharp, Kornegay et al. 1992). It shows electrocardiogram abnormalities similar to DMD patients such as sinus tachycardia, shortened PR interval, prolonged QT interval, reduction of the Q/R ratio (Fine, Shin et al. 2011). Echocardiographic findings in these dogs are remarkably like the ones found in DMD boys including myocardial fibrosis, left ventricle systolic and diastolic disfunction, and the enlargement of the left ventricle chamber, which are all symptoms of a progressive cardiomyopathy. In

this thesis I used cardiac sections from a different DMD dog model: the deltaE50-MD dog. The deltaE50-MD dog carries a mutation in exon 50 (**Figure 6**) that was initially found as a spontaneous mutation in Cavalier King Charles spaniels (Walmsley, Arechavala-Gomeza et al. 2010) and is now maintained on a beagle background (Amoasii, Hildyard et al. 2018). The advantage to choose the deltaE50-MD dog over the GRMD is mostly due to their smaller size, making them easier to handle and less expensive to maintain. The cardiac evaluation of the deltaE50-MD dogs is ongoing at the Royal Veterinary College by Professor Richard Piercy's group, and the data generated in my thesis will be added to their work.
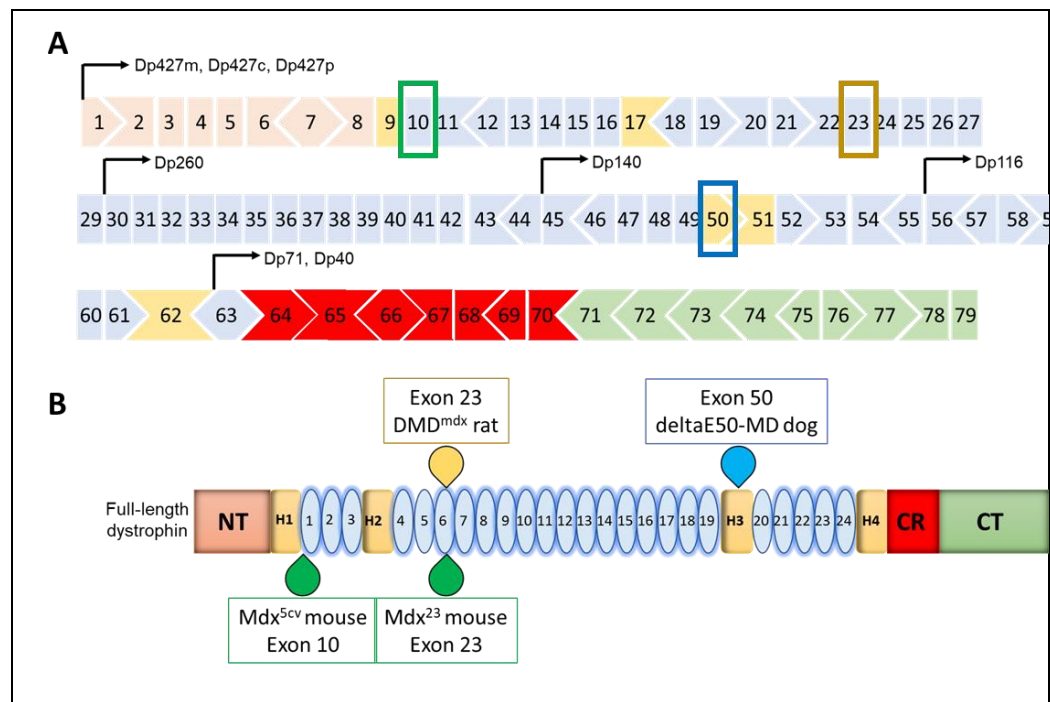
Figure 6. Dystrophin mutations affecting the DMD animal models used for my PhD thesis.

***A.** Dystrophin exons affected by the different mutations in DMD mouse, dog, and rat models with the corresponding affected protein domains (**B**).*

1.4 Pharmacological cardiac therapies and AAV gene therapy

1.4.1 Pharmacological therapies for dilated cardiomyopathy

The available pharmacological therapies intend to control symptoms, delay the onset of dilated cardiomyopathy and improve the quality of life. One of the therapeutic strategies used to prevent early symptoms of dilated cardiomyopathy in DMD children is the use of perindopril. Perindopril is an angiotensin-converting enzyme inhibitor (ACEi) and its efficacy have been tested in a 5 year multicentre study involving 57 children, showing its efficacy in preventing DCM in terms of reducing left ventricle dysfunction (Duboc, Meune et al. 2005).

The combined used of ACEi (perindopril) and eplerenone have been also found to have a cardioprotective effects in a placebo-controlled trial (Raman, Hor et al. 2015). Eplerenone is an aldosterone antagonist type of potassium-sparing diuretic, used to reduce fluid around the heart and decrease blood pressure, which is elevated in patients with DMD. ACEi are widely used in clinical practice for DMD compared to eplerenone that is less available and more expensive (Birnkrant, Bushby et al. 2018, Raman, Hor et al. 2019).

Another drug that is routinely used for heart failure treatment in adults are β-blockers, that are used to specifically decrease the heart rate and reduce cardiac stress. In children, the effectiveness of β-blockers has been tested in several studies, in particular the use of β-blockers in combination with ACEi showed 5 years increased survival rate in DMD patients with heart failure, particularly in asymptomatic patients with ventricular dysfunction (Ogata, Ishikawa et al. 2009). In another two

studies, the beneficial effects of β-blockers were not seen (Saito, Matsumura et al. 2001, Viollet, Thrush et al. 2012) and these conflicting results contributed to their delayed initiation in DMD patients (Adorisio, Mencarelli et al. 2020). Currently, the followed treatment strategies for DCM in Duchenne and Becker patients are in line with the ones used to treat heart failure endorsed by the 2018 DMD Care Considerations (Birnkrant, Bushby et al. 2018). None of the pharmacological treatments used are able to prevent dilated cardiomyopathy: they only delay the onset of the disease.

1.4.2 Rationale for AAV gene therapy constructs

Adeno-associated virus (AAV) gene therapy is a promising approach to treat DMD, aiming to deliver a cDNA coding for a functional dystrophin. The chosen vehicle to deliver a functional dystrophin cDNA in skeletal and cardiac muscle is the AAV vector. AAV is a 25 nm virus from the Parvoviridae family and its genome consists of a linear single-stranded DNA of 4.7 kilo-bases (Naso, Tomkowicz et al. 2017). The advantages of using AAV vectors include their capacity to infect dividing and non-dividing cells allowing the infection of a wide range of cell types (Podsakoff, Wong et al. 1994) and low rates of off-target genomic integration that could lead to tumorigenesis (Chandler, Sands et al. 2017). Depending on the chosen serotype, AAV can be delivered via the vascular system for body wide gene delivery and they are not pathogenic (Balakrishnan and Jayandharan 2014). Moreover, depending on their serotype, AAV vectors can transduce different types of tissues (Podsakoff, Wong et al. 1994). One of the limitations in the use of AAV vectors to deliver a functional dystrophin gene is their packaging capacity. In fact, AAV vectors can accommodate a maximum 5 kb

(Srivastava, Lusby et al. 1983) and at 14 kb the size of dystrophin cDNA exceeds this capacity. (Naso, Tomkowicz et al. 2017). This limitation is addressed by designing a shorter dystrophin gene that can fit in an AAV vector and that carries the dystrophin domains needed for skeletal and cardiac muscle function. This idea of creating a shorter but functional dystrophin came from a discovery made by England and colleagues in 1990 (England, Nicholson et al. 1990), who found a family in which one member showed a very mild BMD (still ambulant at the age of 61) despite having a deletion in the central part of the dystrophin gene leading to a half-sized dystrophin protein, called Δ17–48 mini-dystrophin. This discovery showed that parts of the dystrophin protein can be omitted with minimal impact on its function. The therapeutic potential of the mini-dystrophin genes was subsequentially confirmed by several genotype-phenotype correlation studies that will be described in the next paragraphs (Harper, Hauser et al. 2002, Li, Kimura et al. 2006, Lai, Thomas et al. 2009, Wasala, Shin et al. 2018).

1.4.3 Genotype phenotype correlation of cardiomyopathy in Becker muscular dystrophy patients

Since the packaging capacity of AAV vectors is 5 kb (Srivastava, Lusby et al. 1983) and the size of dystrophin cDNA is 14 kb (Naso, Tomkowicz et al. 2017), the choice of the dystrophin exons to be included in gene therapy constructs is crucial as they must be functional for both skeletal and cardiac muscle. The genotype-phenotype correlation studies are a very useful tool for the design of the micro and mini-dystrophin constructs. The micro-dystrophin constructs are about 4 kb while the mini-dystrophin constructs are 6 kb length. Therefore, they cannot be packed into an AAV vector. Recently Zhou and colleagues performed a

meta-analysis of 18 studies performed in 9 countries on crucial genotype parameters of cardiomyopathy in BMD, finding that mutations affecting exons 45 and 46 are highly associated with cardiac dysfunction in these patients (Zhou, Fu et al. 2021). Exons 45 and 46 encode for repeats 17 and 18. Studies in dystrophin-null mdx mice expressing a mini-dystrophin lacking the region from exon 45 to exon 49 but with an intact Hinge 3 showed a complete rescue of skeletal muscle pathology but only a partial improvement of cardiac function, suggesting that this dystrophin region is particularly important for cardiac function and not for skeletal muscle function (Bostick, Yue et al. 2009). Another study published by Montanaro and colleagues analysed the impact of this mutation (exons 45 to 49) on the dystrophin protein structure (Kaspar, Allen et al. 2009). They found that different combinations of exon deletion can preserve or disrupt the known spectrin-like repeat pattern (Cross, Stewart et al. 1990) that, when disrupted, is associated with an earlier onset of dilated cardiomyopathy. This is because the physical boundaries of each spectrin-like repeat do not correlate with the exon boundaries. They found that BMD patients with mutation in the rod domain that disrupt the spectrin-like repeat pattern as well as patients with deletion in the N-terminal actin binding domain develop cardiomyopathy at an early age (Kaspar, Allen et al. 2009). Another study performed by Tandon and colleagues on 247 DMD and BMD patients found the association between the presence of the C-terminus with a milder cardiac phenotype (Tandon, Jefferies et al. 2015) but there seems to be no correlation with skeletal muscle pathology (Crawford, Faulkner et al. 2000). The exact correlation between specific mutations and the onset and severity of cardiomyopathy is still unclear, but an understanding of this is crucial in

order to design a micro-dystrophin construct that includes dystrophin domains that are effective in both skeletal and cardiac muscle.

1.4.4 Optimization of micro-dystrophin construct design for functional rescue of skeletal and cardiac muscle

So far, around 40 micro-dystrophin constructs have been tested in animal models but the cardiac rescue potential of the micro-dystrophin constructs have been assessed only in few studies and mostly with the ΔR4-R23/ΔCT micro-dystrophin (Yue, Li et al. 2003, Gregorevic, Allen et al. 2006, Townsend, Blankinship et al. 2007, Bostick, Yue et al. 2008, Bostick, Shin et al. 2011, Shin, Nitahara-Kasahara et al. 2011, Bostick, Shin et al. 2012, Wang, Marrosu et al. 2021).

Currently three AAV gene therapy constructs (**Figure 7**) have been utilised for clinical trial from Pfizer (https://clinicaltrials.gov/ct2/show/NCT04281485), Sarepta (https://www.clinicaltrials.gov/ct2/show/NCT03375164) and Solid Biosciences (https://www.clinicaltrials.gov/ct2/show/NCT03368742).

All three constructs are under the control of a muscle specific promoter to avoid off target expression of the constructs in non-muscle tissue.

The construct from Pfizer is driven by the muscle creatine kinase (MCK) promoter (Wang, Li et al. 2008). The Pfizer clinical trial was paused in September 2021 for three serious adverse events that led them to change the patient inclusion criteria.

Sarepta's construct is driven by the murine muscle creatine kinase (CK) and the cardiac enhancer α-myosin heavy-chain genes (MHCK7 promoter) (Salva, Himeda et al. 2007).

Solid Bioscience chose the CK8 promoter that is the MHCK7promoter with two copies of the MCK enhancer instead of the α-myosin heavy-chain enhancer (Hakim, Wasala et al. 2017).

It was decided to insert the N-terminus that is essential for the binding with the actin cytoskeleton (Norwood, Sutherland-Smith et al. 2000) in all of them. As mentioned in **1.4.3**, the presence of the N-terminal is also important for cardiac function and studies in the skeletal muscle of transgenic mice expressing micro-dystrophin constructs lacking the N-terminus showed myofiber degeneration and the inability of these to correctly localise at the skeletal muscle fibres (Banks, Gregorevic et al. 2007). Hinge 1 and the first repeats were inserted in all the constructs in order to avoid misfolding of the N-terminus (Acsadi, Moore et al. 2012). Moreover, spectrin-like repeats 1-3 were shown to be important for dystrophin interaction with the sarcolemma in a study that compared the membrane localisation of constructs including different spectrin-like repeats expressed in dystrophin-null mdx[23] mice skeletal muscle (Zhao, Kodippili et al. 2016). The construct used for Sarepta's clinical trials also includes hinge 2 but this may not be the best choice, as hinge 2 contains a polyproline site that in the mdx[23] mouse influenced the functional capacity of micro-dystrophin (Banks, Judge et al. 2010). In particular, Banks and colleagues found that the insertion of hinge 2 in this micro-dystrophin construct reduces myofiber size, alters the normal structure of both muscle tendentious and neuromuscular junctions and also contributes to the formation of abnormal ring-shaped myofibers. In their mouse study they tested another construct that did not carry hinge 2 but instead carried hinge 3 that improved these impaired parameters (Banks, Judge et al. 2010). In support of these data, a study from 2002 with

mdx[23] mice expressing two similar constructs, one with hinge 3 and the other without hinge 3, revealed the amelioration of the muscle pathology and muscle force in mice expressing the construct with hinge 3 (Harper, Hauser et al. 2002). The discussion on the insertion of the central hinges in the micro-dystrophin construct is still ongoing and is quite controversial. In fact, Harper and colleagues (Harper, Hauser et al. 2002) compared transgenic mdx[23] mice expressing a micro-dystrophin construct without hinge 2 and hinge 3 with mdx[23] mice expressing another micro-dystrophin construct with hinge 3, finding that the removal of hinge 3 resulted in an efficient restoration of the histological and functional parameters (less fibre degeneration and higher force). Another study, this time on DMD and BMD patients, revealed that mutations causing the loss of hinge 3 lead to a significantly milder disease progression (Carsana, Frisso et al. 2005).

Moving further, the construct used for the Solid Biosciences clinical trials carries the spectrine-like repeats 16 and 17 that have been shown to be involved in the interaction of dystrophin with nNOS in skeletal muscle. Studies in mouse and dog models for DMD expressing micro-dystrophin constructs carrying these repeats show improved skeletal muscle pathology (Lai, Thomas et al. 2009, Shin, Pan et al. 2013, Hakim, Wasala et al. 2017).

All the clinical trial constructs carry the cysteine-rich domain that is essential for the interaction between dystrophin and the sarcolemma in both skeletal and cardiac muscle (Bies, Caskey et al. 1992, Anderson, Rogers et al. 1996, Ayalon, Davis et al. 2008). None of the clinical trial constructs carry the C-terminal domain, and this decision was made based on a study that Crawford and colleagues (Crawford, Faulkner et

al. 2000) made on mdx[23] mice expressing a C-terminus truncated dystrophin construct. They found that muscle histology and the muscle force of these transgenic mice was identical to wild-type mice, suggesting that the C-terminus was not crucial for skeletal muscle function. However, as mentioned in **1.4.3**, the C-terminus might be important for the cardiac muscle function (Tandon, Jefferies et al. 2015). Moreover, studies in mice and DMD patients suggest that the C-terminus could be also important to preserve cognitive function (Daoud, Candelario-Martínez et al. 2008, Ricotti, Mandy et al. 2016).

Taken together, these studies show how challenging it is to find the best micro-dystrophin design that includes all the domains that are important for both skeletal and cardiac muscle function (Harper, Hauser et al. 2002, Yue, Li et al. 2003, Bostick, Shin et al. 2011, Shin, Nitahara-Kasahara et al. 2011). The results from these three clinical trials will give new knowledge about their therapeutical capacity in humans. Unfortunately, of all these clinical trial constructs, only the one from Sarepta, ΔR4-R23/ΔCT micro-dystrophin, has been studied for its ability to rescue both skeletal and cardiac muscle impairments in mdx[23] mice (Yue, Li et al. 2003, Gregorevic, Allen et al. 2006, Townsend, Blankinship et al. 2007, Bostick, Yue et al. 2008, Bostick, Shin et al. 2011, Bostick, Shin et al. 2012).
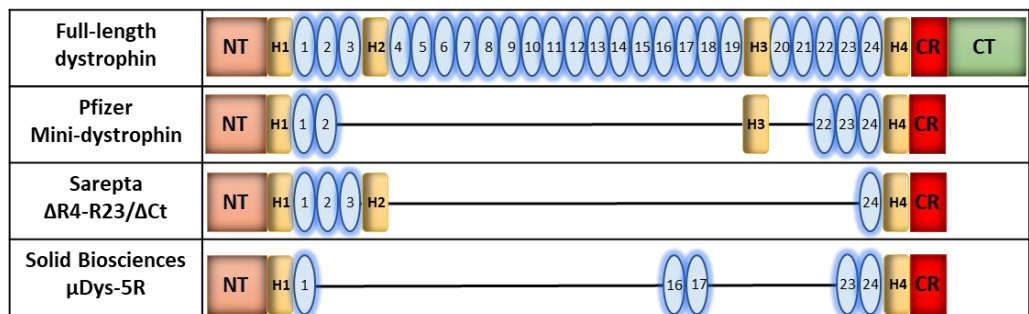
Figure 7. AAV gene therapy constructs currently on clinical trial.

*Graphic representation of the of the proteins encoded by the Pfizer, Sarepta and Solid Bioscience micro-dystrophin constructs currently in clinical trial. N-terminus (**NT**), hinges (**H1**, **H2**, **H3**, **H4**), Cysteine-rich domain (**CR**), C-terminus (**CT**), spectrin-like repeats (light blue numbered ovals).*

1.5 Dystrophin expression and its molecular association in the heart

My PhD thesis focuses on the cardiac aspect of DMD, therefore, in the next sections I will go through what is known about dystrophin in the heart according to the literature.

1.5.1 Cardiac sub-cellular distribution of dystrophin

The sub-cellular distribution of dystrophin in cardiac muscle is not identical to skeletal myocytes. Full-length dystrophin is localised at the sarcolemma in both cardiomyocytes (Stevenson, Rothery et al. 1997, Stevenson, Cullen et al. 2005) and skeletal muscle fibres (Torelli, Ferlini et al. 1999). However, only in cardiac muscle full-length dystrophin and the shorter dystrophin isoform Dp71 are found at the t-tubules (Klietsch, Ervasti et al. 1993, Fabbrizio, Nudel et al. 1994, Masubuchi, Shidoh et al. 2013). The t-tubules are invagination of the membrane where ion channels are highly expressed. In fact, the majority of the calcium influx

triggering the release of intracellular calcium enters across the t-tubular fraction (Scriven, Dan et al. 2000). T-tubules are crucial for the excitation–contraction coupling (the process whereby an action potential triggers a myocyte to contract, followed by subsequent relaxation) (Orchard, Pásek et al. 2009) suggesting that dystrophin in the heart plays additional roles compared to skeletal muscle. Dystrophin is also expressed at the intercalated discs (Anastasi, Cutroneo et al. 2009, Di Mauro, Gaeta et al. 2009) that connect adjacent cardiomyocytes to each other allowing the cell-to-cell propagation of action potentials. The sub-cellular distribution of dystrophin is not the only difference between cardiac and skeletal muscle.

1.5.2 Cardiac dystrophin new binding partners

In **1.4.4** the lack of correlation between skeletal and cardiac muscle disease in patients with BMD has been described. This raises questions on the cause of the different effect that mutation of the dystrophin gene can have on skeletal and cardiac muscle disease. One of the reasons why this happens may lie in the possibility that in the heart, dystrophin associates with different or additional proteins that are not present in the skeletal muscle dystrophin protein complex. In this regard Montanaro and colleagues performed proteomic analysis to compare the dystrophin interactome of skeletal and cardiac muscle (Johnson, Zhang et al. 2012). They found that dystrophin in the heart establishes associations with proteins that are not present in skeletal muscle DGC. In the heart, dystrophin associates with β2-syntrophin and α3-dystrobrevin, and four proteins that are important for cardiac function: ahnak1, cypher, αB-crystallin, and cavin-1. Mutations affecting ahnak1, cypher, αB-crystallin, and cavin-1 are associated with arrhythmias, long QT syndrome and

contractile dysfunction (Vatta, Mohapatra et al. 2003, Haase, Alvarez et al. 2005, Rajab, Straub et al. 2010, Shastry, Delgado et al. 2010, Sacconi, Féasson et al. 2012, Mahmoodzadeh, Koch et al. 2021) also observed in DMD and BMD patients (Chenard, Becane et al. 1993, Ashford, Liu et al. 2005, Khan, Almashham et al. 2013). This discovery suggests a direct relation between dystrophin and cardiac function. In fact, Johnson and colleagues also found that ahnak1 and cavin-1 were present in dystrophin immunoprecipitations of human cardiac biopsies. Ahank1 and cavin-1 were absent from the immunoprecipitations of mdx^{5cv} hearts performed using β-dystroglycan that instead was preserved at the cardiomyocyte membrane of mdx^{5cv} mice (Johnson, Zhang et al. 2012). During my PhD thesis I have explored more in-depth the link between cavin-1 and dystrophin as well as the link between dystrophin and other cavin family members - cavin-2 and -4. Cavin-1, -2 and -4 are all key protein components of membrane structures called caveolae (Rothberg, Heuser et al. 1992) that are in crucial for cardiac function and disease

1. 6 Cardiac dystrophin association with caveolar proteins

In **1.1.2** proteins that comprise the dystrophin glycoprotein complex have been described, but the study of the dystrophin interactome is ever-changing. New dystrophin binding partners in skeletal and cardiac muscle have been discovered in the last decade (**1.5.2**). Since my PhD focuses on the cardiac aspect of DMD and the molecular interactions that are disrupted due to dystrophin loss in the heart specifically, the following **1.6.1** aims to address the new findings in terms of cardiac dystrophin protein binding partners that could be involved in the DMD patient's cardiac impairments.

1.6.1 Caveolae and caveolar proteins

Caveolae are 50-100nm omega-shaped invaginations of the plasma membrane present in the cells of wide variety of tissues. Before 1992 caveolae were only described for their morphology until the discovery of a marker that allowed scientists to separate caveolae from other lipid-rafts, a protein that was named caveolin (Rothberg, Heuser et al. 1992). This finding led to the discovery that caveolins are 3 distinct proteins called caveolin-1 (CAV1), caveolin-2 (CAV2) and caveolin-3 (CAV3). Caveolin-1 and caveolin-2 are both expressed in different cell types including endothelial cells and fibroblasts (Schubert, Frank et al. 2001, Wheaton, Sampsel et al. 2001) while caveolin-3 is the only caveolin that is muscle-specific and is component of the sarcolemma found to co-precipitate with dystrophin and the DGC (Tang, Scherer et al. 1996). Caveolin-1 and -3 are both expressed in cardiac cells (Song, Scherer et al. 1996, Cho, Chow et al. 2010). Caveolins are synthesised in the endoplasmic reticulum and via their three C-terminal palmitoylation site are rapidly transported to the Golgi complex (Parat, Stachowicz et al. 2002), then transported to the plasma membrane in vesicular carriers where they meet other caveolar proteins called cavins (Hayer, Stoeber et al. 2010) (**Figure 8**). Cavin-1, -2 and -3 are expressed in a wide variety of cells such as endothelial cells (Hansen, Shvets et al. 2013) while cavin-4 is expressed exclusively in smooth (Ogata, Ueyama et al. 2008) and striated muscles (Tagawa, Ueyama et al. 2008). Cavins are characterised by 2 basic (coiled-coil) helical regions (HR) flanked by acidic disordered regions (DR) (**Figure 8**). The first helical region (HR1) is responsible for the formation of the trimers, consisting in 2 molecules of cavin-1 associated with one molecule of cavin-2 or cavin-3, but cavin-2

and cavin-3 do not associate with each other (Gambin, Ariotti et al. 2013, Ludwig, Howard et al. 2013, Kovtun, Tillu et al. 2014). Cavins interact with the membrane phospholipids with their two helical regions (Kovtun, Tillu et al. 2014) and are not interchangeable proteins: cavin-1 plays a crucial role in the biogenesis of caveolae, and cavin-1 knock-out animal models have a complete loss of caveolae in all tissues (Hill, Bastiani et al. 2008, Liu, Brown et al. 2008, Taniguchi, Maruyama et al. 2016). Cavin-4 also associates with caveolae by binding cavin-1 and is not essential for caveolar formation but plays a role in caveolar morphology in cardiomyocytes (Ogata, Naito et al. 2014). Moreover, when the heart is under stress cavin-4 plays an important role in mediating cardio-protective signalling via the α1-adrenergic receptors, recruiting the extracellular signal-regulated kinase 1/2 (ERK) to caveolae where it can be phosphorylated following activation of α1-adrenergic receptors by catecholamines. Then cavin-4 and the phosphorylated ERK translocate to the nucleus to allow gene activation for preventing cardiomyocyte apoptosis and activating adaptive cardiomyocyte hypertrophy to preserve contractile strength (Ogata, Naito et al. 2014). Cardiac caveolae and the proteins related to them play important roles such as cardiac protection from mechanical stress (Patel, Tsutsumi et al. 2007, Cheng, Mendoza-Topaz et al. 2015). They are involved in calcium signalling (Balijepalli, Foell et al. 2006), cardiac conduction (Tyan, Turner et al. 2021), and cardiac contraction (Grivas, González-Rajal et al. 2020).
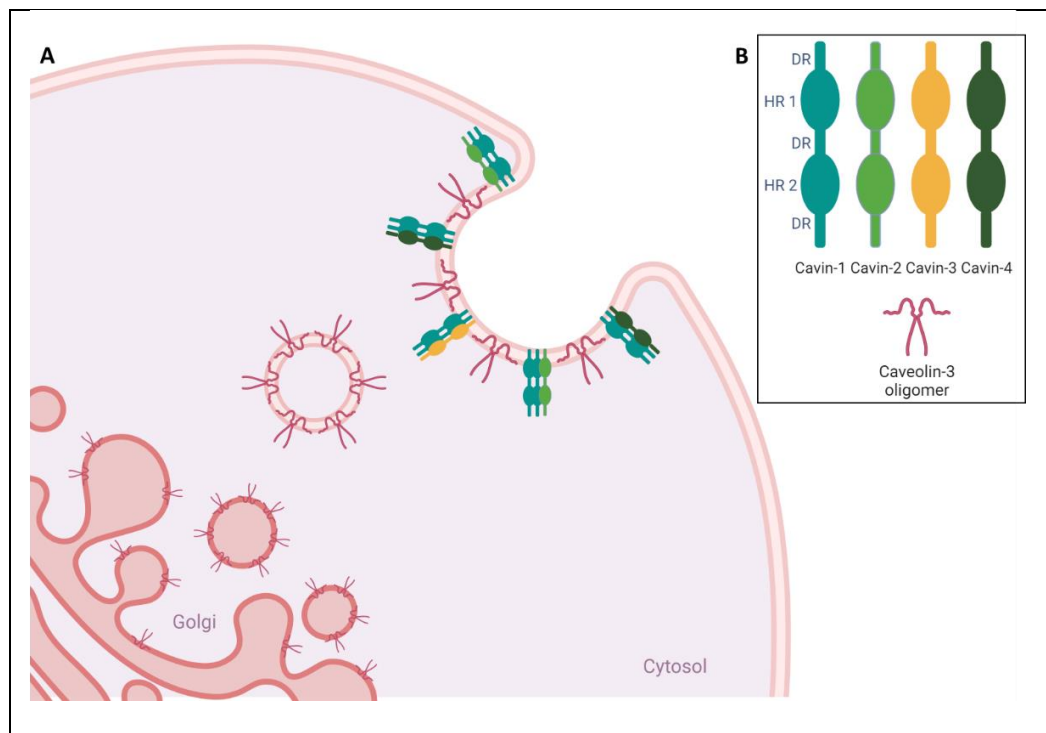
Figure 8. Schematic representation of the formation of a muscle caveola.

A. *After being synthesised in the endoplasmic reticulum, caveolins are transported to the Golgi apparatus and then transferred to the plasma membrane.* ***B.*** *Schematic representation of cavin-1, -2, -3 and -4 with their 2 helical regions (HR1 and HR2) and the disordered regions (DR). Caveolin-3 oligomer. As the real number of cavin-4 involved in each trimer is not known, this diagram is meant only to be a schematic representation of cavin trimer formation.*

1.6.3 Caveolar proteins and cardiac disease

Several studies found that mutation in the genes encoding for cavin-1 and cavin-4 are associated with cardiac disease. Specifically, studies in mice link the deficiency of cavin-1 with a cardiomyopathic phenotype, with cardiomyocyte hypertrophy, cardiac fibrosis, and electrocardiographic abnormalities (Taniguchi, Maruyama et al. 2016). Moreover, the loss-of-function mutation of cavin-1 in human patients causes congenital generalized lipodystrophy type 4 and some of these patients show cardiac impairments such as long-QT syndrome and fatal

cardiac arrhythmia (Rajab, Straub et al. 2010). Molecular genetic studies on human patients (Nouhravesh, Ahlberg et al. 2016) as well as *in vitro* studies (Rodriguez, Ueyama et al. 2011) found an association between loss-of-function cavin-4 mutations and dilated cardiomyopathy.

1.7 Research Hypothesis and Aims

The molecular principles behind DCM associated with DMD mutations are poorly understood and current cardiac therapies show limited efficiency due to their lack of specificity. This project arose from the findings that dystrophin associates with cavin-1 in the heart, suggesting the existence of cardiac-specific functions of dystrophin that are currently undefined, and also reinforced from the evidence that cavin-1 mutations cause cardiac disease. My hypothesis is that the association of dystrophin and cavin-1 is critical for optimal cardiac function and that dystrophin mutations that disrupt the binding site of dystrophin for cavin-1 lead to the loss of proper cavin-1 expression and localisation in the heart of patients with DMD and BMD. As mentioned in **1.6.1** cavin-1 is part of a complex that includes also other proteins such as cavin-2, -3, -4 and caveolins. Cavin-4 has also been shown to be causative in DCM. Therefore, characterising the effect of the loss of dystrophin on caveolar proteins will be beneficial for understanding mechanisms of cardiac disease in DMD and BMD patients. Further to this, my thesis aimed to narrow down the number of potential dystrophin domains known to be critical in the binding of caveolar proteins. This knowledge will be fundamental in guiding the design of the next generation of gene therapy constructs.

To test this hypothesis, I proposed the following aims. To:

- Investigate the effect of loss dystrophin on caveolar proteins in Duchenne mouse models (mdx[23] and mdx[5cv]), and also in rats and dogs Duchenne animal models that showed several cardiac disease similarities with DMD and BMD patients.

- Test different micro and mini-dystrophin constructs for their capacity to bind with caveolar proteins and also use them as a tool to narrow down the dystrophin domains involved in the binding with caveolar proteins.

Combine the data collected from the studies of caveolar protein localisation in wild-type animal models with the ones collected from human heart to understand which animal model best mirrors the human caveolar proteins localisation.

Chapter 2. Materials and methods

2.1 Animal work

For my PhD thesis, multiple mouse strains and animal models have been used. Described below is the establishment of the mdx^{5cv} and the ΔR4-R23/ΔCT micro-dystrophin mouse colonies. For these live mice, breeding and experimental procedures were carried out at the UCL Biological Service Unit in accordance with the Animals (Scientific Procedures) Act 1986. For other transgenic mice and DMD animal models, we received and processed post-mortem cardiac samples from our collaborators. These animals were maintained by our collaborators at their institutions under their animal licenses following country-specific guidelines.

2.1.1 Establishment of the mdx^{5cv} mouse colony

Cryopreserved embryos of B6Ros.Cg-Dmdmdx-5Cv/J (Stock No: 002379) were obtained from the Jackson Laboratories and the colony was established by UCL Biological Services. Female embryos were heterozygous for the DMD$^{mdx-5cv}$ mutation (**1.3.2**), and all male embryos were wild-type. After the first generation was born and genotyped (**2.2**), wild-type males were crossed with heterozygous females. From this second generation, males carrying the DMD$^{mdx-5cv}$ mutation were identified by genotyping and bred with heterozygous females for the DMD$^{mdx-5cv}$ mutation in order to generate homozygous DMD$^{mdx-5cv}$ females to establish the mdx^{5cv} colony. Wild-type males and females generated during the mdx^{5cv} colony establishment were kept and bred to be used as a control strain-matched line.

2.1.2 ΔR4-R23/ΔCT micro-dystrophin mice

The ΔR4-R23/ΔCT micro-dystrophin mice used for this project were generated in the transgenic core facility of the University of Missouri. Very briefly, the sequence of the ΔR4-R23/ΔCT micro-dystrophin construct was inserted in a multi-cloning vector between the α-myosin heavy chain promoter and the bovine growth hormone polyadenylation signal. Transgenic mice were created via fertilized egg pronuclear injection, embryo culture and transplantation into FVB mice (University of Missouri Transgenic Core). The micro-dystrophin transgene was transferred onto the mdx^{5cv} background by crossing transgenic males with mdx^{5cv} female mice for 6 generations. The choice of transferring the transgene onto the mdx^{5cv} (**1.3.2**) background was made for the purpose of studies involving a high sensitivity method such as the proteomic based on the evidence that mdx^{5cv} mice have a 10-fold lower frequency of revertant fibres compared to wild-type mice (Danko, Chapman et al. 1992). Cardiac samples from the mdx^{5cv} ΔR4-R23/ΔCT micro-dystrophin mice (mdx^{5cv}-μDys) were transported on dry ice to the Great Ormond Street Institute of Child Health and kept at -80°C. A live colony of mdx^{5cv}-μDys mice was then established *de novo* at UCL (see section 2.1.3 below)

2.1.3 Generation of ΔR4-R23/ΔCT micro-dystrophin mouse colony

B10.Cg-Dmdmdx Tg(Myh6-DMD*)47Dua/Mmjax cryopreserved sperm was purchased from the Jackson Laboratories and an *in vitro* fertilization procedure was performed on C57BL/6 females by UCL Biological Services. The cryopreserved sperm is from an mdx^{5cv} mouse carrying the ΔR4-R23/ΔCT micro-dystrophin construct driven by the α-myosin heavy chain promoter. From the first generation, males positive for the

ΔR4-R23/ΔCT transgene were selected by genotyping (**2.2.1**) and crossed with mdx[5cv] female mice and vice versa.

2.1.4 Other transgenic mice

Other transgenic mice used in this project for immunohistochemical analysis, were kindly provided by Dr. Dongsheng Duan's research group at the University of Missouri School of Medicine. Each of these mice carry 4 different micro and mini-dystrophin constructs (**Figure 9**), the ΔR4-R23 micro-dystrophin (Harper, Crawford et al. 2002), the ΔH2-R19/ΔCT mini-dystrophin (Li, Kimura et al. 2006), ΔH2-R19 mini-dystrophin (Li, Kimura et al. 2006) and the ΔH2-R15 mini-dystrophin (Lai, Thomas et al. 2009, Wasala, Shin et al. 2018). The ΔR4-R23 micro-dystrophin, the ΔH2-R19 and the ΔH2-R19/ΔCT mini-dystrophins are expressed on mdx[23] mice that are on C57BL/10 background (**4.3**). The ΔH2-R15 mini-dystrophin is expressed on mdx[23] mice that are on a FVB background. All of these constructs are described in detail in sections **4.3**.
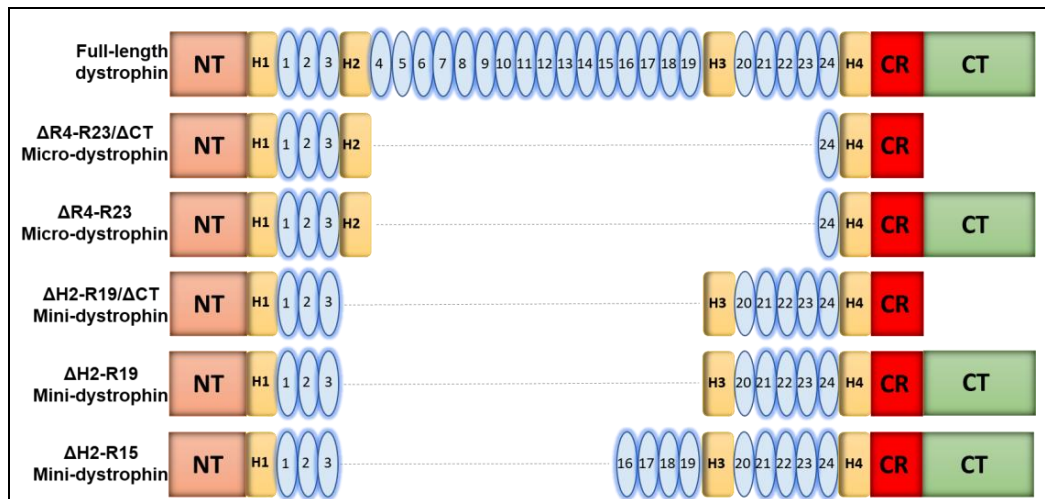
Figure 9. Schematic representation of the micro and mini-dystrophin constructs used for this project.

*Orange boxes represent the N-terminus, yellow boxes are hinges (**H1**, **H2**, **H3**, **H4**), the red boxes represent the cysteine-rich domain (**CR**), C-terminus represented by the green boxes (**CT**), spectrin-like repeats (light blue numbered ovals). These constructs contain the N-terminus, hinge 1 and the first 3 spectrin-like repeats. Hinge 2 is included only in the ΔR4-R23/ΔCT and the ΔR4-R23 constructs but they do not contain Hinge 3. All the constructs include hinge 4, the cysteine-rich domain and only the ΔR4-R23/ ΔCT and the ΔH2-R19/ΔCT do not have the C-terminus. The ΔH2-R15 also contains spectrin-like repeats 16-19.*

2.1.5 Cardiac samples from different DMD animal models

The wild-type and DMD[mdx] rat cardiac tissues used for the immunohistochemical experiments in chapter 5 were provided by Dr. Caroline Le Guiner from the University of Nantes, and they were all obtained from 7-month-old rats. DMD[mdx] rats carry an out-of-frame mutation in exon 23 of the dystrophin gene (Larcher, Lafoux et al. 2014, Szabo, Ebner et al. 2021). The samples were shipped on dry ice and once arrived were mounted with OCT before being sectioned with an OTF5000 Cryostat (Bright Instruments) for immunofluorescence experiments (**2.4.2**). The 3 month-old wild-type and the ΔE50-MD dog cardiac tissue samples were provided by Professor Richard Piercy and Dr John Hildyard from the Royal Veterinary College and were used to generate the data presented in **6.2**. The ΔE50-MD dogs carry a mutation in exon 50 and are described in detail in **1.3.4.** Dr John Hildyard prepared the sections of cardiac tissue from both wild-type and ΔE50-MD dogs and I performed the immunostaining.

2.1.6 Human cardiac samples

The human cardiac samples used for the immunohistochemistry experiments in chapter 5 were collected by a colleague from a pediatric patient affected by Tetralogy of Fallot (Gualandi, Trabanelli et al.) during corrective surgery. Tetralogy of Fallot is a combination of four congenital abnormalities (ventricular septal defect, pulmonary valve stenosis, an overriding aorta and a thickened right ventricular wall). These patients do not show any dystrophin defect in the heart. Therefore, I have used them to visualize the cardiomyocyte localization of caveolar proteins and to investigate any differences between human and animal models.

2.2 Mdx[5cv] mouse genotyping

DNA was extracted from ear biopsies collected from each mouse. The ear samples were incubated in a sterile 1.5ml centrifugation tube (Fisherbrand) with 40µL lysis buffer (NaOH 25mM, EDTA 0.2mM made up in distilled water) for 1 hour at 100°C. The ear biopsies and the lysis buffer were centrifugated at 16000 g for 30 seconds at room temperature and then cooled on ice for 5 minutes. The neutralisation buffer (40mM Tris-HCl made up in distilled water, pH 7.5) was added to stop the lysis. DNA concentration was measured with the NanoDrop 1000 (Thermo Fisher). A polymerase chain reaction (PCR) was performed according to Chamberlain's published protocol (Banks, Combs et al. 2010), detailed below.

2.2.1 Polymerase chain reaction

Two hundred nanograms of DNA were used for the polymerase chain reaction (PCR). The primers for the DNA amplification were designed according to Bank's paper (Banks, Combs et al. 2010) in order to amplify the region of exon 10, of the *DMD* gene where the mdx[5cv] mutation is situated (Im, Phelps et al. 1996).The sequence of the forward primer was ATTTGGAAGCTCCCAGAGAC and the sequence of the reverse primer was TGCTTTAGCTTCAGAAGTCA. Primers were ordered from Invitrogen and shipped as desalted stocks. Primer stock was diluted in RNAase and DNAase free water to a concentration of 100 µM and stored at -20°C. The reaction mix was prepared with 10µM of each primer, 200ng DNA and 12,5µL of Q5 Hot Start 2x master mix (BioLab, M0494S). The PCR was performed under the following conditions: 94°C for 5′, followed by 35 cycles of 94°C for 30″, 60°C for 30″ and 72°C for 30″ followed by an extension of 72°C for 3′ on a thermocycler and a final

4°C step (Applied Biosystems Veriti 96-Well). A negative control was prepared substituting the volume corresponding to the samples with distilled water.

2.2.2 PCR product purification

In order to verify that the correct PCR product of 221 bp was amplified, 5µl of each PCR product was run on a 1.25% agarose gel for 30 minutes at 100V. The agarose gel was prepared adding 1.25g of UltraPure™ Agarose (Invitrogen, 16500500) to 198.75mL of Tris-Borate-EDTA buffer (1.25%) (Merk, T4415) and 10µL of SYBR® Safe (Invitrogen S33102). The PCR product were purified using the Qiaquick PCR purification kit (Qiagen, 28104) and measured with the NanoDrop 1000 (Thermo Fisher).

2.2.3 Sanger sequencing

5 ng/µl of DNA was required for sequencing performed by Source BioScience UK. The chromatogram shows a single peak corresponding to an adenine nucleotide for wild-type mice and a single peak corresponding to a thymine nucleotide for mdx[5cv] mice. A double peak was only detected in DNA samples from heterozygous female mice (**Figure 10**).
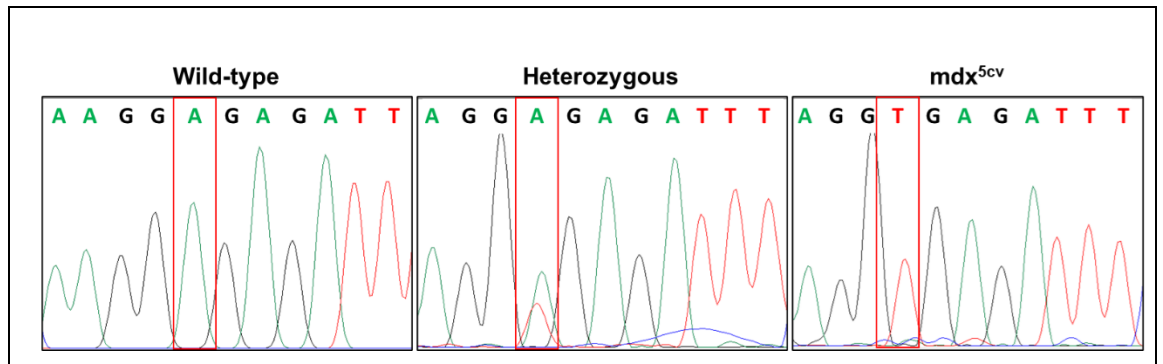
Figure 10. Example of chromatogram resulting after Sanger sequencing.

Point mutation representative chromatogram from wild-type, heterozygous and mdx^{5cv} mice. The red rectangle indicates the mutated nucleotide and the correspondent green peak for wild-type and red peak for mdx^{5cv}. The heterozygous shows both peaks.

2.2.4 ΔR4-R23/ΔCT micro-dystrophin mouse genotyping

DNA was extracted and measured as described in **2.2**. The mdx[5cv]-μDys mice genotyping was performed with a forward primer designed against exon 16 that corresponds to the spectrin-like repeat 3 and a primer reverse designed against exon 59 that corresponds to spectrin-like repeat 24 (**Figure 1 A and Figure 11 A**) producing a band of 300bp used to distinguish mice carrying the transgene from wild-type mice that express full-length dystrophin (**Figure 11 B**). The reaction mix was prepared with 200ng of the extracted DNA, forward and reverse primers (**Figure 11 A**) (10μM) and 13 μL of Q5 Hot Start 2x master mix (BioLab, M0494S) and incubated in a thermocycler (Applied Biosystems Veriti 96-Well) with the following programme:1 cycle at 95°C for 10 minutes, followed by 35 cycles at 95°C for 30 seconds, 61°C for 30 seconds, 72°C for 1 minutes and finished by an extension cycle at 72°C for 7 minutes. The electrophoresis gel was made with 1.25g of UltraPure™ Agarose (Invitrogen, 16500500) and 198.75mL of Tris-Borate-EDTA buffer (1.25%) (Merk, T4415) and 10μL of SYBR® Safe (Invitrogen S33102) in order to label and visualise the PCR product. The first lane of the agarose gel was used to load the 100bp ladder from Promega (G2101), 5 μL of the PCR product were run on the agarose gel for maximum of 40 minutes at 100V (**Figure 11 B**). The samples that did not show the 300bp product (named as 5cv in **Figure 11 B**) were tested with a set of primers for an internal control in order to verify the presence of DNA and validate the negative results, namely mdx[5cv] mice.
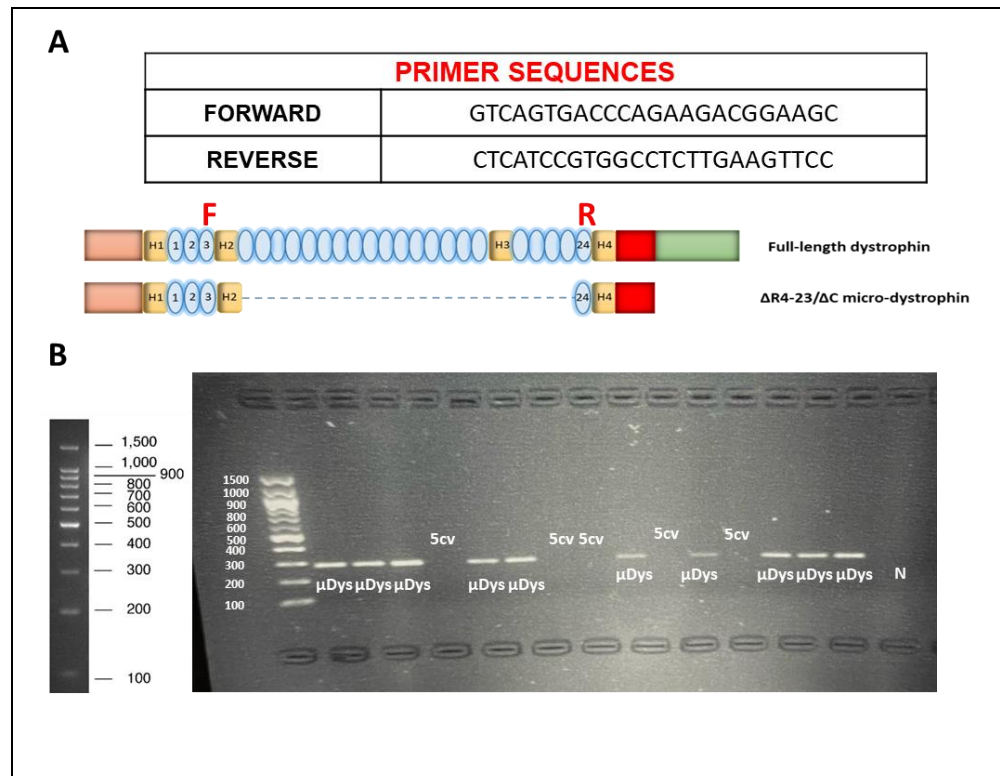
Figure 11. ΔR4-R23/ΔCT micro-dystrophin mice genotyping.

*Schematic representation of full-length dystrophin and the ΔR4-R23/ΔCT micro-dystrophin, the letters F and R in green represent the Forward primer and the Reverse primer. **B**. Representative example of genotyping results in an electrophoresis gel. The bands at 300bp represent the ΔR4-R23/ΔCT micro-dystrophin samples (μDys). Negative control, last well labelled with N. The 100 bp ladder from Promega was run alongside the samples*

2.3 Western Blot

2.3.1 Samples preparation for western blot

The cardiac lysate from wild-type (C57BL/6J) and mdx^{5cv} cardiac muscle was made using the following protocol:

1) Hearts from wild-type (C57BL/6J) and mdx^{5cv} mice were prepared as described in **2.4.3** and 30 sections of 25µm were cut using OTF5000 Cryostat (Bright Instruments) and place in labelled 1.5mL sterile tubes (Fisherbrand). Tubes with cryosections were kept in dry ice during this process.

2) The lysis buffer was prepared by dissolving at room temperature one tablet of protease inhibitor (Pierce, 88668) in 500µl of distilled water in a 1.5mL sterile tube (Fisherbrand). Separately, a mix of Tris (Sigma E17-1321-01) 125mM (the pH was adjusted at 6.8 with HCl 37%), urea 4M, SDS 4% in distilled water was prepared and 50µl of the previously prepared protease inhibitor was add to the mix.

3) Keeping the 1.5mL tubes with the cryosections in dry ice 150µl of lysis buffer were add to each tube. The tubes with cryosections and the lysis buffer were quickly mixed using a vortex and placed into sonicating water bath (filled with wet ice to keep the temperature down) for 5-10 minutes or until lysates showed low viscosity. During the 5-10 minutes the tubes were mixed using a vortex for a few seconds and then placed again in the sonicating water bath.

4) The tubes with the cardiac lysate were incubated in a heat block for 3 minutes at 95°C and then centrifugated for 15 minutes at 15,000 g at

4°C. Then the supernatant was collected in a clean 1.5mL tube and kept on wet ice until protein quantification.

The protein quantification of the cardiac lysates was performed using the DC™ (detergent compatible) protein assay (Bio-Rad) according with manufacturer protocol and a plate reader.

2.3.2 Western blot protocol and antibodies

The western blot results for the DGC members showed in chapter 3 (**Figure 24**) were generated by my colleague Ms Charlotte Scott. Briefly, the cardiac lysate from wild-type (C57BL/6J), mdx^{5cv} and mdx^{5cv}-µDys mice was prepared as described in **2.3.1**. In each lane of a in NuPAGE™ bis-tris protein gels (Invitrogen) 30µg protein were loaded and run for 1 hour at 200V using NuPAGE™ MOPS SDS running buffer (Invitrogen, NP0001). The protein transfer stage was performed using a 0.45-micron nitrocellulose membrane run for 1.5 hours at 30V. The nitrocellulose membrane was then blocked for 1 hour at room temperature with 5% milk in wash buffer (20mM Tris-HCL pH 7.5, 150mM NaCl, and 0.1% Tween-20). The primary antibodies for the detection of the DGC members (**Table 2**) were incubated in blocking buffer solution with 5% milk at 4°C overnight. The next day the nitrocellulose membrane was incubated with the appropriate secondary antibodies conjugated to HRP for 30 minutes at room temperature. The ChemiDoc XRS+ machine (Bio-Rad) has been used to visualise the signal. The densitometric analysis was performed using the Image™ Lab 6.0 Software (Bio-Rad) and the intensity of each band of interest was normalised to the loading control probed with GAPDH or cardiac troponin on the same membrane. The

wild-type samples (N=4) run on the same membrane were used to normalise the relative band intensity.

Table 2. Summary of the antibodies using for western blot analyses.

TARGET PROTEINS	VENDOR	CAT #	HOST SPECIES	DILUTION WB
β-dystroglycan (β DG)	DSHB	MANDAG2	Mouse	1:500
β-sarcoglycan (β SARC)	Abcam	ab83699	Rabbit	1:500
α1-syntrophin (α1 SYN)	Abcam	ab11187	Rabbit	1:500
a-Dystrobrevin (DTNA)	BD Biosciences	610766	Mouse	1:500
cardiac troponin (cTN)	Abcam	ab47003	Rabbit	1:400
GAPDH	Millipore	MAB374	Mouse	1:5000

2.4 Immunofluorescence

2.4.1 Antibodies produced from hybridoma cells

MANEX1011B and MANDYS1 antibodies against dystrophin N-terminus and dystrophin rod domain respectively, were produced from hybridoma cell lines from the Developmental Studies Hybridoma Bank (DSHB) following three steps:

1) Culture of hybridoma cells in serum free medium (SFM) to avoid introduction of non-relevant immunoglobulins. The cells were rapidly thawed in 37°C water bath and then transferred to a 15mL conical tube (Applewood, 352097). Ten millilitres of SFM (Invitrogen 12045-076) were add slowly to the thawed cells. The cells suspended in the SFM were then transferred to a T-75 flask (Appleton Woods, BC301) with another 10 ml of SFM (20 ml total). The cells were grown for 2 days in an incubator set at 37°C and 5% CO_2 at which point 80 mL of SFM was

added. The lid of the T-75 flask was place on a 100mm petri dish to avoid the SFM touching the filter of the T-75 flask lid.
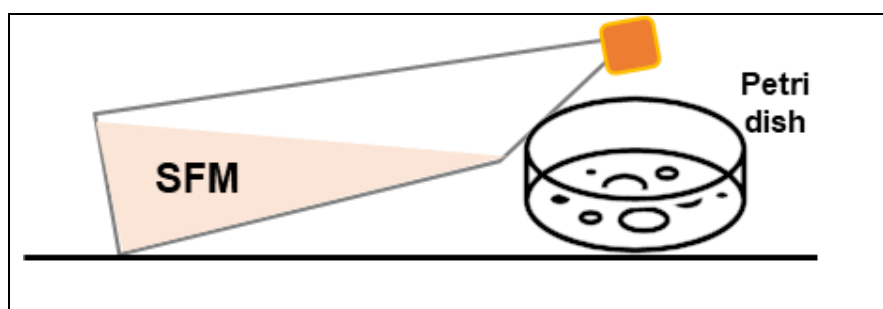
Figure 12. Graphic representation of how the hybridoma cells were grown in the incubator.

After 10 days without changing the SFM medium, the cells and the medium were transferred to two 50 mL conical tubes and centrifuged for 10 minutes at 1500 g to remove cells and any debris, the pellet was discarded, and the supernatant was used for the second step of the antibody production.

2) The supernatant was added to an Amicon™ Ultra-15 Centrifugal Filter Units (Millipore, 10781543) to harvest the culture medium and concentrate it from 80ml down to 5ml. The membrane cut-off of the Amicon™ Ultra-15 Centrifugal Filter Units was 30,000 kDa molecular weight too ensures a highly concentrated preparation of antibody was obtained (MANEX1011B and MANDYS have a molecular weight of 50kDa). The culture medium was centrifuged for 10 minutes at 3000 g.

3) Quantification of immunoglobulins in the preparation using a Western Blot assay as described below (Johnson, Zhang et al. 2012).

A standard curve was created using a MANEX1011B previously produced by a colleague with a known concentration of 3.84µg/µl (called

reference antibody). A stock solution of 0.6µg/µl of the reference antibody was made and a standard curve was created diluting the stock solution from 0.5µg/µl to 0.1µg/µl. Different volumes of the stock solution of MANDYS1 and MANEX1011B with unknown concentration were loaded in the same gel with the reference antibody (**Figure 13**). All the antibodies were suspended in Laemmli sample buffer (Bio-rad, 1610737) and boiled at 95°C for 5 minutes before being loaded in the 4-12% NuPAGE™ bis-tris protein gel (Invitrogen) and then run for 1 hour at 200V. The 4-12% gel was chosen to separate a wide range of molecular weight proteins. Proteins were transferred for 1.5 hours at 30V to a 0.45µm nitrocellulose membrane and probed over night with an anti-mouse immunoglobulin antibody conjugated to horse radish peroxidase at 4°C in a cold room in the dark (1:2000, Stratech). The membrane was washed 3 times for 15 minutes in wash buffer on shaker at room temperature and then incubated for 5 minutes at room temperature with the Supersignal West Pico Plus ECL (Thermofisher 34579). Images of the nitrocellulose membrane were acquired using a ChemiDoc XRS+ machine (Bio-Rad) with exposures from 2 to 30 seconds (**Figure 13**). Subsequently, the intensity of protein bands at 50kDa corresponding to the IgG heavy chain were quantified using Chemidoc image analysis software (Image lab version 6.0).
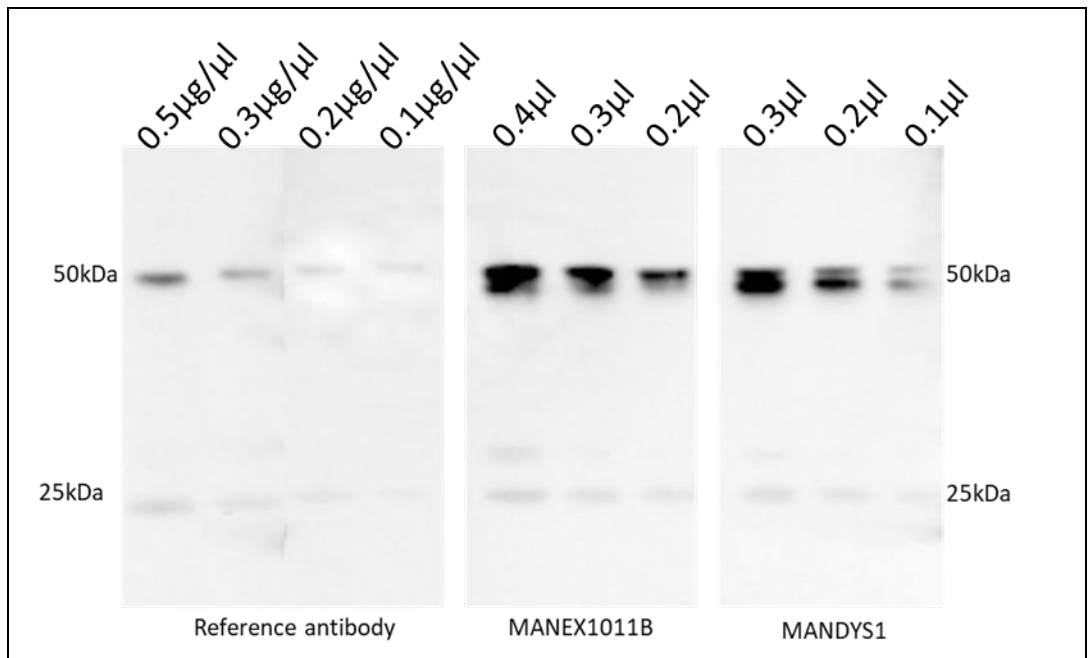
Figure 13. Western blot quantification for antibodies produced form hybridoma cells (MANEX1011B and MANDYS1) and reference antibody.

The reference antibody was diluted from 0.5µg/µl to 0.1µg/µl to create a standard curve and MANEX1011B and MANDYS1 were loaded at different volumes in a 4-12% bis-tris protein gel. The resulted 50kDa bands correspond to the molecular weight of the reference antibody, MANEX1011B and MANDYS1.

Using the intensity values of the 50kDa band of the reference antibody, a standard curve was generated based on the absorbance and the concentration of the reference antibody (**Figure 14**).
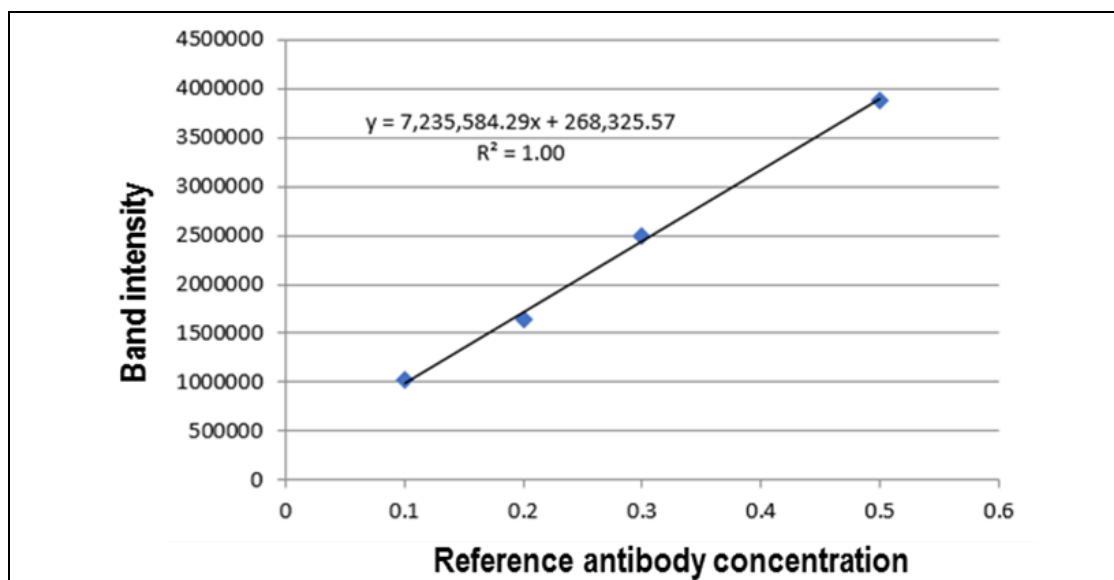
Figure 14. Standard curve generated using the reference antibody.
The reference antibody stock solution (0.6µg/µl) was serially diluted for the western blot analysis to create a standard curve and the equation y=mx+b.

Using the resulting equation (**Figure 14**), the concentration of MANDYS1 and MANEX1011B in µg/µl was calculated and multiplied by the dilution factor (**Table 3**).

Table 3.Calculation of the concentrations of MANEX1011B and MANDYS1 produced from hybridoma cells.

MANEX1011B						
Intensity		3802545	2529390	2118960		
Concentration of sample from curve	µg/µl	0.51	0.33	0.27		
Dilution factor		0.08	0.06	0.04		
Concentration of antibody	µg/µl	6.42	5.44	6.65	**Average**	6.17
MANDYS1						
Intensity		2887320	2151735	1454400		
Concentration of sample from curve	µg/µl	0.38	0.27	0.17		
Dilution factor		0.06	0.04	0.02		
Concentration of antibody	µg/µl	6.32	6.77	8.40	**Average**	6.54

The intensity of each volume of MANEX1011B and MANDYS1 was added to the equation resulting in their concentration in µg/µl. This concentration was then multiplied for the dilution factor to deduct the original stock concentration. This determined that MANEX1011B had a concentration of 6.169125 µg/µl whilst MANDYS1 was 6.542336 µg/µl.

Once the concentrations of MANEX1011B and MANDYS1 were determined the next step was to test both antibodies for their ability to recognize dystrophin. A Western blot analysis was performed using cardiac lysate of wild-type (C57BL/6J) and mdx[5cv] mice (**2.3.1**) The cardiac lysates were also probed with a commercially available antibody against the C-terminus of dystrophin (Abcam, Ab15277) used as a positive control.

Table 4. Information of the different dystrophin antibodies used for the western blot analyses.

TARGET PROTEINS	VENDOR	CAT #	HOST SPECIES	DILUTION WB
Dystrophin C-terminus	Abcam	Ab15277	Rabbit	1:50
Dystrophin N-terminus	DSHB	MANEX1011B	Mouse	1:2000
Dystrophin rod domain	DSHB	MANDYS1	Mouse	1:2000

The western blot was performed with 10µg of protein of each sample. Samples were mixed with reducing sample buffers (RSB) buffer up to 10µL and boiled for 5 minutes at 95°C and then loaded in 4-12% NuPAGE™ bis-tris protein gel (Invitrogen) with the BenchMark™ pre-stained protein ladder (6 to 180 kDa, Invitrogen 10748010). The gel was run in 1X NuPAGE™ MOPS SDS running buffer (Invitrogen, NP0001) for 1 hour at 200V. Proteins were then transferred for 1.5 hours at 30V on a 0.45µm nitrocellulose membrane using a transfer buffer prepared with 50mL of MOPS SDS Transfer Buffer 20X (Invitrogen, NP0006-1), 100mL of methanol 100% and 850mL of MilliQ water. After the transfer the membrane was blocked for 1 hour at room temperature with a blocking buffer prepared with 5% milk in 20mM Tris (the pH was adjusted at 7.5 with HCl), 150mM NaCl and 0.1% Tween-20. The membrane was cut in to 3 pieces, each piece contained 2 lanes, one with the proteins transferred from wild-type cardiac lysate and one with the proteins transferred from mdx^{5cv} cardiac lysate. This was made to probe the wild-type and the mdx^{5cv} samples separately with MANEX1011B, MANDYS1 and dystrophin C-terminus antibody (Abcam, Ab15277). Each piece of membrane was placed in a 15mL conical tube (Applewood, 352097) and incubated with MANEX1011B and MANDYS1 at 1:2000 in blocking buffer and with the Ab15277 at 1:500 in blocking buffer, overnight in a

cold room at 4°C in the dark. After the overnight incubation, membranes were washed 3 times for 15 minutes in wash buffer at room temperature on shaker in dark small plastic boxes. Then were placed in a 15mL conical tube (Applewood, 352097) covered with aluminum foil to keep them in the dark and incubated with the secondary antibodies conjugated with horseradish peroxidase (1:2000, Stratech) in blocking buffer for 1 hour on a tube roller. Following incubation, the membrane was washed 3 times for 15 minutes in wash buffer on shaker at room temperature. The membrane was then incubated for 5 minutes at room temperature with the Supersignal West Pico Plus ECL (Thermofisher 34579) before the image acquisition. Images of the membranes were acquired using a ChemiDoc XRS+ machine (Bio-Rad) (**Figure 15**). In the wild-type heart protein extract, the commercial dystrophin C-terminus antibody (Ab15277) recognises bands at 427kDa, around 230kDa, around 140kDa and at 71-75kDa (**Figure 15**), indicating a complex pattern of dystrophin isoform expression in the wild-type mouse heart (**Figure 1 B**). In the mdx[5cv] protein extract, the 427kDa full length dystrophin is absent as expected due to the mutation in exon 10 of the *Dmd* gene. Some of the lower molecular weight bands are also missing, indicating that additional dystrophin isoforms are disrupted in the mdx[5cv] heart, although their promoters lie downstream of the mutation (Im, Phelps et al. 1996). In samples probed with MANEX1011B and MANDYS1, a single high molecular weight band at approximately 430kDa was present only in wild-type samples, as expected. The 50kDa band in the lanes probed with MANEX1011B and the MANDYS1 antibodies correspond to the heavy chain of the immunoglobulins detected by the goat anti-mouse IgG secondary antibody (**Figure 15**).
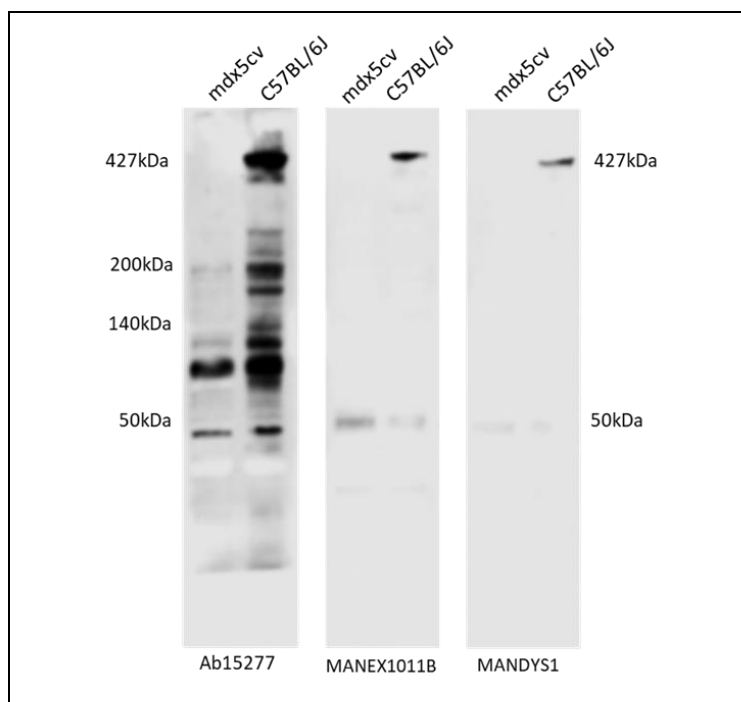
Figure 15. Western blot characterization of the MANEX1011B and MANDYS1 antibodies produced from hybridoma cells in comparison with the commercially available Abcam antibody to the C-terminus of dystrophin.

Cardiac lysates from 8 month old mdx^{5cv} and wild-type (C57BL/6J) male mice probed with the Abcam 15277 antibody that recognises multiple dystrophin isoforms in wild-type mice, some of which are preserved in mdx^{5cv} cardiac lysate and MANEX1011B and MANDYS1 antibodies. MANEX1011B and MANDYS1 only recognise full length dystrophin in wild-type cardiac lysate.

MANDYS1 and MANEX1011B were also tested for their ability to detect dystrophin by immunohistochemistry on heart sections from wild-type, ΔR4-R23/ΔCT micro-dystrophin and mdx^{5cv} mice. Both showed a clear staining at 1:200 concentration. On tissue sections from wild-type mice, MANEX1011B and MANDYS1 staining was visible at the cardiomyocyte lateral membrane (**Figure 16**). As expected, there was no staining on

cardiac sections from mdx^{5cv} mice due to the absence of dystrophin and ΔR4-R23/ΔCT micro-dystrophin protein (**Figure 16**).

On sections from ΔR4-R23/ΔCT micro-dystrophin hearts (**Figure 16**), MANEX1011B labelled the cardiomyocyte membrane, as its epitope is located on the N-terminus of the protein that is present on the micro-dystrophin construct. In contrast, when MANDYS1 was tested on ΔR4-R23/ΔCT micro-dystrophin hearts, there was no staining, except for a nonspecific light background. MANDYS1 is a good antibody to discriminate micro-dystrophin from full-length dystrophin as its epitope is on exon 32 (rod domain) that is absent in micro-dystrophin.
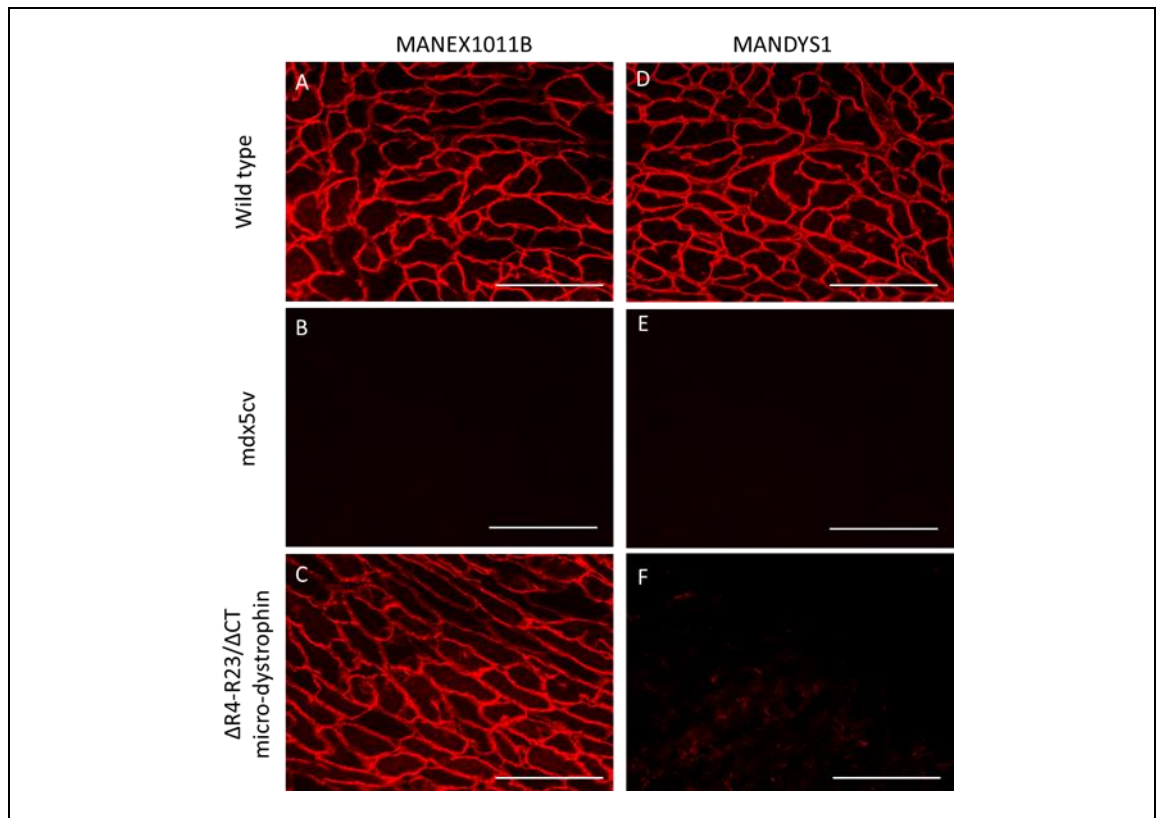
Figure 16. MANEX1011B immunolabelling showed dystrophin in wild-type and mdx^{5cv}-µDys hearts and MANEX1011B and MANDYS1 immunolabelling showed no revertant fibers in mdx^{5cv} hearts.

*Immunolabelling for MANEX1011B and MANDYS1 both at 1:200 of cardiac sections from wild-type (C57BL/6J) (figure **A** and **D**), mdx^{5cv} (figure **B** and **E**) and ΔR4-R23/ΔCT micro-dystrophin mice (Figure **C** and **F**). 40X magnification, scale bar 300µm.*

2.4.2 Antibody optimization

In order to choose the appropriate sample preparation and antibody conditions for the immunohistochemistry experiments with antibodies against cavin-1, -2, -4 and full-length dystrophin (MANEX1011B) several conditions were tested (**Table 5**). With the aim of preserving these membrane associate proteins, cardiac sections were fixed with 2% paraformaldehyde in PBS 1X for 15 minutes at room temperature and

then permeabilized with 0.1% Triton-X for 5 minutes at room
temperature.

Table 5. List of different concentrations and conditions tested in order to obtain optimal immunofluorescence results for cavin-1, cavin-2, cavin-4 and dystrophin N-terminus (MANEX1011B) antibodies.

Antibody optimisations		
TARGET PROTEIN	*CONDITIONS TESTED*	*CONCENTRATIONS TESTED*
CAVIN-1	PFA 2% Triton-X 0.1%	1:50, 1:100
	No PFA Triton-X 0.1%	1:50, 1:100
	Fresh frozen	1:50
CAVIN-2	PFA 2% Triton-X 0.1%	1:50, 1:100
	Fresh frozen	1:50
CAVIN-4	PFA 2% Triton-X 0.1%	1:50, 1:100
	Fresh frozen	1:50
MANEX1011B	PFA 2% Triton-X 0.1%	1:50, 1:100, 1:200
	Fresh frozen	1:200

The conditions that allowed a clear visualization of caveolar proteins and
dystrophin was the fresh frozen protocol where the cardiac sections were
not fixed and permeabilized before incubation with the blocking buffer
(described in detailed in **2.3.4**) The optimal concentration for cavin-1
(Ab48824, Abcam), cavin-2 (NBP1-44090, Novus Biological) and cavin-4
(Ab121647, Abcam) was 1:50 in blocking buffer and for MANEX1011B
1:200 in blocking buffer (**2.3**).Using these conditions, cavin-1 and cavin-2

are clearly visible at the cardiomyocyte lateral membrane, indicated with a white arrow in figure **17 C** and **17 F** and at the capillaries (yellow arrow figure **17 C** and **17 F**).
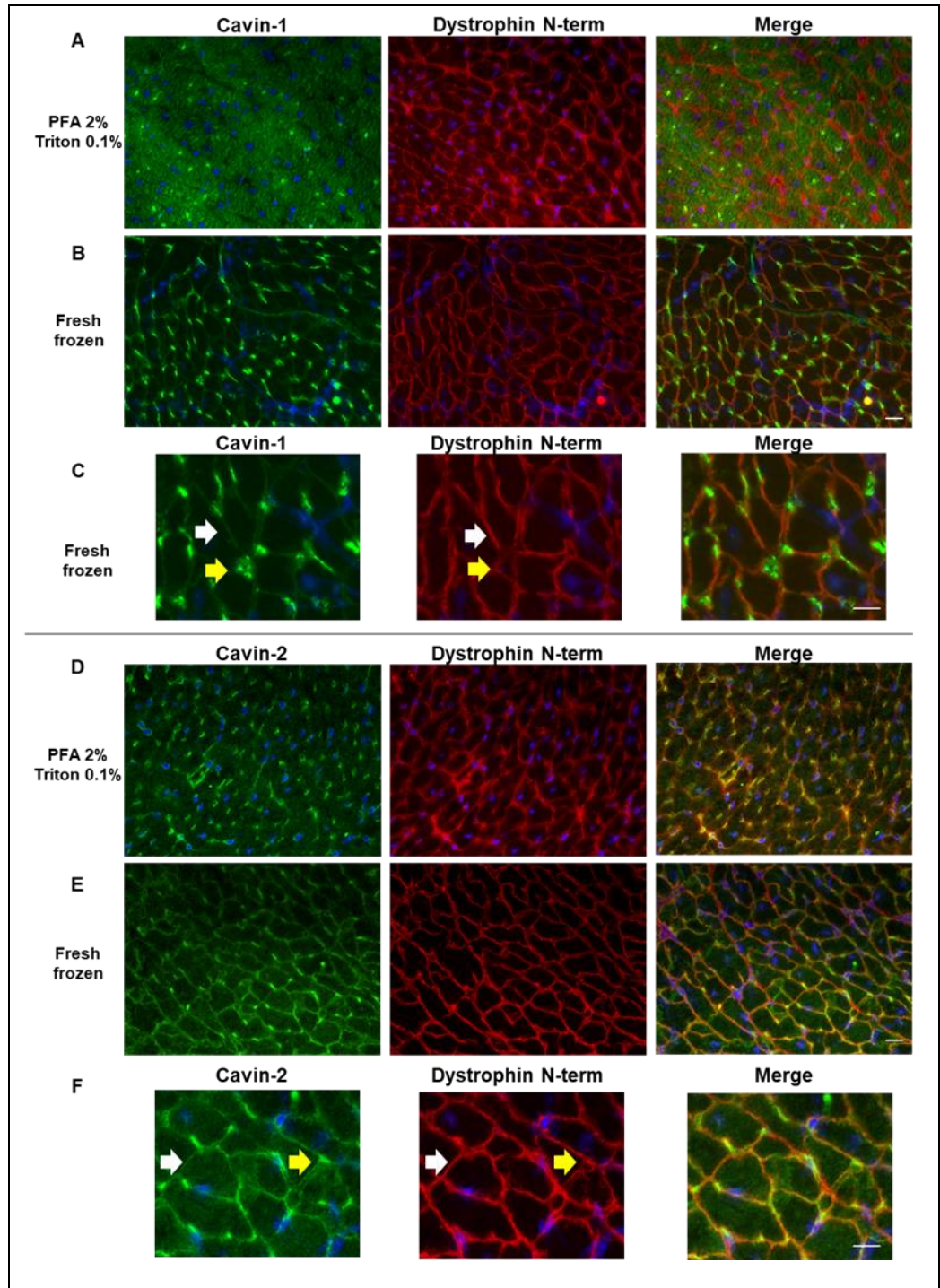
Figure 17. Optimisation of cavin-1, cavin-2 and dystrophin N-terminus (MANEX1011B) antibodies.

*Cardiac tissue from an 8-month-old C57BL/6J male mouse stained with antibodies against cavin-1 (green **A**, **B**, **C**) cavin-2 (green **D**, **E**, **F**) and dystrophin N-terminus (red **A**, **B**, **C**, **D**, **E**, **F**). Cardiac tissue sections **A** and **D** were treated with PBS 1X for 15 minutes at room temperature and then permeabilized with 0.1% Triton-X for 5 minutes at room temperature. Cardiac tissue sections **B** and **E** were stained fresh frozen. (**C**) Enlarged picture from **B**, white arrows point to cardiomyocyte membranes and yellow arrows point to capillaries. (**F**) Enlargement of picture **D**, cardiomyocyte membrane indicated by white arrows and capillaries by yellow arrows. Nuclei stained with DAPI which labels nucleic acid structures are shown in blue. 40x magnification, scale bar 25µm (**A**, **B**, **D**, **E**) and 10µm (**C** and **F**).*

When fixed and permeabilised, the cardiac tissues stained with cavin-4 had a diffuse intracellular staining and a faint membrane stained of both cavin-4 and MANEX1011B (**Figure 18 A**). A strong membrane staining of cavin-4 and MANEX1011B was instead achieved on fresh frozen cardiac sections (**Figure 18 B**).
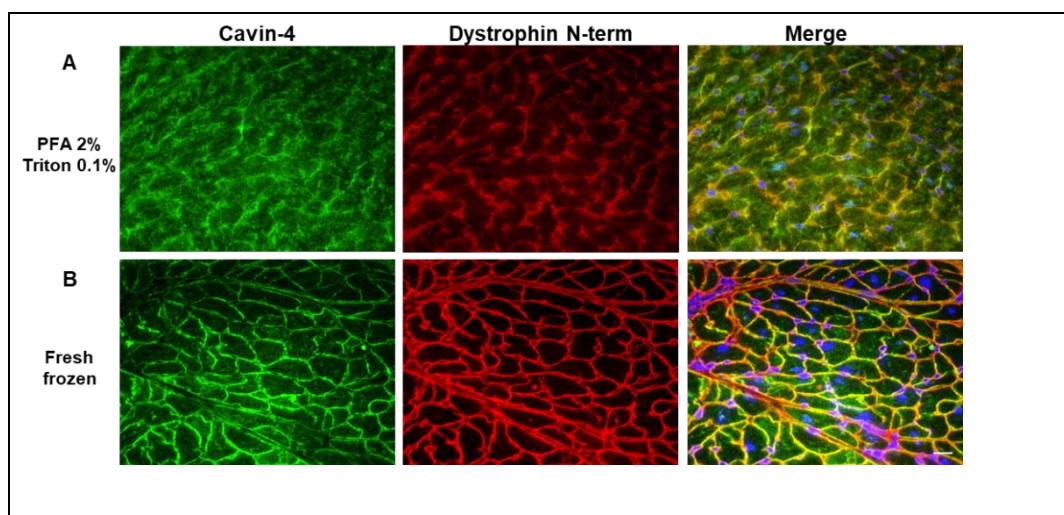
Figure 18. Cavin-4 antibody optimization.

*Cardiac tissue from an 8-month-old C57BL/6J male mouse stained with antibodies against cavin-4 (green) and dystrophin N-terminus (red). Cardiac tissue sections in **A** were treated with PBS 1X for 15 minutes and then permeabilized with 0.1% Triton-X for 5 minutes at room temperature. Cardiac tissue sections in **B** were stained fresh frozen. Nuclei stained with DAPI are shown in blue (merge). 40X magnification, scale bar 25 µm.*

Table 6 below shows all the commercial antibodies used, except for cavin-1, -2, -4 and MANEX1011B, they did not necessitate special optimisation but only concentration adjustments. In table 3 the optimal concentration of each used antibody is identified as "DILUTION IF".

Table** 6**. Detailed list of the antibodies used for this project

TARGET PROTEINs	VENDOR	CAT #	HOST SPECIES	DILUTION IF	DILUTION WB
CAVIN-1	Abcam	ab48824	Rabbit	1:50	-
CAVIN-2	Novus Biologicals	NBP1-44090	Rabbit	1:50	-
CAVIN-4	Abcam	ab121647	Rabbit	1:50	-
CAVEOLIN-3	BD Biosciences	BD 601420	Mouse	1:50	-
LAMININ-A2	Sigma	L0663	Rat	1:500	-
N-CADHERIN	Proteintech	22018-1-AP	Rabbit	1:100	-
B-CATENIN	R&D systems	AF1329	Goat	1:200	
DYSTROPHIN N-TERMINUS	DSHB	MANEX1011B	Mouse	1:200	1:2000
DYSTROPHIN C-TERMINUS	Abcam	ab15277	Rabbit	1:50	1:50
DYSTROPHIN ROD DOMAIN	DSHB	MANDYS1	Mouse	1:200	1:2000
A-DYSTROBREVIN	BD Biosciences	BD610766	Mouse	1:200	-
A1-SYNTROPHIN	Abcam	ab11187	Rabbit	1:100	-
B-DYSTROGLYCAN	DSHB	MANDAG2	Mouse	1:200	-
B-SARCOGLYCAN	Abcam	ab83699	Rabbit	1:50	-
UTROPHIN			Goat	1:100	-

The secondary antibodies were purchased from Jackson ImmunoResearch Laboratories (Table 4) and were all used at 1:200 in blocking buffer (**table 7 and Figure 19**). All the immunofluorescence experiments were designed and performed including one cardiac section in each slide stained only with the secondary antibodies used for the experiment. This was done in order to be sure that the observed labelling was exclusively due to the binding of the secondary antibody with the primary antibody.

*Table 7. **List of secondary antibodies used for immunofluorescence analysis.***

SECONDARY ANTIBODY	CONJUGATE	VENDOR
Donkey anti-mouse IgG (H+L)	Alexa Fluor® 594	Jackson ImmunoResearch Laboratories
Donkey anti-rabbit IgG (H+L)	Alexa Fluor® 488	Jackson ImmunoResearch Laboratories
Donkey anti-rat IgG (H+L)	Rhodamine Red™-X	Jackson ImmunoResearch Laboratories
Donkey anti-goat IgG (H+L)	Alexa Fluor® 488	Jackson ImmunoResearch Laboratories
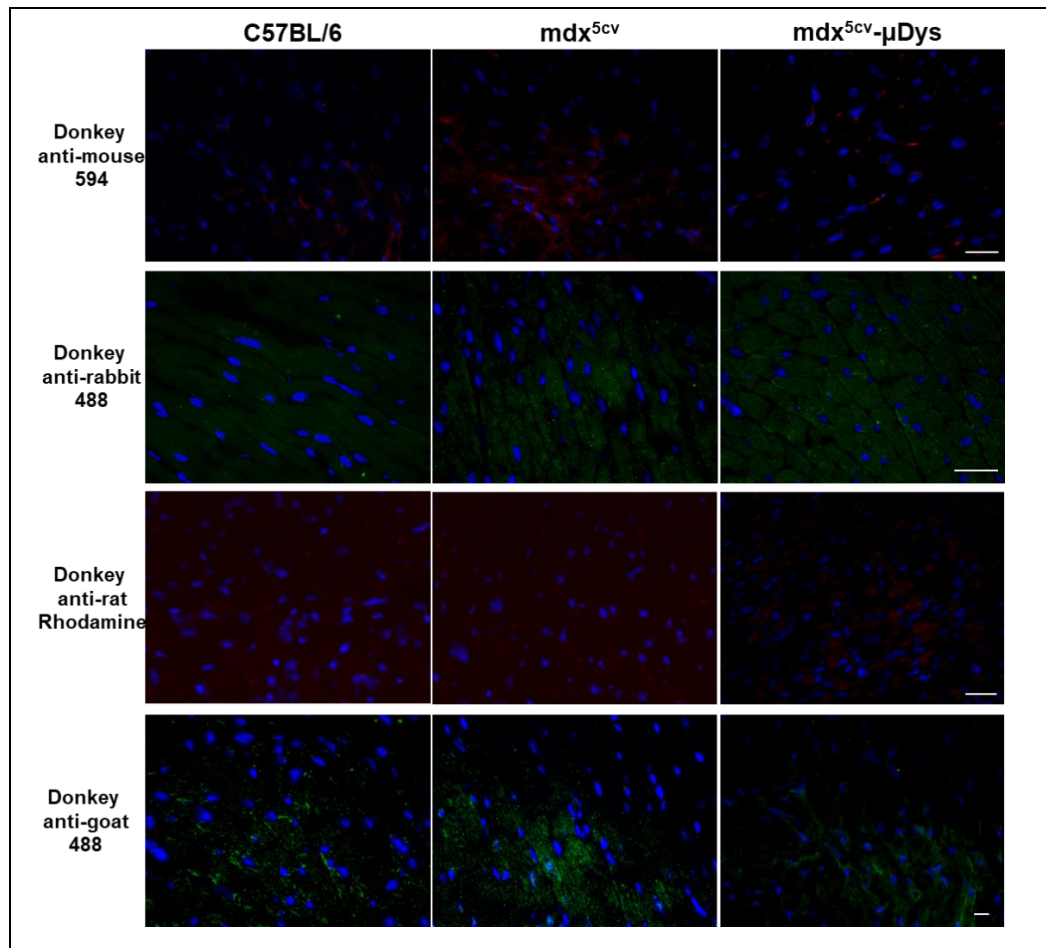
Figure 19.Secondary antibody staining on cardiac sections from wild-type, mdx^{5cv} and mdx^{5cv}-μDys mice.

*Cardiac sections from wild-type, mdx^{5cv} and mdx^{5cv}-μDys mice stained only with secondary antibodies listed in table 4. Sections stained with the donkey anti-mouse 594 were incubated with the FAB fragment after the incubation with blocking buffer as described in **2.3.4**. Pictures taken at 40X magnification and acquired with the maximum exposure time (500ms). Nuclei stained with DAPI in blue, scale bar 25μm.*

2.4.3 Sample preparation for immunohistochemistry experiments

Mice were killed by a schedule 1 procedure (cervical dislocation). After spraying the mouse chest with 70% ethanol the chest was opened with a longitudinal incision. The heart was lifted with curved forceps and a cut was made close to the superior vena cava with small scissors to excise the heart. Once the heart was removed it was squeezed very gently to remove excess blood and dabbed with a clean tissue paper. Then the atria were removed, and the heart was mounted on oak chucks using 7% tragacanth gum. The tragacanth gum (Sigma G1128-500) was prepared days before the heart collection dissolving it in sterile water (6% w/v) for 4 hours and heated overnight at 60°C in a water bath. Then it was allowed to cool, and stored at 4°C. Once mounted in the oak chucks, the hearts were frozen in isopentane cooled in liquid nitrogen for 18 seconds and then transferred to dry ice. The samples were then stored in labelled boxes at -80°C until needed.

2.4.4 Immunohistochemistry

Serial 5μm cryosections were cut on an OTF5000 Cryostat (Bright Instruments) and transferred to a room temperature microscope slide (Superfrost® Plus slides, VWR). The slides were stored in a plastic box at -80°C until needed.

Frozen sections were ringed with a ImmEDGE™ hydrophobic barrier pen (Fisher scientific, H4000), a 30μL drop of blocking buffer containing 5% heat inactivated horse serum in 1X PBS was added to each section and then incubated in a humidified chamber for 1 hour at room temperature. When a primary antibody made in mouse was used, the blocking buffer incubation was followed by a 2-hour incubation in a humidified chamber with 0.1mg/ml donkey-anti-mouse Fab fragments (Jackson

ImmunoResearch Laboratories) in 1X PBS in order to block endogenous immunoglobulins. Sections were then incubated overnight at 4°C with the primary antibodies diluted in blocking buffer. On the following day, after 3 washes of 5 minutes in 1X PBS at room temperature, sections were incubated at room temperature in a dark humidified chamber for 1 hour with the appropriate secondary antibodies. The sections were then washed 3 times for 5 minutes in 1X PBS and stained for 5 minutes with 4′, 6-diamidino-2-phenylindole (DAPI 1µl/10mL dilution in double-distilled water) to identify the nuclei, at room temperature. Sections were then quickly rinsed in double-distilled water and mounted with n-propyl-gallate mounting medium (NPG mounting medium). The NPG mounting medium was prepared following the protocol from Jackson ImmunoResearch Laboratories

(https://www.jacksonimmuno.com/technical/products/protocols/anti-fade). Briefly, a stock solution of 20% (w/v) NPG in dimethyl sulfoxide (Sigma D2650) was prepared. Nine parts of glycerol (ACS grade 99-100% purity, Sigma) were mixed with 1 part of 10X PBS and then 0.1 part of 20% NPG were slowly added to this mix stirring it rapidly. The NPG mounting medium was kept at -20°C before use and on ice during the slide mounting step. A borosilicate glass coverslip (Thermo Fisher Scientific) was applied on top of the sections covered by NPG mounting medium. Nail polish was applied around the coverslip to seal it. Immunolabelled sections were viewed under the Leica DMR fluorescence microscope and images were acquired using Metamorph software (Universal Imaging). Exposure settings for each antibody were fixed based on the wild-type sample signal and then used for the other dystrophin deficient and micro or mini-dystrophin samples.

2.5. Cardiac perfusion for electron microscopy

Mice were anesthetized with a combination of fentanyl-fluanisone and midazolam mixed in equal volume in sterile water (10mL/kg). Once the mouse was fully anesthetized (no reaction to foot pinch), it was culled by a schedule 1 procedure (cervical dislocation). Then the chest of the mouse was sprayed with 70% ethanol and a longitudinal incision was made to open the chest and expose the heart. Using curved forceps, the heart was grasped and lifted in order to create a space to cut the superior vena cava with small scissors, being extra careful to not damage the aorta. The heart was then immersed in Hank's balanced salt solution at room temperature and the fat trimmed away under an inverted microscope to reveal the aorta. A small incision was made in the aortic arch to insert an 18G blunt cannula (Covidien). The aorta was grasped with two pairs of fine forceps to carefully pull the opening of the aorta over the cannula. Then the aorta was secured to the cannula by tying 2 loops of silk suture thread size 6/0 (Fine Science Tool, 18020-60) around the aorta (**Figure 20**).
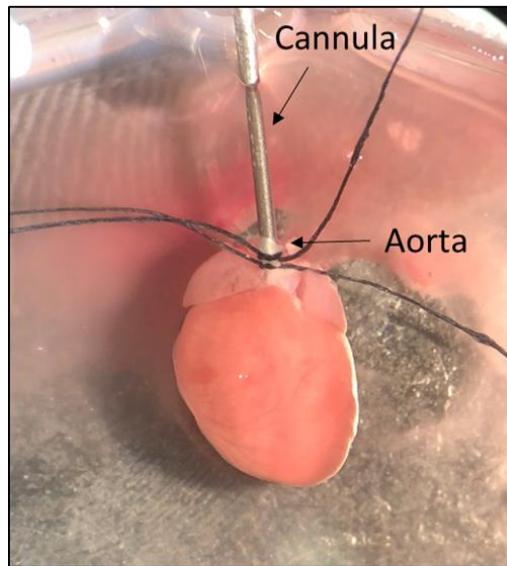
Figure 20. Cannulation of the aorta.

Picture of a mouse heart during cardiac perfusion. The 18G cannula is inserted in the aorta and secures with 2 loops of silk suture thread.

The cannula was connected with a micro tube to a peristaltic pump (Eyela MP3 Microtube) that allows the perfusion buffer to enter the heart via the coronary vasculature. The buffer used for the first experiments was 2.5% potassium citrate in Hank's balanced salt solution which has been used to arrest hearts in diastole (Dae, Heymann et al. 1982). The heart was then placed in a fixation solution of 0.1M sodium cacodylate and 3% EM grade glutaraldehyde in distilled H_2O at 4°C. After 2 hours, the heart was bisected transversally in order to visualize the ventricles (black line **Figure 21 B**). Then a sagittal cut was made on each half (red line **Figure 21 B**). After these two steps, the heart was cut in 4 pieces and each quarter was cut again in a small piece (approximately 2mm) (green areas **Figure 21 B**). This procedure was used in order to collect the upper and the lower part of each ventricle (**Figure 21 B**).
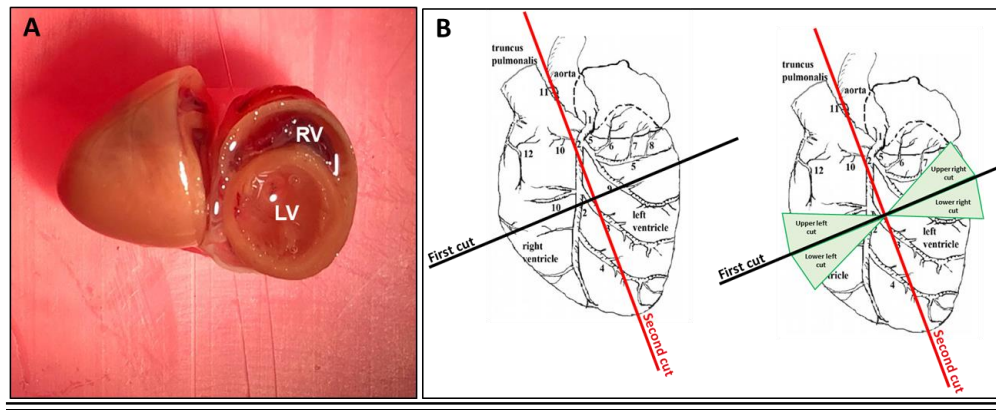
Figure 21. Heart after the first transversal cut and diagram of the cuts.

*Heart after the first transversal cut. The left ventricle (**LV**) and the right ventricle (**RV**) are dilated after the diastolic buffer perfusion (**A**). Diagram of the cuts made for the sample preparation. In green the areas used for the EM (**B**).*

2.5.1 Samples preparation for electron microscopy

After cardiac perfusion and fixation the cardiac samples were processed at the EM facility at the UCL Queen Square Institute of Neurology (ION) by the technical manager Kerrie Venner.

2.6 RNA extraction and quantification

All the microcentrifuge tubes (Fisherbrand) used for the RNA extraction and quantification were autoclaved at 120°C for 1 hour.

Thirty cardiac tissue sections of 20µm were cut with the OTF5000 Cryostat (Bright Instruments) and placed in a sterile 1.5mL microcentrifuge tube (Fisherbrand) kept on dry ice. 500µL of TRIzol™ (ThermoFisher cat no. 15596026) were added to each microcentrifuge tube containing the frozen cryosections. The mixture of TRIzol™ and cryosections was brought to room temperature and vortexed for a few

seconds. The microcentrifuge tubes were then centrifuged at 17000 g for 1 minute at room temperature to remove tissue debris. Then, the supernatant was collected and mixed thoroughly with an equal volume of ethanol (95-100%) (500µL). RNA purification was performed using the Direct-zol RNA kit (Zymo Research; R2062) according to the manufacturer's protocol. The mixture was then placed in a Zymo-Spin™ IC Column and centrifuged for 30 seconds at 17000 g. The flow-through was discarded and 400µL of RNA PreWash buffer were added to the column and centrifuged for 30 seconds at 16000g. This step was repeated once and then, after discarding the flow-through, 700µL of RNA Wash Buffer were placed into the column. The column was centrifuged at 16000 g for 1 minute to achieve the complete removal of the buffer. After discarding the flow-through, the column was placed in a sterile 1.5 mL microcentrifuge tube and the RNA was eluted by placing 50µL of DNase/RNase-free water into the column and centrifuging for 30 seconds at 16000 g. The RNA was measured with the NanoDrop 1000 Spectrophotometer (Fisher Scientific) and then stored at -80°C until needed.

2.6.1 cDNA preparation

cDNA was prepared using the High-Capacity RNA-to-cDNA kit (Applied Biosystems; 4387406) from 800ng of RNA, 10µL of RT Buffer, 1µL of RT enzyme in a total volume of 20µL. All the reagents were kept on ice and the RNA was kept on dry ice until needed. The mix was prepared in 100µL sterile polypropylene tubes (Starlab) and incubated in a thermal cycler (Applied Biosystems) for 1 hour at 37°C and then for 5 minutes at 95°C.

2.6.2 TaqMan probes for DAPC and quantitative RT-PCR

Quantitative real-time PCR (qRT-PCR) performed to assess possible changes in the expression of the DGC mRNA in mdx[5cv] and ΔR4-R23/ΔCT micro-dystrophin hearts compared to wild-type mice was conducted using the cDNA (cDNA preparation described in **2.6.1**) prepared from hearts of 3 wild-type, 3 mdx[5cv] and 3 ΔR4-R23/ΔCT micro-dystrophin mice. The TaqMan method was chosen for this purpose for its high sensitivity (Tajadini, Panjehpour et al. 2014). Predesigned assays from Integrated DND Technologies (IDT) were used for the qRT-PCR, consisting of two primers and a hydrolysis probe for each gene of interest. The genes of interest encode members of the DGC (**3.3.1**), Dag1 (β-dystroglycan), Dtna (α-dystrobrevin), Stna1 (α1-syntrophin), Sgcb (β-sarcoglycan) (**Table 8**). HPRT1 (hypoxanthine phosphoribosyltransferase1) was chosen as housekeeping gene for its stable expression and similar Ct values with the gene of interests. Moreover, HPRT1 has also stable expression during heart failure (Molina, Jacquet et al. 2017) to normalize the gene of interest. Each probe for the genes of interest was labelled with FAM (6-Carboxyfluorescein) and the HPRT1 probe was labelled with VIC (2′-chloro-7′phenyl-1,4-dichloro-6-carboxyfluorescein) (**Table 8**).

Table** 8**. Pre-designed primers and probes used for the qRT-PCR experiments.

TARGET GENE	FLUORESCENT DYE	CAT #	VENDOR
Dag1	FAM	Mm.PT.58.5524327	IDT
Dtna	FAM	Mm.PT.58.12547497	IDT
Stna1	FAM	Mm.PT.58.32407120	IDT
Sgcb	FAM	Mm.PT.58.1305984	IDT
Hprt	VIC	Mm00446968_m1	IDT

Each set of primers and probe was validated separately (singleplex) by preparing a dilution series (6 points) from the cDNA prepared from RNA extracted from the heart of an adult wild-type (C57BL/6J) male mouse. The amplification efficiency of each gene assay was between 94 and 111% (**Figure 22**) and calculated by the StepOnePlus™ Software v2.3 (Applied Biosystem).
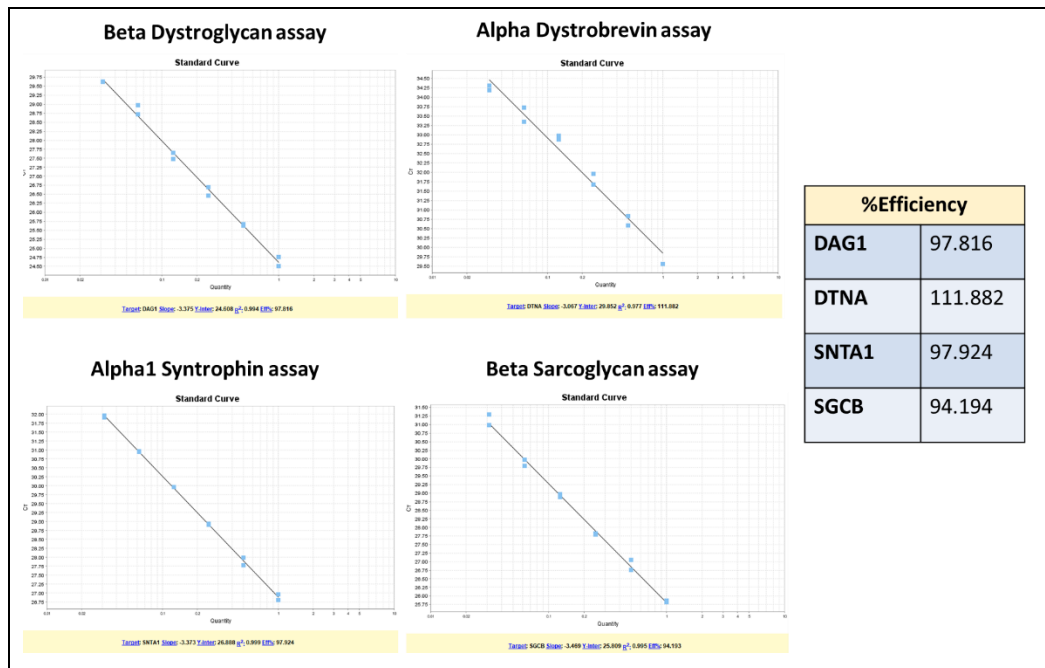
Figure 22. Amplification efficiency of each gene assay.

Graphic representation of the 6 dilution points for each pre-designed set of primers and probe and the resulting amplification efficiency percentage for each of them.

Multiplexed quantitative RT-PCR was performed with a total of 20ng of cDNA from each sample as template, mixed with the Taqman Fast Advanced Master Mix (Life Technologies) and the primers and probes of the gene of interest and of HPRT1 in a total of 10µL volume. The mix was incubated in a StepOne Plus Real-Time PCR machine (Applied Biosystem) for 2 minutes at 50°C, for another 2 minutes at 95°C and for 40 cycles at 95°C for 1 second each, followed by 20 seconds at 60°C. The analysis was performed with StepOnePlus™ Software v2.3 (Applied Biosystem) (**2.6.1**).

2.7 Data analyses

2.7.1 ΔΔCt comparative qPCR analysis

The aim of the qRT-PCR experiments was to assess whether the loss of dystrophin could have an impact on the amount of the mRNA transcript of the DGC members compared to wild-type levels. For this purpose, the ΔΔCt method was used to analyse the qRT-PCR data and calculate the gene fold expression change. First, the average of the Ct values for the target genes and the housekeeping gene was calculated for the wild-type, the mdx[5cv] and micro-dystrophin mice. Then the difference between the averaged Ct of genes of interest and the housekeeping gene was calculated, to arrive at the ΔCt values of the wild-type (control), mdx[5cv] and micro-dystrophin samples. The ΔΔCt was calculated as the difference between the ΔCt values of the mdx[5cv] and micro-dystrophin and the ΔCt values of the wild-type samples. In order to get the expression fold change, data were transformed by applying the formula $2^{-(\Delta\Delta Ct)}$ as Cts are in logarithm base 2.

2.7.2 Quantification of Cavin-4 positive nuclei

The cardiac sections were stained with cavin-4 and laminin-α2 antibodies, nuclei were stained with DAPI (**4.2.2** and **Figure 36 B**). Laminin-α2 antibody was chosen in order to visualize the basal lamina of the cardiomyocytes (Klietsch, Ervasti et al. 1993) and to avoid the counting of the nuclei present in the interstitial spaces in which dystrophin (**Figure 30**) and cavin-4 are not expressed.

Four random but not overlapping pictures for each cardiac sample were taken with a 20X objective and the exposure time was fixed based on the wild-type samples. Using the ImageJ counter tool, a minimum of 200 nuclei localized in the cardiomyocytes were counted for each sample (N=3 mice/group).

2.7.3 Quantification of membrane fluorescence intensity

The quantification of the cardiomyocyte lateral membrane fluorescence intensity was performed according to Arechavala-Gomeza's protocol (Arechavala-Gomeza, Kinali et al. 2010).

The immunostaining for the fluorescence intensity quantification was performed on cardiac tissue sections stained with antibodies against the protein of interest and against laminin-α2. Laminin-α2 fluorescence intensity values were chosen as a normalisation factor as it did not show any significant expression differences among the 3 groups (wild-type, mdx^{5cv} and ΔR4-R23/ΔCT micro-dystrophin) (**Figure 23**). Three samples for each group were used to reach statistical significance (3 wild-type, 3 mdx^{5cv} and 3 ΔR4-R23/ΔCT micro-dystrophin). After staining 4 images of each sample were taken at 20X magnification with the same exposure settings, using MetaMorph software. Following acquisition, 10 random circular regions of interest containing 30 pixels were acquired for each

picture, a total of 40 regions were selected for each sample of each group in order to have 120 selected regions per mouse group (N=3 mice/group). When the random region was on interstitial spaces, it was manually adjusted to be placed on the nearest section of cardiomyocyte lateral membrane. Two values were measured for both laminin-α2 and the protein of interest, the minimum and the maximum fluoresce intensity. The maximum fluorescence intensity was taken from the staining present at the cardiomyocyte lateral membrane and the minimum fluorescence intensity was the background from the nearest cytoplasm.

- The measurements of the minimum fluorescence intensity were subtracted from the measurements of maximum fluorescence intensity.
- The average of the resulted values from the subtraction was calculated for each sample for both laminin-α2 and protein of interest.
- The average of the laminin-α2 values for each sample was calculated.
- The average of the values of laminin-α2 from the control samples were used to calculate the "normalization factor" of each sample from each group dividing the control average with the average of the laminin-α2 values of each sample from each group.
- The "normalization factor" was used to normalize all the protein of interest intensity measurements, by dividing the values of the protein of interest for the "normalization factor" of the corresponding sample.
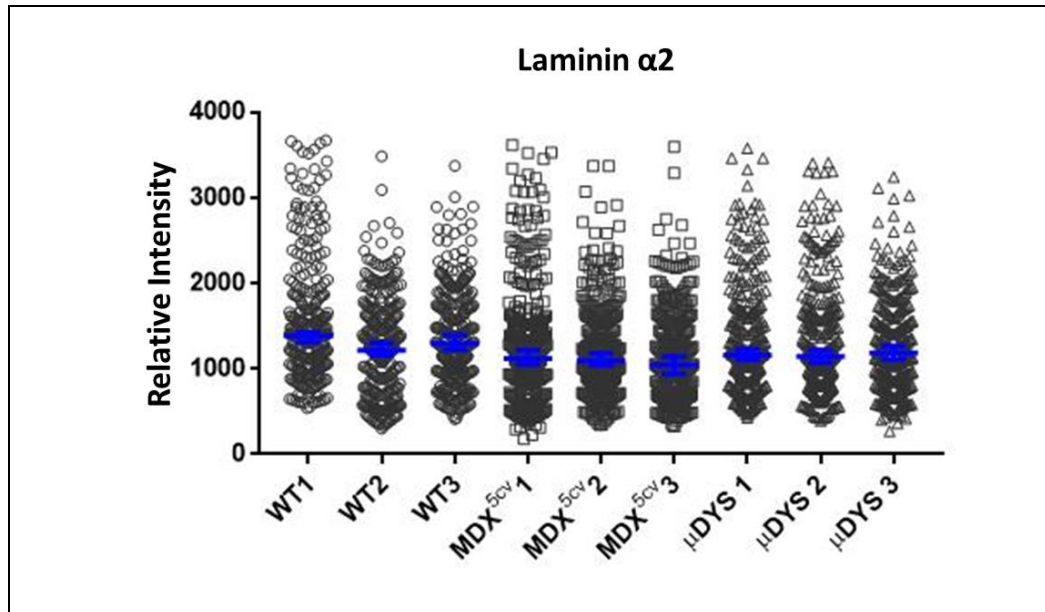
Figure 23. Measurements of laminin-α2 fluorescence intensity showed no significant difference between wild-type, mdx5cv and micro-dystrophin hearts.

Comparison of the laminin-α2 fluorescence intensity between the 3 wild-type, 3 mdx^{5cv} and 3 micro-dystrophin cardiac samples. Each dot corresponds to each measurement taken for each mouse, mixed-effect model was applied. Although, there were significant differences between individual mice, there were not significant genotype specific changes (P=0.0512). The blue bar represents means ± SEM.

.

2.8 Statistics

Non-normally distributed data were analysed using the non-parametric Kruskal-Wallis (comparison between three groups or more) analysis followed by the Dunn's test for pair-wise comparisons. Normally distributed data were analysed using a one-way ANOVA followed by a Bonferroni test for pair-wise comparisons. A two-way repeated measure ANOVA was used for SuperPlots involving nested measurements of membrane fluorescence intensity for n=3 mice per group. The SuperPlots were created to visualise the distribution of the entire dataset where the large, coloured symbols represent the samples belonging to a specific genotype (circles for wild-types, squares for mdx^{5cv} and triangles for mdx^{5cv}-µDys), the small, coloured symbols correspond to each measurement took for each mouse. Statistical significance was set at P-values below 0.05.

Chapter 3. Characterisation of the ΔR4-R23/ ΔCT micro-dystrophin mouse.

3.1 Background and objectives

The work presented in this chapter intends to characterise the main transgenic mouse model that I used for this PhD project, the ΔR4-R23/ ΔCT micro-dystrophin mouse (mdx^{5cv}-μDys). The ΔR4-R23/ΔCT micro-dystrophin construct lacks hinge 3, almost the whole rod domain and the C-terminus domain (**Figure 24 A**). Mice expressing this construct carry the mdx^{5cv} mutation in exon 10 of the gene coding for dystrophin and therefore lack expression of Dp427. The construct is only expressed in cardiomyocytes under the control of the α-myosin heavy chain (αMHC) promoter. The choice of this construct was initially made because it fully restores membrane integrity but only partially rescues cardiac function in the mdx[23] mouse model (Bostick, Shin et al. 2012). Therefore, it was important to ask whether this micro-dystrophin construct can associate with the newly-identified cardiac-specific DGC proteins, some of which are involved in cardiac disease.

The characterisation of the ΔR4-R23/ΔCT micro-dystrophin mouse was carried out by Dr. Hong Wang, Ms Charlotte Scott and myself. Dr. Wang showed that expression of this micro-dystrophin prevented the development of cardiac fibrosis, decreases in capillary density, cardiomyocyte hypertrophy and also normalised electrocardiogram parameters (Wang, Marrosu et al. 2021). These results confirmed that this transgenic mouse model expresses a functional micro-dystrophin. In this chapter, I describe my contribution to the characterisation of the ΔR4-R23/ ΔCT micro-dystrophin mouse.

My specific objectives were to:

1- test that the micro-dystrophin protein is correctly expressed at the cardiomyocyte lateral membrane.

2- assess its ability to restore membrane expression of DGC proteins.

3- determine the effects of loss of dystrophin and of micro-dystrophin expression on the mRNA transcript levels of DGC components in the heart.

For the protein localization studies, I used semi-quantitative immunohistochemical analyses (Arechavala-Gomeza, Kinali et al. 2010). My transcript analyses by quantitative RT-PCR were accompanied by quantifications of total protein expression of DGC components and dystrophin/micro-dystrophin in heart protein lysates performed by Ms. Scott. These biochemical protein analyses are included in section **3.3** with her consent to provide a richer context for my RNA and immunohistochemical analyses and facilitate discussion of the data that I collected. The results in this chapter were recently published (Wang, Marrosu et al. 2021).

3.2 Expression and localisation of the ΔR4-R23/ ΔCT micro-dystrophin protein at the cardiomyocyte membrane of transgenic mdx^{5cv} mice

To assess whether the ΔR4-R23/ ΔCT micro-dystrophin protein (**Figure 24 A**) is correctly localised at the cardiomyocyte membrane, immunohistochemical analyses were performed on cardiac sections from wild-type (C57BL/6J), and ΔR4-R23/ ΔCT micro-dystrophin mice (mdx^{5cv}-µDys) using the MANEX1011B antibody (**Figure 24 B**). MANEX1011B

recognizes both full-length dystrophin and micro-dystrophin as its epitope is located in spectrin-like repeat 1 (R1) that is present in both proteins. (**Figure 24 A**). Mdx[5cv] were used as a negative control, as these mice do not express either dystrophin (Im, Phelps et al. 1996) or micro-dystrophin. The ΔR4-R23/ ΔCT micro-dystrophin protein showed a continuous and strong immunostaining in mdx[5cv]-µDys cardiac sections similar to dystrophin in wild-type mice. As expected, no dystrophin staining was detected in sections of mdx[5cv] hearts (**Figure 24 B**). The dystrophin and ΔR4-R23/ ΔCT micro-dystrophin protein staining can be seen also in cardiac longitudinal sections (**Figure 24 D**) where the lateral membrane is visible along the cardiomyocyte length. The staining of longitudinal cardiomyocytes allows the visualisation of dystrophin and ΔR4-R23/ΔCT micro-dystrophin protein at the intercalated discs where they overlap with N-cadherin (Kostetskii, Li et al. 2005), a marker for the intercalated discs (schematically represented in **Figure 24 C**). I also quantified the membrane fluorescence intensity of dystrophin and ΔR4-R23/ΔCT micro-dystrophin protein. I used laminin-α2 together with MANEX1011B not only to delineate the basal lamina of the cardiomyocytes but also to use it as a normalisation protein in all the three groups (wild-type, mdx[5cv] and ΔR4-R23/ΔCT micro-dystrophin) (**2.6.3**) (Arechavala-Gomeza, Kinali et al. 2010). Quantification of fluorescence intensity at the cardiomyocyte lateral membrane of wild-type and mdx[5cv]-µDys mice revealed a difference in the expression of full-length dystrophin and the ΔR4-R23/ΔCT micro-dystrophin protein. Specifically, the ΔR4-R23/ΔCT micro-dystrophin protein had a 1.7-fold higher expression at the cardiomyocyte lateral membrane of mdx[5cv]-µDys mice compared to full-length dystrophin in wild-type mice (**Figure 24 E**).
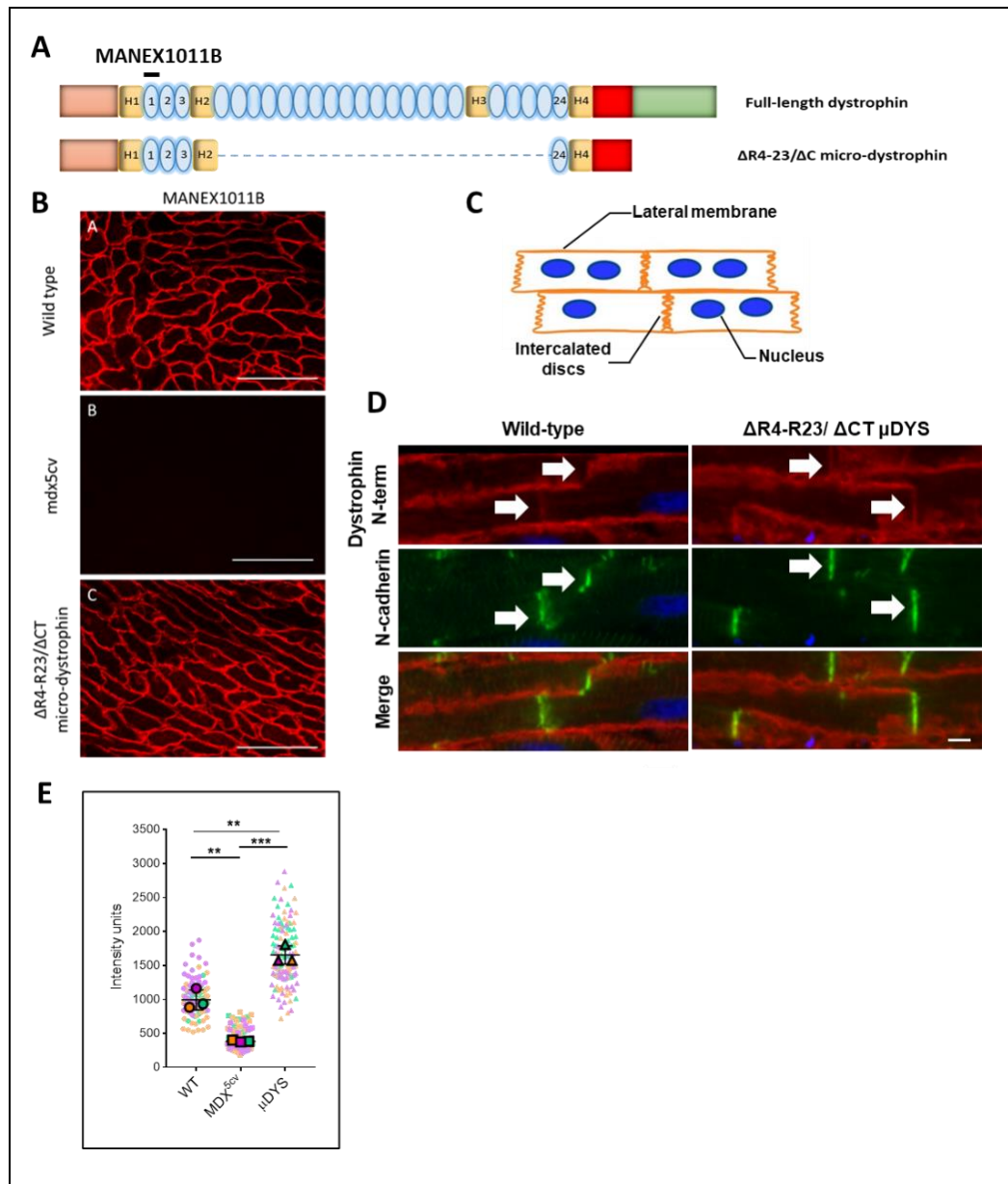
Figure 24. Characterisation of the ΔR4-R23/ ΔCT micro-dystrophin mouse

A. *Diagram representing full-length dystrophin and the ΔR4-R23/ ΔCT micro-dystrophin constructs expressed by the ΔR4-R23/ ΔCT micro-dystrophin mice. The line indicates the epitope recognized by the MANEX1011B antibody.* **B**. *Immunolabelling of full-length dystrophin on cardiac sections from 8-month-old male wild-type (C57BL/6J), mdx^{5cv} and ΔR4-R23/ ΔCT micro-dystrophin mice. There was no dystrophin staining in the mdx^{5cv} hearts. 40X magnification, scale bar 300μm.* **C**. *Schematic representation of cardiac cells, with labelled lateral membrane, nuclei and intercalated discs.* **D**. *Immunolabelling of cardiac tissue sections from wild-type (C57BL/6J) mouse with full-length dystrophin (red) and ΔR4-R23/ ΔCT micro-dystrophin (red) and N-*

*cadherin (green) (C57BL/6J male mouse, 8 months old). White arrows pointing to intercalated discs where dystrophin, ΔR4-R23/ ΔCT micro-dystrophin and N-cadherin are co-localised. Nuclei stained with DAPI (blue), 40X magnification, scale bar 20μm. **E.** Quantification of the dystrophin and micro-dystrophin staining fluorescence intensity at the cardiomyocyte lateral membrane of wild-type (C57BL/6J), mdx^{5cv} and ΔR4-R23/ ΔCT micro-dystrophin mice represented with a Superplot. 40 measurements were taken for each of the 3 mice used for each group (C57BL/6J , mdx^{5cv} and μDys) and are identifiable with the small, coloured dots. The bigger dots represent the mean of the measurements taken for each mouse (N=3). * p<0.05; ** p<0.01; *** p<0.005. Two-way repeated measures ANOVA followed by a Bonferroni test adjusted for multiple comparisons.*

3.3. Protein analysis of the members of the DGC in wild-type, mdx[5cv] and mdx[5cv]-µDys hearts

Previous studies showed that the ΔR4-R23/ΔCT micro-dystrophin construct is able to restore the dystrophin-glycoprotein complex (DGC) in the heart of mdx[23] mice (Yue, Li et al. 2003, Townsend, Blankinship et al. 2007). Therefore, I wanted to assess the condition of the cardiac DGC in the hearts from mdx[5cv] and mdx[5cv]-µDys mice. Firstly, I assessed the total protein expression levels of the DGC using western blot and as mentioned in **3.1** these data were generated by my colleague Ms Charlotte Scott (Wang, Marrosu et al. 2021). In addition, I also wanted to investigate the cellular localisation of the DGC members in mdx[5cv] mice expressing the ΔR4-R23/ΔCT micro-dystrophin construct and compared them with wild-type and mdx[5cv] mice to have a better understanding of the status of the DGC in these mice.

The western blot analyses (**Figure 25 A**) were performed on cardiac lysates of male wild-type, mdx[5cv] and mdx[5cv]-µDys mice between 6 and 12 months of age. The densitometric quantification of the levels of the DGC protein expression (β-dystroglycan, β-sarcoglycan, α1-sytrophin and α-dystrobrevins) in the mdx[5cv] cardiac lysate showed a significant reduction compared to wild-type mice (**Figure 25 B**). Analysing the expression of the same DGC proteins in the mdx[5cv]-µDys hearts revealed that, compared to wild-type, the expression of β-dystroglycan and β-sarcoglycan were significantly increased in mdx[5cv]-µDys mice. The expression of α1-sytrophin and α1, α2 and α3-dystrobrevins in mdx[5cv]-µDys hearts were significantly increased compared to wild-type levels (**Figure 25 B**). These results indicate that the protein expression of DGC members is disrupted in the mdx[5cv] heart, and that the ΔR4-R23/ΔCT

micro-dystrophin protein is able to restore their expression up to and above wild-type levels. However, it was important to assess whether these proteins were correctly localised at the cardiomyocyte membrane of mdx^{5cv}-μDys mice.
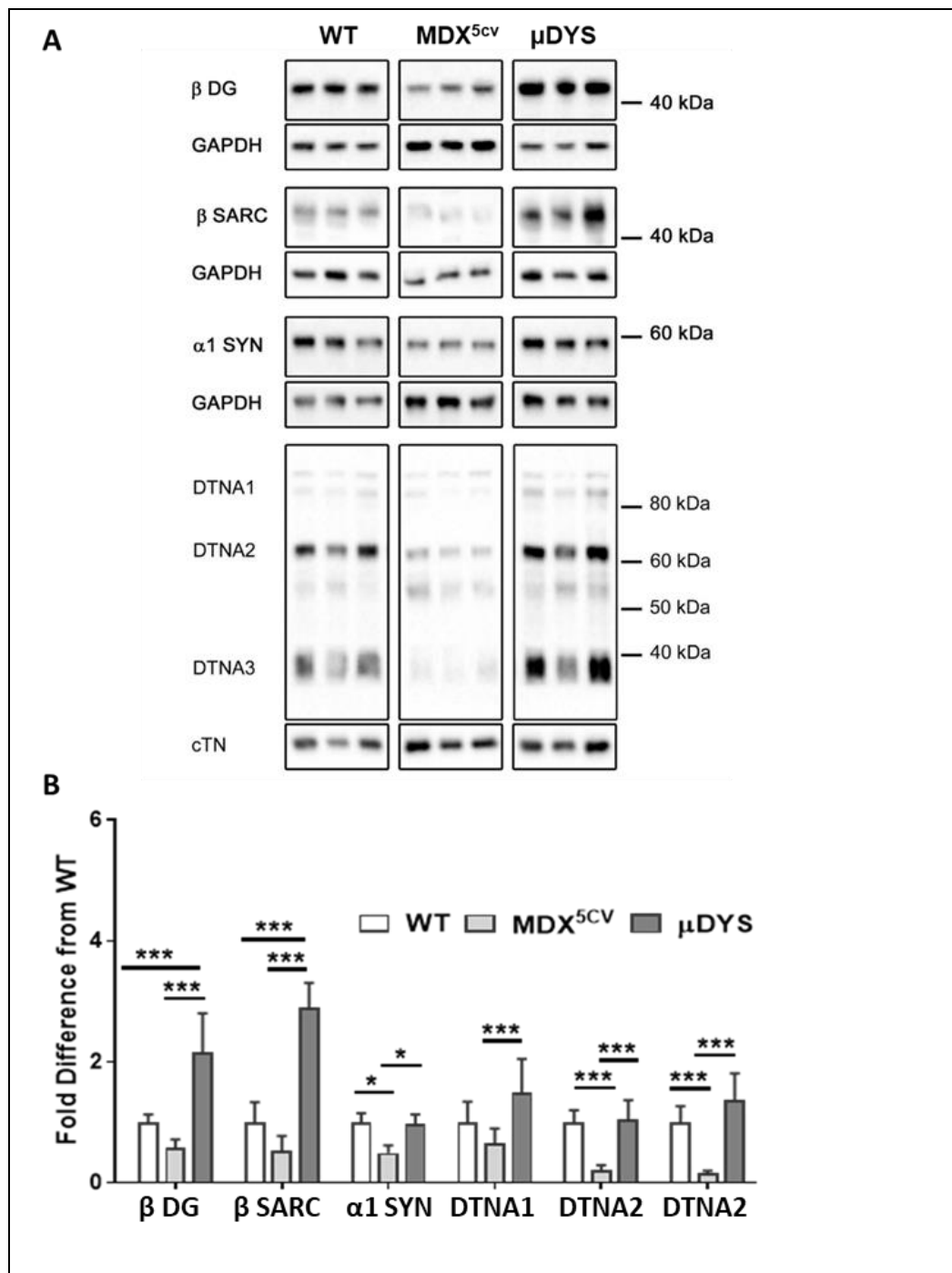
Figure 25. Total protein expression of cardiac DGC in wild-type, mdx^5cv and ΔR4-R23/ΔCT micro-dystrophin mice.

(B) Densitometric quantification of western blot (A) obtained probing cardiac lysates from male wild-type (C57BL/6J), mdx^5cv and ΔR4-R23/ΔCT micro-dystrophin (μDys) mice between 6 and 12 months of age for β-dystroglycan (βDG), β-sarcoglycan (βSG), α1-sytrophin (STNA1) and α-dystrobrevin (DTNA1, A2, A3). The values of mean ± standard deviations are normalised to wild-type. * p<0.05, *** p<0.001, one-way

To do this, I performed immunohistochemistry and membrane fluorescence intensity quantifications for antibodies against β-dystroglycan, β-sarcoglycan, α1-syntrophin and α-dystrobrevin. Cardiac sections from 8-month-old wild-type, mdx^{5cv} and mdx^{5cv}-μDys mice were stained with laminin-α2 and the same DGC antibodies used for the western blots (**Figure 25 A**). The immunofluorescence quantification confirmed that there was a significant reduction of β-dystroglycan, β-sarcoglycan and α1-syntrophin at the cardiomyocyte membrane of mdx^{5cv} mice compared to wild-type mice, reflecting the decreased protein expression observed in the western blot analysis (**Figure 26**). However, α1-syntrophin showed a consistently diffuse intracellular staining in cardiomyocytes from mdx^{5cv} mice (**Figure 26 C**).

Western blot showed a significant decreased in the expression of α2- and α3-dystrobrevins in mdx^{5cv} compared to wild-type mice. Using an antibody that recognises all α-dystrobrevins, I could not detect a significant difference in α-dystrobrevin fluorescence intensity at the cardiomyocyte membrane between wild-type and mdx^{5cv} mice (**Figure 26 E**).

In the mdx^{5cv}-μDys hearts, the membrane fluorescence intensity of β-dystroglycan was significantly increased above wild-type levels in agreement with the western blot results (**Figure 25**).

The protein expression of β-sarcoglycan was increased above wild-type level in mdx^{5cv}-μDys mice (**Figure 25**) but this increase is not visible at the membrane level where β-sarcoglycan immunofluorescence intensity does not reach the wild-type levels. The presence of β-sarcoglycan in

mdx^{5cv}-µDys hearts is probably not directly dependent on the micro-dystrophin construct but it may be due to the presence of β-dystroglycan that is reported to bind to the sarcoglycans (Chan Y. M. 1998).

The membrane fluorescence intensity quantification of α1-sytrophin on mdx^{5cv}-µDys hearts is in line with the western blot results showing a significant normalisation of this protein at membrane level. However, α1-syntrophin was still predominantly seen in the cardiomyocyte cytoplasm in the mdx^{5cv}-µDys hearts (**Figure 26 C**), meaning that even if in the mdx^{5cv}-µDys hearts α1-sytrophin protein expression is normalised at wild-type level by the ΔR4-R23/ΔCT micro-dystrophin construct, the membrane localisation is not completely restored by this construct.

Finally, α-dystrobrevin fluorescence intensity was not significantly increased at the cardiomyocyte membrane of mdx^{5cv}-µDys mice.

Taking together the results of the protein expression and the membrane expression/localisation of the DGC, only β-dystroglycan showed the same level of increase in its protein expression and membrane fluorescence intensity in the cardiomyocytes of mdx^{5cv}-µDys mice.
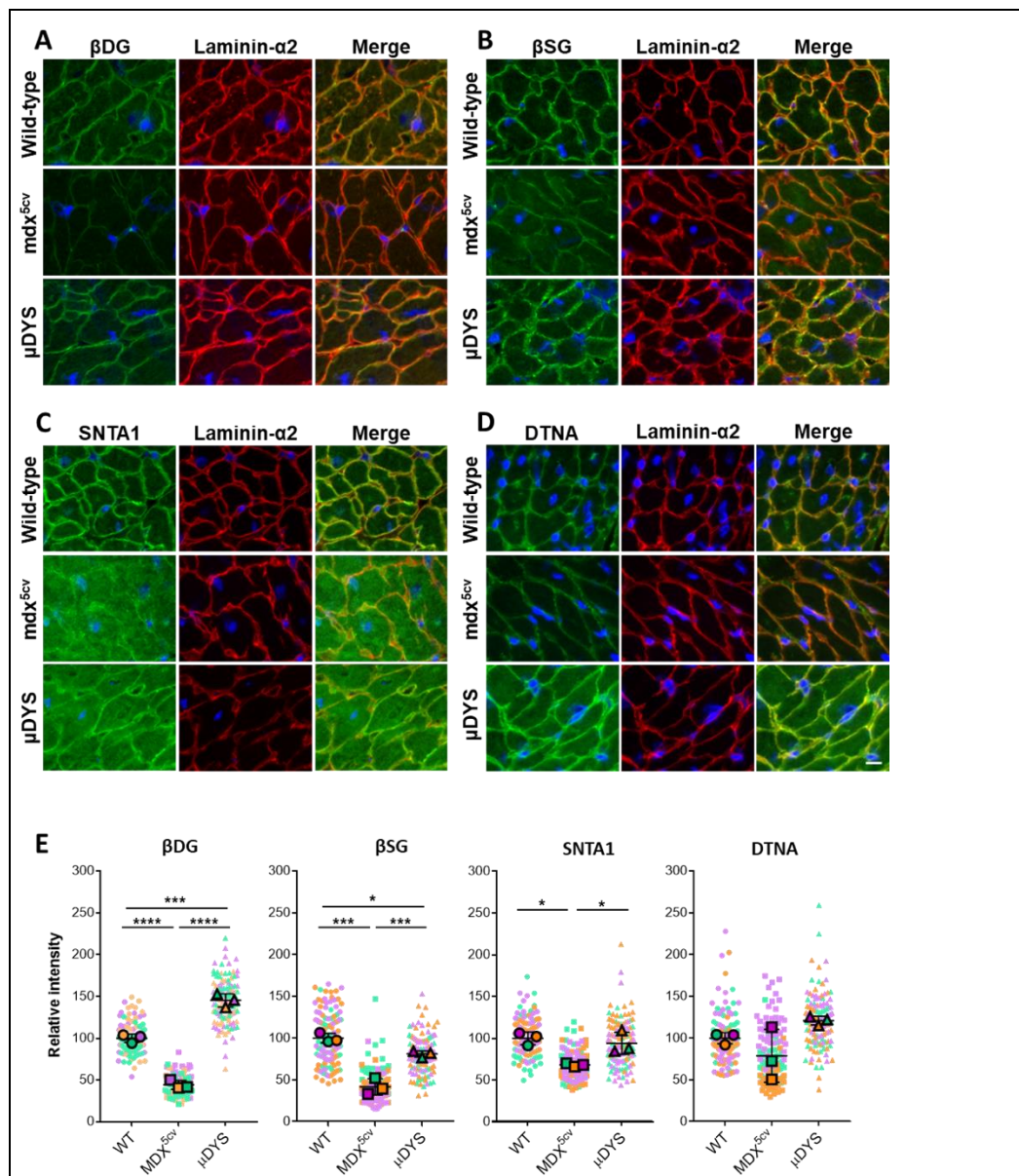
Figure 26. Membrane immunofluorescence quantification of the dystrophin glycoprotein complex.

A, B, C, D. *Immunolabelling for laminin-α2 in red, and β-dystroglycan (βDG), β-sarcoglycan (βSG), α1-sytrophin (STNA1) or pan-dystrobrevin (DTNA) in green on cardiac tissue sections from 8 months old male wild-type, mdx^{5cv} and ΔR4-R23/ ΔCT micro-dystrophin (µDYS) mice (N=3/group). Nuclei were stained with DAPI (blue), 40X magnification, scale bar 15µm.* **E.** *Quantification of the β-dystroglycan, β-sarcoglycan, α1-syntrophin and pan-dystrobrevin fluorescence intensity at the cardiomyocyte lateral membrane of wild-type, mdx^{5cv} and the ΔR4-R23/ ΔCT micro-dystrophin mice represented using Superplots. The small dots represent the measurements (n=40) taken for each mouse of each*

group (wild-type, mdx^{5cv} and ΔR4-R23/ ΔCT micro-dystrophin), the bigger dots are the mean of the 40 measurements took for each mouse (N=3 per group). The grand mean ± standard deviation is indicated by the lines. * p<0.05, ** p<0.01, *** p<0.005, **** p<0.001, two-factor repeated measures ANOVA

3.3.1 ΔR4-R23/ΔCT micro-dystrophin normalizes expression levels of DGC mRNA transcripts in the heart

After analysing the protein expression and the localisation of the members of the DGC, I next investigated whether the total protein overexpression of the members of the DGC on mdx^{5cv}-μDYS was due to mRNA overexpression by the ΔR4-R23/ΔCT micro-dystrophin construct. To quantify the mRNA transcript of each member of the DGC quantitative RT-PCR analysis was performed using pre-designed assays that consist of a primer pair and a probe. The TaqMan method was chosen for its high sensitivity (Tajadini, Panjehpour et al. 2014) and HPRT1 was chosen as reference gene for its stable expression and similar Ct values with the gene of interests (**2.5.2**). The mdx^{5cv} mice showed an increase of 1.5-fold-change in the mRNA expression for all the analysed genes except for α-dystrobrevin compared to wild-type (**Figure 27**). The pre-designed assay for α-dystrobrevin is not designed to distinguish between the different isoforms. In mdx^{5cv}-μDYS mice, the expression of DGC transcripts is normalised to wild-type levels (**Figure 27**). Overall, these results indicate that there is not a correlation between the increased amount of mRNA transcript for β-dystroglycan, β-sarcoglycan and α1-syntrophin and the corresponding protein expression.
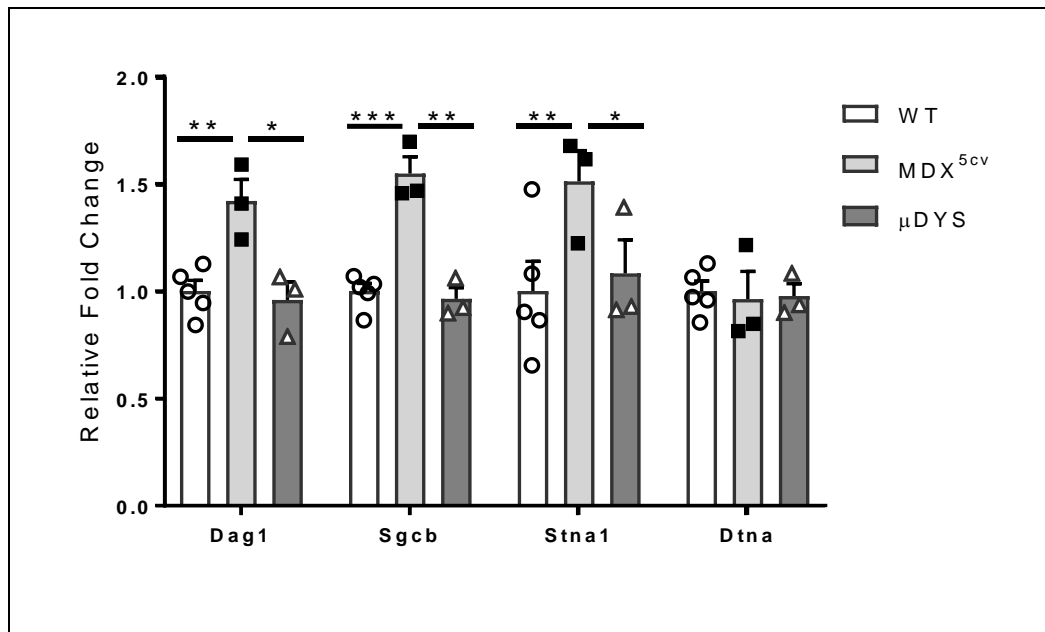
Figure 27.Quantitative RT-PCR analysis of the DGC mRNA transcripts in hearts from WT (wild-type), mdx^5cv and ΔR4-R23/ ΔCT micro-dystrophin (µDYS) mice.

The ΔΔCt method was used to quantify the transcript amounts for Dag1 (ß-dystroglycan), Sgcb (ß-sarcoglycan), Stna1 (α1-syntrophin) and Dtna (α-dystrobrevin) in hearts from WT, mdx^5cv and µDYS mice. The mRNA transcript levels were normalized to HPRT and are expressed as a fold-change relative to the wild-type levels. Statistical analysis: two-way ANOVA followed by the Tuckey test with correction for multiple comparisons. * p<0.05; ** p<0.01; *** p<0.005. WT (n=5), mdx^5cv (n=3) and µDYS (n=3).

3.4 Discussion

Transgenic mice expressing ΔR4-R23/ΔCT micro-dystrophin in their hearts showed that the ΔR4-R23/ΔCT micro-dystrophin protein has the same localisation pattern observed for dystrophin in cardiomyocytes from wild-type mice. Both full-length dystrophin and the ΔR4-R23/ΔCT micro-dystrophin protein are localised at the cardiomyocyte lateral membrane and at the intercalated discs. The only difference between full-length dystrophin and the ΔR4-R23/ΔCT micro-dystrophin proteins is the expression level, in fact this micro-dystrophin had a 2-fold increased expression at the cardiomyocyte lateral membrane of ΔR4-R23/ΔCT micro-dystrophin compared to wild-type mice. This is likely to be due to the fact that the ΔR4-R23/ ΔCT micro-dystrophin expression is driven by the αMHC promoter that has been shown to boost the transgene expression in the heart (Salva, Himeda et al. 2007). These results showed the ΔR4-R23/ ΔCT micro-dystrophin construct to be expressed and correctly localised in the heart of mdx[5cv] transgenic mice.

I used different experimental approaches to characterize the DGC status in the heart of mdx[5cv] and mdx[5cv]-μDYS mice. One of the major findings is that there is no correlation between the levels of mRNA and the levels of DGC proteins in mdx[5cv] and mdx[5cv]-μDYS hearts. In fact, the decreased levels of β-dystroglycan, β-sarcoglycan and α1-syntrophin in mdx[5cv] hearts quantified by immunofluoresce are not reflected by their mRNA levels. The increased DGC mRNA levels in mdx[5cv] hearts could be attributable to a compensatory mechanism triggered by the loss of full-length dystrophin. This mechanism has been already described for utrophin in mdx[23] mice as a compensatory response to dystrophin deficiency (Chen, Chin et al. 2017). ΔR4-R23/ ΔCT micro-dystrophin

improves the stabilisation of the sarcolemma of mdx[23] hearts (Yue, Li et al. 2003) , the normalisation of the DGC mRNA levels I observed in mdx[5cv]-µDys hearts could be in part due to membrane stabilisation. A possible explanation is that the membrane damage caused by the loss of dystrophin in mdx[5cv] mice could triggers transcription factors that regulate the expression of the DGC proteins. In other words, it is possible that in mdx[5cv] hearts the DGC proteins are degraded when they cannot bind dystrophin at the cardiomyocyte membrane (as reflected in the low or unchanged protein expression seen in Western blot analysis). However, such changes could trigger increased transcription of genes encoding the DGC proteins, which may be reflected in increased mRNA levels. These are only speculations and they must be further investigated.

These results are in partial contrast with what Turk and colleagues observed in the skeletal muscle of mdx[23] mice where they found a downregulation of the mRNA levels of β-dystroglycan and β-sarcoglycan but an upregulation of α-dystrobrevin (Turk, Sterrenburg et al. 2005).

As I mentioned **3.1**, the ΔR4-R23/ΔCT micro-dystrophin construct does not have the C-terminus domain, that is involved in the binding with α1-syntrophin, α-dystrobrevins. The data I collected from the immunofluorescence quantifications showed that even if the dystrophin C-terminus is not included in the ΔR4-R23/ΔCT micro-dystrophin construct, α1-syntrophin is brought back to the cardiomyocyte membrane of mdx[5cv]-µDys mice. However, mdx[5cv]-µDys mice show the same intracellular staining observed in mdx[5cv] mice indicating a non complete

rescue of its localisation from the ΔR4-R23/ΔCT micro-dystrophin construct.

Stevenson showed a close interaction of β-dystroglycan with the C-terminus and the cysteine-rich domain of dystrophin (Stevenson, Rothery et al. 1998). In agreement with this I observed total protein expression levels and membrane intensities of β -dystroglycan in mdx[5cv]-μDys mice were higly increased above wild-type levels. Therefore, the presence of the cysteine-rich domain is enough to bring β-dystroglycan to the cardiomyocyte membrane of mdx[5cv]-μDys mice confirming what was seen by Yue and colleagues in mdx[23] mice expressing the same construct, but only using immunofluorescence analysis (Yue et al 2003). The total protein expression of β-sarcoglycan was increased in mdx[5cv]-μDys mice beyond wild-type levels but expression at the membrane of mdx[5cv]-μDys mice though increased compared to mdx[5cv] mice was below wildtype levels. . Alpha-dystrobrevin, a DGC member that is known to bind with the C-terminus of dystrophin shown to be increased at protein expression level in mdx[5cv]-μDys mice but did not show any significant changes at the cardiomyocyte membrane of both mdx[5cv] and mdx[5cv]-μDys mice.

In conclusion, the ΔR4-R23/ ΔCT micro-dystrophin protein is correctly expressed at the cardiomyocyte lateral membrane of trangenic mice and normalise the DGC mRNA levels and it increases their total protein expression. However, it shows differences in the membrane rescue efficacy of some DGC members.

Chapter 4. Cavin membrane localisation is disrupted in transgenic mouse hearts expressing different micro and mini-dystrophin constructs

4.1 Background and objectives

As mentioned in **1.4.4**, among the micro-dystrophin constructs currently in clinical trial, only the ΔR4-R23/ΔCT micro-dystrophin (**Figure 7**) has been studied for its capacity to rescue the impaired cardiac parameters of dystrophin deficient mice (mdx[23]). Yue and collaborators showed that this construct stabilises the DGC at the membrane of mdx[23] hearts and restores sarcolemma integrity (Yue, Li et al. 2003). However, this construct is not able to restore all affected cardiac parameters (Townsend, Blankinship et al. 2007, Bostick, Shin et al. 2011, Bostick, Shin et al. 2012). The ΔR4-R23/ΔCT micro-dystrophin construct lacks hinge 3, almost the whole rod domain and the C-terminus domain. The molecular basis for the incomplete cardiac rescue provided by ΔR4-R23/ΔCT micro-dystrophin is currently unknown. Therefore, a deeper understanding of the molecular interactions of dystrophin in the heart is needed in order to design more efficient constructs in the future. Johnson and colleagues discovered that the cardiac DGC includes a set of proteins that are absent in the skeletal muscle DGC and are important for cardiac function and disease (ahnak1, cypher, αB-crystallin, and cavin-1) (Johnson, Zhang et al. 2012). Among these proteins, cavin-1 has been described as essential for the formation of caveolae (Taniguchi, Maruyama et al. 2016). As mentioned in **1.6.1**, caveolae and the proteins related to them play an important role protecting the heart from mechanical stress (Patel, Tsutsumi et al. 2007, Cheng, Mendoza-Topaz

et al. 2015). They are involved in calcium signalling (Balijepalli, Foell et al. 2006), cardiac conduction (Tyan, Turner et al. 2021), and cardiac contraction (Grivas, González-Rajal et al. 2020).

In addition to cavin-1, other key accessory proteins have been identified, which include cavin-2 and -3 and the muscle-specific cavin-4 that is expressed in smooth, skeletal and cardiac muscle (Ogata, Ueyama et al. 2008). Interestingly, both cavin-1 and cavin-4 are associated with cardiac disease. Specifically, studies in mice link the deficiency of cavin-1 with a cardiomyopathic phenotype, with cardiomyocyte hypertrophy, cardiac fibrosis, and electrocardiographic abnormalities (Taniguchi, Maruyama et al. 2016). Moreover, the loss-of-function mutation of cavin-1 in human patients causes congenital generalised lipodystrophy type 4 and some of these patients show cardiac impairments such as long-QT syndrome and fatal cardiac arrhythmia (Rajab, Straub et al. 2010). Molecular genetic studies on human patients (Nouhravesh, Ahlberg et al. 2016) as well as *in vitro* studies (Rodriguez, Ueyama et al. 2011) found an association between loss-of-function cavin-4 mutations and dilated cardiomyopathy. These observations leave some open questions:

- Since cavin-1 is part of the cardiac DGC (Johnson, Zhang et al. 2012), does it localise with dystrophin at the cardiomyocyte lateral membrane?
- Do the other cavins share the same membrane localisation?
- Is their localisation disrupted when full-length dystrophin is not expressed?
- Which dystrophin domains are involved in the association with cavins?

- Do the micro and mini-dystrophin constructs contain the binding domain for the cavins?

In this chapter I aim to answer to these questions by:

-Characterising the localisation of cavin-1, -2, -3 and -4 in wild-type hearts.

-Investigating whether the sub-cellular localisation of these proteins is disrupted in mdx^{5cv} and mdx^{23} hearts (in which full-length dystrophin is not expressed).

-Investigating the localisation of cavins in the heart of mdx^{5cv} and mdx^{23} mice expressing different micro and mini-dystrophin constructs (**Figure 28**).

The use of mdx^{5cv} and mdx^{23} transgenic mice expressing different micro and mini-dystrophin constructs could also help with the identification of dystrophin domains that may be involved in binding with cavins.
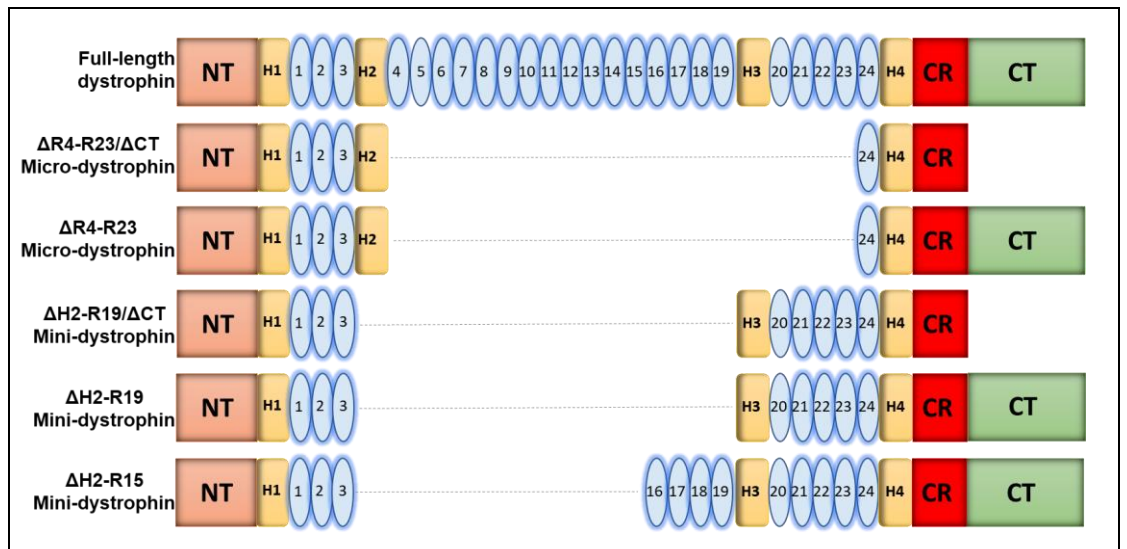
Figure 28. Graphic representation of the full-length dystrophin and the micro and mini-dystrophin proteins.

Orange boxes represent the N-terminus (NT), hinges are represented by the yellow boxes (H1, H2, H3, H4), the red boxes represent the cysteine-rich domain (CR), C-terminus represented by the green boxes (CT), spectrin-like repeats (light blue numbered ovals).

4.2 Results

4.2.1 Cavin-1, -2 and -4 are lost or disrupted at the mdx[5cv] cardiomyocyte lateral membrane and are not rescued by ΔR4-R23/ ΔCT micro-dystrophin

- **Cavin-1**

The distribution of cavin-1 in heart has not been studied in detail, as studies assessing an involvement of cavin-1 in cardiac disease did look at the localisation of this protein with immunofluorescence only in blood vessels (Rajab, Straub et al. 2010, Hansen, Shvets et al. 2013, Taniguchi, Maruyama et al. 2016, Kaakinen, Reichelt et al. 2017). Here, I investigated the cardiac distribution of cavin-1 using immunofluorescence (**Figure 29**) finding that in wild-type (C57BL/6J) hearts, cavin-1 localises at the cardiomyocyte lateral membrane with a continuous and homogenous staining. The overlapping of cavin-1 staining and the laminin-α2 staining became an orange staining at the cardiomyocyte lateral membrane of wild-type mice membrane (**Figure 29 B**, white arrow). Consistently with the abundance of caveolae in the vascular endothelial cells (Hansen et al. 2013), cavin-1 is also present at the capillaries that are located outside the laminin-α2 boundary (**Figure 29 B**, yellow arrows). In mdx[5cv] hearts, where full-length dystrophin is absent, cavin-1 is lost from the cardiomyocyte lateral membrane and this membrane localisation is not rescued by expression of ΔR4-R23/ΔCT micro-dystrophin. The absence of full-length dystrophin does not have any effect on the presence of cavin-1 at the capillaries (**Figure 29 B**) due to the fact that dystrophin is not expressed in the capillaries (**Figure 30**).

Cavin-1 is also localised at the intercalated discs of wild-type, mdx^{5cv} and mdx^{5cv}-μDys mice (**Figure 31**). The loss of cavin-1 from the cardiomyocyte lateral membrane of mdx^{5cv} and mdx^{5cv}-μDys hearts is confirmed by the quantification of cavin-1 membrane fluorescence intensity when compared to the wild-type levels (**Figure 29 C**). The membrane intensity quantification was performed by staining sections from 3 wild-type (C57BL/6J), 3 mdx^{5cv} and 3 mdx^{5cv}-μDys mouse hearts with cavin-1 and laminin-α2 (as in **Figure 29 A and B**). The fluorescence intensity measurements of cavin-1 were normalised to the intensity of laminin-α2 (Materials and Methods, **Figure 23**) showing the decreased cavin-1 fluorescence at the cardiomyocyte lateral membrane of both mdx^{5cv} and mdx^{5cv}-μDys mice. These data show that the cardiomyocyte membrane localisation of cavin-1 depends on the presence of full-length dystrophin at the cardiomyocyte membrane, confirming previous biochemical findings (Johnson, Zhang et al. 2012) that showed that cavin-1 is a member of the DGC in the heart. Moreover, these data show that the ΔR4-R23/ΔCT micro-dystrophin construct does not rescue the membrane localisation of cavin-1 in mdx^{5cv}-μDys mice.
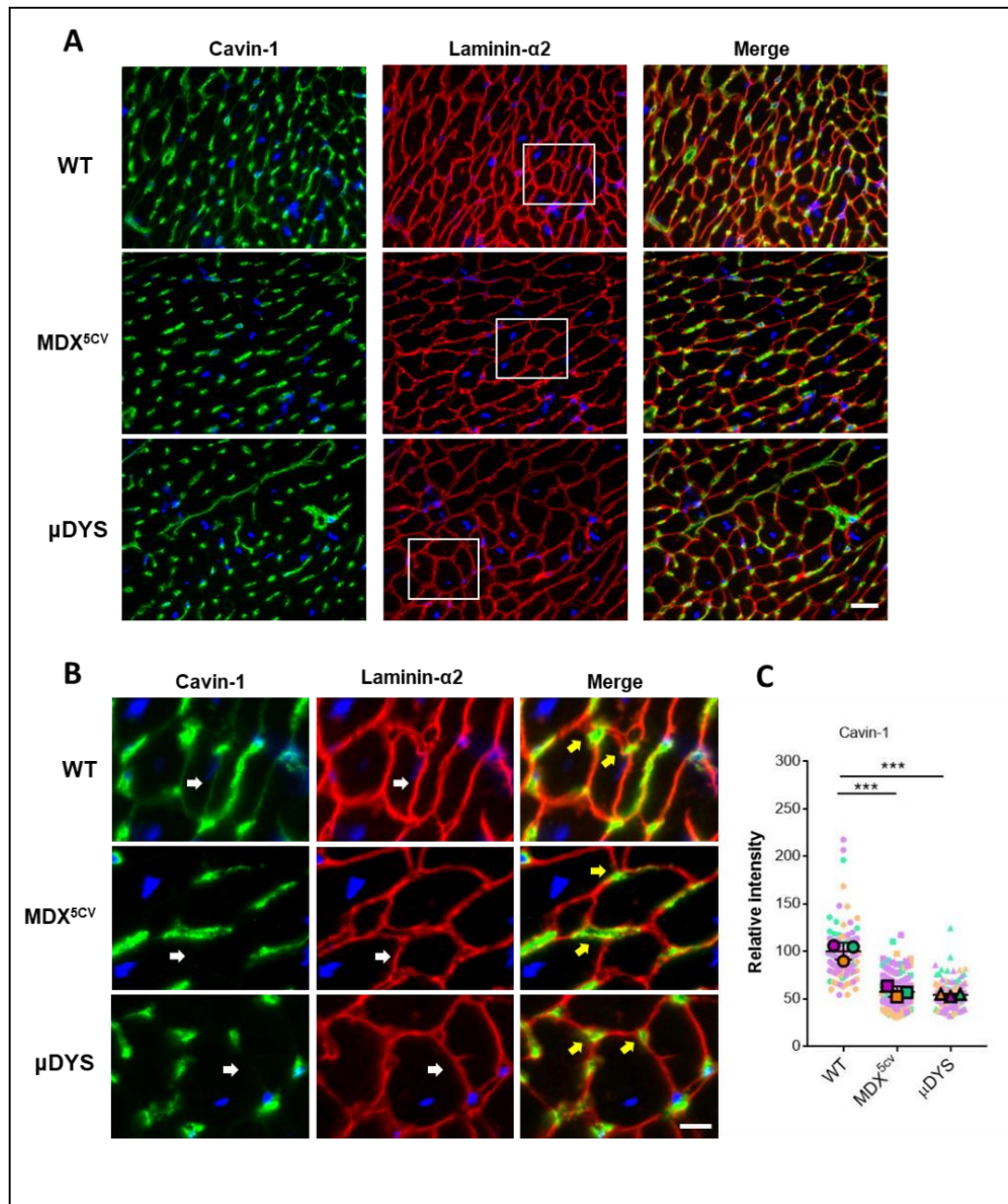
Figure 29.Cavin-1 is lost from the mdx^{5cv} and µDys cardiomyocyte lateral membrane.

A, B. Cardiac tissue cryosections from 8-month-old male C57BL/6J (WT), mdx^{5cv} and µDys mice stained with cavin-1 and laminin-α2 (red). Nuclei stained with DAPI (blue). 40X magnification, scale bar: 25µm. (N=3 mice/group) B. Enlargements of the immunostainings showed in A. Cardiomyocyte lateral membranes are indicated with white arrows. Capillaries are surrounded by laminin-α2 (red) and indicated with yellow arrows in the merged pictures. Scale bar: 10µm. C. Superplot of cavin-1 fluorescence intensity at the cardiomyocyte lateral membrane normalised for the membrane fluorescence intensity of laminin-α2. The small dots represent the 40 measurements taken for each of the 3 mice used for

each group (WT, mdx^{5cv} and µDys). The mean of the measurements for each mouse is depicted by the bigger dots (N=3/group). The mean ± standard deviation is indicated by the lines. *** p<0.005.
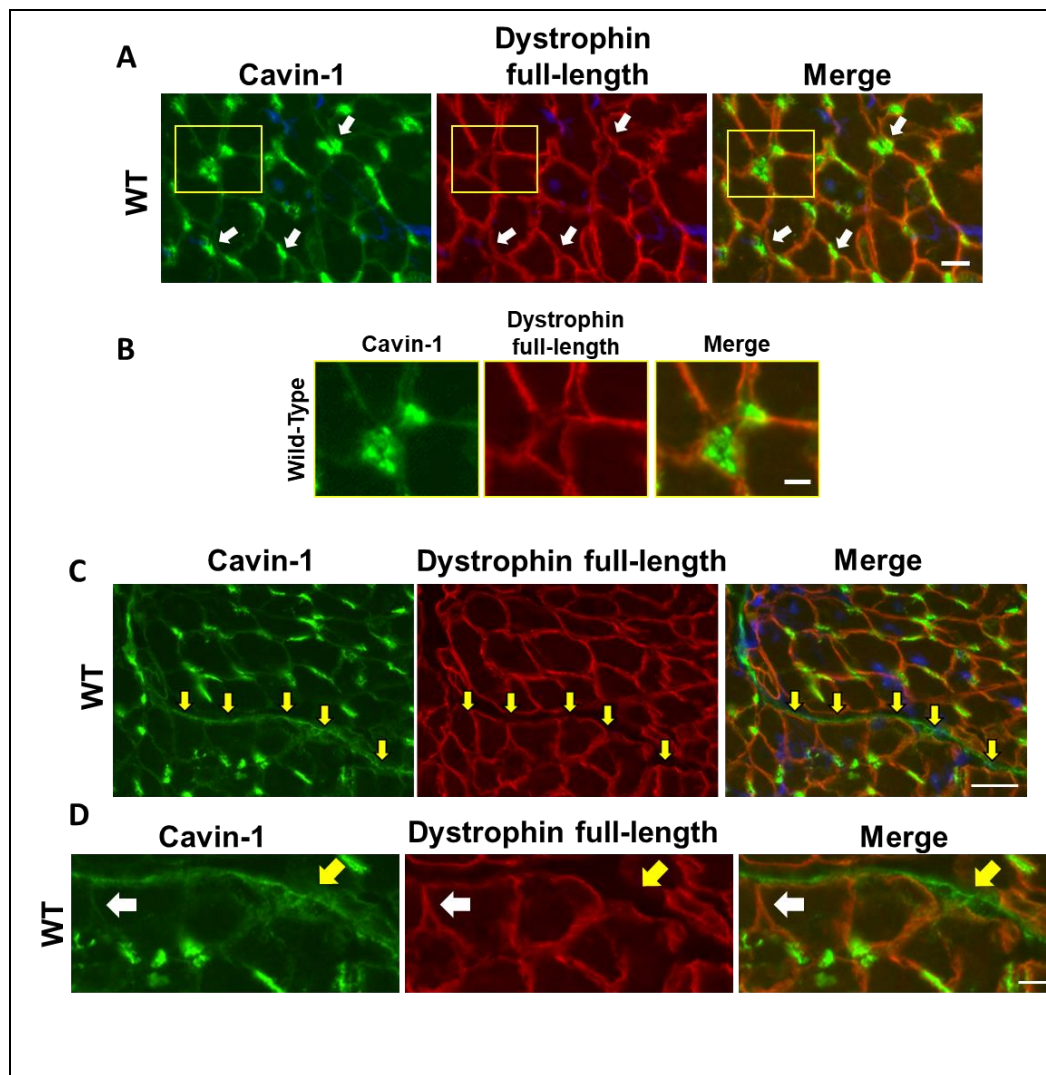
Figure 30. Full-length dystrophin is not expressed in capillaries.

A. Representative image of cardiac sections from an 8-month wild-type (C57BL/6J) male mouse immunolabelled with cavin-1 and dystrophin N-terminus antibodies. Dystrophin staining is visible only at the lateral membrane of the cardiomyocytes and is not present at the capillaries. White arrows pointing to capillaries stained with cavin-1. Nuclei stained with DAPI. 40x magnification, Scale bar 10µm B. Enlarged pictures of the areas delineated by the yellow boxes in A where cavin-1 staining at the capillaries, as well as the absence of dystrophin, is more visible. Scale bar = 5µm. C. Immunolabelling of cardiac section from an 8-month wild-type (C57BL/6J) male mouse immunolabelled with cavin-1 and dystrophin N-terminus antibodies. Yellow arrow point to a longitudinal capillary stained with cavin-1. 40X magnification, scale bar 25µm. D. Enlarged pictures of C, white arrows pointing to cavin-1 membrane

staining in overlap with dystrophin and yellow arrows pointing a longitudinal capillary stained with cavin-1 and not dystrophin. 40X magnification, scale bar 10µm.
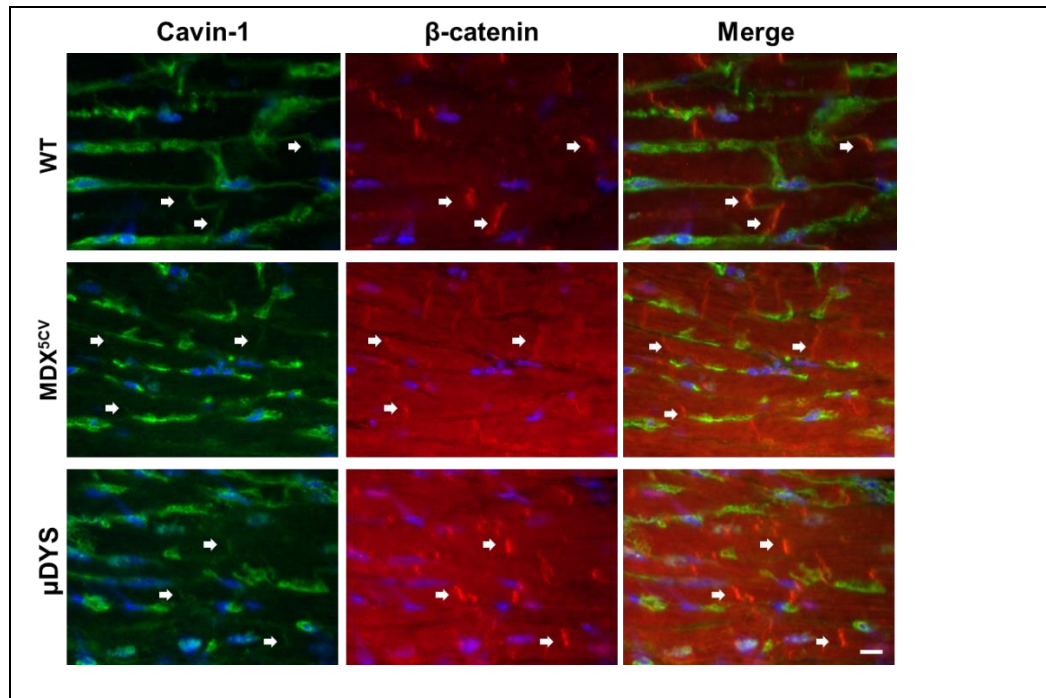
Figure 31. Cavin-1 is expressed at the intercalated discs of wild-type, mdx^{5cv} and ΔR4-R23/ΔCT micro-dystrophin mice.

Double labelling of cardiac tissue sections from wild-type, mdx^{5cv} and ΔR4-R23/ΔCT micro-dystrophin mice for cavin-1 (green) and β-catenin (red). White arrows pointing to intercalated discs positive for cavin-1 and β-catenin. Nuclei stained with DAPI (blue). 40X magnification. Scale bar: 25µm. (N=3 mice/group).

- **Cavin-2**

Experiments on cavin-1 knock-out mice show that the loss of cavin-1 in the myocardium is accompanied by the loss of cavin-2 (Ogata, Ueyama et al. 2008, Taniguchi, Maruyama et al. 2016). The studies of Ogata and Taniguchi were made on cardiac lysate from wild-type (C57BL/6J) and cavin-1 knock out mice, but they did not study cavin-2 protein localisation in these mice. The immunofluorescence results reported in **Figure 29** show the loss of cavin-1 at the cardiomyocyte membrane of mdx[5cv] and ΔR4-R23/ΔCT micro-dystrophin hearts. Therefore, it was worth asking whether the loss of cavin-1 at the cardiomyocyte membrane level was followed by the loss of cavin-2. Using immunofluorescence (**Figure 32 and 33**) the presence of cavin-2 at the cardiomyocyte membrane was first assessed in the heart from wild-type (C57BL/6J) mice, revealing the expression of cavin-2 at the membrane and at the capillaries (**Figure 32 B**, white arrows indicating the cardiomyocyte membrane and yellow arrows pointing to the capillaries). When full-length dystrophin is absent from the membrane of mdx[5cv] cardiomyocytes, cavin-2 appears to be discontinuous and punctate at the membrane and diffuse in the cytoplasm (**Figure 32 B**). In the hearts of mice expressing the cardiac ΔR4-R23/ΔCT micro-dystrophin construct, cavin-2 staining remains disrupted at the membrane. As per cavin-1, cavin-2 localisation is preserved at the capillaries (Hansen, Shvets et al. 2013) of mdx[5cv] and mdx[5cv]-µDys mice where dystrophin and micro-dystrophin are not expressed (**Figure 30**). Overall, cavin-2 membrane localisation seems to be affected by the loss of full-length dystrophin appearing punctate and discontinuous. It was not possible to quantify cavin-2 membrane

fluorescence intensity, due to the increased intracellular staining in cardiomyocytes from mdx^{5cv} and mdx^{5cv}-µDys mice.
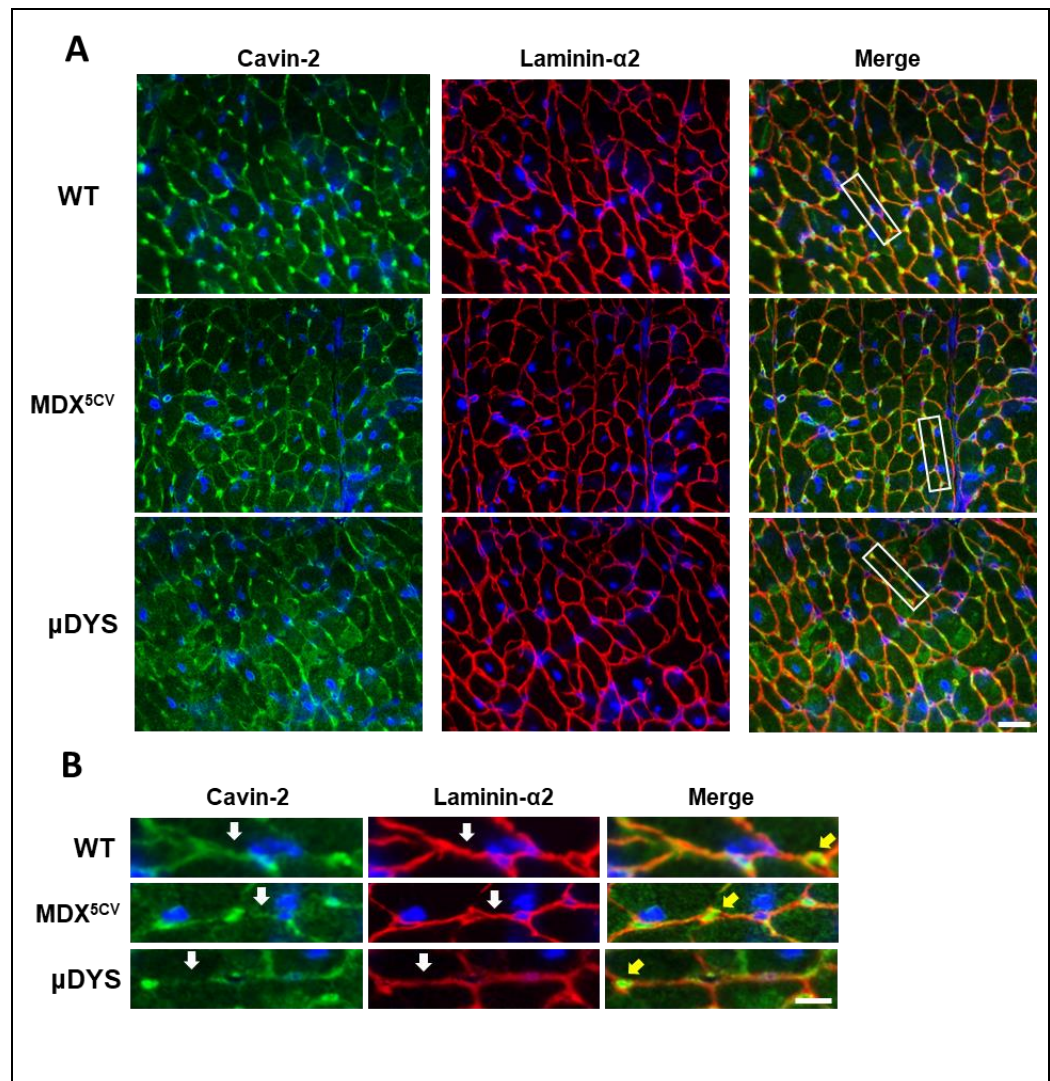
Figure 32.Disruption of cavin-2 cardiomyocyte lateral membrane localisation in absence of full-length dystrophin.

A. Immunostaining of cardiac cryosections from 8-month-old male C57BL/6J, mdx^{5cv} and µDys mice with antibodies against cavin-2 and laminin-α2 (red). 40X magnification, scale bar: 25µm. (N=3/genotype group). **B**. Enlarged pictures of figure **A** with cardiomyocyte lateral membranes indicated with white arrows and capillaries indicated with yellow arrows. 40X magnification, scale bar: 15µm. Nuclei stained with DAPI (blue).
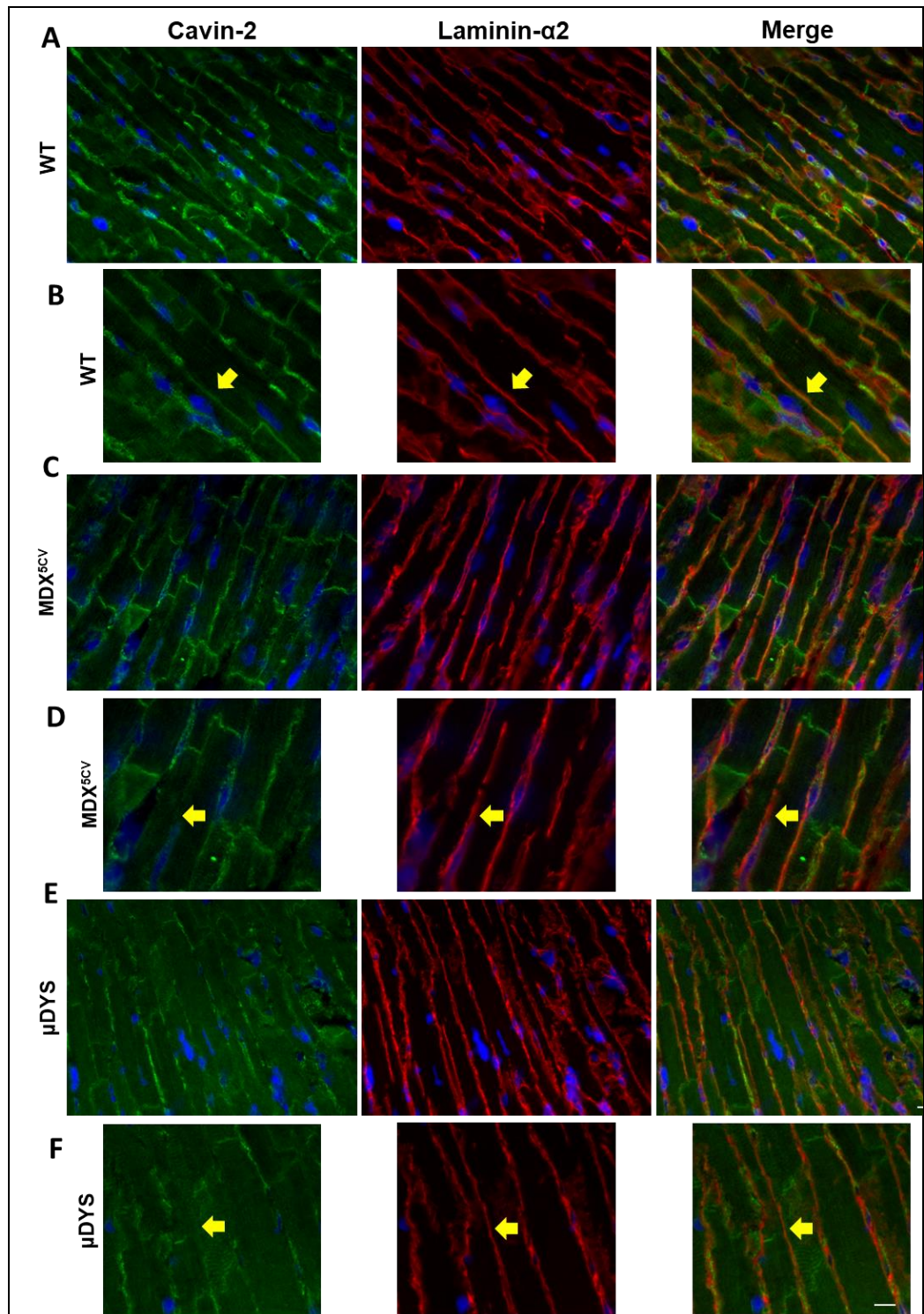
Figure 33.Cavin-2 staining is discontinuous at the cardiomyocyte lateral membrane of mdx^{5cv} and µDys mice.

A, C and E. Immunolabelling for cavin-2 (green) and laminin-α2 (red) on cardiac sections from 8-month-old male C57BL/6J (WT), mdx^{5cv} and µDys mice. Nuclei stained with DAPI (blue). 40X magnification, scale bar: 15µm. **B, D and F**. Enlarged pictures of A with yellow arrows pointing to

cardiomyocyte membrane. Nuclei stained with DAPI (blue). 40X
magnification, scale bar: 10µm (N=3/genotype group).

- ## Cavin-4

Cavin-4 is the only muscle-specific cavin and is expressed in smooth,
skeletal, and cardiac muscle (Ogata, Ueyama et al. 2008). Although it
has been described as a dispensable protein for the formation of
caveolae it appears to have a role in their morphology (Ogata, Naito et
al. 2014). Ogata and colleagues showed the capacity of cavin-4 to
increase the area of cardiac caveolae of transgenic mice that over
express cavin-4 compared to wild-type mice (Ogata, Naito et al. 2014).
Moreover, it has been reported that in the heart, cavin-4 is involved in
signalling pathways affecting calcium homeostasis (Malette,
Degrandmaison et al. 2019), cardiac function and conduction disturbance
(Ogata, Ueyama et al. 2008) and the gene encoding for cavin-4 is also
been associated with dilated cardiomyopathy (Nouhravesh, Ahlberg et al.
2016). An association between cavin-2 and cavin-4 has been reported
(Ogata, Ueyama et al. 2008). None of the studies reported above
assessed the cardiac localisation of the cavin-4 protein. As shown in
Figure 32 and **33** cavin-2 is located at the cardiomyocyte membrane of
wild-type (C57BL/6J) mice and is disrupted when full-length dystrophin is
not expressed in mdx[5cv] and mdx[5cv]-µDys hearts. As well as cavin-1 and
cavin-2, cavin-4 is localised at the cardiomyocyte lateral membrane of
wild-type (C57BL/6J) mice, exhibiting a strong and homogenous staining.
The cavin-4 staining diminishes appreciably at the cardiomyocyte
membrane of mdx[5cv] and mdx[5cv]-µDys mice (**Figure 34 A and B**). Cavin-
4 is localized at the intercalated discs of wild-type, mdx[5cv] and mdx[5cv]-
µDys mouse hearts (**Figure 35**) suggesting that its localisation is not

dependent on full-length dystrophin that is not expressed in mdx^{5cv} and mdx^{5cv}-µDys hearts. The quantification of cavin-4 fluorescence intensity shows a >2-fold reduction of cavin-4 staining at the cardiomyocyte membrane of mdx^{5cv} and mdx^{5cv}-µDys mice confirming that the loss of full-length dystrophin is associated with the disruption of cavin-4 at the sarcolemma.
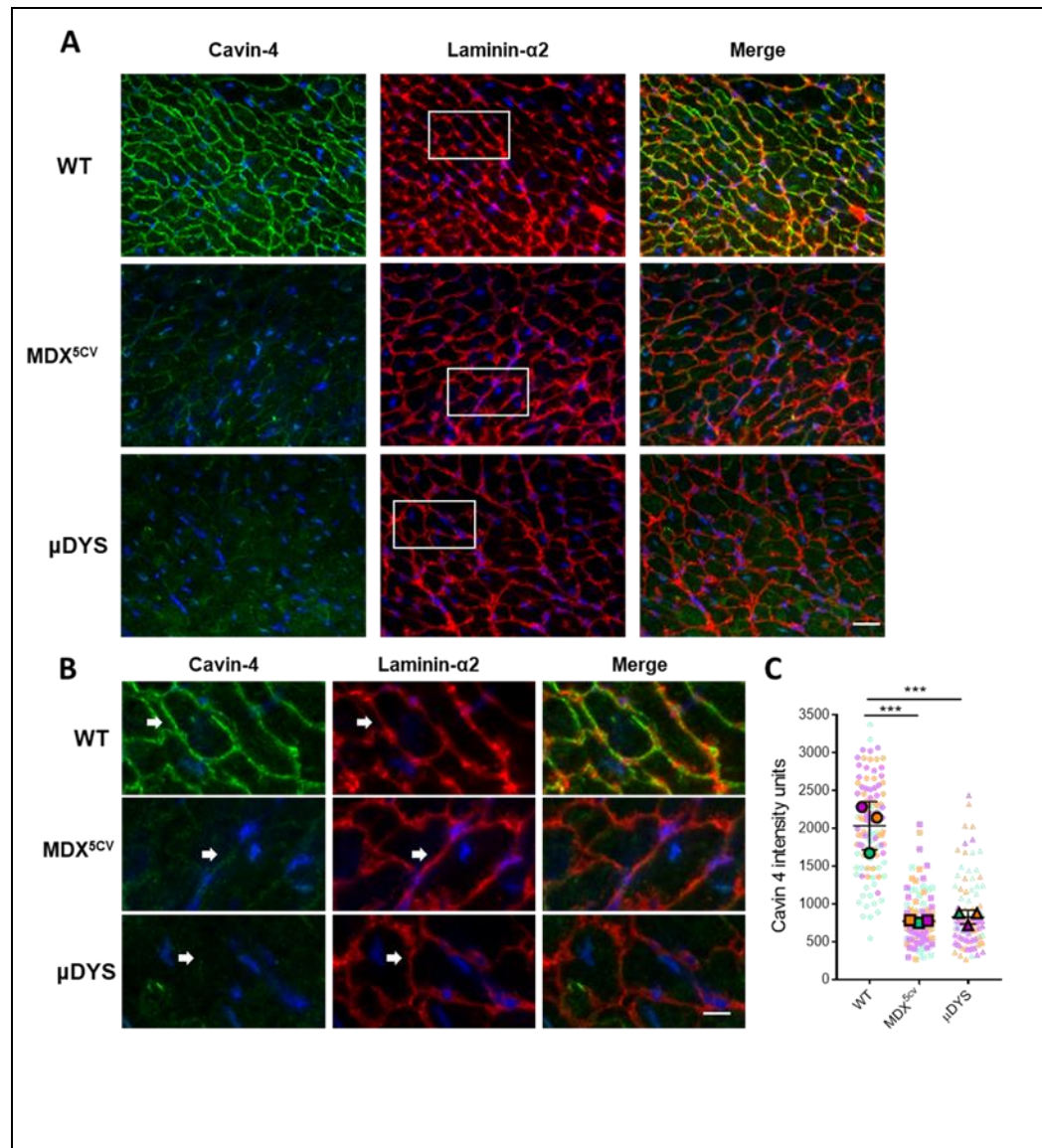
Figure 34. Cavin-4 membrane expression is lost in mdx^{5cv} and µDys hearts.

A. Immunolabelling of cardiac cryosections from 8-month-old male WT, mdx^{5cv} and micro-dystrophin mice for cavin-4 (green) and laminin-α2 (red). Nuclei stained with DAPI (blue). 40X magnification, scale bar: 25µm. B. Magnified pictures of panel A showing in more detail the cavin-

4 staining at the WT cardiomyocyte lateral membrane (white arrows) and its disruption in the mdx^{5cv} and μDys lateral membrane. Scale bar: 15μm.
C. Cavin-4 membrane intensity quantification represented by superplots where the small dots depict the 120 measurements taken for each of 3 sample of each group (groups= C57BL/6J, mdx^{5cv} and ΔR4-R23/ΔCT micro-dystrophin). The mean of the measurements for each mouse is depicted by the bigger dots (N=3/group). The mean ± standard deviation is indicated by the lines. *** p<0.005.
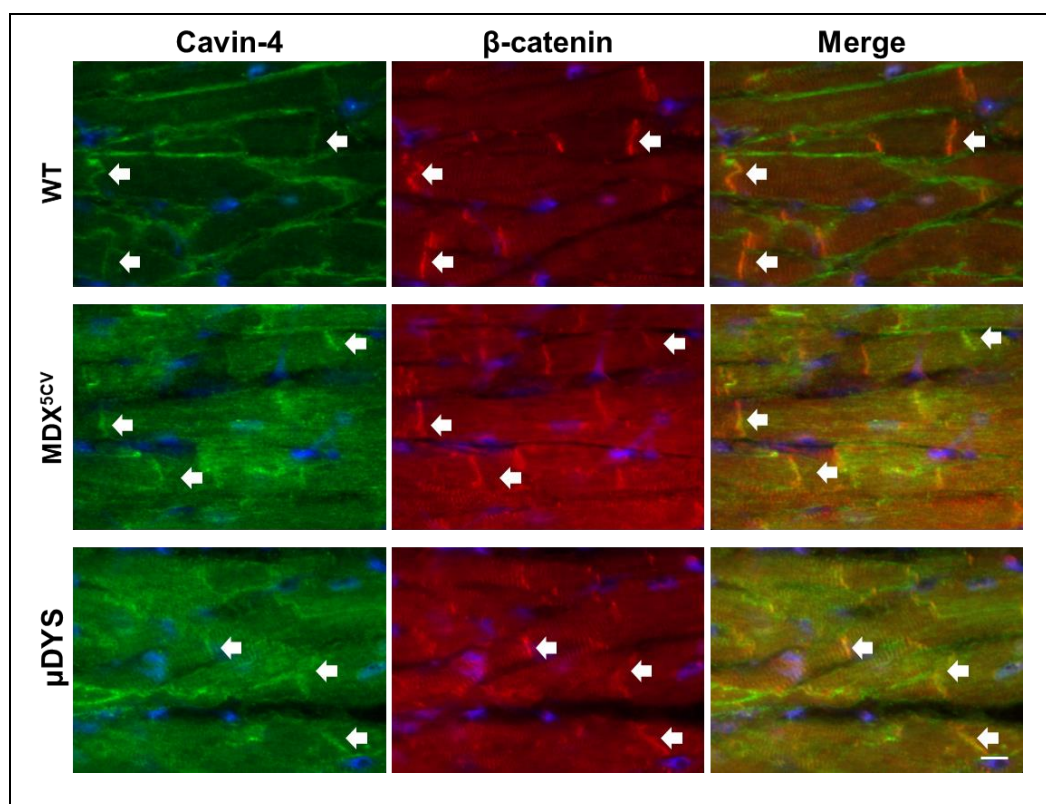
Figure 35. Cavin-4 is expressed at the intercalated discs of wild-type, mdx^{5cv} and ΔR4-R23/ΔCT micro-dystrophin mice.

Double labelling of cardiac tissue sections from wild-type, mdx^{5cv} and ΔR4-R23/ΔCT micro-dystrophin mice for cavin-4 (green) and β-catenin (red). White arrows pointing to intercalated discs positive for cavin-4 and β-catenin. Nuclei stained with DAPI (blue). 40X magnification. Scale bar: 25μm. (N=3 mice/group).

4.2.2 Cavin-4 abnormal peri-nuclear localisation in mdx^{5cv} and ΔR4-R23/ΔCT micro-dystrophin mice

Another interesting finding arose from my observations of cardiac tissue sections from wild-type (C57BL/6J), mdx^{5cv} and mdx^{5cv}-μDys mice stained for cavin-4 and DAPI to visualize the nuclei. Cavin-4 appears to be abnormally localized in the peri-nuclear region when full-length dystrophin is absent (**Figure 36 A**). Using DAPI and laminin-α2 in order to identify nuclei present inside the cardiomyocytes and to distinguish them from the nuclei present in the interstitial space (**Figure 36 B**), the number of nuclei stained with cavin-4 found inside the cardiomyocytes were counted. Two hundred nuclei were counted for each sample of each of the 3 genotype groups (N=3/group) (**Figure 36 C**). In wild-type mice, cavin-4 is present in 26% ± 6 of nuclei while in mdx^{5cv} 67% ± 10 of nuclei had cavin-4 staining. In the hearts of mdx^{5cv}-μDys mice, cavin-4 is present in 85% ± 3 of nuclei. These results suggest that the cavin-4 peri-nuclear localization is associated with its loss from the cardiomyocyte membrane.
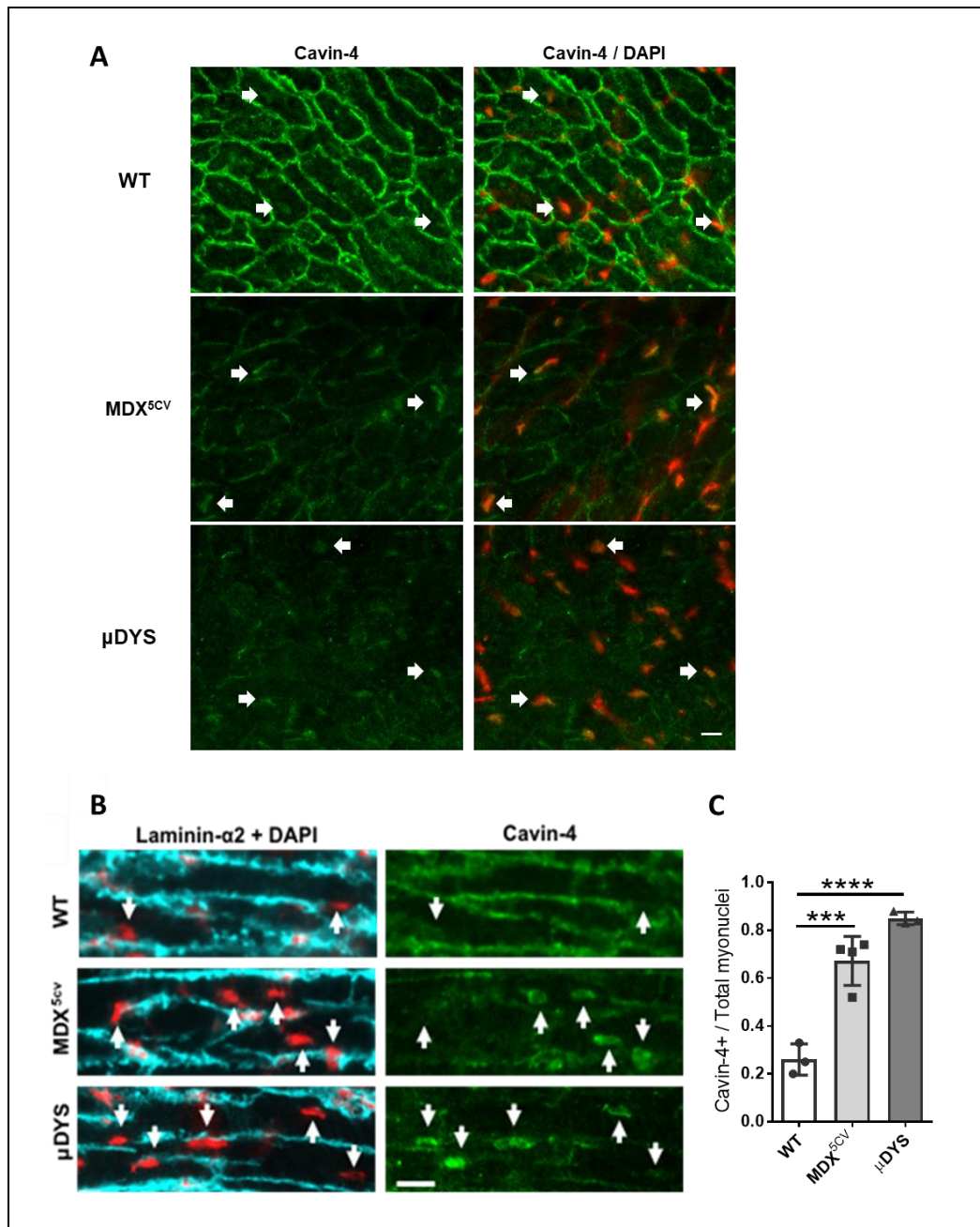
Figure 36. Peri-nuclear abnormal localisation of cavin-4 in hearts of mdx^5cv and micro-dystrophin mice.

A*. Cardiac sections from 8-month-old male mice wild-type, mdx^5cv and micro-dystrophin mice stained with cavin-4 with nuclei stained with DAPI (red). White arrows indicate nuclei stained with cavin-4. 40X magnification, scale bar 10µm. **B**. Triple staining of wild-type, mdx^5cv and micro-dystrophin hearts for laminin-α2 (light blue), cavin-4 and nuclei stained with DAPI (red). White arrows indicate only the nuclei located within cardiomyocytes. 40X magnification, scale bar 25µm. **C**.*

Quantification of nuclei stained with cavin-4 relative to the total number of nuclei located within the cardiomyocyte. N=3 mice/group.

4.2.3 Evaluation of caveolae by Electron Microscopy

In **4.2.1**, I assessed the effect that the loss of full-length dystrophin has on the cardiac localisation of cavin-1, -2 and -4. I showed that the expression of full-length dystrophin at the cardiomyocyte membrane is necessary for the membrane localisation of the cavins. This begs the question of how the loss of the cavins at the cardiomyocyte membrane impact caveolae in the heart. In fact, electron microscopy studies on the heart from cavin-1 knock-out mice revealed an almost flat cardiomyocyte membrane in these mice (Taniguchi, Maruyama et al. 2016) demonstrating the essential role of cavin-1 in the biogenesis of caveolae. It is fair to hypothesise that the disruption of cavin-1 at the cardiomyocyte membrane of mdx^{5cv} mice could cause the reduction or a disruption of caveolae in their hearts. To visualise the ultrastructure of caveolar in wild-type and mdx^{5cv} mice and to assess potential changes in the number (reduction) and the shape (disruption) of caveolae per cardiomyocyte I have performed electron microscopy (EM) experiments. During the systolic phase the cardiac muscle is contracted to pump the blood out of the heart whereas during the diastolic phase the heart is relaxed, and the cardiac chambers are filled with blood (**Figure 37**).
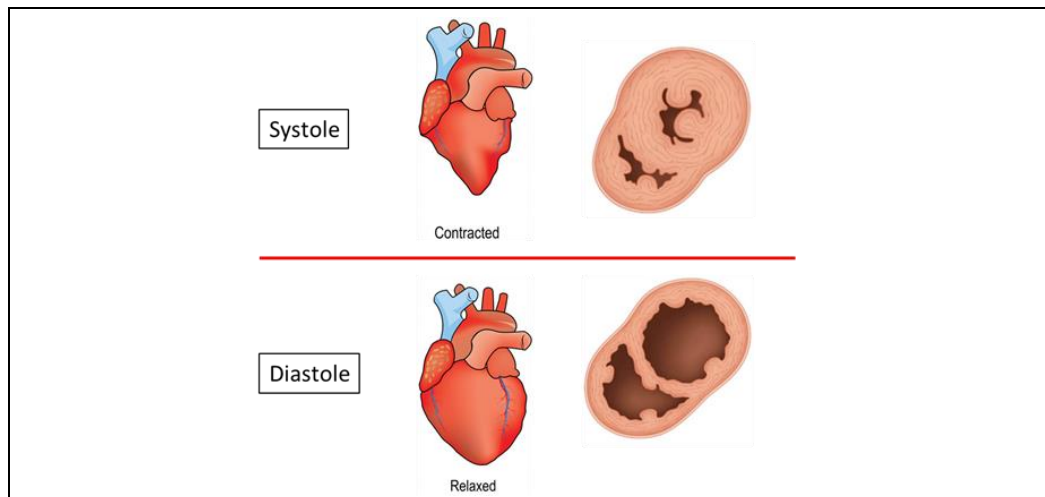
Figure 37. Diagrammatic representations showing the morphology of the heart during systole and diastole.

Diagram of the hearts during systole and diastole showing that during systole the cardiac muscle is contracted and during diastole the cardiac muscle is relaxed, and ventricles are dilated.

The morphology of the membrane changes when the cardiac muscle is contracted during systole and is stretched during diastole (Hanft, Korte et al. 2008). Studies on rabbit (Pfeiffer, Wright et al. 2014) and mouse (Kohl, Cooper et al. 2003) hearts showed a decreased number of caveolae when the heart is relaxed and cardiomyocytes are stretched (diastole) and an increased number of caveolae during cardiac contraction when cardiomyocytes are shortened (systole). Moreover, during cardiac contraction and relaxation, the sarcomere length changes from ~1.8 µm to 2.3 µm respectively (Wu, Cazorla et al. 2000, Hanft, Korte et al. 2007).

The first experiments I performed were conducted in order to find the best cardiac preparation for the electron microscopy experiments, to visualise caveolae in the heart of wild-type and mdx[5cv] mice. Therefore, two different buffers were used to achieve systolic and diastolic cardiac

arrest in wild-type mice (**2.5** materials and methods) and the sarcomere length was measured to assess the relaxed or contracted status of the hearts. The buffers were administered by intra-aortic infusion (**Figure 38**) (**2.5** materials and methods).
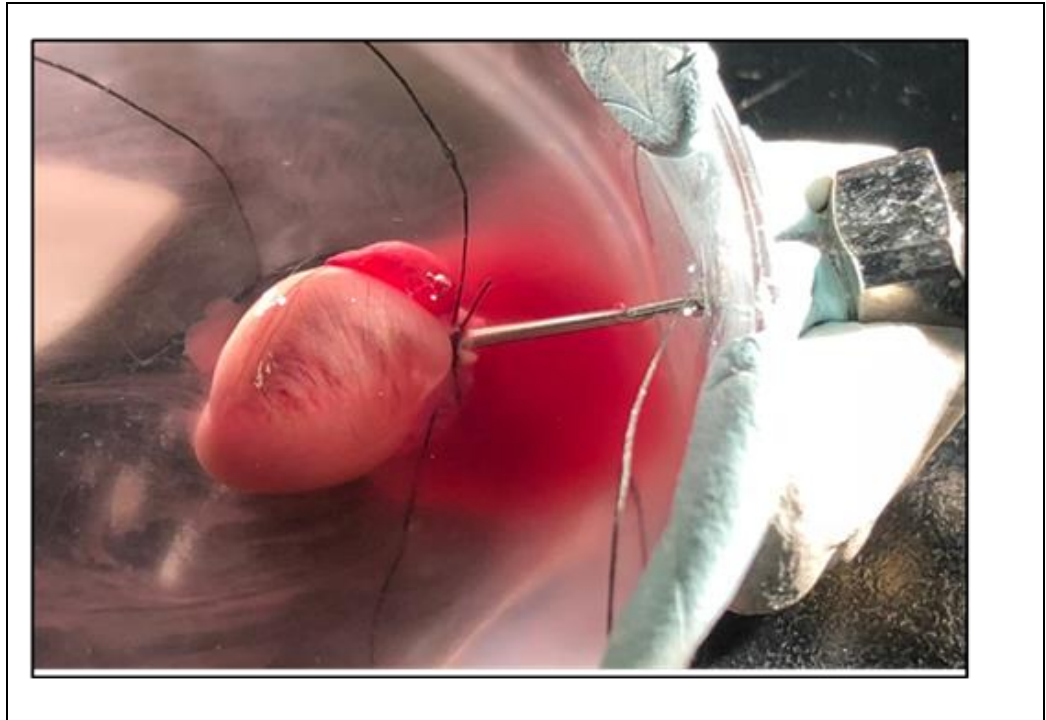
Figure 38. Heart during the perfusion with the diastolic buffer.

Picture showing heart perfusion. The heart was placed on a petri dish filled with the perfusion buffer. An 18G cannula is inserted in the aorta and secured with 2 loops of black silk suture thread

Cutting the heart transversally (**Figure 39**) gave me the possibility to check the relaxed or contracted status of the ventricles in order to assess the efficacy of the diastolic and systolic buffer.
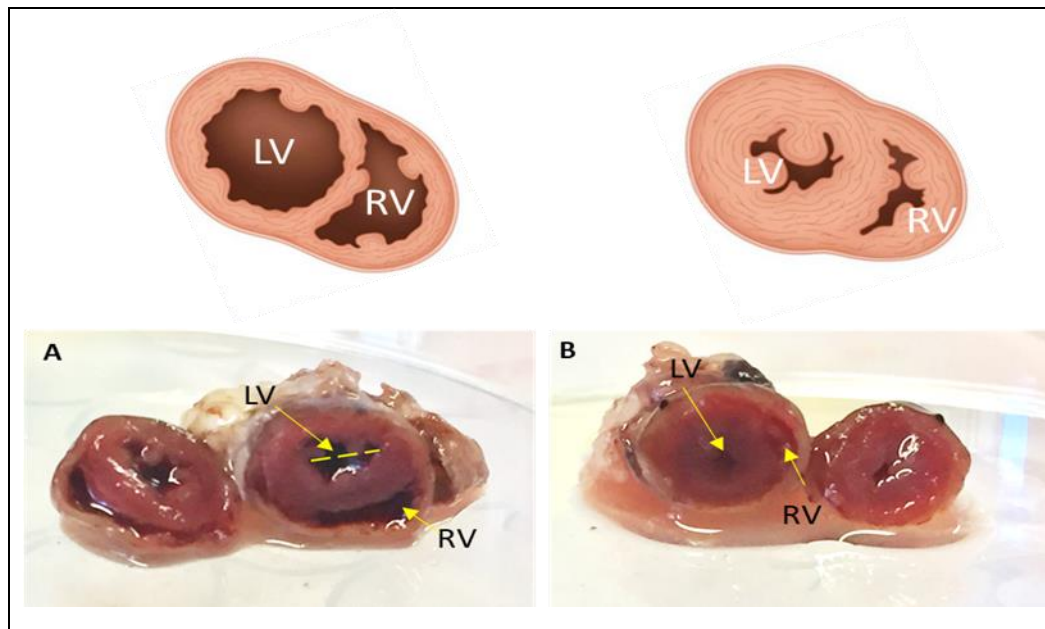
Figure 39. Transversal cut of the perfused hearts to assess their status.

Cardiac arrest in diastole (A) were the left and right ventricles (LV and RV) are dilated and in systole (B) where the ventricles are contracted following perfusion with the diastolic and systolic buffer.

The first sets of cardiac sample preparations for EM were performed by the UCL Electron Microscopy Laboratory Core Facility that processed the whole perfused heart. Because of the impossibility to cut the heart transversally and check the status of the hearts before the sample processing for EM, I have assessed the systolic and diastolic arrest directly on EM measuring the sarcomere length (**Figure 40**). Measuring the sarcomere length, I found no differences between the measurements of the hearts arrested with the diastolic and the systolic buffers (~2.5µm) and I concluded that while the diastolic arrest was consistently achievable, the systolic arrest was not achievable with consistency (**Figure 40**).
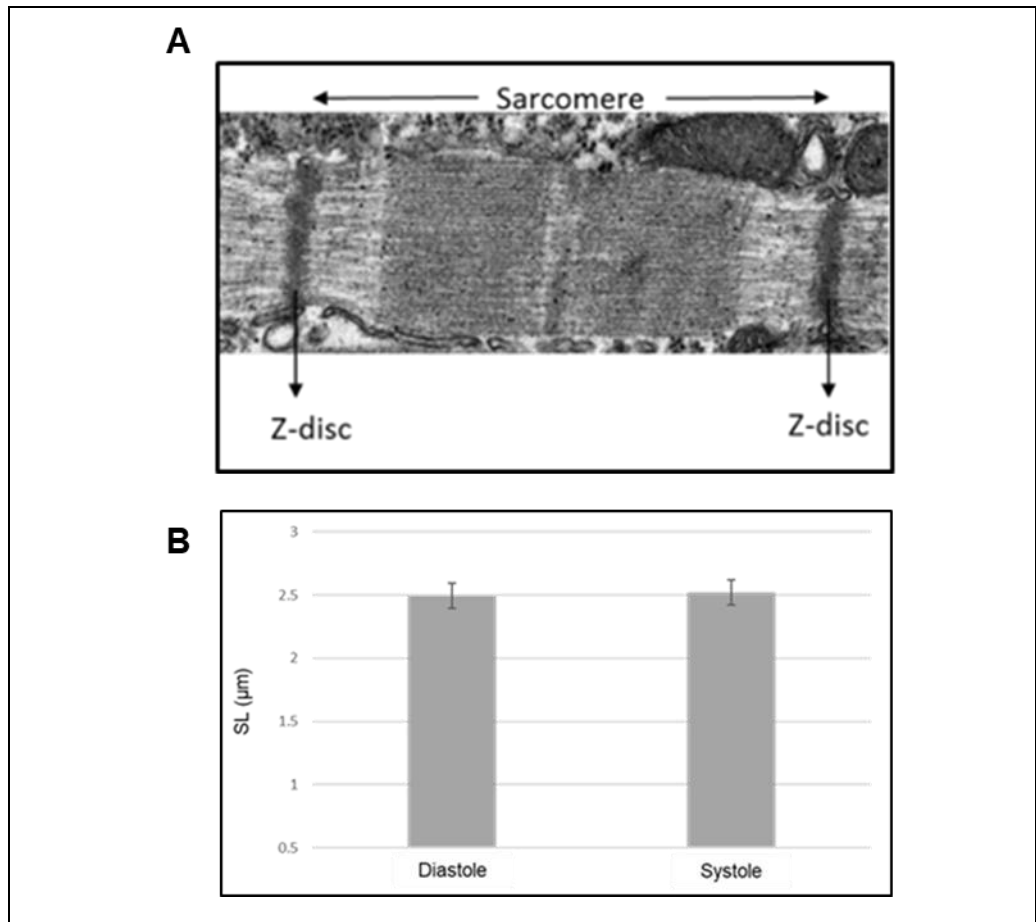
Figure 40. Calculation of sarcomere length between Z-discs using the ImageJ software.

(A) The sarcomere length was calculated as the distance between two Z-lines. (B) No difference was detected in the sarcomere length of the samples perfused with the diastolic and the systolic buffers.

Therefore, I opted for perfusing the hearts with a diastolic buffer and then compered the number of caveolae in wild-type and mdx[5cv] hearts. I have used a buffer made with 2.5% potassium citrate in Hank's balanced salt solution to arrest the mouse heart in diastole (Dae, Heymann et al. 1982). These second attempts at cardiac perfusion were performed by the UCL Queen Square Institute of Neurology (ION) where the technical manager Kerrie Venner and her group prepared the hearts for electron

microscopy acquisitions that I conducted after being trained. After

perfusion, the heart was placed in fixative solution (**2.4** materials and

methods) for two hours at 4°C and sent to the EM facility. I observed

signs of good perfusion such as the absence of blood into the capillary

lumen (**Figure 41 A**). A good tissue preservation was achieved as the Z-

lines (Z) that delineate the sarcomeres and the mitochondria (M)

between the myofibrils were clearly visible (**Figure 41 B**). However, I was

not able to consistently achieve well preserved cardiomyocyte

membranes necessary to clearly visualize the caveolae (**Figure 41 B**).
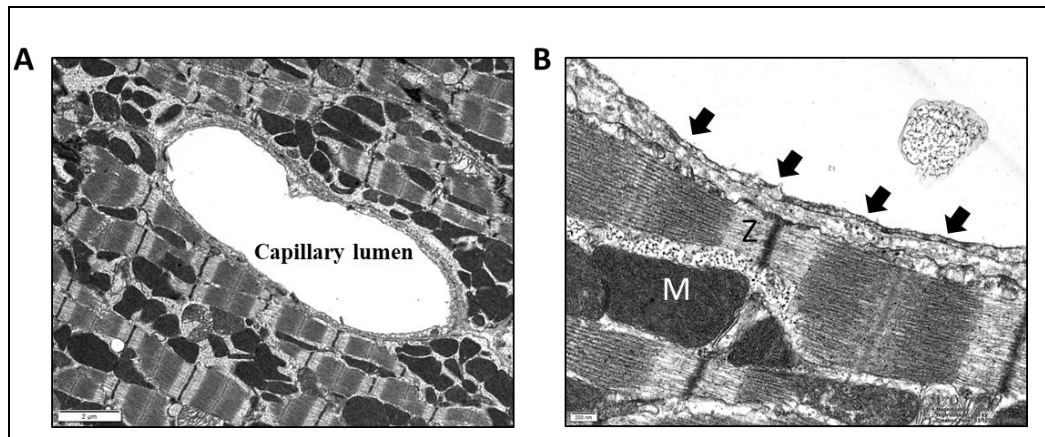
Figure 41. Cardiac section from wild-type mouse acquired with the EM.

*(**A** and **B**). No blood was present into the capillary lumen indicating a good perfusion (**A**). Membrane damage (arrows) on the cardiac EM preparation. Z-lines (**Z**) and mitochondria (**M**) (**B**).*

I was not able to carry on with these experiments because of the covid-

19 pandemic. Due to the lockdown, a limited access to the EM facility

was imposed. The following steps would have focused on finding a

fixation method in order to preserve the membrane integrity. I wanted to

add paraformaldehyde (Roth, Bader et al.) to the fixation buffer as

suggested by Karnovsky (Karnovsky 1965). The addition of PFA to the

glutaraldehyde and cacodylate in the fixation buffer have been described as an optimal solution to improve the quality of fixation in terms of avoiding tissue distortions (Shah, Johansson et al. 2015).

4.2.4 Loss of cavin-1 and cavin-4 in mdx[5cv] cardiomyocytes before the onset of cardiac pathological changes

The mice used for the experiments in section 4.2.1 and 4.2.2 were 8 months of age. Data published from our group showed that mdx[5cv] hearts develop cardiac pathological changes by 6 months of age. Specifically, we reported fibrosis and immune cell infiltration in mdx[5cv] mice between 6 and 12 months of age (Wang, Marrosu et al. 2021). The results of **4.2.1** on mdx[5cv] hearts, showed a disruption of cavin-1 and cavin-4 at 8 months of age, when the heart has already been subject to damage caused by the loss of dystrophin at the plasma membrane (Han, Bansal et al. 2007). Therefore, it was important to assess whether the loss of cavin-1 and cavin-4 observed in mdx[5cv] hearts at 8 months of age when the cardiomyocyte membrane is damaged could be attributed to the loss of dystrophin, or as consequence of the membrane fragility. The mdx[5cv] mice show late onset of cardiac fibrosis, similar to the mdx[23] mice (Gavillet, Rougier et al. 2006, Dorchies, Reutenauer-Patte et al. 2013). Therefore, in order to investigate the localisation of cavin-1 and cavin-4 before the onset of cardiac histopathology, hearts from wild-type (C57BL/6J) and mdx[5cv] mice of 9 weeks of age were immunolabelled for cavin-1 and cavin-4 (**Figure 42**). Mdx[5cv] showed the same cavin-1 and -4 impairment observed in older mdx[5cv] mice (8 months of age) (**Figure 29 and 34**). These data are also in agreement with the immunofluorescence analysis (**4.2.1**) showing that mdx[5cv]-μDys hearts have a disruption in

cavin-1 and cavin-4, even though this construct is able to prevent cardiac pathological changes (Wang, Marrosu et al. 2021).
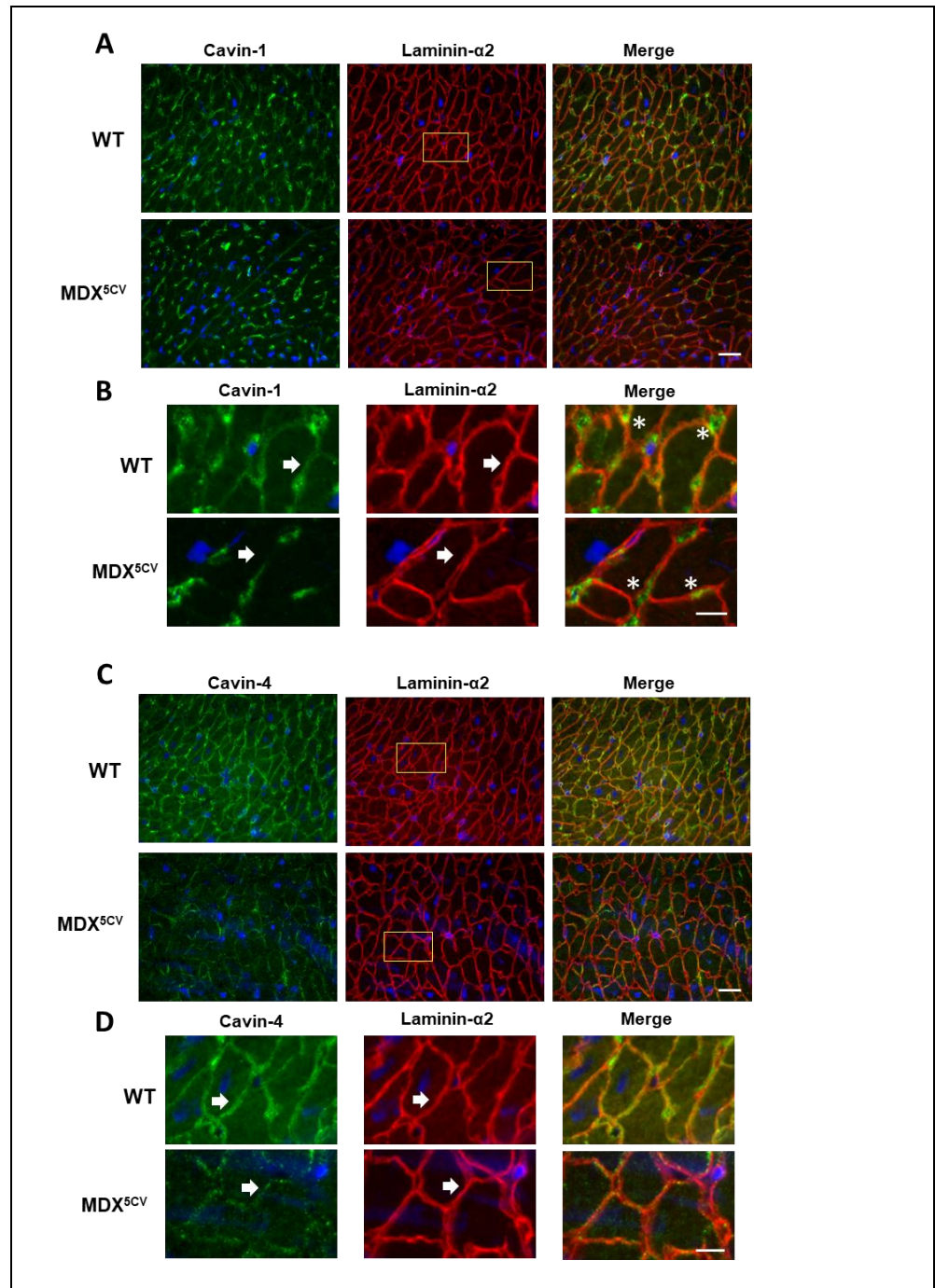
Figure 42. Cavin-1 and cavin-4 are disrupted before the onset of cardiac histopathology in mdx^{5cv} mice.

A and B. Triple staining of cardiac tissue sections from 9-week-old male wild-type and mdx^{5cv} mice for cavin-1 (green) and laminin-α2 (red). Nuclei stained with DAPI (blue). B. Enlargements of figure A showing the cavin-1 lost at the cardiomyocyte lateral membrane (white arrows) of mdx^{5cv} mouse. Cavin-1 is preserved at the capillaries (white asterisks) in mdx^{5cv} hearts. Scale bar 10um. C and D Immunolabelling for cavin-4 and laminin-α2 (red) on cardiac tissue sections from 9-week-old wild-type and mdx^{5cv} mice. Nuclei stained with DAPI (blue). D. Enlarged pictures from panel C where the loss of cavin-4 from the mdx^{5cv} cardiomyocyte lateral membrane is appreciable. Scale bar 10um. A and C. 40X magnification; Scale bar 25um.

4.3 Hinge 2, Hinge 3, repeats 20-24 and the C-terminus of dystrophin are not involved in the binding with cavin-4

The data collected on transgenic mice expressing the cardiac ΔR4-R23/ΔCT micro-dystrophin revealed its inability to restore cavin-1, cavin-2 and the muscle specific cavin-4 membrane localisation (**4.2**). The cause of this lack of restoration of the cavins could be attributed to the possibility that this dystrophin construct does not have specific domains that are involved in the binding with the cavins. These findings leave open the question concerning the identification of the dystrophin binding site for caveolar proteins in the heart. In order to narrow down the possible dystrophin domain involved in the link between cavin-1 and the muscle specific cavin-4, I performed immunohistochemical analyses in transgenic mice expressing different micro- and mini-dystrophin constructs (**Figure 43**). The four transgenic mdx[23] mouse lines (**Figure 43**) were generated by Dr Duan's lab at the University of Missouri and

express the following constructs under the control of the cardiac myosin promoter:

1. The **ΔR4-R23 micro-dystrophin** (Harper, Crawford et al. 2002) that is identical to the ΔR4-R23/ΔCT micro-dystrophin, except that it includes the unique C-terminus of dystrophin.

2. The **ΔH2-R19/ΔCT mini-dystrophin** that, compared to ΔR4-R23/ΔCT micro-dystrophin, lacks hinge 2 but includes hinge 3 and spectrin repeats 20 to 23.

3. The **ΔH2-R19 mini-dystrophin** (Li, Kimura et al. 2006) that is identical to ΔH2-R19/ΔCT mini-dystrophin (Li, Kimura et al. 2006) except that it includes the C-terminal domain.

4. The **ΔH2-R15 mini-dystrophin** (Lai, Thomas et al. 2009, Wasala, Shin et al. 2018) that carries the C-terminus domain and spectrin repeats 16-19.
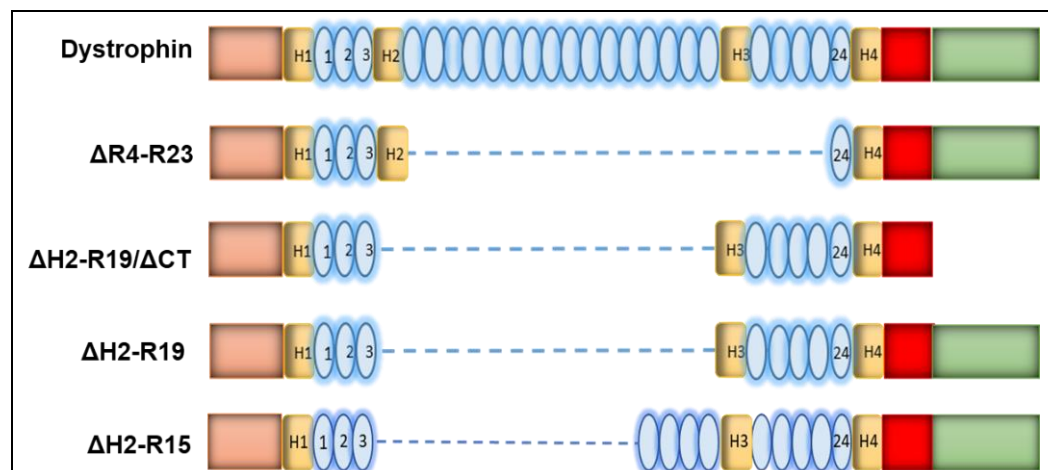
Figure 43. Schematic representation of the micro and mini-dystrophin constructs used for this project.

*Orange boxes represent the N-terminus, hinges in yellow (**H1**, **H2**, **H3**, **H4**), the red boxes represent the cysteine-rich domain, C-terminus represented by the green boxes, spectrin-like repeats (light blue numbered ovals).*

4.4 The disruption of cavin-1 and cavin-4 is influenced by the genetic background of mdx[23] mice.

These transgenic mice expressing the constructs represented on **figure 43** are mdx[23] (**1.3.2**), on C57BL/10 background except for the ΔH2-R15 mini-dystrophin that are mdx[23] on the FVB background. Therefore, I first checked whether I could detect the same cavin-1 and cavin-4 mis-localisation observed in mdx[5cv] on the C57BL/6J background and whether the different genetic background of the mdx[23] (C57BL/10 and FVB) could differently affects cavin-1 and cavin-4 localisation.

I first performed immunofluorescence experiments on C57BL/10 and FVB hearts (**Figure 44 A and B**) to assess any difference in the cavin-1 localisation. Cavin-1 is expressed at the cardiomyocyte lateral membrane and at the capillaries in both C57BL/10 and FVB mice.

In mdx[23] mice on an FVB background, cavin-1 is not lost at the cardiomyocyte membrane and preserved at the capillaries (**Figure 44 C and D**). In the heart from mdx[23] mice on a C57BL/10 background, cavin-1 is lightly diffuse in the cytoplasm and a faint staining is visible at the cardiomyocyte membrane (**Figure 44 C and D**).
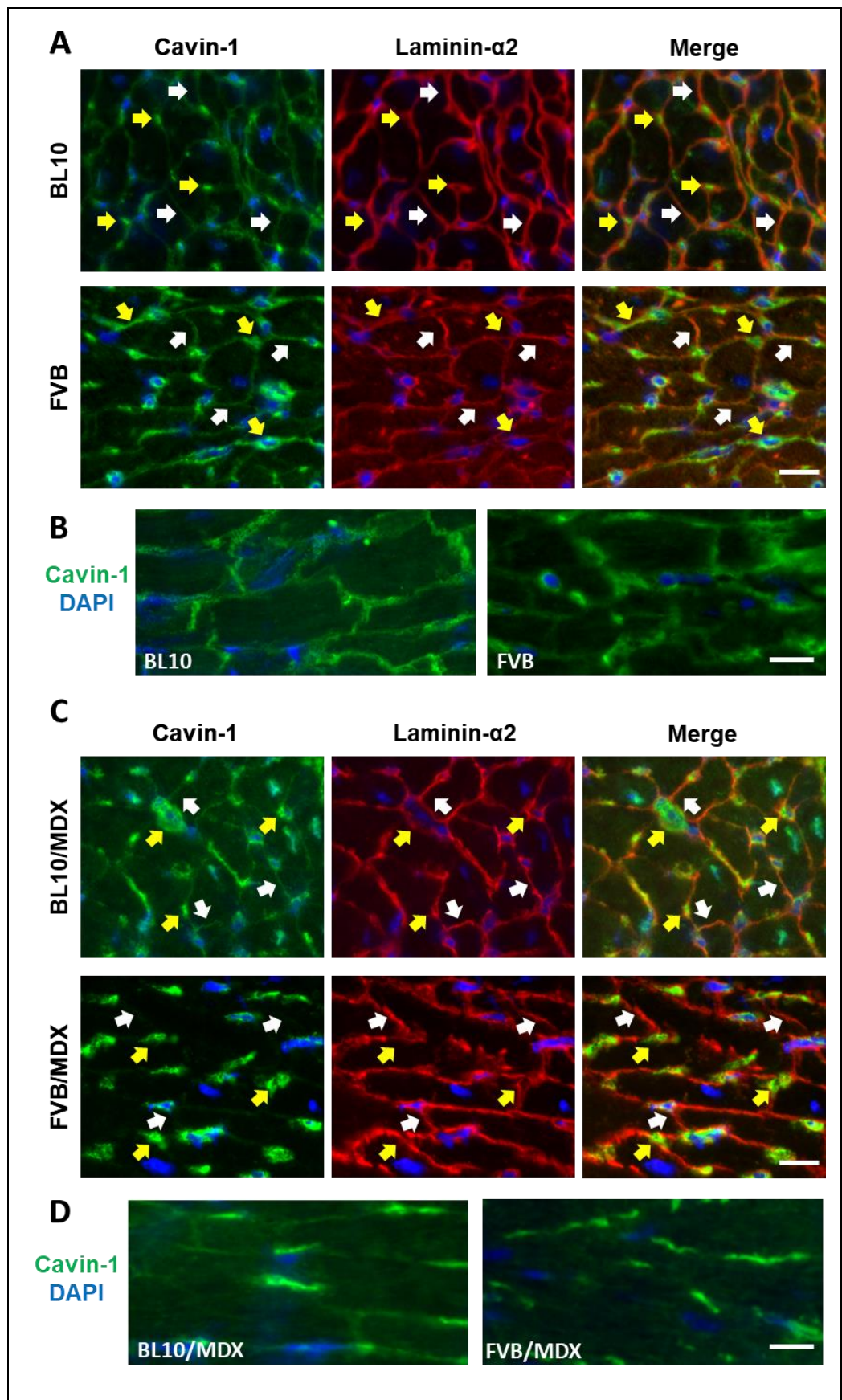
Figure 44. Different disruption levels of cavin-1 in hearts from mdx[23] mice on C57BL/10 and FVB background.

A and B. Cardiac sections from C57BL/10 and FVB mice stained for cavin-1 (green) and laminin-α2 (red). A. White arrows pointing to the membrane staining of cavin-1 and the yellow arrows pointing to cavin-1 at the capillaries. Capillaries are surrounded by the laminin-α2 staining. Nuclei stained with DAPI (blue). 40X magnification. Scale bar 15 μm (A), 10μm (B). C. Cardiac sections from mdx[23] mice on C57BL/10 and FVB background stained for cavin-1 (green) and laminin-α2 (red). Membrane staining of cavin-1 pointed with white arrows and capillaries pointed with yellow arrows. D. Cardiac sections from mdx[23] mice on C57BL/10 and FVB background stained for cavin-1. Nuclei stained with DAPI (blue). 40X magnification. Scale bar 15 μm (C), 10μm (D).

Cavin-4 (**Figure 45 A and B**) staining is visible at the cardiomyocyte lateral membrane of both C57BL/10 and FVB mice. In the hearts from mdx[23] mice on C57BL/10 background (**Figure 45 C and D**), a residual staining of cavin-4 is visible at the cardiomyocyte lateral membrane and also appears to distribute in the cytoplasm of mdx[23] mice in straight striations reminiscent of the t-tubules. This peculiar cytoplasmic distribution is not seen in mdx[23] mice on an FVB background. These data showed a different disruption of cavin-1 and -4 in the heart of mdx[23] mice that are on a different genetic background. Comparing them with the immunofluorescence data for cavin-1 and -4 collected from mdx[5cv] mice (C57BL/6J background), in the mdx[23] mice both cavin-1 and -4 are disrupted but not to the same extent as mdx[5cv]. The mdx[5cv] mice share the same pattern of disruption of cavin-1 and -4 staining with the mdx[23] mice that are on the FVB background where the loss of full-length dystrophin at the cardiomyocyte membrane is accompanied by the complete loss of both cavin-1 and -4 at the cardiomyocyte membrane.

Moreover, neither mdx^{5cv} mice nor mdx^{23} (FVB background) showed the striated cavin-4 staining observed in the cytoplasm of mdx^{23} mice (C57BL/10 background). These differences should be taking in account when choosing the best DMD mouse model for the study of caveolar proteins.
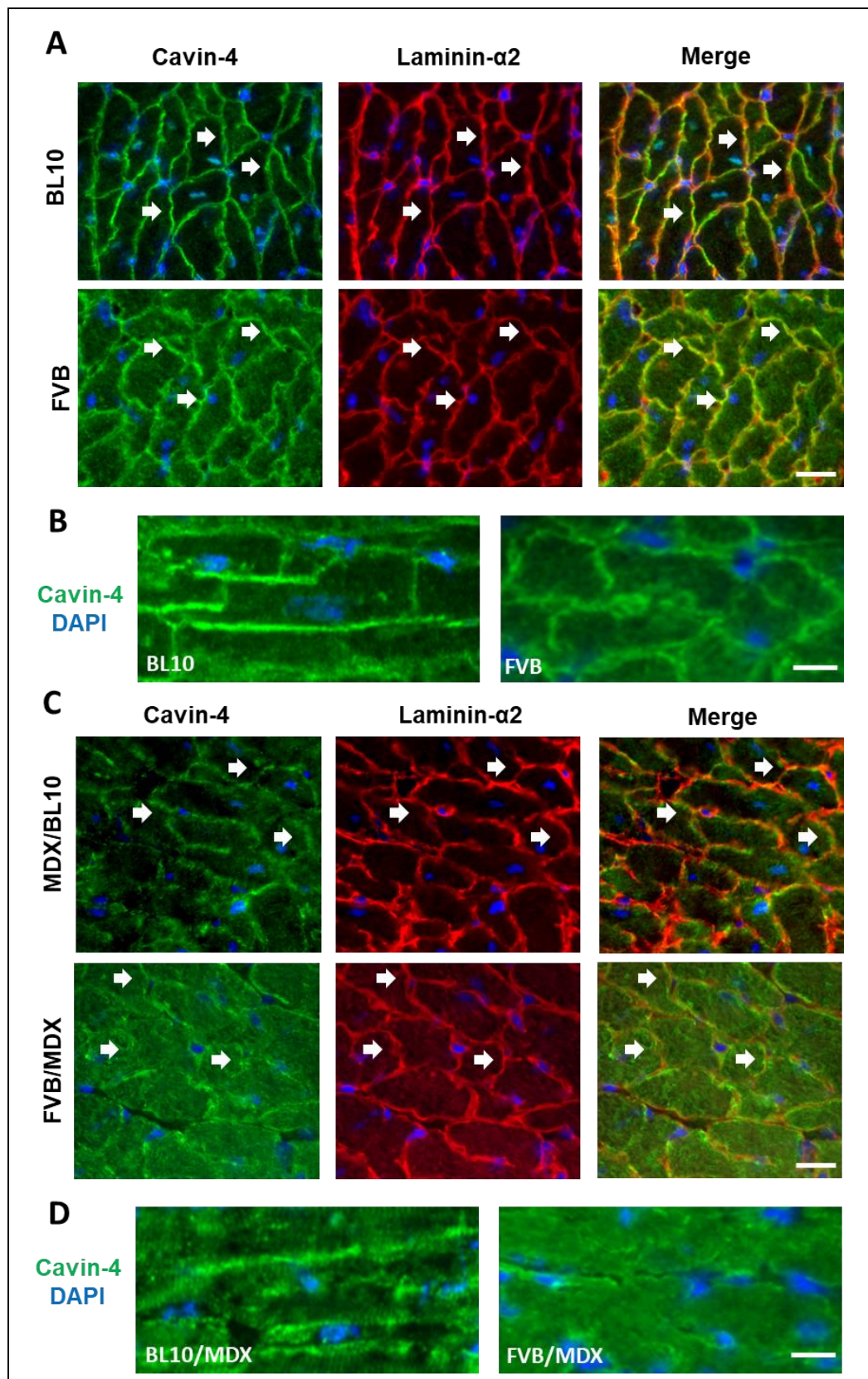
Figure 45. Different disruption levels of cavin-4 in hearts from mdx[23] mice on C57BL/10 and FVB background.

A and B. Cardiac sections from C57BL/10 and FVB mice stained for cavin-4 (green) and laminin-α2 (red). *A*. White arrows pointing to the

membrane staining of cavin-4 Nuclei stained with DAPI (blue). 40X magnification. Scale bar 15 µm (A), 10µm (B).C. Cardiac sections from mdx[23] mice on C57BL/10 and FVB background stained for cavin-4 (green) and laminin-α2 (red). Membrane staining of cavin-4 pointed with white arrows. D. Cardiac sections from mdx[23] mice on C57BL/10 and FVB background stained for cavin-4. Nuclei stained with DAPI (blue). 40X magnification. Scale bar 15 µm (C), 10µm (D).

The constructs showed in **figure 43** contain dystrophin regions that are not present in the ΔR4-R23/ΔCT micro-dystrophin construct. Three of them contain Hinge 3 and the C-terminus that are not present in the ΔR4-R23/ΔCT micro-dystrophin and one of them contains the spectrin repeats 16-19 that are candidates for a cardioprotective function (Kaspar, Allen et al. 2009) (**Figure 43**). The first three constructs were investigated only by immunofluorescence for cavin-4, due to insufficient samples being available to me, while the fourth construct (ΔH2-R15) was tested for both cavin-1 and cavin-4.

The wild-type samples (C57BL/10) showed a strong cavin-4 staining at the lateral membrane of the cardiomyocytes co-localizing with full-length dystrophin (**Figure 46 B and C**). In the mdx[23] hearts (C57BL/10), cavin-4 is present at the intercalated discs and, unlike mdx[5cv] mice where cavin-4 is barely visible at the cardiomyocyte lateral membrane, in the mdx[23] it is fainter and discontinuous compared to the control mice (C57BL/10). In hearts expressing **ΔH2-R19/ΔCT mini-dystrophin** and **ΔH2-R19 mini-dystrophin**, cavin-4 seems to be localised at the cardiomyocyte lateral membrane. However, at higher magnification (**Figure 46 C**), it was observed that cavin-4 localised at the end of structures, potentially T-tubules, instead of being uniform at the cardiomyocyte membrane as in wild-type (C57BL/10). Hearts from **ΔR4-R23 micro-dystrophin** have a

speckled and faint cavin-4 staining at the lateral membrane of the cardiomyocytes similar to the ΔR4-R23/ΔCT micro-dystrophin mice (**Figure 46 B and C**).

These results led me to exclude the possible involvement of the C-terminal domain of dystrophin in the binding with cavin-4. Moreover, the presence of hinge 2 and hinge 3 as well as the region between repeats 20-24 seems to be necessary for the binding with cavin-4.
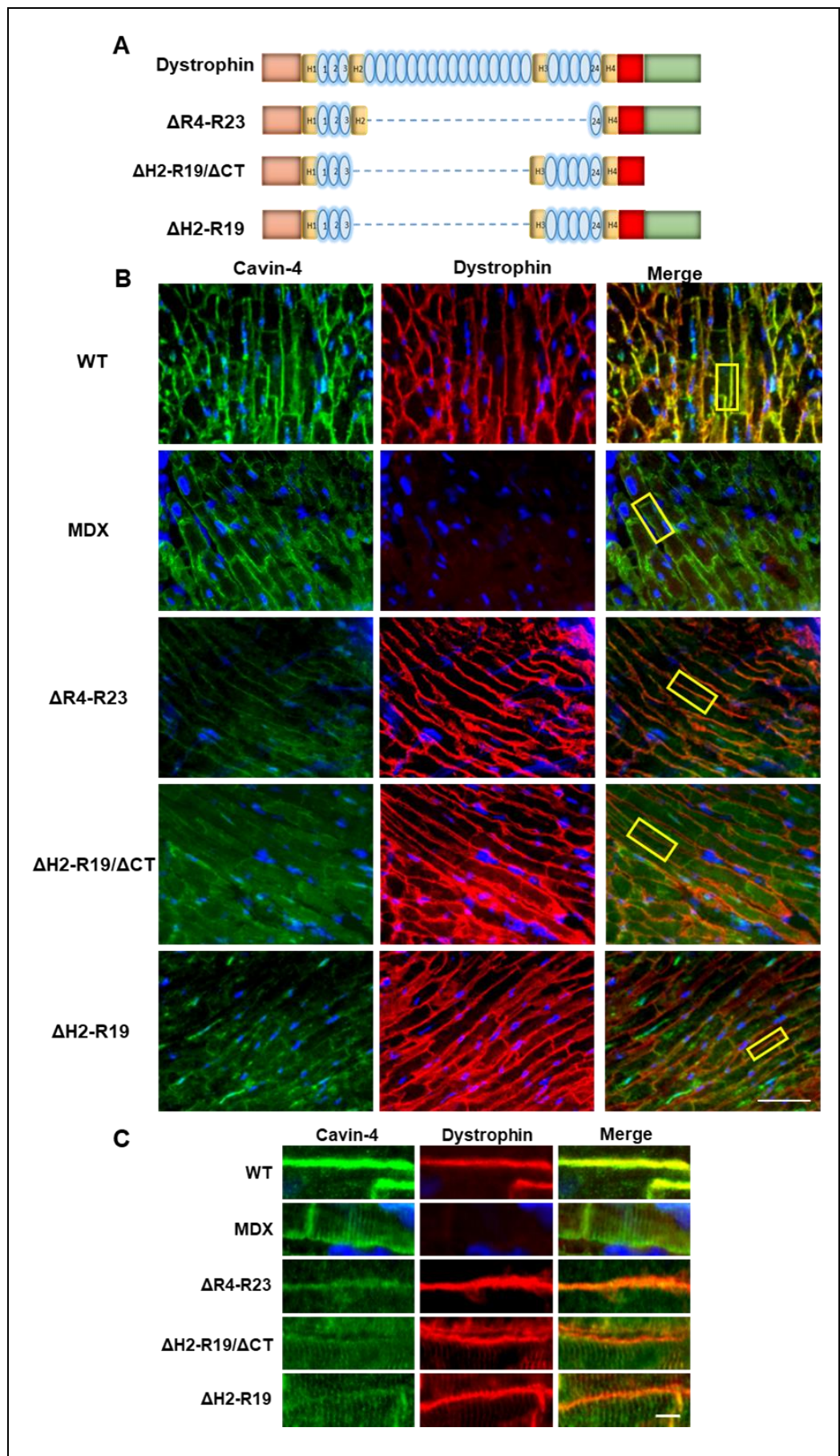
Figure *46.**Cavin-4 membrane localisation is disrupted in the hearts of mini and micro-dystrophin mice.***

A*. Diagram representing full-length dystrophin and the micro and mini dystrophin constructs used for the immunohistochemistry experiments.* ***B****. Immunolabelling for cavin-4 (green) full-length dystrophin (red) of cardiac tissue sections from male wild-type (C57BL/10), mdx[23], ΔH2-R19/ΔCT and ΔH2-R19 mini-dystrophin and ΔR4-R23 micro-dystrophin. Nuclei stained with DAPI (blue). Scale bar 50 μm.* ***C****. Enlargements from images of panel* ***B*** *that help the visualisation of the cardiomyocyte lateral membrane. 40X magnification, scale bar 5μm.*

Twenty one-week-old mice expressing the ΔH2-R15 mini-dystrophin construct (**Figure 47 A**) had a correction of the end-diastolic volume, normalisation of all the aberrant electrocardiogram changes and an improvement of the hemodynamic parameters such as the normalized the end-systolic volume, end-diastolic volume, dP/dt maximum, and ejection fraction. (Wasala, Shin et al. 2018). These mice express the ΔH2-R15 mini-dystrophin construct under the control of the cardiac specific α-myosin heavy chain (αMHC) promoter. The decision of Wasala and colleagues to add the spectrin-like repeats 16-19 was based on the clinical evidence that patients with deletions in the R16-19 region often show a more severe or early-onset cardiac disease (Kaspar, Allen et al. 2009). The reason why this region might be important for cardiac function is unknown, but Adams and colleagues showed that in skeletal muscle R17 is involved in binding with α1-syntrophin (Adams, Odom et al. 2018). They also showed that in skeletal muscle, α1-syntrophin is involved in binding with neuronal nitric oxide synthase nNOS (Adams, Odom et al. 2018). In cardiac muscle, nNOS is not part of the DGC, so adding R17 and bringing back α1-syntrophin could clarify whether α1-syntrophin is

involved in binding with caveolar proteins in the heart. Wasala and collaborators decided to express the ΔH2-R15 mini-dystrophin construct in homozygous mdx[23] female mice (FVB background) (Wasala, Shin et al. 2018), justifying this choice with the evidence that mdx[23] females at 22 month of age display severe end-stage dilated cardiomyopathy not observed in male mdx[23] mice (Bostick, Yue et al. 2010). In order to investigate whether there is a caveolar protein binding site in this region of dystrophin, I performed immunofluorescence analyses on wild-type, mdx[23] and ΔH2-R15 mini-dystrophin hearts using cavin-1 and laminin-α2 antibodies (**Figure 47 B**). While in wild-type hearts (FVB) cavin-1 localises at the cardiomyocyte lateral membrane, in mdx[23] and ΔH2-R15 mini-dystrophin hearts, cavin-1 is absent from the membrane and is expressed only in the capillaries (**Figure 47 B and C**).
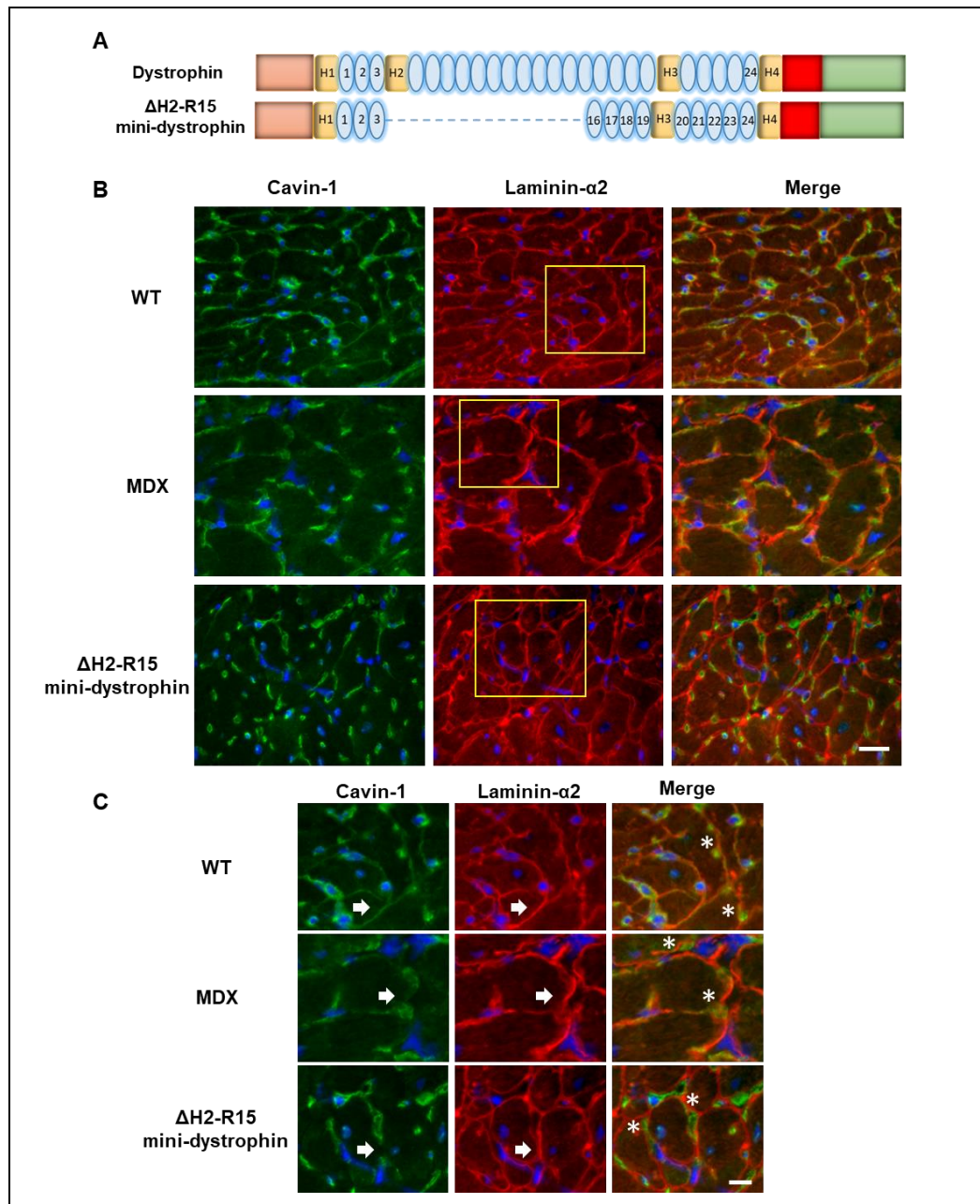
Figure 47. Cavin-1 membrane expression is not seen at the membrane of ΔH2-R15 mini-dystrophin cardiomyocytes.

A*. Diagram representing the domains of the full-length dystrophin and the ΔH2-R15 mini-dystrophin.* ***B****. Immunolabelling for cavin-1 and laminin-α2 (red) of cardiac sections from 21-month-old female wild-type (FVB), mdx[23] and ΔH2-R15 mini-dystrophin mice. (N=3) 40X magnification, scale bar 20μm* ***C****. Enlarged pictures from panel* ***B****, where the cardiomyocyte lateral membrane is indicated by the white arrows and the asterisks indicate the capillaries. Scale bar 10μm.* ***B*** *and* ***C****. Nuclei stained with DAPI (blue).*

The disruption of cavin-4 occurs in mdx[23] and ΔH2-R15 mini-dystrophin hearts, where cavin-4 is absent from the cardiomyocyte lateral membrane (**Figure 48 A and B**).
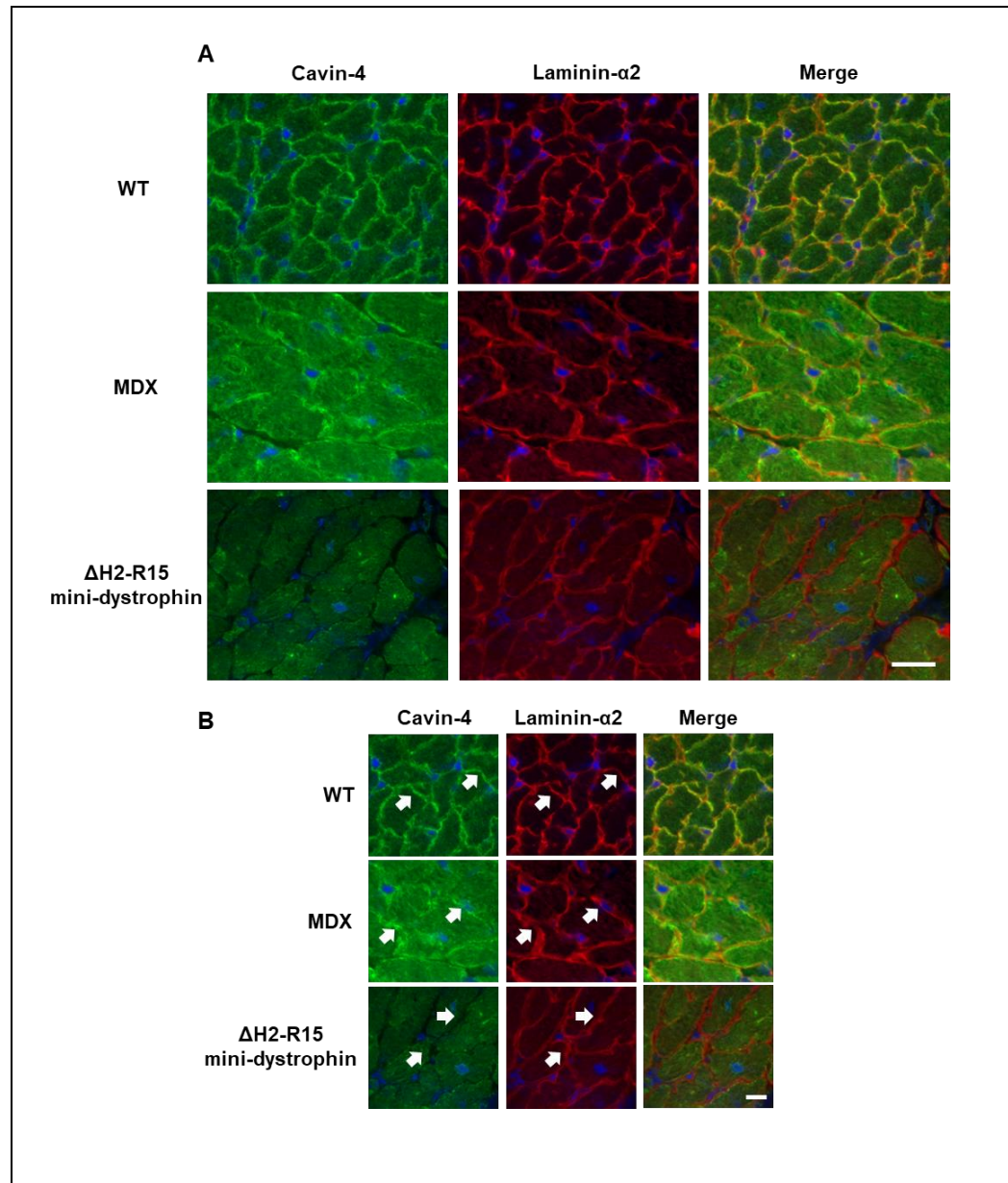
Figure 48.Cavin-4 membrane localisation is not rescued by the ΔH2-R15 mini-dystrophin construct.

A. *Immunolabelling for cavin-4 (green) and laminin-α2 (red) of cardiac tissue sections from 21-month-old female wild-type (FVB), mdx[23] and ΔH2-R15 mini-dystrophin mice. 40X magnification, scale bar 20μm (N=3)* *B*. *Enlarged pictures from panel* *B* *where the cardiomyocyte lateral membrane is indicated by the white arrows. Scale bar 10μm.* *A* *and* *B*. *Nuclei stained with DAPI (blue).*

4.5 Discussion

The first questions asked in this chapter concerned the localisation of cavin-1, -2 and -4 in the hearts of wild-type mice expressing full-length dystrophin and whether the loss of full-length dystrophin in mdx^{5cv} mice influenced their localisation. Immunofluorescence experiments performed on wild-type (C57BL/6J) hearts showed that cavin-1, -2 and -4 are expressed at the cardiomyocyte membrane. In mdx^{5cv} mice, cavin-1 is not detectable at the cardiomyocyte lateral membrane and cavin-2 and cavin-4 appeared to be severely disrupted. Then, I asked whether the ΔR23/ΔCT micro-dystrophin construct was able to restore the membrane localisation of the cavins in mdx^{5cv}-μDys finding that none of the cavins were brought back at the cardiomyocyte membrane of these mice. These data suggest that the expression of full-length dystrophin at the cardiomyocyte membrane is necessary for the correct localisation of the cavins at the membrane and that probably, the ΔR23/ΔCT micro-dystrophin construct does not have the binding domain for the cavins.

I then asked whether the loss of cavin-1 and the disruption of cavin-4 that are involved in cardiac disease were impaired in mdx^{5cv} as a consequence of the cardiac pathological changes that happen in mdx^{5cv} by 6 months of age. The immunofluorescence analysis performed on 9-week mdx^{5cv} hearts showed the loss of cavin-1 and the disruption of cavin-4 at the cardiomyocyte membrane. These results suggest that the loss of cavin-1 and the severe disruption of cavin-4 are directly associated with the loss of full-dystrophin. Cavin-4 also showed an abnormal peri-nuclear localisation in hearts from mdx^{5cv} and mdx^{5cv}-μDys mice. The nuclear accumulation of cavin-4 has been also described in

skeletal muscle of cavin-1 knock-out mice (Lo, Nixon et al. 2015). The cavin-4 data on mdx[5cv] and the mdx[5cv]-µDys mice are in agreement with the findings of Lo and colleagues. In fact, mdx[5cv] and the mdx[5cv]-µDys mice are not knock-out for cavin-1 but they do not express cavin-1 at the membrane as a consequence of the dystrophin loss leading to an abnormal peri-nuclear localisation of cavin-4. The mis-localisation of cavin-4 needs to be further investigated and will be discussed in the final discussion of my PhD thesis.

The other question concerned the identification of dystrophin domains potentially involved in the binding with cavin-1, -2 and -4. To answer this question mdx[23] transgenic mice expressing different micro and mini-dystrophin constructs were used for immunofluorescence analysis. The results from my analyses of hearts from these transgenic mice did not answer this question. However, the use of transgenic mice expressing different mini and micro-dystrophin constructs allowed me to identify dystrophin domains that are not involved in the binding with the cavins or that alone are not enough to bring cavins at the cardiomyocyte membrane. Specifically, the C-terminus, spectrin repeats 16-19, spectrin repeats 20-24 and hinges 2 and 3 are not involved in the binding with the cavins or they might need the insertion of another dystrophin domain to correctly bind with the cavins in the heart.

These data open the possibility that dystrophin plays additional roles in the heart and suggest a role of cavins in cardiac disease caused by loss of dystrophin. These findings will be crucial in enabling the design of the next generation of micro-gene therapy constructs that will almost certainly need to include the cavin binding site. Moreover, these data

could also point towards new research directions for finding targeted therapeutic drugs for DCM in DMD patients.

Another important discovery showed in chapter 4 were the differences in disruption to cavin-1 and cavin-4 in mdx[23] mice on different backgrounds. Specifically, the mdx[23] mice on FVB background showed the same pattern of disruption for cavin-1 and cavin-4 observed in mdx[5cv] mice (C57BL/6J background) with the complete loss of cavin-1 at the cardiomyocyte membrane and a severe membrane disruption of cavin-4 accompanied by diffuse intracellular staining. In contrast, mdx[23] mice on C57BL/10 background, showed a light cavin-1 staining at their cardiomyocyte membrane and a membrane disruption of cavin-4 that is accompanied by an abnormal intracellular distribution. Cavin-4 in mdx[23] mice on C57BL/10 background is distributed in striations that resemble the t-tubules.

The differences in cavin-1 and cavin-4 disruption between mdx[23] and mdx[5cv] mice could be attributed to the effect that the different dystrophin mutations have on the expression of the dystrophin isoforms. In fact, in the mdx[23] hearts Dp71 was described to be expressed in the t-tubules (Masubuchi, Shidoh et al. 2013) while there are not studies assessing dystrophin isoforms expressed in the mdx[5cv] hearts. However, the mdx[5cv] and the mdx[23] mice used for my PhD thesis are also on different genetic backgrounds, C57BL/6 and C57BL/10, FVB respectively. The different genetic background could be also the cause of the difference in the cavin-1 and cavin-4 disruption observed in mdx[23] mice on C57BL/10 and FVB backgrounds. These hypotheses will be discussed in depth in the final discussion (**Chapter 6**).

Chapter 5. Study of caveolar proteins across different species and different DMD animal models

5.1 Background and objectives

Part of chapter 4 was dedicated to determining the distribution of cavin-1, -2 and -4 in the heart of wild-type and DMD murine models. In wild-type mice, cavin-1, -2 and -4 are expressed at the cardiomyocyte lateral membrane and at the intercalated discs. Only cavin-1 and cavin-2 localise at the capillaries. When full-length dystrophin is not expressed, the membrane localisation of cavin-1, -2 and -4 is severely disrupted and a qualitative difference in the mis-localization of cavin-4 in the hearts of different strains of mdx[23] mice was observed. Since mouse models of DMD do not develop cardiac disease as severe as DMD patients, the use of dystrophin-deficient rats and dog models of DMD has increased in recent years for testing of treatments targeting the heart.

As in the mdx[23] mouse, the DMD[mdx] rat model (**1.3.3**) carries a mutation in exon 23 of the dystrophin gene leading to the loss of full-length dystrophin (Larcher, Lafoux et al. 2014). However, compared to the mdx[23] mouse, the DMD[mdx] rat develops a more severe cardiac phenotype, similar to the one observed in DMD boys (Szabo, Ebner et al. 2021). The deltaE50-MD dog (**1.3.4**) carries a mutation in exon 50, initially found in Cavalier King Charles spaniels (Walmsley, Arechavala-Gomeza et al. 2010) and currently maintained on a beagle background (Amoasii, Hildyard et al. 2018). The cardiac evaluation of these dogs is ongoing at the Royal Veterinary College by Professor Piercy's group. However, previous cardiac evaluations on GRMD (**1.3.4**) and on Beagle-

based canine X-linked muscular dystrophy in Japan (CXMDJ) (Shimatsu, Katagiri et al. 2003) found that the DMD dogs have a much stronger cardiac disease than mdx[23] mice and better recapitulate the DMD patient cardiac phenotype (Valentine, Cummings et al. 1989, Moise, Valentine et al. 1991, Yugeta, Urasawa et al. 2006, Fine, Shin et al. 2011).

It is therefore important to investigate whether the localisation of cavins is conserved in wild-type rat and dog hearts and whether their localisation is affected by the loss of full-length dystrophin. The localisation of cavins was investigated via immunofluorescence experiments on cardiac sections from wild-type rats and dogs and on cardiac sections from DMD[mdx] rats and deltaE50-MD dogs.

The last part of this chapter is dedicated to the study of the distribution of cavin proteins in human cardiac samples. The human cardiac samples are from a paediatric patient affected by Tetralogy of Fallot (Gualandi, Trabanelli et al.) (Karl 2008) (**2.1.6**), I have used them to visualize the cardiomyocyte localization of caveolar proteins and to investigate any differences between human and wild-type animal models as TOF patients do not have any dystrophin mutation.

The data generated for this chapter add important pieces of information regarding the effect that loss of dystrophin has on cavin proteins in DMD animal models that show a more severe cardiac disease than DMD mouse models. Moreover, the comparison of the cardiac localisation of cavins in animal models and in humans could help choosing the more appropriate animal model that best recapitulate the human phenotype for future studies of cardiac caveolae and cardiac disease associated with cavin mutations.

5.1.1 Wild-type and DMD^{mdx} rats express cavin-1 at the cardiomyocyte lateral membrane

Immunofluorescence analyses performed on cardiac tissue sections from wild-type and DMD^{mdx} rats at 4 months of age showed the presence of cavin-1 at the cardiomyocyte lateral membrane (**Figure 49 B white arrows**). Cavin-1 is also present at the capillaries (**Figure 49 B yellow arrows**) and at the intercalated discs (**Figure 49 C white arrows**). Wild-type and DMD^{mdx} rats (**Figure 49**) showed the same cavin-1 cardiac distribution observed in wild-type (C57BL/6J, C57BL/10 and FVB) mice where cavin-1 is expressed at the cardiomyocyte lateral membrane, at the intercalated discs and at the capillaries (**Figure 29, Figure 49 A** and **D**). The DMD^{mdx} rat carries the same mutation occurring in the mdx^{23} mouse (exon 23 of the dystrophin gene) and showed a similar disruption of cavin-1 at the cardiomyocyte membrane (**Figure 49**), where cavin-1 is not completely undetectable as in mdx^{5cv} mice (**Figure 29**), but a faint membrane staining is visible (**Figure 49 A** and **D**). Thus, the localisation of cavin-1 at the DMD^{mdx} rat cardiomyocyte membrane is not severely affected by the loss of full-length dystrophin.
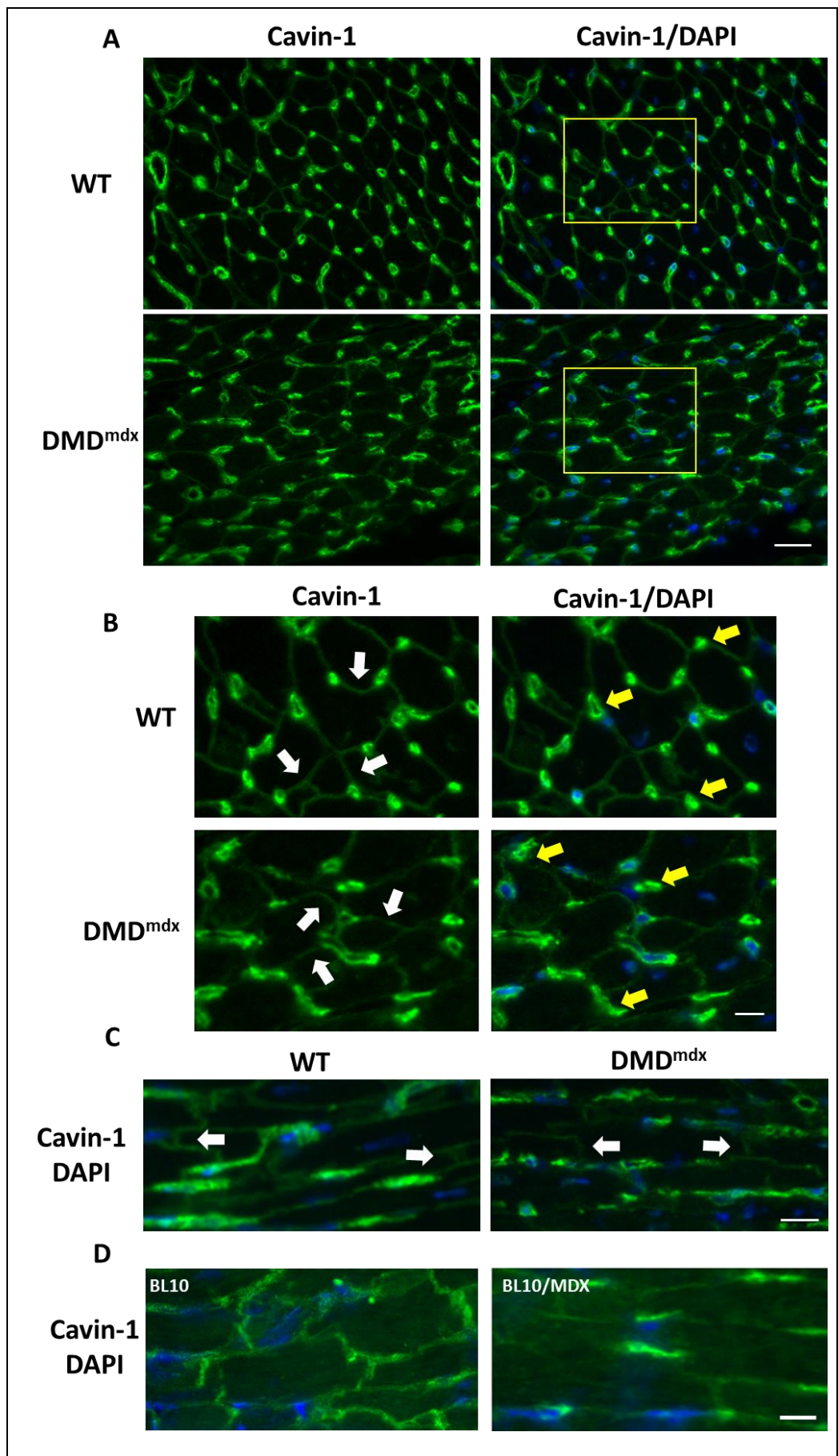
Figure 49. Wild-type and DMD^mdx rats express cavin-1 at the cardiomyocyte lateral membrane.

(A and B). Immunolabelling for cavin-1 on cardiac tissue sections from male rats of 4 months of age. (B) Enlargement of the yellow boxes in figure A. White arrows pointing to the cardiomyocyte lateral membranes and yellow arrows pointing to the capillaries. Nuclei stained with DAPI (blue). 40X magnification. Scale bar 25µm (A), 10µm (B), 20µm (C). (D) Cardiac sections from mdx^23 mice on C57BL/10 background stained for cavin-1 (green). Nuclei stained with DAPI (blue). 40X magnification. Scale bar 15µm.

5.1.2 Low level disruption of cavin-4 at the cardiomyocyte lateral membrane of DMD^mdx rats

Cavin-4 showed a continuous and sharp staining at the cardiomyocyte lateral membrane of wild-type rats (**Figure 50 A and B**) and is also expressed at the intercalated discs visible in longitudinal cardiac sections (**Figure 50 C** intercalated discs indicated with white arrows). In the hearts of DMD^mdx rats, cavin-4 staining appears to be less sharp at the cardiomyocyte membrane compared to the wild-type staining and is also appreciably diffuse in the cytoplasm (**Figure 50 A, B and C**). The distribution of cavin-4 in the cytoplasm is not only diffused but is also organised in striations similar to t-tubules (**Figure 50 C**). This peculiar organisation of cavin-4 in the cytoplasm was also observed in the hearts from mdx^23 mice on C57BL/10 background (**Figure 44 and Figure 50 D)** but is not visible in the hearts from mdx^23 on FVB background (**Figure 44**) and mdx^5cv mice (**Figure 34**).
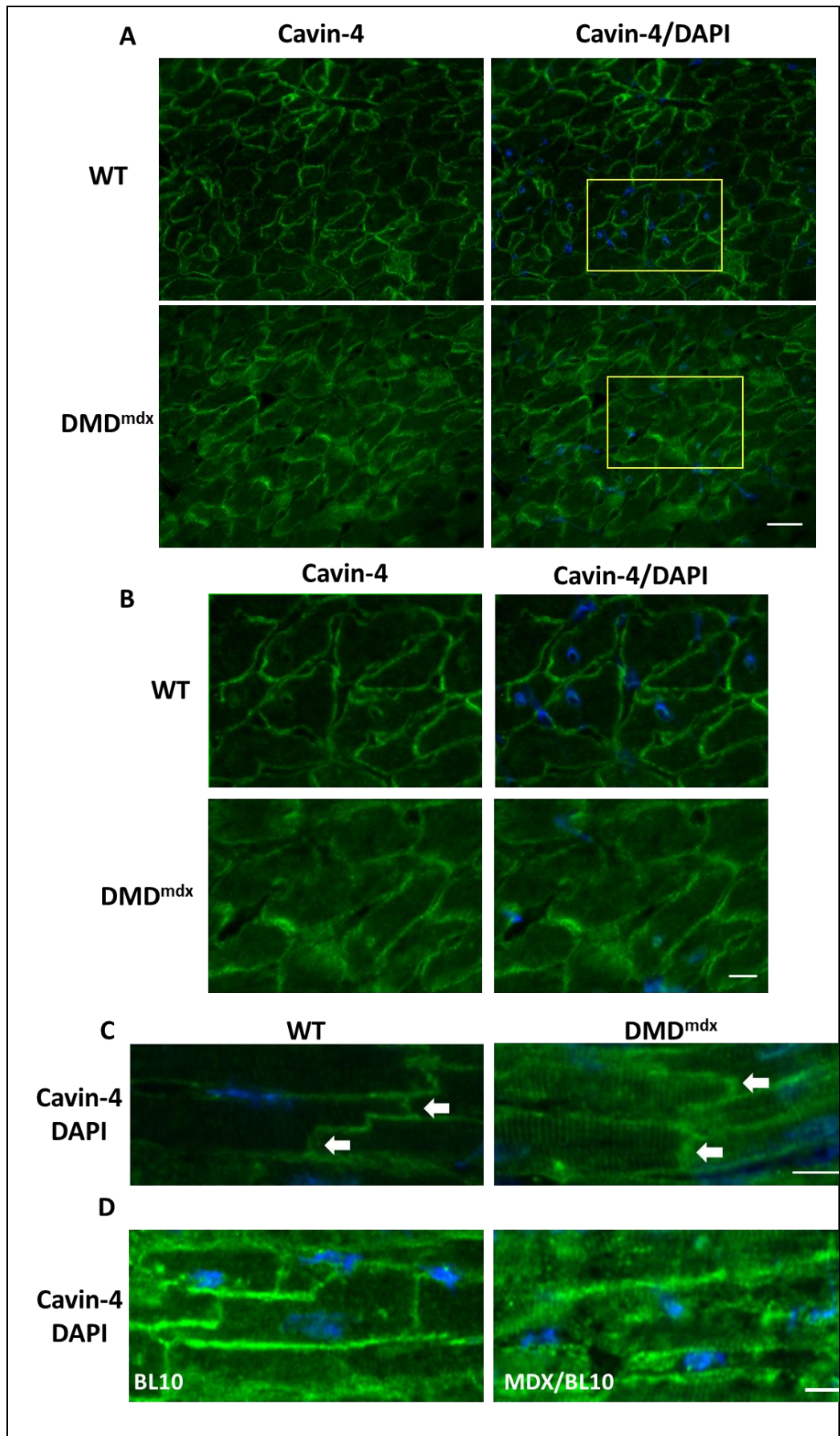
Figure 50. DMD^{mdx} rats show a disrupted cavin-4 staining at the cardiomyocyte lateral membrane.

*(**A** and **B**). Cardiac sections from male wild-type and DMD^{mdx} rats of 4 months of age immunolabelled for cavin-4. (**B**) Pictures of yellow boxed areas in figure **A**. (**C**) Longitudinal cardiac sections from wild-type and DMD^{mdx} rats of 4 months of age immunolabelled for cavin-4. White arrows indicating intercalated discs. Nuclei stained with DAPI (blue). 40X magnification. Scale bar 25µm (**A**) and 10µm (**B** and **C**). (**D**) Cardiac sections from mdx²³ mice on C57BL/10 background stained for cavin-4 (green). Nuclei stained with DAPI (blue). 40X magnification. Scale bar 15µm.*

5.1.3 DMD^{mdx} rats do not express full-length dystrophin but express shorter dystrophin isoforms at the cardiomyocyte lateral membrane

In the literature there are no immunofluorescence studies performed in the heart of wild-type and DMD^{mdx} rats. Larcher and colleagues (Larcher, Lafoux et al. 2014) showed the absence of full-length dystrophin in the heart of 7-month-old DMD^{mdx} rats, by performing western blot using MANEX1011C that has its epitope in the N-terminus domain of dystrophin (exon 10/11). They also performed immunohistochemistry on wild-type and DMD^{mdx} hearts using MANDYS110 that has its epitope in the rod domain (exon 38/39). The MANDYS110 antibody can detect only full-length dystrophin and the isoform Dp260. They found no expression of either full-length or Dp260 dystrophin at the cardiomyocyte lateral membrane of DMD^{mdx} rats (Larcher, Lafoux et al. 2014). However, since DMD^{mdx} rat and the mdx²³ mouse share the same dystrophin mutation in exon 23 and has been found that the mdx²³ mice express Dp71 in their heart (Masubuchi, Shidoh et al. 2013) it is plausible that the DMD^{mdx} rat express Dp71 in their heart. Starting from this hypothesis, the

immunofluorescence experiments for this section have been performed with two different antibodies against dystrophin on cardiac tissue sections from wild-type and DMD[mdx] rats. The first antibody used was the MANEX1011B that has its epitope in the N-terminus domain of dystrophin. Therefore, this antibody is able to recognize full-length dystrophin but not the shorter dystrophin isoforms (**Figure 1 B**). Wild-type rats showed cardiomyocyte membrane expression of full-length dystrophin whereas DMD[mdx] rats had no full-length dystrophin in their hearts (**Figure 51**), confirming previously reported data (Masubuchi, Shidoh et al. 2013, Larcher, Lafoux et al. 2014).
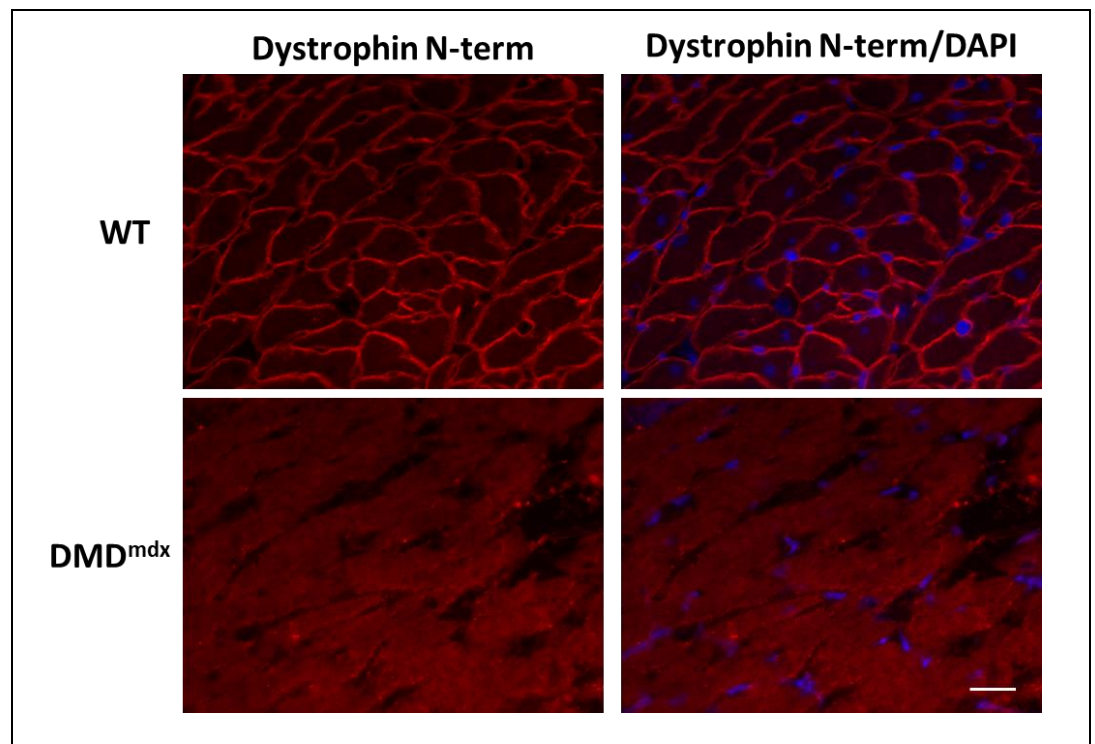
Figure 51.DMD[mdx] rats do not express full-length dystrophin.

Cardiac tissue sections from wild-type and DMD[mdx] male rats of 4 months of age (N=3) stained with a dystrophin antibody against the N-terminal domain. Nuclei stained with DAPI (blue). 40X magnification, 25μm scale bar.

Using another antibody against dystrophin (**Table 6**) that is able to recognize all the dystrophin isoforms (as it has its epitope in the C-

terminal domain) (**Figure 1 B**) the wild-type (**Figure 52 A and B**) rats show dystrophin at the cardiomyocyte membrane and at the intercalated discs (**Figure 52 B** intercalated discs indicated with white arrows). Staining also appear to be localised in structures similar to t-tubules. Interestingly, shorter dystrophin isoforms detected by the dystrophin C-terminus antibody, in the DMD^{mdx} hearts appear disrupted but not completely absent as they are distributed in the cytoplasm in straight striations like the t-tubules as observed for cavin-4 and preserved at the intercalated discs (**Figure 52 B**).
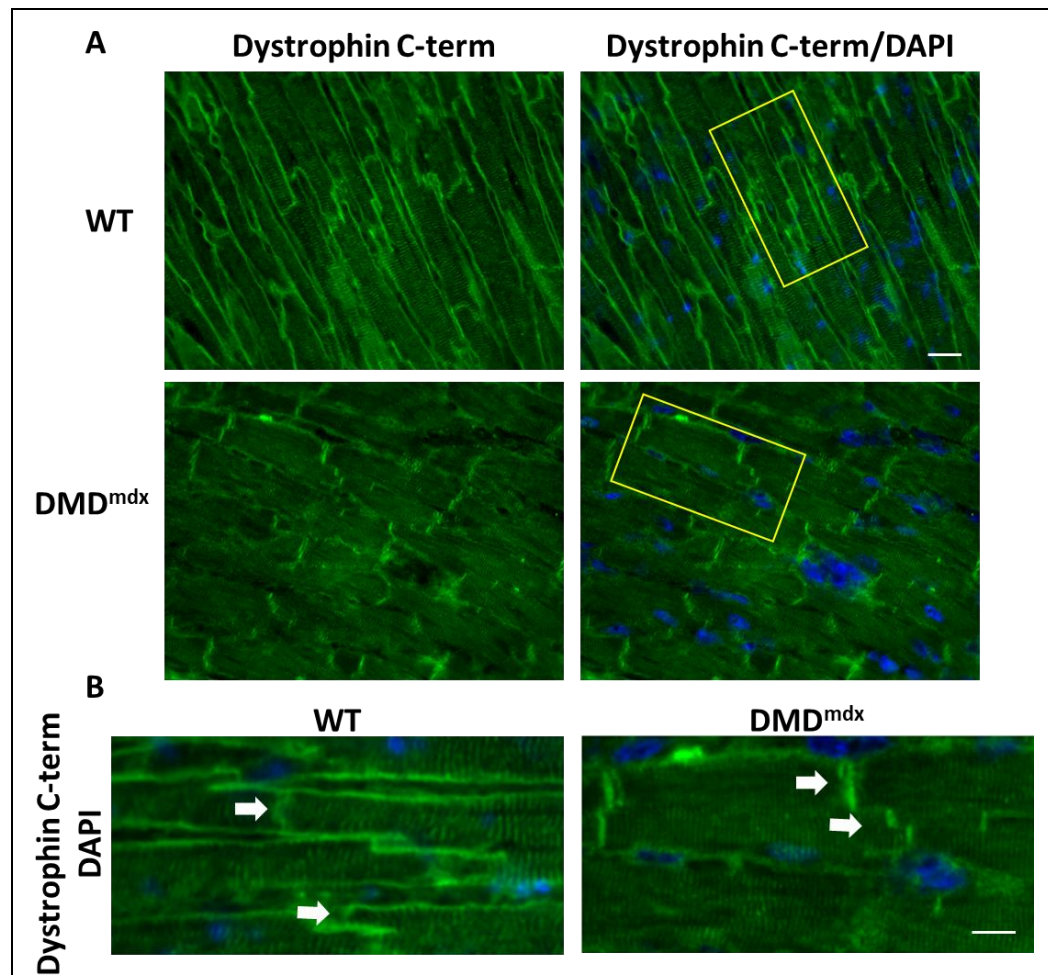
Figure 52.Dystrophin isoforms distribution in wild-type and DMD^{mdx}
hearts.

*(**A** and **B**) Cardiac sections from wild-type and DMD^{mdx} male rats of 4*
months of age stained with a dystrophin antibody against the C-terminus
*domain. (**B**) Enlarged pictures of the yellow boxed areas in **A**. White*
arrow pointing the intercalated discs. Nuclei stained with DAPI (blue).
*40X magnification, scale bar 25µm (**A**) 10µm (**B**). (N=3/group).*

The observation that shorter dystrophin isoforms are expressed at the t-
tubules of mdx[23] mice on C57BL/10 background (Masubuchi, Shidoh et
al. 2013) and DMD^{mdx} hearts, is potentially associated with the presence
of cavin-4 at the t-tubules of DMD^{mdx} rat hearts, and hearts from mdx[23]
mice on C57BL/10 background.

These results show that wild-type rats share the same cardiac
localisation of cavin-1 and cavin-4 observed in wild-type mice. The
disruption of cavin-1 and cavin-4 observed in DMD^{mdx} rats is very similar
to the one observed in mdx[23] mice on a C57BL/10 background. It is very
likely that the Dp71 expressed in mdx[23] mice (C57BL/10 background)
and the shorter dystrophin isoforms expressed in DMD^{mdx} rat hearts
influence the cardiac localisation of cavin-1 and -4. mdx[5cv] mice show the
total loss of cavin-1 and a more severe cavin-4 disruption that is not
characterised by the cytoplasmic cavin-4 distribution. This could be due
to the different mutation that mdx[5cv] mice carry in the dystrophin gene
(exon 10), but also because of their different genetic background
(C57BL/6). Overall, these results showed that DMD^{mdx} rats share the
same cardiac disruption of cavin-1 and cavin-4 observed in mdx[23] mice
on C57BL/10 background.

5.2 Cavin-1 is expressed at the cardiomyocyte lateral membrane of wild-type and ΔE50-MD dogs

The ΔE50-MD canine model of Duchenne Muscular Dystrophy harbours a mutation in exon 50 corresponding to a mutational "hotspot" in the human DMD gene (Bladen, Salgado et al. 2015). This model is still under investigation at the Royal Veterinary College and the cardiac parameters are not available yet. Currently there are no studies on the localisation of caveolar proteins in the heart of wild-type and ΔE50-MD dogs. For these studies 2 wild-type and 2 dystrophin deficient male dogs (ΔE50-MD) of 3 months of age were used. Cavin-1 in heart sections from healthy dogs was present at the cardiomyocyte lateral membrane, the capillaries (**Figure 53 A and B**), and also at the intercalated discs (**Figure 53 C**). In the hearts of ΔE50-MD dogs, cavin-1 staining is visibly reduced at the lateral membrane and is more diffuse in the cardiomyocyte cytoplasm but is preserved at the capillaries (**Figure 53 A and B**) and at the intercalated discs (**Figure 53 C**) as observed in DMD[mdx] rats (**Figure 49**) and mdx[23] mice (C57BL/10 background) (**Figure 44**). Further experiments should be performed using specific markers for capillaries and intercalated discs, these experiments were not performed due to limited time.
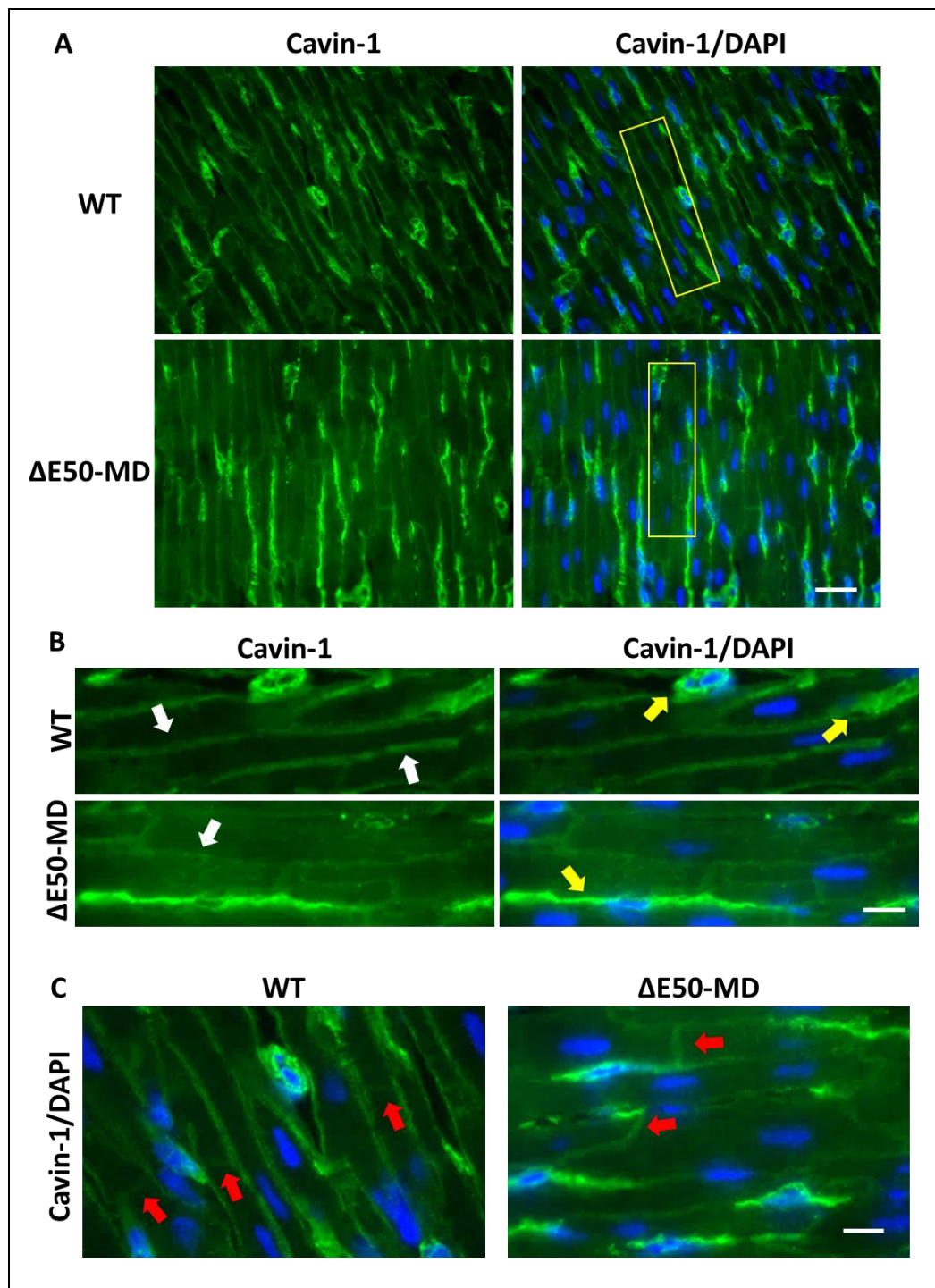
Figure 53.Cavin-1 expression in hearts from wild-type and DMD dogs.

(**A**, **B** and **C**). Cardiac sections from male wild-type and DMD dogs (ΔE50-MD) of 3 months of age stained with cavin-1 antibody (N=2 per genotype). (**B**) Enlarged pictures of figure **A** where with arrows indicate cavin-1 staining at the cardiomyocyte membrane and the yellow arrows indicate cavin-1 at the capillaries. (**C**) Red arrows indicating intercalated

*discs. Nuclei stained with DAPI (blue), 40X magnification. Scale bar 25μm (**A**) and 10μm (**B** and **C**).*

5.2.1 ΔE50-MD dogs and mdx[23] mice share the same cavin-4 cardiac impairment

In healthy dogs, cavin-4 localised at the cardiomyocyte lateral membrane and at the intercalated discs (**Figure 54 A and B**). At the membrane of wild-type dogs, cavin-4 staining is homogeneous as previously observed in wild-type mice (**Figure 34** and **Figure 45**) and rats (**Figure 50**). In ΔE50-MD dogs, cavin-4 staining appeared diffuse within the cardiomyocyte cytoplasm and localised in structures similar to the t-tubules (**Figure 54 A and B**) as has been seen in mdx[23] mouse on a C57BL/10 background (**Figure 45**) and DMD[mdx] rat hearts (**Figure 50**). The increased brightness of cavin-4 in ΔE50-MD hearts (**Figure 54**) could be due to the mislocalisation of cavin-4 in striations as a consequence of the loss of full-length dystrophin or to histological changes caused by the cardiac disease of these DMD dog models. The cardiac disease evaluation of the ΔE50-MD dogs is still ongoing at the Royal Veterinary College.
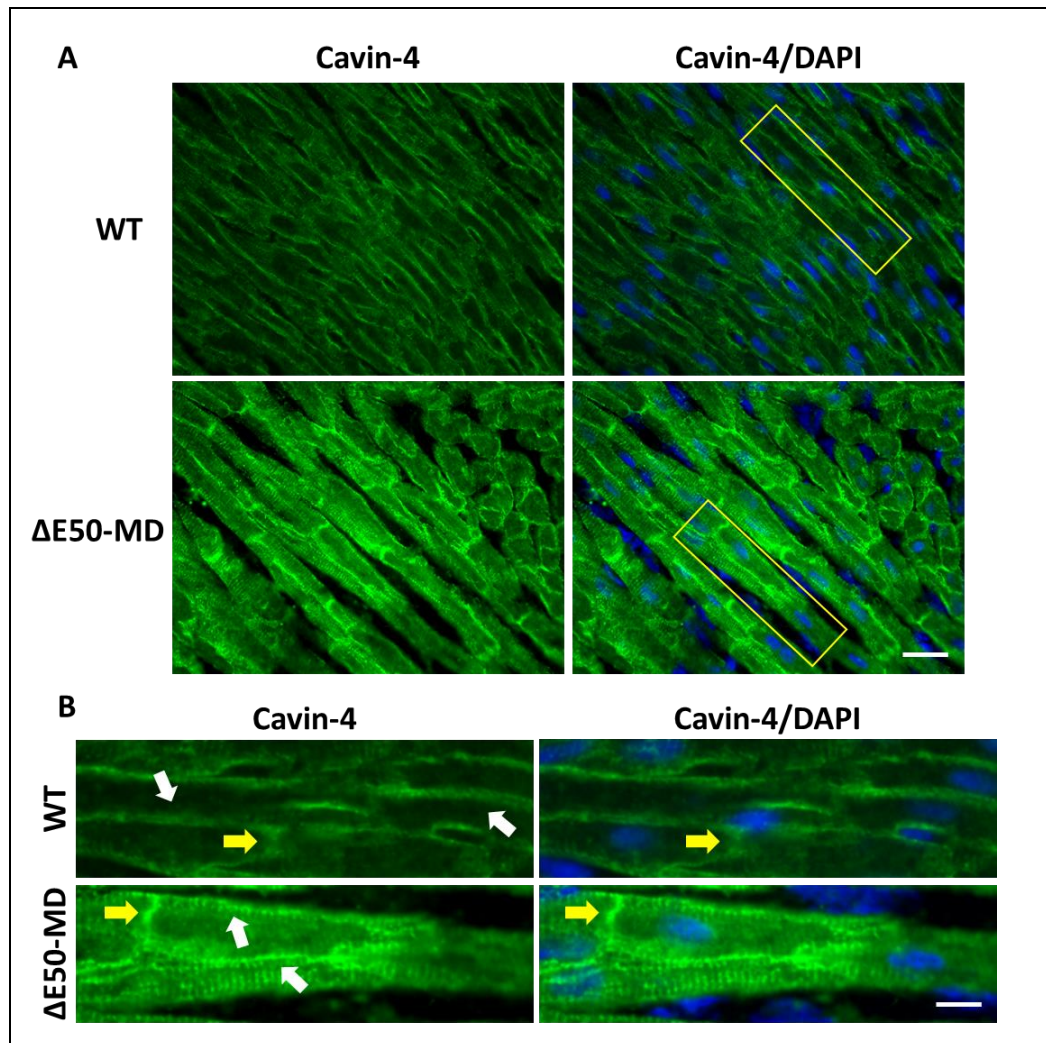
Figure 54. Cavin-4 cardiomyocyte membrane localisation is disrupted in DMD dogs.

(**A** and **B**). Immunolabelling for cavin-4 on cardiac tissue sections from male wild-type and DMD dogs (ΔE50-MD) of 3 months of age (N=2 per genotype). (**B**) Enlarged pictures of the areas surrounded by the yellow boxes in figure **A**. White arrows pointing to cardiomyocyte lateral membranes and yellow arrows pointing to intercalated discs. Nuclei stained with DAPI (blue) 40X magnification, scale bar 25µm (**A**) and 10µm (**B**).

Moreover, in dystrophic dogs (**Figure 55**) cavin-4 staining is also present in the peri-nuclear region as observed in mdx^{5cv} mice (**Figure 36**) and this will be further investigated in future work.
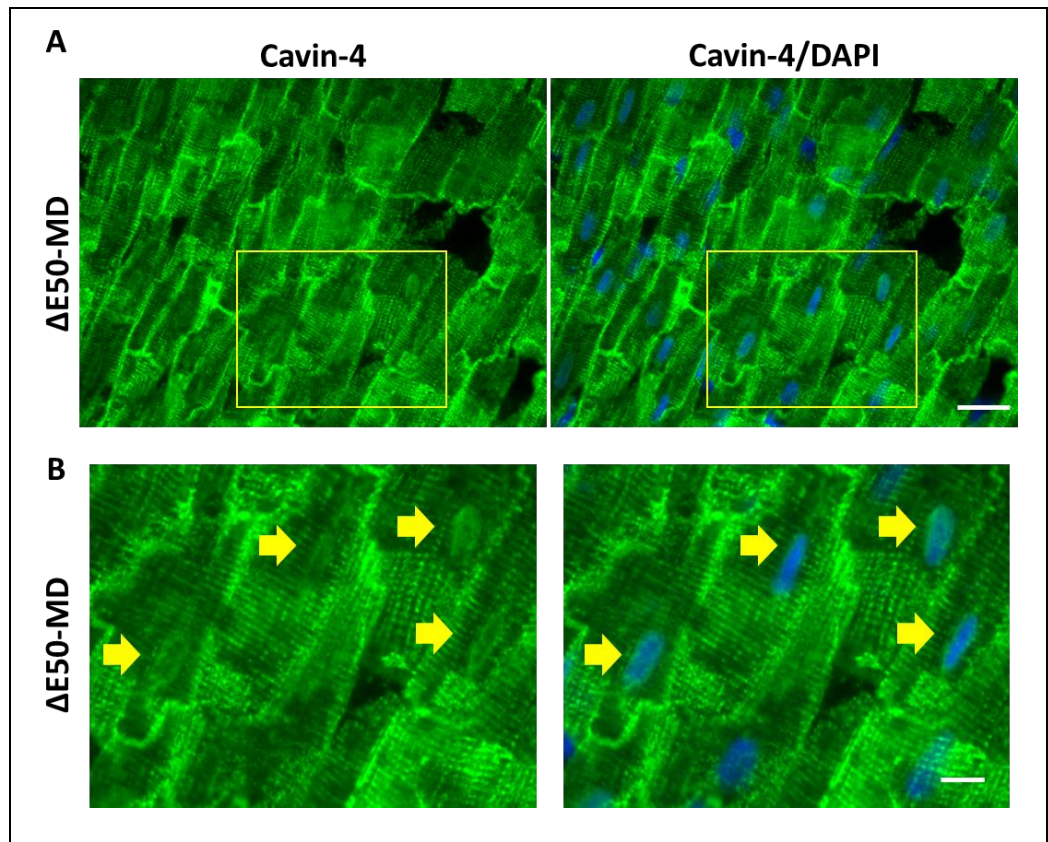
Figure 55.Cavin-4 peri-nuclear localisation in the heart of dystrophin deficient dog.

(A and B) Cardiac tissue sections from male ΔE50-MD dogs of 3 months of age, stained for cavin-4 (green), nuclei stained with DAPI (blue) (N=2 per genotype). (B) Enlarged pictures of the areas surrounded by the yellow boxes in figure A where yellow arrows are pointing the nuclei stained with cavin-4. 40X magnification, scale bar 25µm (A) and 10µm (B).

5.3 Commonalities of cavin-1 cardiac localisation in human and animal models.

In order to study the localisation of cavin-1, cavin-2 and cavin-4 in a human heart, a cardiac ventricular biopsy sample from a paediatric patient affected by tetralogy of Fallot was used (**2.1.6**). As observed in mice, dogs and rats, cavin-1 in the human heart is present at the cardiomyocyte lateral membrane where it co-localizes with full-length dystrophin (**Figure 56 B**). Cavin-1 is also clearly visible at the intercalated discs colocalising with β-catenin (**Figure 56 B**).
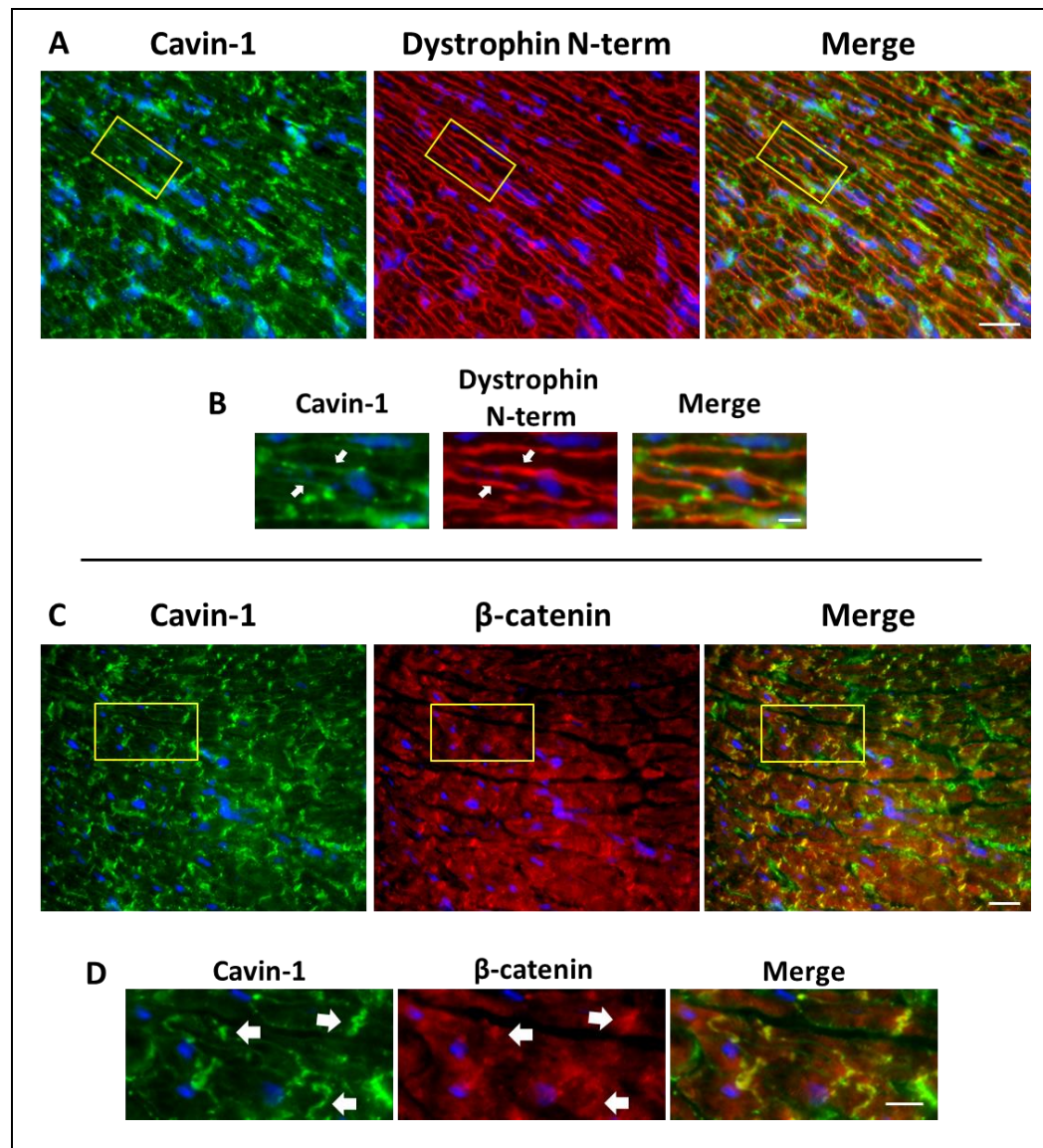
Figure 56. Cavin-1 localises to the cardiomyocyte lateral membrane and at the intercalated discs in human cardiac tissue sections.

*(**A** and **B**). Immunolabelling for cavin-1 (green) and full-length dystrophin (red) on cardiac tissue section from a TOF patient. (**B**) Enlarged area of figure **A**, where white arrows point to cavin-1 and full-length dystrophin at the cardiomyocyte lateral membrane. The membrane colocalisation of cavin-1 and full-length dystrophin is also visible as the cardiomyocyte membrane turns orange in the merge picture of figure **B**. (**C** and **D**) Cardiac tissue sections from a TOF patient stained with cavin-1 (green) and β-catenin (red). (**D**) Enlarged area of figure **C**, intercalated discs indicated with white arrows. (**A, B, C, D**) Nuclei stained with DAPI (blue), 40X magnification. Scale bar 25µm (**A**), 5µm (**B**), 20µm (**C**) and 10µm (**D**). (N=1).*

As observed in wild-type mice (**Figure 32**), in human heart cavin-2 is localised at the cardiomyocyte lateral membrane where it colocalises with full-length dystrophin and at the capillaries (**Figure 57 A** and **B**).

In human heart (**Figure 57 C** and **D**), as in wild-type mouse (**Figure 34** and **45**) and dog hearts (**Figure 54**), cavin-4 is present at the cardiomyocyte lateral membrane co-localising with full-length dystrophin (**Figure 57 C** and **D**).
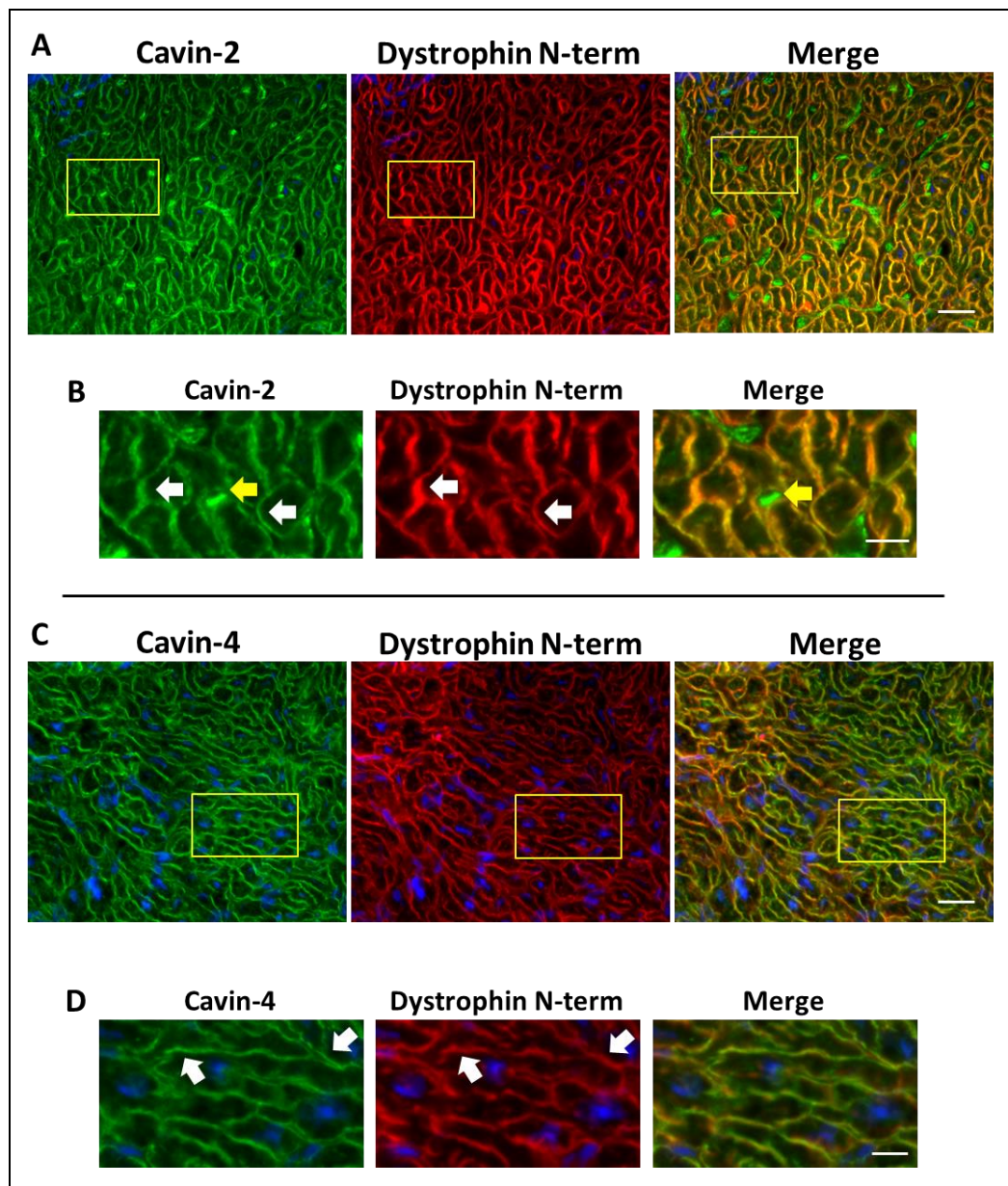
Figure 57.Cavin-2 and cavin-4 cardiomyocyte membrane localisation in human hearts.

(*A* and *B*). Cardiac tissue sections from a TOF human patient stained for cavin-2 (green) and full-length dystrophin (red). (*B*) Enlarged areas of the yellow marked area in figure A where the yellow arrow is pointing at a capillary and the white arrows are pointing to the cardiomyocyte membrane. (*C* and *D*). Immunolabelling for cavin-4 (green) and full-length dystrophin (red) on cardiac tissue sections from a TOF human patient. (*D*) Enlarged areas of figure *C*, white arrows indicate cavin-4 and full-length dystrophin at the cardiomyocyte membrane. (*A*, *B*, *C*, *D*) Nuclei stained with DAPI (blue), 40X magnification. Scale bar 25μm (*A* and *C*), 10μm (*B* and *D*), 20μm (*C*). (N=1).

5.4 Conclusions

The purpose of this chapter was to investigate the cardiac distribution of cavins in different mammalian species in order to look at possible similarities between them and compare them with the distribution of the cavins in human heart. Studying the cardiac distribution of the cavins across different species becomes important when choosing the animal model to study cardiac caveolae, but also to study the cardiac impairments due to mutations in one of the cavin genes in order to choose the animal model that best recapitulates the distribution of these proteins in the human heart. Moreover, the study of cavins in different DMD animal models offered the possibility to assess the effects that the loss of full-length dystrophin has on cavin protein localisation in animal models that show cardiac disease similar to that which is observed in DMD patients.

The major new findings reported in this chapter are that cavin-1 shares the same membrane localisation in the hearts of wild-type rats, dogs and humans and is also expressed at the intercalated discs of all of them. The localisation of cavin-1 found in these species is the same as in wild-type mice (C57BL/6J, C57BL/10 and FVB).

Cavin-4 cardiac localisation is also conserved across the species examined, being present at the cardiomyocyte lateral membrane of rats, dogs, and humans. In rat and dog hearts cavin-4 also localises at the intercalated discs and I cannot exclude the same localisation in humans, because in the samples at my disposal, it was difficult to visualise longitudinal cardiomyocytes due to their small size. Further immunohistochemical studies should be conducted in human cardiac

samples using confocal microscopy to gain more detailed information. Taken together, these data show that cavin-4 localisation is shared by dog, rat, human and mice.

Cavin-2 was found at the cardiomyocyte membrane and at the capillaries of human hearts as observed in wild-type mice. Studies on cavin-2 cardiac localisation were performed only in humans as I did not find an antibody against rat and dog cavin-2.

The other aim of the experiments showed in this chapter was to investigate the effect of the loss of full-length dystrophin on cavin proteins in cardiac samples from different animal species. Both DMD[mdx] rats and ΔE50-MD dogs did not show the same severe cavin-1 disruption observed in mdx[5cv] mice. In DMD[mdx] hearts the localisation of cavin-1 is almost identical to wild-type rats, and it seems that the loss of full-length dystrophin does not have any effect on cavin-1 localisation. In ΔE50-MD dogs, the loss of full-length dystrophin does have a very mild effect on the localisation of cavin-1 especially compared to the effect that the loss of full-length dystrophin has on mdx[5cv] mice.

Cavin-4 in both DMD[mdx] rats and ΔE50-MD dogs lose the homogenous staining at the cardiomyocyte membrane compared to wild-type dogs and rats. Instead, cavin-4 was found into the cytoplasm of both DMD[mdx] rats and ΔE50-MD dogs organised in straight striation similar to the t-tubules. The same cytoplasmic localisation was observed in mdx[23] hearts that are on BL10 background but was not seen either in mdx[23] on FVB background nor in mdx[5cv] mice that carry a different dystrophin mutation (exon 10) that are also on a different background (C57BL/6J). Moreover,

the DMD^{mdx} rats do not express full-length dystrophin as anticipated from their mutation in exon 23 but they express shorter dystrophin isoforms. In fact, using an antibody against the C-terminus of the dystrophin protein, dystrophin was found into the cytoplasm of DMD^{mdx} rats. The expression of shorter dystrophin isoforms in the cytoplasm of these rats could be associated with the cytoplasmic localisation of cavin-4 and also with the presence of cavin-1 at their cardiomyocyte lateral membrane.

It would be beneficial to investigate which dystrophin isoforms are expressed in the heart from DMD^{mdx} rats and ΔE50-MD dogs using western blot analysis with a C-terminus dystrophin antibody. This information would be useful in the investigation of the dystrophin domains potentially involved in the binding with caveolar proteins.

Chapter 6. General discussion and future work

6.1 Background

Patients with Duchenne Muscular Dystrophy lack sufficient expression of
a functional dystrophin protein in all striated muscles, resulting in the loss
of ambulation by 12 years of age, progressive respiratory insufficiency
and dilated cardiomyopathy (Khirani, Ramirez et al. 2014, Yiu and
Kornberg 2015). Currently, cardiac failure is the leading cause of
mortality in DMD (Eagle M. 2002) with available treatment options having
only limited efficacy due to their lack of specificity. The molecular
principles behind DCM are poorly understood and current cardiac
therapies show limited efficacy due to their lack of specificity. One of the
most promising therapeutic approaches is AAV gene therapy that aims to
deliver a functional dystrophin cDNA to skeletal and cardiac muscle. The
packaging capacity of the AAV vectors (4.7 kilo-bases) (Naso,
Tomkowicz et al. 2017) is not enough to fit the whole dystrophin cDNA
(14 kilo-bases). Therefore, several miniaturised versions of dystrophin
have been created for insertion into AAV vectors and tested in animal
models. These miniaturised versions of dystrophin, called mini and
micro-dystrophins contains different combinations of the dystrophin
domains and showed various disease pathology rescue effects. The
ΔR4-R23/ΔCT micro-dystrophin, has been well characterised for its
capacity to rescue both skeletal and cardiac muscle impairments in
mdx[23] mice (Yue, Li et al. 2003, Gregorevic, Allen et al. 2006, Townsend,
Blankinship et al. 2007, Bostick, Yue et al. 2008, Bostick, Shin et al.
2011, Bostick, Shin et al. 2012) and is currently in a phase 1/2a clinical
trial (Duan 2018, Mendell, Sahenk et al. 2020). In mdx[23] mice, this

construct showed a complete rescue of skeletal muscle pathology (Bostick, Yue et al. 2009) but only a partial rescue of the impaired cardiac parameters (Townsend, Blankinship et al. 2007, Bostick, Shin et al. 2011, Bostick, Shin et al. 2012). The incomplete rescue of the cardiac parameters by the ΔR4-R23/ΔCT micro-dystrophin construct needs to be elucidated starting from the investigation of molecular interactions that dystrophin establishes in the heart that are potentially not rescued by this construct. The discovery made by Johnson and colleagues that dystrophin establishes cardiomyocyte specific protein associations suggested the existence of cardiac-specific functions of dystrophin (Johnson, Zhang et al. 2012). Cavin-1 is one of the proteins that was found by Johnson et al to be part of the DGC only in the heart and is part of a complex that also includes cavin-2, -3, -4. Mutations in cavin-1 as well as cavin-4 are associated with cardiac disease. The main hypothesis is that the association of dystrophin and cavin-1 is important for cardiac function and that this association is impaired by the loss of dystrophin in DMD patients. Since cavin-1 is part of a complex, it is fair to hypothesise that cavin-2, -3 and cavin-4 also interact with dystrophin and that they are affected by the loss of dystrophin contributing to cardiac disease in DMD patients. It was also important to assess whether the ΔR4-R23/ΔCT micro-dystrophin construct was able to associate with cavin-1 as full-length dystrophin and potentially with the other cavins. This molecular characterisation is beneficial for several reasons:

-It will add information in terms of the role of dystrophin in the heart.

-It will be informative for the design of the future gene therapy construct.

-It will be beneficial for finding new targeted cardiac therapies for DCM in DMD patients.

In this chapter the results will be consolidated and discussed for their potential contribution in treating DCM in DMD patients.

6.1.1 Characterisation of the ΔR4-R23/ΔCT micro-dystrophin mouse.

In chapter 3, the transgenic mdx[5cv] mouse expressing the ΔR4-R23/ΔCT micro-dystrophin construct (Harper, Hauser et al. 2002) was characterised in terms of the efficiency of this construct to be expressed in cardiomyocytes and for its ability to rescue the members of the DGC. Among other micro and mini-dystrophin constructs, the ΔR4-R23/ΔCT is the most studied in terms of its capacity to rescue impaired cardiac parameters in mdx[23] mice. Townsend and colleagues found that mdx[23] mice expressing the ΔR4-R23/ΔCT construct under the murine cytomegalovirus (CMV) promoter/enhancer showed a restoration of the normal diastolic volume and did not have cardiac pump failure during induced cardiac stress *in vivo*. However, it was not able to correct the systolic pressure that is attenuated in mdx[23] heart, and it did not correct cardiac force development (Townsend, Blankinship et al. 2007). It also been reported that this construct improves the electrocardiographic profile but did not normalise the cardiomyopathy index in mdx[23] mice (Bostick, Yue et al. 2008). The cardiomyopathy index was the calculated value of QT interval (the time in which the ventricles are repolarised) divided by the PQ segment (the time in which the action potential is transmitted from the atria to the ventricles) (Nigro, Comi et al. 1990) and was found reduced compared to mdx[23] mice but not normalised to wild-type level (Bostick, Yue et al. 2008). The ΔR4-R23/ΔCT construct also improved cardiac fibrosis in 24 weeks mdx[23] mice (Shin, Nitahara-Kasahara et al. 2011) but not in aged mdx[23] mice (21 months) (Bostick,

Shin et al. 2012). Bostick and colleagues also showed that mdx[23] mice expressing the ΔR4-R23/ΔCT construct had a normalised PR interval and QRS duration but did not show improvement in other electrocardiographic parameters such as the cardiomyopathy index, the QT interval, and the Q amplitude. These studies highlight the high therapeutical potential of this construct in rescuing skeletal muscle disease and some cardiac parameters but also its limitations. The reason why this construct is more efficient in rescuing skeletal muscle, but not cardiac disease is still unknown. However, a study from Johnson and colleagues (Johnson, Zhang et al. 2012) found that the cardiac DGC includes proteins that are not present in the skeletal muscle DGC. This suggests that dystrophin carries out different or additional roles in the heart that probably involve dystrophin domains that are not included in the ΔR4-R23/ΔCT micro-dystrophin construct.

The ΔR4-R23/ΔCT micro-dystrophin construct (Harper, Hauser et al. 2002) contains the N-terminal domain that is essential for dystrophin to bind with the actin cytoskeleton (Norwood, Sutherland-Smith et al. 2000), it also contains hinge 1 with spectrin repeats 1-3 in order to avoid the misfolding of the N-terminus (Acsadi, Moore et al. 2012). Spectrin repeats 1-3 are also essential for the dystrophin interaction with the sarcolemma (Zhao, Kodippili et al. 2016). It lacks almost all the rod domain and the choice to remove most of the rod domain from this construct was made as in-frame deletions in the rod domain are often found in milder BMD patients (England, Nicholson et al. 1990, Yazaki, Yoshida et al. 1999). The C-terminus was removed based on the

assumption that is not critical for skeletal muscle function (Corrado K. 1996, Crawford G. E. 2000).

The results reported in chapter 3 show that the ΔR4-R23/ΔCT micro-dystrophin protein in the heart of mdx[5cv] transgenic mice is correctly expressed at the cardiomyocyte lateral membrane and at the intercalated discs as in wild-type (C57BL/6J) mice. Moreover, I showed that the micro-dystrophin protein is expressed 1.7-fold higher than dystrophin at the cardiomyocyte lateral membrane of transgenic mdx[5cv] mice compared to wild-type mice. The high expression of the ΔR4-R23/ ΔCT micro-dystrophin in transgenic mdx[5cv] is attributable to the cardiac muscle-specific alpha-myosin heavy chain (αMHC) promoter that drives the expression of this construct (Molkentin, Jobe et al. 1996, Salva, Himeda et al. 2007). As mentioned in **1.1**, dystrophin fulfils its biological function when associated with the other members of the DGC. Yue at al. assessed the capacity of the ΔR4-R23/ΔCT micro-dystrophin construct to restore the dystrophin-glycoprotein complex in the heart of mdx[23] mice (Yue, Li et al. 2003) performing immunofluorescence of only β-sarcoglycan and β-dystroglycan. I looked at the members of DGC (β-dystroglycan, β-sarcoglycan, α1-syntrophin, α-dystrobrevins) in mdx[5cv] and mdx[5cv] expressing ΔR4-R23/ΔCT micro-dystrophin using three different approaches. Firstly, my colleague (Ms Charlotte Scott) quantified protein expression levels of the DGC in cardiac lysate from wild-type, mdx[5cv] and ΔR4-R23/ΔCT micro-dystrophin mice (Wang, Marrosu et al. 2021) finding that mdx[5cv] mice have a significant reduction in the expression levels of α1-syntrophin, and α-dystrobrevins, and a trend for reduced expression of β-dystroglycan and β-sarcoglycan compared to wild-type mice.

In mdx^{5cv}-μDYS hearts, the levels of β-dystroglycan and β-sarcoglycan were increased above wild-type levels (>2-fold), while expression of α1-syntrophin and α-dystrobrevins was normalised to wild-type levels.

I proceeded with the investigation of the members of the DGC and tested whether the protein expression levels matched with their levels of membrane expression, using immunofluorescence and then quantifying the DGC members fluorescence intensity of wild-type, mdx^{5cv} and ΔR4-R23/ΔCT micro-dystrophin mice. The mdx^{5cv} mice showed a significant decrease for all DGC proteins at the cardiomyocyte membrane compared to wild-type, with the exception of α-dystrobrevin. Additionally, α1-syntrophin consistently showed diffuse intracellular immunofluorescence in mdx^{5cv} cardiomyocytes. In mdx^{5cv} -μDYS hearts, membrane expression of β-dystroglycan and α1-syntrophin were increased beyond and up to wild-type levels respectively, in agreement with western blot quantifications. However, diffuse intracellular immunofluorescence was still present for α1-syntrophin in mdx^{5cv} -μDYS cardiomyocytes. Furthermore, although membrane expression of β-sarcoglycan was significantly increased by mdx^{5cv} -μDYS compared to mdx^{5cv} mice, it remained significantly lower than wild-type cardiomyocytes in contrast to our western blot results. The last approach I used to study the cardiac DGC in mdx^{5cv} and mdx^{5cv} -μDYS mice was chosen to assess whether the protein expression of the members of DGC was correlated with the levels of mRNA. I found that whether the loss of dystrophin in in mdx^{5cv} hearts leads to reduction of the DGC protein expression compared to wild-type their mRNA was significantly upregulated in mdx^{5cv} mice with the exception of α-dystrobrevin that did not show any significant change. The upregulation of β-dystroglycan, β-

sarcoglycan and α1-syntrophin in mdx[5cv] suggest a compensatory mechanism triggered by the loss of full-length dystrophin activated only at mRNA level and not at translational level. As regards of ΔR4-R23/ΔCT micro-dystrophin mice, I found that the ΔR4-R23/ΔCT construct normalised the transcripts of the DGC members at wild-type level. Taken together these data showed that in mdx[5cv] hearts there is a correlation between the levels of protein expression of the members of the DGC and the effective protein localised at the membrane of the cardiomyocyte where they are needed. However, these data also tell that looking at the mRNA level is not the best way to study the DGC in mdx[5cv] hearts as the levels of mRNA of the DGC members does not correlate with their protein expression and localisation. More importantly, these data showed that ΔR4-R23/ΔCT construct normalised the level of the DGC members at the cardiomyocyte membrane of mdx[5cv] mice.

The ΔR4-R23/ΔCT construct includes the cysteine-rich domain that appeared to be enough to bring β-dystroglycan at the cardiomyocyte membrane of mdx[5cv] heart and is also able to restore α1-syntrophin and α-dystrobrevin although this construct does not have their binding site (C-terminus). This effect of the ΔR4-R23/ΔCT construct was also seen in a study performed in the skeletal muscle of transgenic mice mdx[23] (Yue, Liu et al. 2006). According with the immunoprecipitation studies on knockout mice performed by Yoshida and colleagues the sarcoglycan-sarcospan complex associates with α-dystrobrevin and α1-syntrophin in skeletal muscle (Yoshida M. 2000). It would be interesting and useful to see whether this association occurs also in cardiac muscle.

Overall, the ΔR4-R23/ΔCT construct normalizes transcript levels of the DGC in mdx[5cv]-μDYS mice and increases the total protein expression levels and membrane localisation of DGC proteins in transgenic mdx[5cv]-μDYS cardiomyocytes. However, there are differences in the efficacy of rescue at the protein level for different DAPC proteins. From these results, I also conclude that an approach that uses multiple techniques to analyse data from different point of views (protein expression, localisation and transcription) is more efficient in order to better evaluate the real rescuing capacity of this or other constructs.

6.1.2 Cavins are disrupted at the cardiomyocyte membrane of mdx[5cv] mice and ΔR4-R23/ΔCT micro-dystrophin does not restore their physiological cardiac localisation

The ΔR4-R23/ΔCT micro-dystrophin construct showed its partial ability to restore the impaired cardiac parameters in mdx[23] mice (Townsend, Blankinship et al. 2007, Bostick, Shin et al. 2011, Bostick, Shin et al. 2012). The reason of this partial restoration still needs to be investigated. The discovery that the DGC includes cavin-1 only in the heart and not in skeletal muscle opened to the possibility that dystrophin plays additional roles in the heart (Johnson, Zhang et al. 2012). The co-immunoprecipitation data generated by Johnson and Zhang published recently showed that not only cavin-1 is part of the cardiac DGC in wild-type mice but also cavin-2, and -4 co-purified with dystrophin and were found significantly decreased in ΔR4-R23/ΔCT micro-dystrophin mice (Wang, Marrosu et al. 2021). The immunofluorescence data I reported in chapter 4 showed that in the heart of wild-type mice cavin-1, -2 and -4 are expressed at the cardiomyocyte membrane. To my knowledge, the immunofluorescence data generated for chapter 4 report for the first time

the expression of cavin-1, -2 and -4 at the intercalated discs. Only caveolin-1 and -3 were found to be localised at the intercalated discs of monkey (*Macaca fascicularis*) heart (Hagiwara, Nishina et al. 2002) suggesting a role for cavins in the electrical or mechanical connections between cardiomyocytes.

In mdx^{5cv} mice where full-length dystrophin is not expressed, cavin-1 is lost from the cardiomyocyte membrane and cavin-2 and cavin-4 are severely disrupted. The fluorescence quantification of cavin-1 and cavin-4 showed the significant reduction of these proteins in mdx^{5cv} hearts compared to wild-type. The immunofluorescence studies of cavin-1, -2 and -4 in ΔR4-R23/ΔCT micro-dystrophin mice showed that the disruption of the cavins observed in mdx^{5cv} hearts is not rescued by the expression of this construct. These data not only showed that inability of the ΔR4-R23/ΔCT micro-dystrophin construct to restore the cardiomyocyte membrane localisation of cavin-1 and -4 but also gave important information on the possible dystrophin binding domains involved with the cavins in the heart. In fact, the domains chosen to be inserted into this construct are very likely not involved in the binding with cavin-1, -2 and -4. I have also found that when full-length dystrophin is not expressed (mdx^{5cv} and ΔR4-R23/ΔCT micro-dystrophin mice) cavin-4 underwent localisation into the cardiomyocyte nuclei. Because Cavin 4 mediates cardioprotection in response to adrenergic stress (Ogata et al), these findings laid the foundation for another study conducted by my colleagues on ERK signalling (Wang, Marrosu et al. 2021).

Because cavin-1 and cavin-4 loss-of-function mutations have been associated with cardiac diseases (Rajab, Straub et al. 2010, Rodriguez,

Ueyama et al. 2011, Taniguchi, Maruyama et al. 2016) finding the dystrophin domains involved in the binding with cavin-1 and -4 could help the design of the next gene therapy constructs and for targeted cardiac therapies.

6.1.3 The C-terminus, spectrin repeats 16-19, spectin repeats 20-24 and hinges 2 and 3 of dystrophin do not associates with cavins.

The use of different transgenic mice expressing different constructs helped me to narrow down the dystrophin domain possibly associated with cavin-1 and -4 (constructs showed in **figure 9**). In fact, from the immunofluorescence data I collected I have been able to conclude that the C-terminus, spectrin repeats 16-19, spectin repeats 20-24 and hinges 2 and 3 are no involved with cavin-1 and cavin-4.

6.2 The genetic background of DMD mice and their dystrophin mutations should be taken in account for the cardiac study of cavin-1 and -4.

The mini and micro-dystrophin constructs that I tested during my PhD project (**Figure 9**) are expressed in mdx[23] on C57BL/10 background, one of them is expressed in mdx[23] mice on FVB background (the ΔH2-R15) and another one (the ΔR4-R23/ΔCT) is expressed in mdx[5cv] on C57BL/6 background. The mdx[23] mice on FVB background showed the same pattern of disruption for both cavin-1 and cavin-4 observed in mdx[5cv] mice (C57BL/6J background) with the complete loss of cavin-1 at the cardiomyocyte membrane and a severe membrane disruption of cavin-4 accompanied by diffuse intracellular staining. The mdx[23] mice on C57BL/10 background, did not show the loss of cavin-1 at their cardiomyocyte membrane, but did display a slight decrease in staining

and a membrane disruption of cavin-4 with an abnormal intracellular distribution that resemble the t-tubules. The differences in the cavin-1 and cavin-4 disruption between mdx[23] and mdx[5cv] mice could be due to the different dystrophin mutations leading to differential expression of smaller isoforms. For example, Dp71 was described to be expressed at the t-tubules of mdx[23] mice (Masubuchi, Shidoh et al. 2013) while there are no reports of dystrophin isoforms expressed in the mdx[5cv] hearts.

The different genetic background of the mdx[23], specifically the C57BL/10 and the FVB may also be the cause of the difference in the cavin-1 and cavin-4 disruption observed in mdx[23] mice.

Duan and colleagues studied the skeletal muscle of these two mdx[23] mice and showed that the dystrophic phenotype did not change dramatically between them (Wasala, Zhang et al. 2015). However, an evaluation of the cardiac parameters of the mdx[23] with different backgrounds have never been done. The only cardiac comparison made on mdx[23] mice with different backgrounds has been done in two studies where the authors compared the C57BL/10 with the DBA/2J background. They found a more severe cardiac phenotype in the mdx[23] with the DBA/2J background that the authors attributed to the presence of genetic modifier loci in the DBA/2J background (Coley, Bogdanik et al. 2016, van Putten, Putker et al. 2019). A similar comparative study should be also done to assess whether mdx[23] on FVB and C57BL/10 backgrounds show differences in cardiac physiology and response to cardiac stress. Previous studies already demonstrated both genetic (McClive, Huang et al. 1994, Slingsby, Hogarth et al. 1996) and behavioural (Deacon, Thomas et al. 2007) differences between C57BL/10 and C57BL/6J. It will

also be interesting to directly compare the cardiac phenotype of the mdx[23] and the mdx[5cv] mice to confront the two different mutations and the different genetic backgrounds. This would be useful in order to find the most suitable mouse model for DMD cardiac studies.

6.3 Cavins have a conserved localisation across different species

The immunofluorescence studies of cavins in other DMD animal models gave me the opportunity to expand the body of knowledge on caveolar proteins expression and localisation in the heart, it offered me also the possibility to consolidate or confront the results obtained in mice with DMD animal models that show cardiomyopathy symptoms that better recapitulate the DMD patient phenotype. The immunofluorescence data I generated in these DMD animal models were also compared with the immunofluorescence data obtained from samples of human heart. One of the major findings was that cavin-1 and cavin-4 showed the same cardiac localisation in all the studied species, including humans making all these animal models suitable for the study of cavins. I also generated interesting results in terms of the effect that the loss of full-length dystrophin has on cavins in dog (ΔE50-MD) and rat (DMD[mdx]) DMD models. I first found that cavin-1 is not dramatically disrupted in DMD[mdx] rats and ΔE50-MD dogs as observed in mdx[23] mice on C57BL/10 background. I also found that cavin-4 has the same abnormal striated cytoplasmic distribution observed in mdx[23] mice on C57BL/10 background. This could be due to the expression of shorter dystrophin isoforms in DMD rat and dog cardiomyocytes such as Dp71 that was found to be expressed in mdx[23] hearts (Masubuchi, Shidoh et al. 2013).

I have tested the cardiac samples from DMD[mdx] rats with an antibody able to recognise shorter dystrophin isoforms and I found that they are expressed and distributed as the dystrophin isoform Dp71 was in the study of Masubuchi on cardiomyocytes of mdx[23] mice on C57BL/10 background (Masubuchi, Shidoh et al. 2013). The observation that cavin-4 in both ΔE50-MD dogs and in DMD[mdx] rats shows the same pattern of disruption observed in mdx[23] (C57BL/10) hearts leads me to hypothesise that cavin-4 localisation could be influenced by shorter dystrophin isoforms. Cardiac tissue from ΔE50-MD dogs should be tested for the expression of shorter dystrophin isoforms as I did for DMD rats in order to assess the expression of Dp71. This was not done because of the limited amount of ΔE50-MD dog cardiac sections.

In conclusion, the cardiac localisations of cavins are conserved across different species making all of these models suitable for the study of cavins in the hearts. The DMD rat and dog models showed the same cardiac disruption of cavin-1 and cavin-4 observed mdx[23] mice on C57BL/10 background. It is difficult to conclude which is the best DMD animal model for the study of DCM since currently there are no data concerning the effect of dystrophin loss on caveolar proteins in DMD patients.

6.4 Future work

The observations and the findings collected from my PhD thesis leaved some open questions that need to be answered to achieve a deeper understanding on the role of dystrophin in the hearts.

The first question concerns the impact that the loss of full-length dystrophin has on cardiac cavin localisation in DMD patients. It would be useful to investigate whether the loss of full-length dystrophin causes the same disruption of cavin-1 and cavin-4 as observed in DMD animal models. From a clinical standpoint, it would be interesting to compare caveolae-associated cardiomyopathies with cardiac disease in DMD but also in BMD patients. Whether caveolar protein localisation is impaired in DMD patients the management of cardiac disease for patients with caveolar dysfunction might provide useful insights to treat DCM in DMD and BMD patients. For this purpose, repeating the same study I did for my PhD on DMD animal models in DMD and BMD patient cardiac samples would be very informative.

The second question concerns the impact that the loss of full-length dystrophin has on the ultrastructure of caveolae in DMD animal models. It would be crucial to perform electron microscopy experiments in DMD animal models since studies on the heart of cavin-1 knock-out mice (Taniguchi, Maruyama et al. 2016) showed the loss of caveolae at the cardiomyocyte membrane. The DMD animal models I studied during my PhD showed a partial or complete loss of cavin-1 at the cardiomyocyte lateral membrane, possible changes in the number and shape of caveolae due to the disruption of cavin-1 at the cardiomyocyte lateral membrane of the examined DMD animal models can be detected with electron microscopy.

Future work should also focus on better characterising the association between dystrophin and the cavins. For this purpose, co-immunoprecipitation using antibodies against cavin-1, cavin-2 and cavin-

4 should be used to test whether they co-purify with dystrophin, thereby clarifying how they interact.

It would be also interesting to study the distribution of different dystrophin isoforms in mdx[5cv] and mdx[23] on both C57BL/10 and FVB backgrounds performing western blot and immunofluorescence using dystrophin C-terminus antibodies and acquiring images with the confocal microscopy to gain a more detailed picture of their cardiac distribution.

It would be also interesting to investigate which dystrophin isoforms are still expressed in the hearts of DMD[mdx] rats and ΔE50-MD dogs in relation to the abnormal distribution of cavin-4 I observed. Potentially, this would reveal new insights as to the nature of cavin-4 binding sites on dystrophin in relevant models providing additional information on the value of comparative studies in DMD research.

6.5 Concluding remarks

The study I conducted during my PhD, has increased the knowledge on the following key areas:

1. It highlighted an association between dystrophin and cavin-1, -2 and -4 that are impaired by the dystrophin loss.
2. It identified previously unrecognised cardiac limitations of the ΔR4-R23/ΔCT micro-dystrophin gene therapy construct in fully rescuing membrane expression of cavins-1, -2 and -4 as well as a subset of core proteins of the cardiac dystrophin-associated proteins complex (namely β-sarcoglycan and α1-syntrophin). This information is extremely important in understanding the molecular

context for the partial rescue of cardiac hemodynamic parameters by this micro-dystrophin.

3. None of the tested micro and mini-dystrophins will likely rescue cavins in the heart and may suffer from the same functional limitations as ΔR4-R23/ΔCT micro-dystrophin.

4. The cardiac localisation of the cavins is the same in humans and the tested animal models. Moreover, cavins localisation is affected in all the tested DMD models due to the loss of full-length dystrophin.

Bibliography

A. J. Kanai, L. L. P., P. R. Clemens, L. A. Birder, M. M. VanBibber, S. Y. Choi, W. C. de Groat, J. Peterson (2001). "Identification of a neuronal nitric oxide synthase in isolated cardiac mitochondria using electrochemical detection." Proc Natl Acad Sci U S A **98**(24): 14126–14131.

Aartsma-Rus, A., J. C. Van Deutekom, I. F. Fokkema, G. J. Van Ommen and J. T. Den Dunnen (2006). "Entries in the Leiden Duchenne muscular dystrophy mutation database: an overview of mutation types and paradoxical cases that confirm the reading-frame rule." Muscle Nerve **34**(2): 135-144.

Acsadi, G., S. A. Moore, A. Chéron, O. Delalande, L. Bennett, W. Kupsky, M. El-Baba, E. Le Rumeur and J. F. Hubert (2012). "Novel mutation in spectrin-like repeat 1 of dystrophin central domain causes protein misfolding and mild Becker muscular dystrophy." J Biol Chem **287**(22): 18153-18162.

Adams, M. E., G. L. Odom, M. J. Kim, J. S. Chamberlain and S. C. Froehner (2018). "Syntrophin binds directly to multiple spectrin-like repeats in dystrophin and mediates binding of nNOS to repeats 16-17." Hum Mol Genet **27**(17): 2978-2985.

Adorisio, R., E. Mencarelli, N. Cantarutti, C. Calvieri, L. Amato, M. Cicenia, M. Silvetti, A. D'Amico, M. Grandinetti, F. Drago and A. Amodeo (2020). "Duchenne Dilated Cardiomyopathy: Cardiac Management from Prevention to Advanced Cardiovascular Therapies." J Clin Med **9**(10).

Amann, K. J., B. A. Renley and J. M. Ervasti (1998). "A cluster of basic repeats in the dystrophin rod domain binds F-actin through an electrostatic interaction." J Biol Chem **273**(43): 28419-28423.

Amoasii, L., J. C. W. Hildyard, H. Li, E. Sanchez-Ortiz, A. Mireault, D. Caballero, R. Harron, T. R. Stathopoulou, C. Massey, J. M. Shelton, R. Bassel-Duby, R. J. Piercy and E. N. Olson (2018). "Gene editing restores dystrophin expression in a canine model of Duchenne muscular dystrophy." Science **362**(6410): 86-91.

Anastasi, G., G. Cutroneo, R. Gaeta, D. Di Mauro, A. Arco, A. Consolo, G. Santoro, F. Trimarchi and A. Favaloro (2009). "Dystrophin-glycoprotein complex and vinculin-talin-integrin system in human adult cardiac muscle." Int J Mol Med **23**(2): 149-159.

Anderson, J. T., R. P. Rogers and H. W. Jarrett (1996). "Ca2+-calmodulin binds to the carboxyl-terminal domain of dystrophin." J Biol Chem **271**(12): 6605-6610.

Angelini, C., M. Fanin, M. P. Freda, F. Martinello, M. Miorin, P. Melacini, G. Siciliano, E. Pegoraro, M. Rosa and G. A. Danieli (1996). "Prognostic factors in mild dystrophinopathies." J Neurol Sci **142**(1-2): 70-78.

Arechavala-Gomeza, V., M. Kinali, L. Feng, S. C. Brown, C. Sewry, J. E. Morgan and F. Muntoni (2010). "Immunohistological intensity measurements as a tool to assess sarcolemma-associated protein expression." Neuropathol Appl Neurobiol **36**(4): 265-274.

Ashford, M. W., Jr., W. Liu, S. J. Lin, P. Abraszewski, S. D. Caruthers, A. M. Connolly, X. Yu and S. A. Wickline (2005). "Occult cardiac contractile dysfunction in dystrophin-deficient children revealed by cardiac magnetic resonance strain imaging." Circulation **112**(16): 2462-2467.

Austin, R. C., , Howard, P. L., D'Souza, V. N., Klamut, H. J., P. N. Ray. (1995). "Cloning and characterization of alternatively spliced isoforms of Dp71." Human Molecular Genetics **4**(9): 1475-1483.

Ayalon, G., J. Q. Davis, P. B. Scotland and V. Bennett (2008). "An ankyrin-based mechanism for functional organization of dystrophin and dystroglycan." Cell **135**(7): 1189-1200.

Balakrishnan, B. and G. R. Jayandharan (2014). "Basic biology of adeno-associated virus (AAV) vectors used in gene therapy." Curr Gene Ther **14**(2): 86-100.

Balijepalli, R. C., J. D. Foell, D. D. Hall, J. W. Hell and T. J. Kamp (2006). "Localization of cardiac L-type Ca(2+) channels to a caveolar macromolecular signaling complex is required for beta(2)-adrenergic regulation." Proc Natl Acad Sci U S A **103**(19): 7500-7505.

Banks, G. B., A. C. Combs and J. S. Chamberlain (2010). "Sequencing protocols to genotype mdx, mdx(4cv), and mdx(5cv) mice." Muscle Nerve **42**(2): 268-270.

Banks, G. B., P. Gregorevic, J. M. Allen, E. E. Finn and J. S. Chamberlain (2007). "Functional capacity of dystrophins carrying deletions in the N-terminal actin-binding domain." Human Molecular Genetics **16**(17): 2105-2113.

Banks, G. B., L. M. Judge, J. M. Allen and J. S. Chamberlain (2010). "The polyproline site in hinge 2 influences the functional capacity of truncated dystrophins." PLoS Genet **6**(5): e1000958.

Beastrom, N., H. Lu, A. Macke, B. D. Canan, E. K. Johnson, C. M. Penton, B. K. Kaspar, L. R. Rodino-Klapac, L. Zhou, P. M. Janssen and F. Montanaro (2011). "mdx(⁵cv) mice manifest more severe muscle dysfunction and diaphragm force deficits than do mdx Mice." Am J Pathol **179**(5): 2464-2474.

Belanto, J. J., T. L. Mader, M. D. Eckhoff, D. M. Strandjord, G. B. Banks, M. K. Gardner, D. A. Lowe and J. M. Ervasti (2014). "Microtubule binding distinguishes dystrophin from utrophin." Proc Natl Acad Sci U S A **111**(15): 5723-5728.

Berko, B. A. and M. Swift (1987). "X-linked dilated cardiomyopathy." N Engl J Med **316**(19): 1186-1191.

Bies, R. D., C. T. Caskey and R. Fenwick (1992). "An intact cysteine-rich domain is required for dystrophin function." J Clin Invest **90**(2): 666-672.

Bies, R. D., M. Maeda, S. L. Roberds, E. Holder, T. Bohlmeyer, J. B. Young and K. P. Campbell (1997). "A 5' dystrophin duplication mutation causes membrane deficiency of alpha-dystroglycan in a family with X-linked cardiomyopathy." J Mol Cell Cardiol **29**(12): 3175-3188.

Bies, R. D., M. Maeda, S. L. Roberds, E. Holder, T. Bohlmeyer, J. B. Young and K. P. Campbell (1997). "A 5′ Dystrophin Duplication Mutation Causes Membrane Deficiency ofα-Dystroglycan in a Family with X-linked Cardiomyopathy." Journal of Molecular and Cellular Cardiology **29**(12): 3175-3188.

Birnkrant, D. J., K. Bushby, C. M. Bann, B. A. Alman, S. D. Apkon, A. Blackwell, L. E. Case, L. Cripe, S. Hadjiyannakis, A. K. Olson, D. W. Sheehan, J. Bolen, D. R. Weber and L. M. Ward (2018). "Diagnosis and management of Duchenne

muscular dystrophy, part 2: respiratory, cardiac, bone health, and orthopaedic management." Lancet Neurol **17**(4): 347-361.

Birnkrant, D. J., K. Bushby, C. M. Bann, S. D. Apkon, A. Blackwell, M. K. Colvin, L. Cripe, A. R. Herron, A. Kennedy, K. Kinnett, J. Naprawa, G. Noritz, J. Poysky, N. Street, C. J. Trout, D. R. Weber and L. M. Ward (2018). "Diagnosis and management of Duchenne muscular dystrophy, part 3: primary care, emergency management, psychosocial care, and transitions of care across the lifespan." The Lancet Neurology **17**(5): 445-455.

Bladen, C. L., D. Salgado, S. Monges, M. E. Foncuberta, K. Kekou, K. Kosma, H. Dawkins, L. Lamont, A. J. Roy, T. Chamova, V. Guergueltcheva, S. Chan, L. Korngut, C. Campbell, Y. Dai, J. Wang, N. Barisic, P. Brabec, J. Lahdetie, M. C. Walter, O. Schreiber-Katz, V. Karcagi, M. Garami, V. Viswanathan, F. Bayat, F. Buccella, E. Kimura, Z. Koeks, J. C. van den Bergen, M. Rodrigues, R. Roxburgh, A. Lusakowska, A. Kostera-Pruszczyk, J. Zimowski, R. Santos, E. Neagu, S. Artemieva, V. M. Rasic, D. Vojinovic, M. Posada, C. Bloetzer, P. Y. Jeannet, F. Joncourt, J. Diaz-Manera, E. Gallardo, A. A. Karaduman, H. Topaloglu, R. El Sherif, A. Stringer, A. V. Shatillo, A. S. Martin, H. L. Peay, M. I. Bellgard, J. Kirschner, K. M. Flanigan, V. Straub, K. Bushby, J. Verschuuren, A. Aartsma-Rus, C. Beroud and H. Lochmuller (2015). "The TREAT-NMD DMD Global Database: analysis of more than 7,000 Duchenne muscular dystrophy mutations." Hum Mutat **36**(4): 395-402.

Blake D. J., T. J. M., Davies K. E., Knight A. E., Winder S. J., Kendrick-Jones J. (1995). "Coiled-coil regions in the carboxy-terminal domains of dystrophin and related proteins: potentials for protein-protein interactions." Trends Biochem Sci. **20**(4): 133-135.

Blake, D. J., J. N. Schofield, R. A. Zuellig, D. C. Górecki, S. R. Phelps, E. A. Barnard, Y. H. Edwards and K. E. Davies (1995). "G-utrophin, the autosomal homologue of dystrophin Dp116, is expressed in sensory ganglia and brain." Proc Natl Acad Sci U S A **92**(9): 3697-3701.

Blake, D. J., A. Weir, S. E. Newey and K. E. Davies (2002). "Function and genetics of dystrophin and dystrophin-related proteins in muscle." Physiol Rev **82**(2): 291-329.

Bostick, B., J. H. Shin, Y. Yue and D. Duan (2011). "AAV-microdystrophin Therapy Improves Cardiac Performance in Aged Female mdx Mice." Mol Ther.

Bostick, B., J. H. Shin, Y. Yue, N. B. Wasala, Y. Lai and D. Duan (2012). "AAV micro-dystrophin gene therapy alleviates stress-induced cardiac death but not myocardial fibrosis in >21-m-old mdx mice, an end-stage model of Duchenne muscular dystrophy cardiomyopathy." J Mol Cell Cardiol **53**(2): 217-222.

Bostick, B., Y. Yue and D. Duan (2010). "Gender influences cardiac function in the mdx model of Duchenne cardiomyopathy." Muscle Nerve **42**(4): 600-603.

Bostick, B., Y. Yue, Y. Lai, C. Long, D. Li and D. Duan (2008). "Adeno-associated virus serotype-9 microdystrophin gene therapy ameliorates electrocardiographic abnormalities in mdx mice." Hum Gene Ther **19**(8): 851-856.

Bostick, B., Y. Yue, C. Long and D. Duan (2008). "Prevention of dystrophin-deficient cardiomyopathy in twenty-one-month-old carrier mice by mosaic dystrophin expression or complementary dystrophin/utrophin expression." Circ Res **102**(1): 121-130.

Bostick, B., Y. Yue, C. Long, N. Marschalk, D. M. Fine, J. Chen and D. Duan (2009). "Cardiac expression of a mini-dystrophin that normalizes skeletal muscle force only partially restores heart function in aged Mdx mice." <u>Mol Ther</u> **17**(2): 253-261.

Buckle, V. J., J. L. Guenet, D. Simon-Chazottes, D. R. Love and K. E. Davies (1990). "Localisation of a dystrophin-related autosomal gene to 6q24 in man, and to mouse chromosome 10 in the region of the dystrophia muscularis (dy) locus." <u>Hum Genet</u> **85**(3): 324-326.

Bulfield, G., W. G. Siller, P. A. Wight and K. J. Moore (1984). "X chromosome-linked muscular dystrophy (mdx) in the mouse." <u>Proc Natl Acad Sci U S A</u> **81**(4): 1189-1192.

Bushby, K., F. Muntoni and J. P. Bourke (2003). "107th ENMC International Workshop: the management of cardiac involvement in muscular dystrophy and myotonic dystrophy. 7th–9th June 2002, Naarden, the Netherlands." <u>Neuromuscular Disorders</u> **13**(2): 166-172.

Byers, T. J., Lidov, H. G. W., Kunkel, L. M. (1993). "An alternative clystrophin transcript specific to peripheral nerve." <u>Nature Genetics</u> **4**: 77-81.

Carsana, A., G. Frisso, M. R. Tremolaterra, R. Lanzillo, D. F. Vitale, L. Santoro and F. Salvatore (2005). "Analysis of dystrophin gene deletions indicates that the hinge III region of the protein correlates with disease severity." <u>Ann Hum Genet</u> **69**(Pt 3): 253-259.

Chamberlain, J. S., J. Metzger, M. Reyes, D. Townsend and J. A. Faulkner (2007). "Dystrophin-deficient mdx mice display a reduced life span and are susceptible to spontaneous rhabdomyosarcoma." <u>Faseb j</u> **21**(9): 2195-2204.

Chan Y. M., B. C. G., Lidov H. G., Kunkel L. M. (1998). "Molecular Organization of Sarcoglycan Complex in Mouse Myotubes in Culture." <u>J Cell Biol</u> **143**(7): 2033-2044.

Chandler, R. J., M. S. Sands and C. P. Venditti (2017). "Recombinant Adeno-Associated Viral Integration and Genotoxicity: Insights from Animal Models." <u>Hum Gene Ther</u> **28**(4): 314-322.

Chelly, J., F. Marlhens, B. Le Marec, M. Jeanpierre, M. Lambert, G. Hamard, B. Dutrillaux and J. C. Kaplan (1986). "De novo DNA microdeletion in a girl with Turner syndrome and Duchenne muscular dystrophy." <u>Hum Genet</u> **74**(2): 193-196.

Chen, H. C., Y. F. Chin, D. J. Lundy, C. T. Liang, Y. H. Chi, P. Kuo and P. C. H. Hsieh (2017). "Utrophin Compensates dystrophin Loss during Mouse Spermatogenesis." <u>Sci Rep</u> **7**(1): 7372.

Chenard, A. A., H. M. Becane, F. Tertrain, J. M. de Kermadec and Y. A. Weiss (1993). "Ventricular arrhythmia in Duchenne muscular dystrophy: prevalence, significance and prognosis." <u>Neuromuscul Disord</u> **3**(3): 201-206.

Cheng, J. P., C. Mendoza-Topaz, G. Howard, J. Chadwick, E. Shvets, A. S. Cowburn, B. J. Dunmore, A. Crosby, N. W. Morrell and B. J. Nichols (2015). "Caveolae protect endothelial cells from membrane rupture during increased cardiac output." <u>J Cell Biol</u> **211**(1): 53-61.

Cho, W. J., A. K. Chow, R. Schulz and E. E. Daniel (2010). "Caveolin-1 exists and may function in cardiomyocytes." <u>Can J Physiol Pharmacol</u> **88**(1): 73-76.

Chung W., C. J. T. (1999). "WW and EF Hand Domains of Dystrophin-Family Proteins Mediate Dystroglycan Binding." Molecular Cell Biology Research Communications **2**(3): 167-171.

Clerk, A., G. E. Morris, V. Dubowitz, K. E. Davies and C. A. Sewry (1993). "Dystrophin-related protein, utrophin, in normal and dystrophic human fetal skeletal muscle." Histochem J **25**(8): 554-561.

Clerk, A., C. A. Sewry, V. Dubowitz and P. N. Strong (1992). "Characterisation of dystrophin in fetuses at risk for Duchenne muscular dystrophy." Journal of the neurological sciences **111**(1): 82-91.

Clerk, A., P. N. Strong and C. A. Sewry (1992). "Characterisation of dystrophin during development of human skeletal muscle." Development **114**(2): 395-402.

Cohen, N. and F. Muntoni (2004). "Multiple pathogenetic mechanisms in X linked dilated cardiomyopathy." Heart **90**(8): 835-841.

Coley, W. D., L. Bogdanik, M. C. Vila, Q. Yu, J. H. Van Der Meulen, S. Rayavarapu, J. S. Novak, M. Nearing, J. L. Quinn, A. Saunders, C. Dolan, W. Andrews, C. Lammert, A. Austin, T. A. Partridge, G. A. Cox, C. Lutz and K. Nagaraju (2016). "Effect of genetic background on the dystrophic phenotype in mdx mice." Hum Mol Genet **25**(1): 130-145.

Corrado K., R. J. A., Mills P. L., Cole N. M., Faulkner J. A., Wang K., Chamberlain J. S. (1996). "Transgenic mdx mice expressing dystrophin with a deletion in the actin-binding domain display a "mild Becker" phenotype." J Cell Biol **134**(4): 873-884.

Cox, G. F. and L. M. Kunkel (1997). "Dystrophies and heart disease." Curr Opin Cardiol **12**(3): 329-343.

Crawford G. E., F. J. A., Crosbie R. H., Campbell K. P., Froehner S. C., Chamberlain J. S. (2000). "Assembly of the Dystrophin-associated Protein Complex Does Not Require the Dystrophin COOH-terminal Domain." The Journal of Cell Biology **150**(6): 1399-1409.

Crawford, G. E., J. A. Faulkner, R. H. Crosbie, K. P. Campbell, S. C. Froehner and J. S. Chamberlain (2000). "Assembly of the Dystrophin-Associated Protein Complex Does Not Require the Dystrophin Cooh-Terminal Domain." Journal of Cell Biology **150**(6): 1399-1410.

Cross, R. A., M. Stewart and J. Kendrick-Jones (1990). "Structural predictions for the central domain of dystrophin." FEBS Lett **262**(1): 87-92.

D.M Pillers, D. E. B., R.G.Weleber, D.A. Sigesmund, M.A. Musarella, B.R. Powell,W.H. Murphey, C. Westall, C. Panton, L.E. Becker, R.G. Worton, P.N. Ray. (1993). "Dystrophin expression in the human retina is required for nonnal function as defined by electroretinography." Nature Genetics: 82-86.

Dae, M. W., M. A. Heymann and A. L. Jones (1982). "A new technique for perfusion fixation and contrast enhancement of foetal lamb myocardium for electron microscopy." J Microsc **127**(Pt 3): 301-305.

Dangain, J. and G. Vrbova (1984). "Muscle development in mdx mutant mice." Muscle Nerve **7**(9): 700-704.

Danialou, G., A. S. Comtois, R. Dudley, G. Karpati, G. Vincent, C. Des Rosiers and B. J. Petrof (2001). "Dystrophin-deficient cardiomyocytes are abnormally

vulnerable to mechanical stress-induced contractile failure and injury." Faseb j **15**(9): 1655-1657.

Danialou, G., Comtois, A. S., Dudley, R., Karpati, G., Vincent, G., Des Rosiers, C., Petrof, B. J. (2001). "Dystrophin-deficient cardiomyocytes are abnormally vulnerable to mechanical stress-induced contractile failure and injury." FASEB J **15**.

Danko, I., V. Chapman and J. A. Wolff (1992). "The frequency of revertants in mdx mouse genetic models for Duchenne muscular dystrophy." Pediatr Res **32**(1): 128-131.

Daoud, F., A. Candelario-Martínez, J. M. Billard, A. Avital, M. Khelfaoui, Y. Rozenvald, M. Guegan, D. Mornet, D. Jaillard, U. Nudel, J. Chelly, D. Martínez-Rojas, S. Laroche, D. Yaffe and C. Vaillend (2008). "Role of mental retardation-associated dystrophin-gene product Dp71 in excitatory synapse organization, synaptic plasticity and behavioral functions." PLoS One **4**(8): e6574.

Deacon, R. M., C. L. Thomas, J. N. Rawlins and B. J. Morley (2007). "A comparison of the behavior of C57BL/6 and C57BL/10 mice." Behav Brain Res **179**(2): 239-247.

Di Mauro, D., R. Gaeta, A. Arco, D. Milardi, S. Lentini, M. Runci, G. Rizzo and L. Magaudda (2009). "Distribution of costameric proteins in normal human ventricular and atrial cardiac muscle." Folia Histochem Cytobiol **47**(4): 605-608.

Doorenweerd, N., A. Mahfouz, M. van Putten, R. Kaliyaperumal, T. H. PAC, J. G. M. Hendriksen, A. M. Aartsma-Rus, J. Verschuuren, E. H. Niks, M. J. T. Reinders, H. E. Kan and B. P. F. Lelieveldt (2018). "Author Correction: Timing and localization of human dystrophin isoform expression provide insights into the cognitive phenotype of Duchenne muscular dystrophy." Sci Rep **8**(1): 4058.

Dorchies, O. M., J. Reutenauer-Patte, E. Dahmane, H. M. Ismail, O. Petermann, O. Patthey- Vuadens, S. A. Comyn, E. Gayi, T. Piacenza, R. J. Handa, L. A. Decosterd and U. T. Ruegg (2013). "The anticancer drug tamoxifen counteracts the pathology in a mouse model of duchenne muscular dystrophy." Am J Pathol **182**(2): 485-504.

Duan, D. (2018). "Systemic AAV Micro-dystrophin Gene Therapy for Duchenne Muscular Dystrophy." Mol Ther **26**(10): 2337-2356.

Duboc, D., C. Meune, G. Lerebours, J. Y. Devaux, G. Vaksmann and H. M. Bécane (2005). "Effect of perindopril on the onset and progression of left ventricular dysfunction in Duchenne muscular dystrophy." J Am Coll Cardiol **45**(6): 855-857.

Duggan, D. J., J. R. Gorospe, M. Fanin, E. P. Hoffman and C. Angelini (1997). "Mutations in the sarcoglycan genes in patients with myopathy." N Engl J Med **336**(9): 618-624.

Eagle M, B. S., Chandler C, Giddings DR, Bullock R, Bushby K. (2002). "Survival in Duchenne muscular dystrophy: improvements in life expectancy since 1967 and the impact of home nocturnal ventilation." Neuromuscular Disorders.

Eagle M., B. S. V., Chandler C., Giddings D. R., Bullock R., Bushby K. (2002). "Survival in Duchenne muscular dystrophy: improvements in lifeexpectancy since 1967 and the impact of home nocturnal ventilation." Neuromuscul Disord **12**(10): 926-929.

England, S. B., L. V. Nicholson, M. A. Johnson, S. M. Forrest, D. R. Love, E. E. Zubrzycka-Gaarn, D. E. Bulman, J. B. Harris and K. E. Davies (1990). "Very mild muscular dystrophy associated with the deletion of 46% of dystrophin." Nature **343**(6254): 180-182.

Ervasti, J. M. and K. P. Campbell (1991). "Membrane organization of the dystrophin-glycoprotein complex." Cell **66**(6): 1121-1131.

Fabbrizio, E., U. Nudel, G. Hugon, A. Robert, F. Pons and D. Mornet (1994). "Characterization and localization of a 77 kDa protein related to the dystrophin gene family." Biochem J **299 (Pt 2)**(Pt 2): 359-365.

Fanin, M., G. A. Danieli, L. Vitiello, L. Senter and C. Angelini (1992). "Prevalence of dystrophin-positive fibers in 85 Duchenne muscular dystrophy patients." Neuromuscul Disord **2**(1): 41-45.

Feng, J., J. Yan, C. H. Buzin, J. A. Towbin and S. S. Sommer (2002). "Mutations in the dystrophin gene are associated with sporadic dilated cardiomyopathy." Mol Genet Metab **77**(1-2): 119-126.

Ferlini, A., N. Galié, L. Merlini, C. Sewry, A. Branzi and F. Muntoni (1998). "A novel Alu-like element rearranged in the dystrophin gene causes a splicing mutation in a family with X-linked dilated cardiomyopathy." Am J Hum Genet **63**(2): 436-446.

Ferrier, P., F. Bamatter and D. Klein (1965). "MUSCULAR DYSTROPHY (DUCHENNE) IN A GIRL WITH TURNER'S SYNDROME." J Med Genet **2**(1): 38-46.

Filareto, A., K. Maguire-Nguyen, Q. Gan, G. Aldanondo, L. Machado, J. S. Chamberlain and T. A. Rando (2018). "Monitoring disease activity noninvasively in the mdx model of Duchenne muscular dystrophy." Proceedings of the National Academy of Sciences **115**(30): 7741-7746.

Fine, D. M., J. H. Shin, Y. Yue, D. Volkmann, S. B. Leach, B. F. Smith, M. McIntosh and D. Duan (2011). "Age-matched comparison reveals early electrocardiography and echocardiography changes in dystrophin-deficient dogs." Neuromuscul Disord **21**(7): 453-461.

Gambin, Y., N. Ariotti, K. A. McMahon, M. Bastiani, E. Sierecki, O. Kovtun, M. E. Polinkovsky, A. Magenau, W. Jung, S. Okano, Y. Zhou, N. Leneva, S. Mureev, W. Johnston, K. Gaus, J. F. Hancock, B. M. Collins, K. Alexandrov and R. G. Parton (2013). "Single-molecule analysis reveals self assembly and nanoscale segregation of two distinct cavin subcomplexes on caveolae." Elife **3**: e01434.

Garcia, S., T. de Haro, M. Zafra-Ceres, A. Poyatos, J. A. Gomez-Capilla and C. Gomez-Llorente (2014). "Identification of de novo mutations of Duchénnè/Becker muscular dystrophies in southern Spain." Int J Med Sci **11**(10): 988-993.

Gavillet, B., J. S. Rougier, A. A. Domenighetti, R. Behar, C. Boixel, P. Ruchat, H. A. Lehr, T. Pedrazzini and H. Abriel (2006). "Cardiac sodium channel Nav1.5 is regulated by a multiprotein complex composed of syntrophins and dystrophin." Circ Res **99**(4): 407-414.

Gregorevic, P., J. M. Allen, E. Minami, M. J. Blankinship, M. Haraguchi, L. Meuse, E. Finn, M. E. Adams, S. C. Froehner, C. E. Murry and J. S.

Chamberlain (2006). "rAAV6-microdystrophin preserves muscle function and extends lifespan in severely dystrophic mice." Nat Med **12**(7): 787-789.

Grivas, D., Á. González-Rajal, C. Guerrero Rodríguez, R. Garcia and J. L. de la Pompa (2020). "Loss of Caveolin-1 and caveolae leads to increased cardiac cell stiffness and functional decline of the adult zebrafish heart." Sci Rep **10**(1): 12816.

Gualandi, F., C. Trabanelli, P. Rimessi, E. Calzolari, L. Toffolatti, T. Patarnello, G. Kunz, F. Muntoni and A. Ferlini (2003). "Multiple exon skipping and RNA circularisation contribute to the severe phenotypic expression of exon 5 dystrophin deletion." Journal of Medical Genetics **40**(8): e100-e100.

Haase, H., J. Alvarez, D. Petzhold, A. Doller, J. Behlke, J. Erdmann, R. Hetzer, V. Regitz-Zagrosek, G. Vassort and I. Morano (2005). "Ahnak is critical for cardiac Ca(V)1.2 calcium channel function and its beta-adrenergic regulation." Faseb j **19**(14): 1969-1977.

Hagiwara, Y., Y. Nishina, H. Yorifuji and T. Kikuchi (2002). "Immunolocalization of caveolin-1 and caveolin-3 in monkey skeletal, cardiac and uterine smooth muscles." Cell Struct Funct **27**(5): 375-382.

Hakim, C. H., N. B. Wasala, X. Pan, K. Kodippili, Y. Yue, K. Zhang, G. Yao, B. Haffner, S. X. Duan, J. Ramos, J. S. Schneider, N. N. Yang, J. S. Chamberlain and D. Duan (2017). "A Five-Repeat Micro-Dystrophin Gene Ameliorated Dystrophic Phenotype in the Severe DBA/2J-mdx Model of Duchenne Muscular Dystrophy." Mol Ther Methods Clin Dev **6**: 216-230.

Hanft, L. M., F. S. Korte and K. S. McDonald (2007). "Cardiac function and modulation of sarcomeric function by length." Cardiovascular Research **77**(4): 627-636.

Hanft, L. M., F. S. Korte and K. S. McDonald (2008). "Cardiac function and modulation of sarcomeric function by length." Cardiovasc Res **77**(4): 627-636.

Hansen, C. G., E. Shvets, G. Howard, K. Riento and B. J. Nichols (2013). "Deletion of cavin genes reveals tissue-specific mechanisms for morphogenesis of endothelial caveolae." Nat Commun **4**: 1831.

Harper, S. Q., R. W. Crawford, C. DelloRusso and J. S. Chamberlain (2002). "Spectrin-like repeats from dystrophin and α-actinin-2 are not functionally interchangeable." Human Molecular Genetics **11**(16): 1807-1815.

Harper, S. Q., M. A. Hauser, C. DelloRusso, D. Duan, R. W. Crawford, S. F. Phelps, H. A. Harper, A. S. Robinson, J. F. Engelhardt, S. V. Brooks and J. S. Chamberlain (2002). "Modular flexibility of dystrophin: implications for gene therapy of Duchenne muscular dystrophy." Nat Med **8**(3): 253-261.

Hayer, A., M. Stoeber, C. Bissig and A. Helenius (2010). "Biogenesis of Caveolae: Stepwise Assembly of Large Caveolin and Cavin Complexes." Traffic **11**(3): 361-382.

Helliwell, T. R., N. T. Man, G. E. Morris and K. E. Davies (1992). "The dystrophin-related protein, utrophin, is expressed on the sarcolemma of regenerating human skeletal muscle fibres in dystrophies and inflammatory myopathies." Neuromuscul Disord **2**(3): 177-184.

Henry, M. D. and K. P. Campbell (1996). "Dystroglycan: an extracellular matrix receptor linked to the cytoskeleton." Curr Opin Cell Biol **8**(5): 625-631.

Hill, M. M., M. Bastiani, R. Luetterforst, M. Kirkham, A. Kirkham, S. J. Nixon, P. Walser, D. Abankwa, V. M. J. Oorschot, S. Martin, J. F. Hancock and R. G. Parton (2008). "PTRF-Cavin, a Conserved Cytoplasmic Protein Required for Caveola Formation and Function." Cell **132**(1): 113-124.

Hillier B. J., C. K. S., Prehoda K. E., Bredt D. S., Lim W. A. (1999). "Unexpected modes of PDZ domain scaffolding revealed by structure of nNOS-syntrophin complex." Science **284**: 812-815.

Hoffman, E. P., K. H. Fischbeck, R. H. Brown, M. Johnson, R. Medori, J. D. Loike, J. B. Harris, R. Waterston, M. Brooke, L. Specht and et al. (1988). "Characterization of dystrophin in muscle-biopsy specimens from patients with Duchenne's or Becker's muscular dystrophy." N Engl J Med **318**(21): 1363-1368.

Hoffman, E. P., J. E. Morgan, S. C. Watkins and T. A. Partridge (1990). "Somatic reversion/suppression of the mouse mdx phenotype in vivo." J Neurol Sci **99**(1): 9-25.

Ibraghimov-Beskrovnaya, O., J. M. Ervasti, C. J. Leveille, C. A. Slaughter, S. W. Sernett and K. P. Campbell (1992). "Primary structure of dystrophin-associated glycoproteins linking dystrophin to the extracellular matrix." Nature **355**(6362): 696-702.

Ilsley, J. L., M. Sudol and S. J. Winder (2002). "The WW domain: linking cell signalling to the membrane cytoskeleton." Cell Signal **14**(3): 183-189.

Im, W. B., S. F. Phelps, E. H. Copen, E. G. Adams, J. L. Slightom and J. S. Chamberlain (1996). "Differential Expression of Dystrophin Isoforms in Strains of mdx Mice with Different Mutations." Human Molecular Genetics **5**(8): 1149-1153.

Ishikawa-Sakurai, M., M. Yoshida, M. Imamura, K. E. Davies and E. Ozawa (2004). "ZZ domain is essentially required for the physiological binding of dystrophin and utrophin to beta-dystroglycan." Hum Mol Genet **13**(7): 693-702.

Ishizaki, M., M. Kobayashi, K. Adachi, T. Matsumura and E. Kimura (2018). "Female dystrophinopathy: Review of current literature." Neuromuscul Disord **28**(7): 572-581.

Johnson, E. K., L. Zhang, M. E. Adams, A. Phillips, M. A. Freitas, S. C. Froehner, K. B. Green-Church and F. Montanaro (2012). "Proteomic analysis reveals new cardiac-specific dystrophin-associated proteins." PLoS One **7**(8): e43515.

Judge, L. M., M. Haraguchiln and J. S. Chamberlain (2006). "Dissecting the signaling and mechanical functions of the dystrophin-glycoprotein complex." J Cell Sci **119**(Pt 8): 1537-1546.

K. Y. Xu, D. L. H., T. M. Dawson, D. S. Bredt, and L. C. Becker (1999). "Nitric oxide synthase in cardiac sarcoplasmic reticulum." PNAS **96**(2): 657–662.

Kaakinen, M., M. E. Reichelt, Z. Ma, C. Ferguson, N. Martel, E. R. Porrello, J. E. Hudson, W. G. Thomas, R. G. Parton and J. P. Headrick (2017). "Cavin-1 deficiency modifies myocardial and coronary function, stretch responses and ischaemic tolerance: roles of NOS over-activity." Basic Res Cardiol **112**(3): 24.

Karl, T. R. (2008). "Tetralogy of Fallot: Current surgical perspective." Ann Pediatr Cardiol **1**(2): 93-100.

Kaspar, R. W., H. D. Allen, W. C. Ray, C. E. Alvarez, J. T. Kissel, A. Pestronk, R. B. Weiss, K. M. Flanigan, J. R. Mendell and F. Montanaro (2009). "Analysis of dystrophin deletion mutations predicts age of cardiomyopathy onset in becker muscular dystrophy." <u>Circ Cardiovasc Genet</u> **2**(6): 544-551.

Khan, M. A., Y. Almashham, A. Almoukirish, T. S. Momenah, A. Alsaman and A. Aljarallah (2013). "Electrocardiographic changes in cases of duchenne muscular dystrophy." <u>Journal of the Saudi Heart Association</u> **25**(2): 154-155.

Khirani, S., A. Ramirez, G. Aubertin, M. Boule, C. Chemouny, V. Forin and B. Fauroux (2014). "Respiratory muscle decline in Duchenne muscular dystrophy." <u>Pediatr Pulmonol</u> **49**(5): 473-481.

Klietsch, R., J. M. Ervasti, W. Arnold, K. P. Campbell and A. O. Jorgensen (1993). "Dystrophin-glycoprotein complex and laminin colocalize to the sarcolemma and transverse tubules of cardiac muscle." <u>Circ Res</u> **72**(2): 349-360.

Koenig, M. and L. M. Kunkel (1990). "Detailed analysis of the repeat domain of dystrophin reveals four potential hinge segments that may confer flexibility." <u>Journal of Biological Chemistry</u> **265**(8): 4560-4566.

Kohl, P., P. J. Cooper and H. Holloway (2003). "Effects of acute ventricular volume manipulation on in situ cardiomyocyte cell membrane configuration." <u>Prog Biophys Mol Biol</u> **82**(1-3): 221-227.

Kostetskii, I., J. Li, Y. Xiong, R. Zhou, V. A. Ferrari, V. V. Patel, J. D. Molkentin and G. L. Radice (2005). "Induced deletion of the N-cadherin gene in the heart leads to dissolution of the intercalated disc structure." <u>Circ Res</u> **96**(3): 346-354.

Kovtun, O., V. A. Tillu, W. Jung, N. Leneva, N. Ariotti, N. Chaudhary, R. A. Mandyam, C. Ferguson, G. P. Morgan, W. A. Johnston, S. J. Harrop, K. Alexandrov, R. G. Parton and B. M. Collins (2014). "Structural insights into the organization of the cavin membrane coat complex." <u>Dev Cell</u> **31**(4): 405-419.

Kunkel, L. M., A. P. Monaco, W. Middlesworth, H. D. Ochs and S. A. Latt (1985). "Specific cloning of DNA fragments absent from the DNA of a male patient with an X chromosome deletion." <u>Proc Natl Acad Sci U S A</u> **82**(14): 4778-4782.

Lai, Y., G. D. Thomas, Y. Yue, H. T. Yang, D. Li, C. Long, L. Judge, B. Bostick, J. S. Chamberlain, R. L. Terjung and D. Duan (2009). "Dystrophins carrying spectrin-like repeats 16 and 17 anchor nNOS to the sarcolemma and enhance exercise performance in a mouse model of muscular dystrophy." <u>J Clin Invest</u> **119**(3): 624-635.

Lai, Y., J. Zhao, Y. Yue and D. Duan (2013). "alpha2 and alpha3 helices of dystrophin R16 and R17 frame a microdomain in the alpha1 helix of dystrophin R17 for neuronal NOS binding." <u>Proc Natl Acad Sci U S A</u> **110**(2): 525-530.

Larcher, T., A. Lafoux, L. Tesson, S. Remy, V. Thepenier, V. Francois, C. Le Guiner, H. Goubin, M. Dutilleul, L. Guigand, G. Toumaniantz, A. De Cian, C. Boix, J. B. Renaud, Y. Cherel, C. Giovannangeli, J. P. Concordet, I. Anegon and C. Huchet (2014). "Characterization of dystrophin deficient rats: a new model for Duchenne muscular dystrophy." <u>PLoS One</u> **9**(10): e110371.

Lebakken C. S., V. D. P., Hrstka R. F., Consolino C. M., Faulkner J. A., Williamson R. A., and Campbell K. P. (2000). "Sarcospan-Deficient Mice

Maintain Normal Muscle Function." Molecular and Cellular Biology **20**(5): 1669-1677.

Lee, T., Y. Takeshima, N. Kusunoki, H. Awano, M. Yagi, M. Matsuo and K. Iijima (2014). "Differences in carrier frequency between mothers of Duchenne and Becker muscular dystrophy patients." J Hum Genet **59**(1): 46-50.

Lester, G., G. Femia, J. Ayer and R. Puranik (2019). "A case report: X-linked dystrophin gene mutation causing severe isolated dilated cardiomyopathy." European Heart Journal - Case Reports **3**(2).

Li, D., A. Bareja, L. Judge, Y. Yue, Y. Lai, R. Fairclough, K. E. Davies, J. S. Chamberlain and D. Duan (2010). "Sarcolemmal nNOS anchoring reveals a qualitative difference between dystrophin and utrophin." J Cell Sci **123**(Pt 12): 2008-2013.

Li, S., E. Kimura, R. Ng, B. M. Fall, L. Meuse, M. Reyes, J. A. Faulkner and J. S. Chamberlain (2006). "A highly functional mini-dystrophin/GFP fusion gene for cell and gene therapy studies of Duchenne muscular dystrophy." Hum Mol Genet **15**(10): 1610-1622.

Lidov, H. G., Kunkel, L.M. (1997). "Dp140: Alternatively Spliced Isoforms in Brain and Kidney." Genomics **45**(1): 132-139.

Lidov, H. G., Selig, S., Kunkel, L. M. (1995). "Dp140: a novel 140 kDa CNS transcript from the dystrophin locus." Human Molecular Genetics **4**(3): 329-335.

Liu, L., D. Brown, M. McKee, N. K. LeBrasseur, D. Yang, K. H. Albrecht, K. Ravid and P. F. Pilch (2008). "Deletion of Cavin/PTRF Causes Global Loss of Caveolae, Dyslipidemia, and Glucose Intolerance." Cell Metabolism **8**(4): 310-317.

Lo, H. P., S. J. Nixon, T. E. Hall, B. S. Cowling, C. Ferguson, G. P. Morgan, N. L. Schieber, M. A. Fernandez-Rojo, M. Bastiani, M. Floetenmeyer, N. Martel, J. Laporte, P. F. Pilch and R. G. Parton (2015). "The caveolin-cavin system plays a conserved and critical role in mechanoprotection of skeletal muscle." J Cell Biol **210**(5): 833-849.

Lu, Q. L., G. E. Morris, S. D. Wilton, T. Ly, O. V. Artem'yeva, P. Strong and T. A. Partridge (2000). "Massive Idiosyncratic Exon Skipping Corrects the Nonsense Mutation in Dystrophic Mouse Muscle and Produces Functional Revertant Fibers by Clonal Expansion." Journal of Cell Biology **148**(5): 985-996.

Ludwig, A., G. Howard, C. Mendoza-Topaz, T. Deerinck, M. Mackey, S. Sandin, M. H. Ellisman and B. J. Nichols (2013). "Molecular composition and ultrastructure of the caveolar coat complex." PLoS Biol **11**(8): e1001640.

Magri, F., A. Govoni, M. G. D'Angelo, R. Del Bo, S. Ghezzi, G. Sandra, A. C. Turconi, M. Sciacco, P. Ciscato, A. Bordoni, S. Tedeschi, F. Fortunato, V. Lucchini, S. Bonato, C. Lamperti, D. Coviello, Y. Torrente, S. Corti, M. Moggio, N. Bresolin and G. P. Comi (2011). "Genotype and phenotype characterization in a large dystrophinopathic cohort with extended follow-up." J Neurol **258**(9): 1610-1623.

Mah, J. K., L. Korngut, J. Dykeman, L. Day, T. Pringsheim and N. Jette (2014). "A systematic review and meta-analysis on the epidemiology of Duchenne and Becker muscular dystrophy." Neuromuscul Disord **24**(6): 482-491.

Mahmoodzadeh, S., K. Koch, C. Schriever, J. Xu, M. Steinecker, J. Leber, E. Dworatzek, B. Purfürst, S. Kunz, D. Recchia, M. Canepari, A. Heuser, S. Di Francescantonio and I. Morano (2021). "Age-related decline in murine heart and skeletal muscle performance is attenuated by reduced Ahnak1 expression." J Cachexia Sarcopenia Muscle **12**(5): 1249-1265.

Malette, J., J. Degrandmaison, H. Giguere, J. Berthiaume, M. Frappier, J. L. Parent, M. Auger-Messier and G. Boulay (2019). "MURC/CAVIN-4 facilitates store-operated calcium entry in neonatal cardiomyocytes." Biochim Biophys Acta Mol Cell Res **1866**(8): 1249-1259.

Masubuchi, N., Y. Shidoh, S. Kondo, J. Takatoh and K. Hanaoka (2013). "Subcellular localization of dystrophin isoforms in cardiomyocytes and phenotypic analysis of dystrophin-deficient mice reveal cardiac myopathy is predominantly caused by a deficiency in full-length dystrophin." Exp Anim **62**(3): 211-217.

McClive, P. J., D. Huang and G. Morahan (1994). "C57BL/6 and C57BL/10 inbred mouse strains differ at multiple loci on chromosome 4." Immunogenetics **39**(4): 286-288.

McNally, E. M., J. R. Kaltman, D. W. Benson, C. E. Canter, L. H. Cripe, D. Duan, J. D. Finder, W. J. Groh, E. P. Hoffman, D. P. Judge, N. Kertesz, K. Kinnett, R. Kirsch, J. M. Metzger, G. D. Pearson, J. A. Rafael-Fortney, S. V. Raman, C. F. Spurney, S. L. Targum, K. R. Wagner, L. W. Markham, L. Working Group of the National Heart, I. Blood and D. Parent Project Muscular (2015). "Contemporary cardiac issues in Duchenne muscular dystrophy. Working Group of the National Heart, Lung, and Blood Institute in collaboration with Parent Project Muscular Dystrophy." Circulation **131**(18): 1590-1598.

Melacini, P., M. Fanin, G. A. Danieli, C. Villanova, F. Martinello, M. Miorin, M. P. Freda, M. Miorelli, M. L. Mostacciuolo, G. Fasoli, C. Angelini and S. Dalla Volta (1996). "Myocardial involvement is very frequent among patients affected with subclinical Becker's muscular dystrophy." Circulation **94**(12): 3168-3175.

Mendell, J. R., Z. Sahenk, K. Lehman, C. Nease, L. P. Lowes, N. F. Miller, M. A. Iammarino, L. N. Alfano, A. Nicholl, S. Al-Zaidy, S. Lewis, K. Church, R. Shell, L. H. Cripe, R. A. Potter, D. A. Griffin, E. Pozsgai, A. Dugar, M. Hogan and L. R. Rodino-Klapac (2020). "Assessment of Systemic Delivery of rAAVrh74.MHCK7.micro-dystrophin in Children With Duchenne Muscular Dystrophy: A Nonrandomized Controlled Trial." JAMA Neurol **77**(9): 1122-1131.

Mendell, J. R., C. Shilling, N. D. Leslie, K. M. Flanigan, R. al-Dahhak, J. Gastier-Foster, K. Kneile, D. M. Dunn, B. Duval, A. Aoyagi, C. Hamil, M. Mahmoud, K. Roush, L. Bird, C. Rankin, H. Lilly, N. Street, R. Chandrasekar and R. B. Weiss (2012). "Evidence-based path to newborn screening for Duchenne muscular dystrophy." Ann Neurol **71**(3): 304-313.

Mercuri, E., C. G. Bönnemann and F. Muntoni (2019). "Muscular dystrophies." The Lancet **394**(10213): 2025-2038.

Moat, S. J., D. M. Bradley, R. Salmon, A. Clarke and L. Hartley (2013). "Newborn bloodspot screening for Duchenne muscular dystrophy: 21 years experience in Wales (UK)." Eur J Hum Genet **21**(10): 1049-1053.

Moise, N. S., B. A. Valentine, C. A. Brown, H. N. Erb, K. A. Beck, B. J. Cooper and R. F. Gilmour (1991). "Duchenne's cardiomyopathy in a canine model: electrocardiographic and echocardiographic studies." J Am Coll Cardiol **17**(3): 812-820.

Molina, C. E., E. Jacquet, P. Ponien, C. Muñoz-Guijosa, I. Baczkó, L. S. Maier, P. Donzeau-Gouge, D. Dobrev, R. Fischmeister and A. Garnier (2017). "Identification of optimal reference genes for transcriptomic analyses in normal and diseased human heart." Cardiovascular Research **114**(2): 247-258.

Molkentin, J. D., S. M. Jobe and B. E. Markham (1996). "Alpha-myosin heavy chain gene regulation: delineation and characterization of the cardiac muscle-specific enhancer and muscle-specific promoter." J Mol Cell Cardiol **28**(6): 1211-1225.

Monaco, A. P., C. J. Bertelson, S. Liechti-Gallati, H. Moser and L. M. Kunkel (1988). "An explanation for the phenotypic differences between patients bearing partial deletions of the DMD locus." Genomics **2**(1): 90-95.

Monaco, A. P., R. L. Neve, C. Colletti-Feener, C. J. Bertelson, D. M. Kurnit and L. M. Kunkel (1986). "Isolation of candidate cDNAs for portions of the Duchenne muscular dystrophy gene." Nature **323**(6089): 646-650.

Muntoni, F., M. Cau, A. Ganau, R. Congiu, G. Arvedi, A. Mateddu, M. G. Marrosu, C. Cianchetti, G. Realdi, A. Cao and et al. (1993). "Brief report: deletion of the dystrophin muscle-promoter region associated with X-linked dilated cardiomyopathy." N Engl J Med **329**(13): 921-925.

Muntoni, F., M. A. Melis, A. Ganau and V. Dubowitz (1995). "Transcription of the dystrophin gene in normal tissues and in skeletal muscle of a family with X-linked dilated cardiomyopathy." Am J Hum Genet **56**(1): 151-157.

Muntoni, F., L. Wilson, G. Marrosu, M. G. Marrosu, C. Cianchetti, L. Mestroni, A. Ganau, V. Dubowitz and C. Sewry (1995). "A mutation in the dystrophin gene selectively affecting dystrophin expression in the heart." J Clin Invest **96**(2): 693-699.

Nakamura, A. (2015). "X-Linked Dilated Cardiomyopathy: A Cardiospecific Phenotype of Dystrophinopathy." Pharmaceuticals (Basel) **8**(2): 303-320.

Nakamura, A., N. Fueki, N. Shiba, H. Motoki, D. Miyazaki, H. Nishizawa, Y. Echigoya, T. Yokota, Y. Aoki and S. Takeda (2016). "Deletion of exons 3-9 encompassing a mutational hot spot in the DMD gene presents an asymptomatic phenotype, indicating a target region for multiexon skipping therapy." J Hum Genet **61**(7): 663-667.

Nakamura, A., N. Shiba, D. Miyazaki, H. Nishizawa, Y. Inaba, N. Fueki, R. Maruyama, Y. Echigoya and T. Yokota (2017). "Comparison of the phenotypes of patients harboring in-frame deletions starting at exon 45 in the Duchenne muscular dystrophy gene indicates potential for the development of exon skipping therapy." J Hum Genet **62**(4): 459-463.

Nakamura, A., K. Yoshida, S. Takeda, N. Dohi and S. Ikeda (2002). "Progression of dystrophic features and activation of mitogen-activated protein kinases and calcineurin by physical exercise, in hearts of mdx mice." FEBS Lett **520**(1-3): 18-24.

Naso, M. F., B. Tomkowicz, W. L. Perry, 3rd and W. R. Strohl (2017). "Adeno-Associated Virus (AAV) as a Vector for Gene Therapy." BioDrugs **31**(4): 317-334.

Nicholson, L. V. B. (1993). "The "rescue" of dystrophin synthesis in boys with Duchenne muscular dystrophy." Neuromuscular Disorders **3**(5): 525-531.

Nigro, G., L. I. Comi, L. Politano and R. J. Bain (1990). "The incidence and evolution of cardiomyopathy in Duchenne muscular dystrophy." Int J Cardiol **26**(3): 271-277.

Nobile, C., F. Galvagni, J. Marchi, R. Roberts and L. Vitiello (1995). "Genomic organization of the human dystrophin gene across the major deletion hot spot and the 3' region." Genomics **28**(1): 97-100.

North, K. N., G. Miller, S. T. Iannaccone, P. R. Clemens, D. A. Chad, I. Bella, T. W. Smith, A. H. Beggs and L. A. Specht (1996). "Cognitive dysfunction as the major presenting feature of Becker's muscular dystrophy." Neurology **46**(2): 461-465.

Norwood, F. L., A. J. Sutherland-Smith, N. H. Keep and J. Kendrick-Jones (2000). "The structure of the N-terminal actin-binding domain of human dystrophin and how mutations in this domain may cause Duchenne or Becker muscular dystrophy." Structure **8**(5): 481-491.

Nouhravesh, N., G. Ahlberg, J. Ghouse, C. Andreasen, J. H. Svendsen, S. Haunsø, H. Bundgaard, P. E. Weeke and M. S. Olesen (2016). "Analyses of more than 60,000 exomes questions the role of numerous genes previously associated with dilated cardiomyopathy." Mol Genet Genomic Med **4**(6): 617-623.

Ogata, H., Y. Ishikawa, Y. Ishikawa and R. Minami (2009). "Beneficial effects of beta-blockers and angiotensin-converting enzyme inhibitors in Duchenne muscular dystrophy." J Cardiol **53**(1): 72-78.

Ogata, T., D. Naito, N. Nakanishi, Y. K. Hayashi, T. Taniguchi, K. Miyagawa, T. Hamaoka, N. Maruyama, S. Matoba, K. Ikeda, H. Yamada, H. Oh and T. Ueyama (2014). "MURC/Cavin-4 facilitates recruitment of ERK to caveolae and concentric cardiac hypertrophy induced by alpha1-adrenergic receptors." Proc Natl Acad Sci U S A **111**(10): 3811-3816.

Ogata, T., T. Ueyama, K. Isodono, M. Tagawa, N. Takehara, T. Kawashima, K. Harada, T. Takahashi, T. Shioi, H. Matsubara and H. Oh (2008). "MURC, a muscle-restricted coiled-coil protein that modulates the Rho/ROCK pathway, induces cardiac dysfunction and conduction disturbance." Mol Cell Biol **28**(10): 3424-3436.

Orchard, C. H., M. Pásek and F. Brette (2009). "The role of mammalian cardiac t-tubules in excitation-contraction coupling: experimental and computational approaches." Exp Physiol **94**(5): 509-519.

Oudet, C., A. Hanauer, P. Clemens, T. Caskey and J. L. Mandel (1992). "Two hot spots of recombination in the DMD gene correlate with the deletion prone regions." Hum Mol Genet **1**(8): 599-603.

Parat, M. O., R. Z. Stachowicz and P. L. Fox (2002). "Oxidative stress inhibits caveolin-1 palmitoylation and trafficking in endothelial cells." Biochem J **361**(Pt 3): 681-688.

Passamano, L., A. Taglia, A. Palladino, E. Viggiano, P. D'Ambrosio, M. Scutifero, M. Rosaria Cecio, V. Torre, D. E. L. F, E. Picillo, O. Paciello, G. Piluso, G. Nigro and L. Politano (2012). "Improvement of survival in Duchenne Muscular Dystrophy: retrospective analysis of 835 patients." Acta Myol **31**(2): 121-125.

Pastoret, C. and A. Sebille (1995). "mdx mice show progressive weakness and muscle deterioration with age." J Neurol Sci **129**(2): 97-105.

Patel, H. H., Y. M. Tsutsumi, B. P. Head, I. R. Niesman, M. Jennings, Y. Horikawa, D. Huang, A. L. Moreno, P. M. Patel, P. A. Insel and D. M. Roth (2007). "Mechanisms of cardiac protection from ischemia/reperfusion injury: a role for caveolae and caveolin-1." Faseb j **21**(7): 1565-1574.

Peters M. F., A. M. E., and Froehner S. C. (1997). "Differential Association of Syntrophin Pairs with the Dystrophin Complex." The Journal of Cell Biology **138**(1): 81-93.

Petrof, B. J., Shrager, J. B., Stedman, H. H., Kelly, A. M., Sweeney, H. L. (1993). "Dystrophin protects the sarcolemma from stresses developed during muscle contraction." Proc Natl Acad Sci U S A **90**: 3710-3714.

Pfeiffer, E. R., A. T. Wright, A. G. Edwards, J. C. Stowe, K. McNall, J. Tan, I. Niesman, H. H. Patel, D. M. Roth, J. H. Omens and A. D. McCulloch (2014). "Caveolae in ventricular myocytes are required for stretch-dependent conduction slowing." J Mol Cell Cardiol **76**: 265-274.

Podsakoff, G., K. K. Wong, Jr. and S. Chatterjee (1994). "Efficient gene transfer into nondividing cells by adeno-associated virus-based vectors." J Virol **68**(9): 5656-5666.

Quinlan, J. G., H. S. Hahn, B. L. Wong, J. N. Lorenz, A. S. Wenisch and L. S. Levin (2004). "Evolution of the mdx mouse cardiomyopathy: physiological and morphological findings." Neuromuscul Disord **14**(8-9): 491-496.

Rafael J. A., C. G. A., Corrado K., Jung D., Campbell K. P., Chamberlain J. S. (1996). "Forced expression of dystrophin deletion constructs reveals structure-function correlations." J Cell Biol **134**(1): 96-102.

Rajab, A., V. Straub, L. J. McCann, D. Seelow, R. Varon, R. Barresi, A. Schulze, B. Lucke, S. Lützkendorf, M. Karbasiyan, S. Bachmann, S. Spuler and M. Schuelke (2010). "Fatal cardiac arrhythmia and long-QT syndrome in a new form of congenital generalized lipodystrophy with muscle rippling (CGL4) due to PTRF-CAVIN mutations." PLoS Genet **6**(3): e1000874.

Rajdev, A. and W. J. Groh (2015). "Arrhythmias in the muscular dystrophies." Card Electrophysiol Clin **7**(2): 303-308.

Raman, S. V., K. N. Hor, W. Mazur, A. Cardona, X. He, N. Halnon, L. Markham, J. H. Soslow, M. D. Puchalski, S. R. Auerbach, U. Truong, S. Smart, B. McCarthy, I. M. Saeed, J. M. Statland, J. T. Kissel and L. H. Cripe (2019). "Stabilization of Early Duchenne Cardiomyopathy With Aldosterone Inhibition: Results of the Multicenter AIDMD Trial." J Am Heart Assoc **8**(19): e013501.

Raman, S. V., K. N. Hor, W. Mazur, N. J. Halnon, J. T. Kissel, X. He, T. Tran, S. Smart, B. McCarthy, M. D. Taylor, J. L. Jefferies, J. A. Rafael-Fortney, J. Lowe, S. L. Roble and L. H. Cripe (2015). "Eplerenone for early cardiomyopathy in Duchenne muscular dystrophy: a randomised, double-blind, placebo-controlled trial." Lancet Neurol **14**(2): 153-161.

Rando, T. A. (2001). "The dystrophin-glycoprotein complex, cellular signaling, and the regulation of cell survival in the muscular dystrophies." Muscle Nerve **24**(12): 1575-1594.

Rapaport, D., D. Lederfein, J. T. den Dunnen, P. M. Grootscholten, G. J. Van Ommen, O. Fuchs, U. Nudel and D. Yaffe (1992). "Characterization and cell type distribution of a novel, major transcript of the Duchenne muscular dystrophy gene." Differentiation **49**(3): 187-193.

Rentschler S., L. H., Deininger K., Bedford M. T., Espanel X. and Sudol M. (1999). "The WW Domain of Dystrophin Requires EF-HandsRegion to Interact with b-Dystroglycan." Biol. Chem. **380**(4): 431-442.

Ricotti, V., W. P. Mandy, M. Scoto, M. Pane, N. Deconinck, S. Messina, E. Mercuri, D. H. Skuse and F. Muntoni (2016). "Neurodevelopmental, emotional, and behavioural problems in Duchenne muscular dystrophy in relation to underlying dystrophin gene mutations." Dev Med Child Neurol **58**(1): 77-84.

Rodriguez, G., T. Ueyama, T. Ogata, G. Czernuszewicz, Y. Tan, G. W. Dorn, 2nd, R. Bogaev, K. Amano, H. Oh, H. Matsubara, J. T. Willerson and A. J. Marian (2011). "Molecular genetic and functional characterization implicate muscle-restricted coiled-coil gene (MURC) as a causal gene for familial dilated cardiomyopathy." Circ Cardiovasc Genet **4**(4): 349-358.

Roth, G. M., D. M. Bader and E. R. Pfaltzgraff (2014). "Isolation and physiological analysis of mouse cardiomyocytes." J Vis Exp(91): e51109.

Rothberg, K. G., J. E. Heuser, W. C. Donzell, Y. S. Ying, J. R. Glenney and R. G. Anderson (1992). "Caveolin, a protein component of caveolae membrane coats." Cell **68**(4): 673-682.

Rybakova, I. N. and J. M. Ervasti (1997). "Dystrophin-glycoprotein complex is monomeric and stabilizes actin filaments in vitro through a lateral association." J Biol Chem **272**(45): 28771-28778.

Rybakova, I. N. and J. M. Ervasti (2005). "Identification of spectrin-like repeats required for high affinity utrophin-actin interaction." J Biol Chem **280**(24): 23018-23023.

Rybakova, I. N., J. R. Patel and J. M. Ervasti (2000). "The dystrophin complex forms a mechanically strong link between the sarcolemma and costameric actin." J Cell Biol **150**(5): 1209-1214.

Sacconi, S., L. Féasson, J. C. Antoine, C. Pécheux, R. Bernard, A. M. Cobo, A. Casarin, L. Salviati, C. Desnuelle and A. Urtizberea (2012). "A novel CRYAB mutation resulting in multisystemic disease." Neuromuscul Disord **22**(1): 66-72.

Sadoulet-Puccio, H. M., M. Rajala and L. M. Kunkel (1997). "Dystrobrevin and dystrophin: an interaction through coiled-coil motifs." Proc Natl Acad Sci U S A **94**(23): 12413-12418.

Saito, T., T. Matsumura, I. Miyai, S. Nozaki and S. Shinno (2001). "[Carvedilol effectiveness for left ventricular-insufficient patients with Duchenne muscular dystrophy]." Rinsho Shinkeigaku **41**(10): 691-694.

Salva, M. Z., C. L. Himeda, P. W. Tai, E. Nishiuchi, P. Gregorevic, J. M. Allen, E. E. Finn, Q. G. Nguyen, M. J. Blankinship, L. Meuse, J. S. Chamberlain and S. D. Hauschka (2007). "Design of tissue-specific regulatory cassettes for high-level rAAV-mediated expression in skeletal and cardiac muscle." Mol Ther **15**(2): 320-329.

Santos, M. A., A. Costa Fde, A. F. Travessa, M. T. Bombig, F. H. Fonseca, B. Luna Filho, A. Mussi, D. Souza, A. Oliveira and R. Povoa (2010). "[Duchenne

muscular dystrophy: electrocardiographic analysis of 131 patients]." <u>Arq Bras Cardiol</u> **94**(5): 620-624.

Satre, V., N. Monnier, F. Devillard, F. Amblard and J. Lunardi (2004). "Prenatal diagnosis of DMD in a female foetus affected by Turner syndrome." <u>Prenat Diagn</u> **24**(11): 913-917.

Schubert, W., P. G. Frank, B. Razani, D. S. Park, C. W. Chow and M. P. Lisanti (2001). "Caveolae-deficient endothelial cells show defects in the uptake and transport of albumin in vivo." <u>J Biol Chem</u> **276**(52): 48619-48622.

Scriven, D. R., P. Dan and E. D. Moore (2000). "Distribution of proteins implicated in excitation-contraction coupling in rat ventricular myocytes." <u>Biophys J</u> **79**(5): 2682-2691.

Shah, F. A., B. R. Johansson, P. Thomsen and A. Palmquist (2015). "Ultrastructural evaluation of shrinkage artefacts induced by fixatives and embedding resins on osteocyte processes and pericellular space dimensions." <u>J Biomed Mater Res A</u> **103**(4): 1565-1576.

Sharp, N. J., J. N. Kornegay, S. D. Van Camp, M. H. Herbstreith, S. L. Secore, S. Kettle, W. Y. Hung, C. D. Constantinou, M. J. Dykstra, A. D. Roses and et al. (1992). "An error in dystrophin mRNA processing in golden retriever muscular dystrophy, an animal homologue of Duchenne muscular dystrophy." <u>Genomics</u> **13**(1): 115-121.

Shastry, S., M. R. Delgado, E. Dirik, M. Turkmen, A. K. Agarwal and A. Garg (2010). "Congenital generalized lipodystrophy, type 4 (CGL4) associated with myopathy due to novel PTRF mutations." <u>Am J Med Genet A</u> **152a**(9): 2245-2253.

Shimatsu, Y., K. Katagiri, T. Furuta, M. Nakura, Y. Tanioka, K. Yuasa, M. Tomohiro, J. N. Kornegay, I. Nonaka and S. Takeda (2003). "Canine X-linked muscular dystrophy in Japan (CXMDJ)." <u>Exp Anim</u> **52**(2): 93-97.

Shin, J. H., Y. Nitahara-Kasahara, H. Hayashita-Kinoh, S. Ohshima-Hosoyama, K. Kinoshita, T. Chiyo, H. Okada, T. Okada and S. Takeda (2011). "Improvement of cardiac fibrosis in dystrophic mice by rAAV9-mediated microdystrophin transduction." <u>Gene Ther</u> **18**(9): 910-919.

Shin, J. H., X. Pan, C. H. Hakim, H. T. Yang, Y. Yue, K. Zhang, R. L. Terjung and D. Duan (2013). "Microdystrophin ameliorates muscular dystrophy in the canine model of duchenne muscular dystrophy." <u>Mol Ther</u> **21**(4): 750-757.

Sicinski, P., Y. Geng, A. S. Ryder-Cook, E. A. Barnard, M. G. Darlison and P. J. Barnard (1989). "The molecular basis of muscular dystrophy in the mdx mouse: a point mutation." <u>Science</u> **244**(4912): 1578-1580.

Singh, S. M., S. Bandi, D. D. Shah, G. Armstrong and K. M. Mallela (2014). "Missense mutation Lys18Asn in dystrophin that triggers X-linked dilated cardiomyopathy decreases protein stability, increases protein unfolding, and perturbs protein structure, but does not affect protein function." <u>PLoS One</u> **9**(10): e110439.

Slingsby, J. H., M. B. Hogarth, E. Simpson, M. J. Walport and B. J. Morley (1996). "New microsatellite polymorphisms identified between C57BL/6, C57BL/10, and C57BL/KsJ inbred mouse strains." <u>Immunogenetics</u> **43**(1-2): 72-75.

Song, K. S., P. E. Scherer, Z. Tang, T. Okamoto, S. Li, M. Chafel, C. Chu, D. S. Kohtz and M. P. Lisanti (1996). "Expression of caveolin-3 in skeletal, cardiac, and smooth muscle cells. Caveolin-3 is a component of the sarcolemma and co-fractionates with dystrophin and dystrophin-associated glycoproteins." J Biol Chem **271**(25): 15160-15165.

Srinivasan, R., J. E. Hornyak, D. T. Badenhop and L. G. Koch (2005). "Cardiac rehabilitation after heart transplantation in a patient with Becker's muscular dystrophy: a case report." Arch Phys Med Rehabil **86**(10): 2059-2061.

Srivastava, A., E. W. Lusby and K. I. Berns (1983). "Nucleotide sequence and organization of the adeno-associated virus 2 genome." J Virol **45**(2): 555-564.

Stevenson, S., S. Rothery, M. J. Cullen and N. J. Severs (1997). "Dystrophin is not a specific component of the cardiac costamere." Circ Res **80**(2): 269-280.

Stevenson, S., S. Rothery, M. J. Cullen and N. J. Severs (1998). "Spatial relationship of the C-terminal domains of dystrophin and beta-dystroglycan in cardiac muscle support a direct molecular interaction at the plasma membrane interface." Circ Res **82**(1): 82-93.

Stevenson, S. A., M. J. Cullen, S. Rothery, S. R. Coppen and N. J. Severs (2005). "High-resolution en-face visualization of the cardiomyocyte plasma membrane reveals distinctive distributions of spectrin and dystrophin." Eur J Cell Biol **84**(12): 961-971.

Stone, M. R., A. O'Neill, D. Catino and R. J. Bloch (2005). "Specific interaction of the actin-binding domain of dystrophin with intermediate filaments containing keratin 19." Mol Biol Cell **16**(9): 4280-4293.

Suhr, F., S. Gehlert, M. Grau and W. Bloch (2013). "Skeletal muscle function during exercise-fine-tuning of diverse subsystems by nitric oxide." Int J Mol Sci **14**(4): 7109-7139.

Szabo, P. L., J. Ebner, X. Koenig, O. Hamza, S. Watzinger, S. Trojanek, D. Abraham, H. Todt, H. Kubista, K. Schicker, S. Remy, I. Anegon, A. Kiss, B. K. Podesser and K. Hilber (2021). "Cardiovascular phenotype of the Dmd(mdx) rat - a suitable animal model for Duchenne muscular dystrophy." Dis Model Mech **14**(2).

Tagawa, M., T. Ueyama, T. Ogata, N. Takehara, N. Nakajima, K. Isodono, S. Asada, T. Takahashi, H. Matsubara and H. Oh (2008). "MURC, a muscle-restricted coiled-coil protein, is involved in the regulation of skeletal myogenesis." Am J Physiol Cell Physiol **295**(2): C490-498.

Takeshita, E., N. Minami, K. Minami, M. Suzuki, T. Awashima, A. Ishiyama, H. Komaki, I. Nishino and M. Sasaki (2017). "Duchenne muscular dystrophy in a female with compound heterozygous contiguous exon deletions." Neuromuscul Disord **27**(6): 569-573.

Tandon, A., J. L. Jefferies, C. R. Villa, K. N. Hor, B. L. Wong, S. M. Ware, Z. Gao, J. A. Towbin, W. Mazur, R. J. Fleck, J. J. Sticka, D. W. Benson and M. D. Taylor (2015). "Dystrophin genotype-cardiac phenotype correlations in Duchenne and Becker muscular dystrophies using cardiac magnetic resonance imaging." Am J Cardiol **115**(7): 967-971.

Tang, Z., P. E. Scherer, T. Okamoto, K. Song, C. Chu, D. S. Kohtz, I. Nishimoto, H. F. Lodish and M. P. Lisanti (1996). "Molecular cloning of caveolin-

3, a novel member of the caveolin gene family expressed predominantly in muscle." J Biol Chem **271**(4): 2255-2261.

Taniguchi, T., N. Maruyama, T. Ogata, T. Kasahara, N. Nakanishi, K. Miyagawa, D. Naito, T. Hamaoka, M. Nishi, S. Matoba and T. Ueyama (2016). "PTRF/Cavin-1 Deficiency Causes Cardiac Dysfunction Accompanied by Cardiomyocyte Hypertrophy and Cardiac Fibrosis." PLoS One **11**(9): e0162513.

Tasaki, N., K. Yoshida, S. I. Haruta, H. Kouno, H. Ichinose, Y. Fujimoto, N. Urasawa, T. Kawakami, M. Taniguchi, S. Kurushima and T. Shimakura (2001). "X-linked dilated cardiomyopathy with a large hot-spot deletion in the dystrophin gene." Intern Med **40**(12): 1215-1221.

Tennyson, C. N., H. J. Klamut and R. G. Worton (1995). "The human dystrophin gene requires 16 hours to be transcribed and is cotranscriptionally spliced." Nat Genet **9**(2): 184-190.

Thrush, P. T., H. D. Allen, L. Viollet and J. R. Mendell (2009). "Re-examination of the electrocardiogram in boys with Duchenne muscular dystrophy and correlation with its dilated cardiomyopathy." Am J Cardiol **103**(2): 262-265.

Tinsley, J. M., D. J. Blake, A. Roche, U. Fairbrother, J. Riss, B. C. Byth, A. E. Knight, J. Kendrick-Jones, G. K. Suthers, D. R. Love and et al. (1992). "Primary structure of dystrophin-related protein." Nature **360**(6404): 591-593.

Torelli, S., A. Ferlini, L. Obici, C. Sewry and F. Muntoni (1999). "Expression, regulation and localisation of dystrophin isoforms in human foetal skeletal and cardiac muscle." Neuromuscul Disord **9**(8): 541-551.

Towbin, J. A., J. F. Hejtmancik, P. Brink, B. Gelb, X. M. Zhu, J. S. Chamberlain, E. R. McCabe and M. Swift (1993). "X-linked dilated cardiomyopathy. Molecular genetic evidence of linkage to the Duchenne muscular dystrophy (dystrophin) gene at the Xp21 locus." Circulation **87**(6): 1854-1865.

Townsend, D., M. J. Blankinship, J. M. Allen, P. Gregorevic, J. S. Chamberlain and J. M. Metzger (2007). "Systemic administration of micro-dystrophin restores cardiac geometry and prevents dobutamine-induced cardiac pump failure." Mol Ther **15**(6): 1086-1092.

Tozawa, T., K. Itoh, T. Yaoi, S. Tando, M. Umekage, H. Dai, H. Hosoi and S. Fushiki (2012). "The shortest isoform of dystrophin (Dp40) interacts with a group of presynaptic proteins to form a presumptive novel complex in the mouse brain." Mol Neurobiol **45**(2): 287-297.

Turk, R., E. Sterrenburg, E. J. de Meijer, G. J. van Ommen, J. T. den Dunnen and P. A. t Hoen (2005). "Muscle regeneration in dystrophin-deficient mdx mice studied by gene expression profiling." BMC Genomics **6**: 98.

Tyan, L., D. Turner, K. R. Komp, R. Y. Medvedev, E. Lim and A. V. Glukhov (2021). "Caveolin-3 is required for regulation of transient outward potassium current by angiotensin II in mouse atrial myocytes." Am J Physiol Heart Circ Physiol **320**(2): H787-h797.

V N D'Souza, T. M. N., G. E. Morris, W. Karges, D. A. Pillers, P. N. Ray. (1995). "A novel dystrophin isoform is required for normal retinal electrophysiology." Human Molecular Genetics **4**: 837-842.

Valentine, B., J. Cummings and B. Cooper (1989). "Development of Duchenne-type cardiomyopathy. Morphologic studies in a canine model." <u>The American journal of pathology</u> **135**(4): 671.

van Bockel, E. A., J. S. Lind, J. G. Zijlstra, P. J. Wijkstra, P. M. Meijer, M. P. van den Berg, R. H. Slart, L. P. Aarts and J. E. Tulleken (2009). "Cardiac assessment of patients with late stage Duchenne muscular dystrophy." <u>Neth Heart J</u> **17**(6): 232-237.

van Ommen, G. J., J. M. Verkerk, M. H. Hofker, A. P. Monaco, L. M. Kunkel, P. Ray, R. Worton, B. Wieringa, E. Bakker and P. L. Pearson (1986). "A physical map of 4 million bp around the Duchenne muscular dystrophy gene on the human X-chromosome." <u>Cell</u> **47**(4): 499-504.

van Putten, M., K. Putker, M. Overzier, W. A. Adamzek, S. Pasteuning-Vuhman, J. J. Plomp and A. Aartsma-Rus (2019). "Natural disease history of the D2-mdx mouse model for Duchenne muscular dystrophy." <u>Faseb j</u> **33**(7): 8110-8124.

Vatta, M., B. Mohapatra, S. Jimenez, X. Sanchez, G. Faulkner, Z. Perles, G. Sinagra, J. H. Lin, T. M. Vu, Q. Zhou, K. R. Bowles, A. Di Lenarda, L. Schimmenti, M. Fox, M. A. Chrisco, R. T. Murphy, W. McKenna, P. Elliott, N. E. Bowles, J. Chen, G. Valle and J. A. Towbin (2003). "Mutations in Cypher/ZASP in patients with dilated cardiomyopathy and left ventricular non-compaction." <u>J Am Coll Cardiol</u> **42**(11): 2014-2027.

Verghese, E. (2021). "The variability in neurological deficits in Duchenne muscular dystrophy patients may be explained by differences in dystrophin glycoprotein complexes in the brain and muscle." <u>Neuroreport</u> **32**(15): 1229-1233.

Viollet, L., P. T. Thrush, K. M. Flanigan, J. R. Mendell and H. D. Allen (2012). "Effects of angiotensin-converting enzyme inhibitors and/or beta blockers on the cardiomyopathy in Duchenne muscular dystrophy." <u>Am J Cardiol</u> **110**(1): 98-102.

Walmsley, G. L., V. Arechavala-Gomeza, M. Fernandez-Fuente, M. M. Burke, N. Nagel, A. Holder, R. Stanley, K. Chandler, S. L. Marks, F. Muntoni, G. D. Shelton and R. J. Piercy (2010). "A duchenne muscular dystrophy gene hot spot mutation in dystrophin-deficient cavalier king charles spaniels is amenable to exon 51 skipping." <u>PLoS One</u> **5**(1): e8647.

Wang, B., J. Li, F. H. Fu, C. Chen, X. Zhu, L. Zhou, X. Jiang and X. Xiao (2008). "Construction and analysis of compact muscle-specific promoters for AAV vectors." <u>Gene Ther</u> **15**(22): 1489-1499.

Wang, H., E. Marrosu, D. Brayson, N. B. Wasala, E. K. Johnson, C. S. Scott, Y. Yue, K. L. Hau, A. J. Trask, S. C. Froehner, M. E. Adams, L. Zhang, D. Duan and F. Montanaro (2021). "Proteomic analysis identifies key differences in the cardiac interactomes of dystrophin and micro-dystrophin." <u>Hum Mol Genet</u> **30**(14): 1321-1336.

Wasala, N. B., J. H. Shin, Y. Lai, Y. Yue, F. Montanaro and D. Duan (2018). "Cardiac-Specific Expression of DeltaH2-R15 Mini-Dystrophin Normalized All Electrocardiogram Abnormalities and the End-Diastolic Volume in a 23-Month-Old Mouse Model of Duchenne Dilated Cardiomyopathy." <u>Hum Gene Ther</u> **29**(7): 737-748.

Wasala, N. B., K. Zhang, L. P. Wasala, C. H. Hakim and D. Duan (2015). "The FVB Background Does Not Dramatically Alter the Dystrophic Phenotype of Mdx Mice." <u>PLoS Curr</u> **7**.

Way M. , P. B., Cross R. A. , Kendrik-Jones J. , Weeds A. G. (1992). "Expression of the N-terminal domain of dystrophin in E. coli and demonstration of binding to F-actin." <u>FEBS</u> **301**(3): 243-245.

Weir, A. P., E. A. Burton, G. Harrod and K. E. Davies (2002). "A- and B-utrophin have different expression patterns and are differentially up-regulated in mdx muscle." <u>J Biol Chem</u> **277**(47): 45285-45290.

Wheaton, K., K. Sampsel, F. M. Boisvert, A. Davy, S. Robbins and K. Riabowol (2001). "Loss of functional caveolae during senescence of human fibroblasts." <u>J Cell Physiol</u> **187**(2): 226-235.

Wilson, J., W. Putt, C. Jimenez and Y. H. Edwards (1999). "Up71 and Up140, Two Novel Transcripts of Utrophin That Are Homologues of Short Forms of Dystrophin." <u>Human Molecular Genetics</u> **8**(7): 1271-1278.

Wu, Y., O. Cazorla, D. Labeit, S. Labeit and H. Granzier (2000). "Changes in titin and collagen underlie diastolic stiffness diversity of cardiac muscle." <u>J Mol Cell Cardiol</u> **32**(12): 2151-2162.

Yazaki, M., K. Yoshida, A. Nakamura, J. Koyama, T. Nanba, N. Ohori and S. Ikeda (1999). "Clinical characteristics of aged Becker muscular dystrophy patients with onset after 30 years." <u>Eur Neurol</u> **42**(3): 145-149.

Yiu, E. M. and A. J. Kornberg (2015). "Duchenne muscular dystrophy." <u>J Paediatr Child Health</u> **51**(8): 759-764.

Yoshida, K., S. Ikeda, A. Nakamura, M. Kagoshima, S. Takeda, S. Shoji and N. Yanagisawa (1993). "Molecular analysis of the Duchenne muscular dystrophy gene in patients with Becker muscular dystrophy presenting with dilated cardiomyopathy." <u>Muscle Nerve</u> **16**(11): 1161-1166.

Yoshida, M., H. Hama, M. Ishikawa-Sakurai, M. Imamura, Y. Mizuno, K. Araishi, E. Wakabayashi-Takai, S. Noguchi, T. Sasaoka and E. Ozawa (2000). "Biochemical evidence for association of dystrobrevin with the sarcoglycan-sarcospan complex as a basis for understanding sarcoglycanopathy." <u>Hum Mol Genet</u> **9**(7): 1033-1040.

Yoshida M., H. H., Ishikawa-Sakurai M., Imamura M., Mizuno Y., Araishi K., Wakabayashi-Takai E., Noguchi S., Sasaoka T., Ozawa E. (2000). "Biochemical evidence for association of dystrobrevin with the sarcoglycan-sarcospan complex as a basis for understanding sarcoglycanopathy." <u>Hum Gene Ther</u> **9**(7): 1033-1040.

Young, H. K., B. A. Barton, S. Waisbren, L. Portales Dale, M. M. Ryan, R. I. Webster and K. N. North (2008). "Cognitive and psychological profile of males with Becker muscular dystrophy." <u>J Child Neurol</u> **23**(2): 155-162.

Yue, Y., Z. Li, S. Q. Harper, R. L. Davisson, J. S. Chamberlain and D. Duan (2003). "Microdystrophin gene therapy of cardiomyopathy restores dystrophin-glycoprotein complex and improves sarcolemma integrity in the mdx mouse heart." <u>Circulation</u> **108**(13): 1626-1632.

Yue, Y., M. Liu and D. Duan (2006). "C-terminal-truncated microdystrophin recruits dystrobrevin and syntrophin to the dystrophin-associated glycoprotein

complex and reduces muscular dystrophy in symptomatic utrophin/dystrophin double-knockout mice." Mol Ther **14**(1): 79-87.

Yugeta, N., N. Urasawa, Y. Fujii, M. Yoshimura, K. Yuasa, M. R. Wada, M. Nakura, Y. Shimatsu, M. Tomohiro, A. Takahashi, N. Machida, Y. Wakao, A. Nakamura and S. Takeda (2006). "Cardiac involvement in Beagle-based canine X-linked muscular dystrophy in Japan (CXMDJ): electrocardiographic, echocardiographic, and morphologic studies." BMC Cardiovasc Disord **6**: 47.

Zhao, J., K. Kodippili, Y. Yue, C. H. Hakim, L. Wasala, X. Pan, K. Zhang, N. N. Yang, D. Duan and Y. Lai (2016). "Dystrophin contains multiple independent membrane-binding domains." Hum Mol Genet **25**(17): 3647-3653.

Zhou, H., M. Fu, B. Mao and L. Yuan (2021). "Cardiac Phenotype-Genotype Associations in DMD/BMD: A Meta-Analysis and Systematic Review." Pediatr Cardiol **42**(1): 189-198.